The mechanisms of latrophilin 1-mediated control of spontaneous exocytosis at the mouse neuromuscular junction

EVELINA PETITTO

A thesis submitted in partial fulfilment of the requirements of the University of Kent and the University of Greenwich for the Degree of Doctor of Philosophy

November 2015

DECLARATION

I certify that this work has not been accepted in substance for any degree, and is not concurrently being submitted for any degree other than of Doctor of Philosophy being studied at the University of Greenwich and Kent. I also declare that this work is the result of my own investigations except where otherwise identified by references and that I have not plagiarised the work of others.

Candidate: Evelina Petitto

Signed: _____

Supervisor: Prof. Yuri Ushkaryov

Signed: _____

Date: 16/11/2015

AKNOWLEDGEMENTS

"It would be possible to describe everything scientifically, but it would make no sense; it would be without meaning, as if you described a Beethoven symphony as a variation of wave pressure."

Albert Einstein

A lot of science will follow in the next pages. However, life would be meaningless if science was all that matters. This is the place where I take the opportunity to express my gratitude to all the people that were by my side during this life-changing experience, sharing with me every moment, good and bad, and every feeling, from joy to sadness, from satisfaction to frustration.

First of all I want to thank my exceptional supervisor, Prof. Yuri Ushkaryov; all of this wouldn't have been possible without him, who gave me the possibility to work in his lab, tempered my spirit, and helped me with his (apparently) infinite knowledge. A special thank goes also to Vera Lelyanova, who assisted me during the beginning of my PhD.

Thanks to former and present members of the lab, Nickolai Vysokov and Jen Blackburn for the useful discussions, help with lab work, and for the much-needed chats in the lab.

In this contest I cannot avoid to say how grateful I am to have met wonderful colleagues that turned out to be very special friends too: my time spent at Kent would not have been the same without Carmen Piras, Colin Moore, Filip Kunc, Francesca Ferrara, Stefania Lettieri, Stuart Mather.

Finally, a big thank you to the people that more closely have been with me: Jared, the best partner I could ever have wished for, who was patient enough to tolerate my mood swings and my long list of complaints especially in the period when this thesis was written. And last but not least thanks to my mother Alessandra and to her partner Sandro for all the support they gave me not only during these years, but for all my life. I cannot thank you enough for making me who I am.

ABSTRACT

Latrophilin1 (LPHN1) is a presynaptic adhesion G protein-coupled receptor involved in the control of spontaneous exocytosis of neurotransmitters. The effects of LPHN1 activation on exocytosis have been described on several model systems, such as cultured hippocampal neurons and neuromuscular junction (NMJ) using its well known agonist LTX^{N4C}, and include a massive increase in exocytosis characterised by periods of intense release (bursts) interspersed with periods of moderate activity (interburst intervals).

However, the molecular mechanisms underlying these effects were yet to be determined. Based on previous observations that LPHN1 is associated to G proteins, and that its activation leads to activation of PLC and increased IP_3, we hypothesize that LPHN1 controls exocytosis via the $G\alpha_q$ protein pathway, whose activation ultimately results in the release of Ca^{2+} from IP_3-sensitive Ca^{2+} stores.

Using a pharmacological approach and the current clamp method at the mouse NMJ, we first used LPHN1 KO preparations to study the role of LPHN1 on spontaneous exocytosis in resting conditions, and to show that LPHN1 is the only receptor mediating the effects observed upon stimulation by LTX^{N4C}.
Then, we interfered with several molecules involved in the $G\alpha_q$ pathway to test their involvement in LPHN1 activation, and we investigated the role of store-operated (SOCCs) and voltage-gated (VGCCs) Ca^{2+} channels in mediating the Ca^{2+} influx that is necessary for the development of LPHN1 effects.

Our results support the hypothesis LPHN1 is involved in the regulation of spontaneous exocytosis at rest and that it is the receptor mediating the increased exocytosis following stimulation by LTX^{N4C}; the suggestions that $G\alpha_q$ and its intracellular pathway mediate the effects of LPHN1 activation on spontaneous exocytosis, and that SOCCs and VGCCs (particularly $Ca_v2.1$) mediate the Ca^{2+} influx necessary for the development of LPHN1 effects are also supported by our findings.

Altogether, this work uncovered the mechanisms by which G protein-coupled receptors, in this case LPHN1, can regulate the rate of spontaneous neurotransmitter release at the mouse NMJ.

TABLE OF CONTENTS

FIGURES

CHAPTER 1

in untransfected cells (first five lanes), suggesting that the binding is non specific and the toxin is not active due to incorrect folding.

CHAPTER 4

CHAPTER 5

CHAPTER 7

CHAPTER 8

TABLES

LIST OF ABBREVIATIONS

2APB	2-Aminoethoxydiphenyl borate
3D	three-dimensional
Ach	acetylcholine
aGPCR	adhesion G protein-coupled receptor
ALR	ankirin-like repeat
AP	action potential
ATP	adenosine triphosphate
BDNF	brain derived neurotrophic factor
CaM	calmodulin
CC	coil-coiled domain
CNS	central nervous system
CRAC	Ca^{2+} release-activated Ca^{2+} channel
CTF	C-terminal fragment
EB 1	microtubule end binding protein 1
EFs	Ca^{2+} binding EF-hands
EGF	epidermal growth factor
EM	electron microscopy
EPSCs	excitatory postsynaptic currents
ER	endoplasmic reticulum
GABA	gamma-aminobutyric acid
GAPs	GTPase activating proteins
GBL	galactose binding lectin
GDP	guanosine diphosphate
GPCR	G protein-coupled receptor
GPS	GPCR proteolysis site
GTP	guanosine triphosphate
HRM	hormone receptor motif
$\mathbf{I_{CRAC}}$	Ca^{2+} release-activated Ca^{2+} current
$\mathbf{IP_3}$	inositol triphosphate
$\mathbf{IP_3R}$	inositol triphosphate receptor

IPSCs	inhibitory postsynaptic currents
IPTG	isopropyl b-D thiogalactoside
K_d	equilibrium dissociation constant
KO	knock out
LDCV	large dense core vesicle
LNS	laminin G/NRX/sex hormone-binding like
LPHN	latrophilin
LTX	latrotoxin
MEPPs	miniature end-plate potentials
mEPSCs	miniature excitatory postsynaptic currents
NMJ	neuromuscular junction
NRX	neurexin
NSF	N-ethylmaleimide sensitive factor
NTF	N-terminal domain
PFOA	perflourooctanoic acid
PIP_2	phosphatidylinositol 4,5-biphosphate
PKC	protein kinase C
PLC	phospholipase C
PM	plasma membrane
PNS	peripheral nervous system
PTPσ	protein tyrosine phosphatase σ
RIM	Rab3 interacting molecule
ROCs	receptor operated channels
RT	room temperature
SAM	Sec1-Munc18 like
SNAP-25	25 kDa synaptosomal-associated protein
SNAPs	soluble NSF attachments proteins
SNARE	soluble NSF attachment receptor
SOCCs	store-operated calcium channels
SOCE	store-operated calcium entry
SP	signal peptide
SSV	small synaptic vesicle

STIM	stromal interaction molecule
STP	Ser-, Thr- and Pro-rich domain
TCAP	teneurin C-terminal associated peptide
TG	thapsigargin
TMR	transmembrane region
TRPCs	transient receptor potential channels
TTX	tetrodotoxin
VAMP	vesicle associated membrane protein
VGCCs	voltage-gated calcium channels
WT	wild type

CHAPTER 1
INTRODUCTION

1.1 Exocytosis

Exocytosis is the process by which cells release the content of an intracellular vesicle to the extracellular space. It is a fundamental process in multicellular organisms that permits the passage of material and information from cell to cell.

Exocytosis can be constitutive or regulated; the first type occurs continuously in all eukaryotic cell types without the need of any stimulus and it is necessary to maintain the plasma membrane identity. Through constitutive exocytosis, for example, a cell delivers its surface proteins that will be incorporated in the plasma membrane. In contrast, regulated exocytosis only occurs when cells are stimulated, and is limited to specialised cells such as neurons or endocrine cells. In this case, the content of intracellular vesicles is released when the stimulation of the cell triggers an elevation of intracellular Ca^{2+} or other second messengers. Constitutive and regulated exocytosis can coexist in the same cell (Burgess and Kelly 1987).

Regardless of the cell type involved, the final stage of the exocytosis is the fusion of the membrane belonging to the vesicle and the membrane belonging to the cell, with consequent release of material in the extracellular space. This whole process is highly regulated and mediated by specific proteins that define the exocytic apparatus.

1.1.1 Early evidences of vesicular release

The first evidences that cells, more specifically neurons at the synaptic terminals, contain membrane-bound vesicles come from electric micrographs of lizard neuromuscular junctions (NMJs) showing that small vesicles were always

present in each preparation at the presynaptic side (Robertson 1956; De Robertis 1958).

These early observations constituted the foundation of the "vesicle hypothesis", according to which neurotransmitters are stored inside synaptic vesicles that are released in the synapse upon their fusion with the plasma membrane and get then recycled in a Ca^{2+}-dependent manner (del Castillo and Katz 1956; Hubbard and Kwanbunbumpen 1968; Ceccarelli and Hurlbut 1980a; Ceccarelli and Hurlbut 1980b)

However, the correlation between synaptic vesicles and synaptic activity was not directly obvious, as the chances of observing by electron microscopy (EM) one of these vesicles fusing with the plasma membrane and releasing its content were very small (Birks, Huxley and Katz 1960). The situation was resolved with the discovery that La^{3+} is able to stimulate massive neurotransmitter release at the frog NMJ. Using this stimulation, for the first time it was possible to establish a link between increased neurotransmitter release and reduction in synaptic vesicle number (Miledi 1966).

Another evidence in support of the vesicular hypothesis of neurotransmitter release came from studies at the frog NMJ using α -latrotoxin (αLTX), a black widow spider venom's toxin that is able to trigger a dramatic increase in neurotransmitter release; when observed using EM, terminals treated with αLTX appear swollen and, most importantly, depleted of synaptic vesicles, confirming the hypothesis that these structures are the ones implicated in the exocytosis of neurotransmitter (Frontali et al. 1976).

1.1.2 Exocytosis of neurotransmitter

Communication between neurons takes place in a specialised structure called synapse, where axons and dendrites belonging to different neurons come in close proximity and exchange information in a unidirectional way (Purves 2012).

In the mammalian central nervous system (CNS) the majority of neurons are connected by chemical synapses, in which neurotransmitter molecules stored in synaptic vesicles are released during a highly regulated process that starts when an

action potential (AP) reaches the presynaptic terminal. The change in membrane potential causes the opening of the presynaptic voltage-gated Ca^{2+} channels (VGCCs), leading to the influx of Ca^{2+} into the cytosol. The elevation in the cytosolic Ca^{2+} concentration allows the fusion of the synaptic vesicles to the plasma membrane, so that neurotransmitters are released in the synaptic cleft where they can interact with the corresponding postsynaptic receptors, leading to the opening/closing of specific ions channels. In this way the signal is transmitted to the postsynaptic cells, and the result is the increased (in the case of excitatory neurotransmitters) or decreased (in the case of inhibitory neurotransmitters) probability that an AP will be generated (Purves 2012).

Two classes of vesicles are found in neurons: small synaptic vesicles (SSVs) and large dense core vesicles (LDCVs). Classical neurotransmitters such as glutamate, acetylcholine, dopamine, gamma-aminobutyric acid (GABA) and serotonin are stored in SSVs, that are located mainly in the CNS, have a diameter of approximately 30 nm and appear as clear circles in electron microscopy (EM) images. Neuropeptides, amine and neurohormones are instead stored in LDCVs, that are mainly located in the peripheral nervous system (PNS), have a diameter ranging from 100 to 300 nm and look as having a dense core in EM images (Park and Kim 2009).

These two classes of synaptic vesicles have different mechanisms of exocytosis: being mainly localised at the active zone, SSVs are released rapidly after a single AP and undergo a cycle of exocytosis/endocytosis and refilling of neurotransmitter. Neurotransmitters released from SSVs elicit fast electrical signals in the postsynaptic neurons by activating ion channels on their plasma membrane and thus mediate synaptic transmission. On the other hand, LDCVs are localised homogenously in the cytoplasm, and they are released only upon prolonged stimulation. Differently from SSVs, neurotransmitters stores in LDCVs do not produce fast synaptic transmission, but they modulate it by acting primarily on G protein-coupled receptors (GPCRs) (Park and Kim 2009; Xu and Xu 2008).

1.1.3 Evoked and spontaneous exocytosis

When we talk about exocytosis of neurotransmitter we usually think of the process initiated by an action potential, which, by depolarising the plasma membrane, allows the opening of VGCCs and the influx of Ca^{2+} into the cytosol. The increased cytosolic Ca^{2+} concentration then promotes fusion of vesicles with the plasma membrane and neurotransmitter release. This is known as evoked exocytosis.

However, release of neurotransmitter also happens independently from an action potential. This is called spontaneous exocytosis, and was first described on the basis of postsynaptic recordings at the neuromuscular junction by Fatt and Katz (1952). Here they observed small postsynaptic depolarisations occurring continuously in the absence of any stimulation (Fatt and Katz 1952). These events, constant in amplitude (about 0.5 mV), led to the formulation of the "quantal hypothesis", stating that: (i) the quantum of neurotransmission at the basis of spontaneous miniature end-plate potentials (MEPPs) and evoked end-plate potentials (EPPs) are the same; (ii) the release of each quantum is random, that is, independent from the release of other quanta; (iii) the evoked EPPs are the result of the synchronous release of several quanta (Fatt and Katz 1952; del Castillo and Katz 1954).

The constant amplitude of MEPPs is one of the most important features of this phenomenon. However, different factors can have an influence on it. First, the input resistance of the fibre, that defines the change in voltage associated to the injection of a current. An increased input resistance will generate a bigger membrane voltage change and vice versa (Katz and Thesleff 1957; Harris and Ribchester 1979). Second, the resting membrane potential have an influence on the driving force (defined as the difference between resting potential and the reverse potential for the action of Ach on its receptor) of different ions; as a result, more negative membrane potentials generate bigger driving forces (and so stronger inward currents) and this translates in larger voltage responses; on the contrary, more positive membrane potentials will generate smaller voltage responses because the driving forces generated (and the corresponding inward currents) will be weaker (McLachlan and Martin 1981).

The dependency on Ca^{2+} is also true for spontaneous release: in fact, spontaneous exocytosis is sensitive to both intracellular and extracellular Ca^{2+} concentrations. Intracellularly, the elevation of cytosolic Ca^{2+} due to release from intracellular Ca^{2+} stores (mediated by both inositol triphosphate (IP_3) and ryanodine receptors), increases the rate of spontaneous exocytosis; in a similar way, elevations of extracellular Ca^{2+} concentration increase the frequency of neurotransmitter release, whilst reductions of extracellular Ca^{2+} concentration decrease it (Grassi et al. 1994; Li et al. 1998; Mozrzymas, Barberis and Cherubini 1999; Giovannini et al. 2002; Awatramani, Price and Trussell 2005; Glitsch 2008).

Both evoked and spontaneous forms of neurotransmitter exocytosis have physiological roles. Evoked release is used by neurons to signal rapidly between one to another. Spontaneous release can regulate dendritic protein synthesis and expression of postsynaptic receptors. For example, spontaneous glutamate release regulates mRNA translation, enhancing it or inhibiting it according to the frequency of release (Sutton et al. 2004). Moreover, spontaneous glutamate release is essential to maintain dendritic spines by activating AMPA receptor (McKinney et al. 1999).

1.1.4 Mechanisms of exocytosis

Synaptic vesicles undergo a series of steps before their content can be released. In the first step, called docking, the vesicles come in close proximity with where they are tethered to the plasma membrane; this is followed by a priming step, in which the vesicles are made competent for exocytosis. Finally, when an elevation in cytosolic Ca^{2+} concentration occurs, the membrane of the vesicles fuse with the plasma membrane, connecting the vesicle lumen to the extracellular space where the content of the vesicle can be released.

The molecular machinery that governs the exocytic process consists of many interacting proteins. The main group of transmembrane proteins, collectively called "soluble N-ethylmaleimide-sensitive factor (NSF) attachment protein receptors" (SNAREs), drives vesicle fusion and includes synaptobrevin, also called VAMP2 (integral protein of SSVs), SNAP-25 and syntaxin-1 (located on the plasma membrane). There are also cytosolic proteins: Sec1-Munc18 like (SM) proteins, NSF and soluble NSF attachments proteins (SNAPs). Other important cytosolic molecules that modulate the process are synaptotagmin-1, Munc-13, Rab3 interacting molecule (RIM) and complexins (Sudhof 2004; Sudhof and Rizo 2011; Südhof 2013)

SNAREs are the initial components for the docking of the vesicles to the plasma membrane. VAMP2 and syntaxin-1 each contain a single SNARE motif (an extended coiled-coil stretch), while SNAP-25 contains two SNARE motifs. When these three proteins assemble, their four SNARE motifs come together pulling the vesicular and plasma membrane close to each other (Sollner et al. 1993b; Sutton et al. 1998). At this stage, the two membranes still have different identities, and form a *trans*-SNARE complex. After the zippering of this complex in an amino-to-carboxy-terminal direction forces the two membranes to close proximity and fusion, VAMP2, syntaxin-1 and SNAP-25 are all localised on the plasma membrane, forming a *cis*-SNARE complex.

SM protein Munc 18-1 is essential for the SNARE complex formation; however its role is still controversial and not completely understood. Munc 18-1 is known to bind to the closed conformation of syntaxin-1, preventing it from interacting

with other SNAREs; when syntaxin-1 "opens" in preparation for the formation of the SNARE complex, Munc 18-1 remains attached to it, changing its binding mode to an interaction with the complex (Khvotchev et al. 2007). It was first proposed that Munc 18-1 acted by inhibiting the activation of syntaxin-1 (Yang et al. 2000; Wu et al. 2001); however, deletion of Munc 18-1 results in a complete loss of exocytosis (Verhage et al. 2000). It is proposed that Munc 18-1 is needed to guide syntaxin-1 to an appropriate SNARE complex formation, or to prevent a premature SNARE assembly (Jahn and Fasshauer 2012).

Other proteins, RIM and Munc-13 are involved in the vesicle docking and priming steps and in recruiting Ca^{2+} channels next to the docked vesicles. RIM has several functions: it binds to Rab3 and Rab27 GTP-binding proteins on synaptic vesicles, therefore contributing to the docking; it binds to Ca^{2+} channels recruiting them to the active zone; finally, it binds to Munc-13, activating it. In turn, Munc-13 acts as a priming factor that promotes SNARE assembly by catalysing the conformational change of syntaxin-1 from closed to open (Südhof 2013).

Other molecules involved in priming are the complexins, which bind on the surface of the SNARE complex once it is already partially assembled. Complexins have both a stimulatory and an inhibitory function: they stabilise partially zipped SNARE complexes preparing them to be activated by synaptotagmin, and at the same time they block the progression of the zippering competing with VAMP2 until Ca^{2+} enters the cell, when most likely synaptotagmin releases the cluster (Jahn and Fasshauer 2012).

The principal Ca^{2+} sensor for the fusion mediated by SNARE appears to be synaptotagmin-1, an integral membrane protein located on the synaptic vesicles (Koh and Bellen 2003; Brose et al. 1992), whose cytoplasmic domain contains repeats of a region homologous to the C2 domains of the protein kinase C. Synaptotagmin-1 has two C2 domains, C2A and C2B, that can bind 3 and 2 Ca^{2+} ions respectively (Ubach et al. 1998; Fernandez et al. 2001).

In response to elevations in cytosolic Ca^{2+} concentration, synaptotagmin-1 can bind to the plasma membrane lipids (Brose et al. 1992) and can also bind to phosphatidylinositol 4,5-biphosphate (PIP_2) located within the inner leaflet of the

plasma membrane (Schiavo et al. 1996; Hu et al. 2002). Most interestingly, synaptotagmin-1 also binds SNAREs syntaxin and SNAP-25 in a Ca^{2+} dependent manner (Sollner et al. 1993a; Schiavo et al. 1997; Chapman et al. 1995).

Far from being simply a sensor for Ca^{2+}, synaptotagmin-1 regulates synaptic vesicles exocytosis modulating various steps of the cycle: it interacts with SNAP-25 in a Ca^{2+} dependent manner promoting the docking of the vesicles to the plasma membrane (Chieregatti, Witkin and Baldini 2002); it contributes to the opening of the fusion pore through rearrangements that alter the distance and orientation of the synaptotagmin-1-SNAP-25 complex (Bai et al. 2004); finally, synaptotagmin-1 is also necessary for the endocytosis of SSVs once exocytosis is completed (Poskanzer et al. 2003).

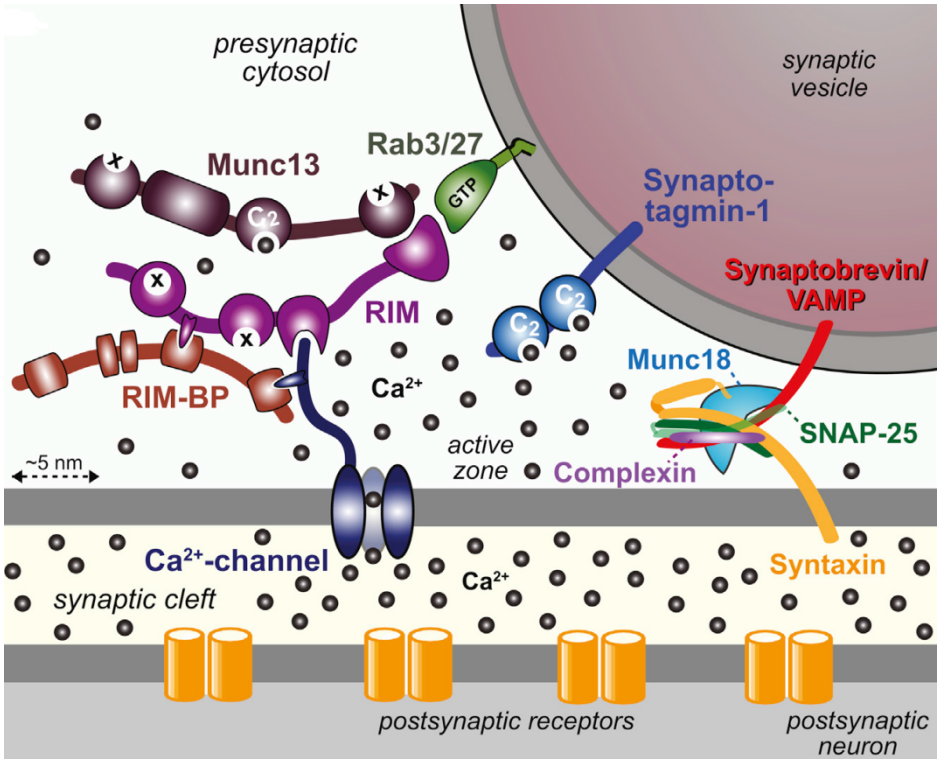

Figure 1.1. Schematic representation of the molecular machinery involved in vesicle exocytosis. On the top right, a synaptic vesicle is shown, being docked to the active zone (Südhof 2013).

Once fusion has occurred, the SNARE complexes are disassembled by NSF, a member of the AAA^+ (ATPases Associated with various cellular Activities plus) family. NSF acts by binding to the SNAPs and freeing VAMP2, thus allowing its recycling through endocytosis (Sollner et al. 1993a; Zhao et al. 2010).

1.1.5 Full fusion and kiss and run

The mode of fusion of synaptic vesicles to the plasma membrane during exocytosis has been long studied and two distinct mechanisms have been proposed in the early 1970s: full fusion of the vesicle and kiss and run.

According to the first model, when a vesicle undergoes exocytosis its membrane fully collapses and fuses with the plasma membrane, becoming part of it. At a later stage, the vesicle is retrieved at a distal location and refilled with neurotransmitter to become fully operational again (Heuser and Reese 1973; Heuser 1989).

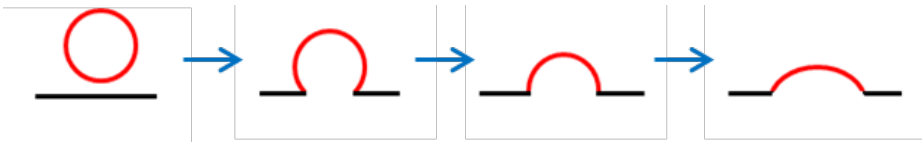

Figure 1.2. Full fusion model of vesicle exocytosis. The vesicle undergoing exocytosis fully fuses and becomes part of the plasma membrane.

In the same years, Ceccarelli and collaborators noticed that upon prolonged stimulation at the neuromuscular junction the number of vesicles in the terminal remained constant for a long period of time, and only after several hours the release would stop, probably due to the lack of newly synthetized neurotransmitter. Using EM, they also visualised the omega membrane profile connecting the vesicle and the plasma membrane at the active zone. Therefore they came up with another model, known as “kiss and run”, according to which the vesicle only partially fuses with the plasma membrane, resulting in the opening of a small fusion pore. The neurotransmitter is quickly released and soon

after the pore closes, maintaining the integrity of the synaptic vesicle (Ceccarelli, Hurlbut and Mauro 1972; Ceccarelli, Hurlbut and Mauro 1973).

Figure 1.3. Kiss and run model of vesicle exocytosis. The vesicle membrane only partially fuses with the plasma membrane, generating an omega structure and a fusion pore. After the closure of the pore the vesicle is back at the active zone where it can be exocytosed again.

Whilst the existence of full fusion has been widely accepted for a long time, the idea that kiss and run fusion can exist in neurons has been debated until recently. With time, evidence in favour of the existence of kiss and run fusion have been collected in endocrine cells, calyx of Held synapse, neuromuscular junction, goldfish retinal bipolar synapses (He and Wu 2007), cultured hippocampal synapses (Stevens and Williams 2000) and dopaminergic neurons (Wightman and Haynes 2004).

With the accumulation of data suggesting that kiss and run fusion exists at synapses, the focus of the debate is now switching to whether this form of exocytosis is the major form of fusion.

Regardless of the debate about what form of fusion is predominant, some works suggests that these two forms are both present at synapses and can coexist in the same terminal. The switch from one mechanism to the other could be a method to regulate synaptic strength and plasticity, as they would allow to release different quantities of neurotransmitter, different rates of release and also different times (Choi, Klingauf and Tsien 2000; Choi, Klingauf and Tsien 2003; He and Wu 2007).

1.2 α-Latrotoxin as a tool to study LPHN1-mediated exocytosis

The black widow spider (genus *Lactrodectus*) is a venomous spider whose bite causes a variety of symptoms including difficult breathing, muscle cramps and spasms, high blood pressure, anxiety, nausea and restlessness. Severe symptoms usually last for a couple of days and mild symptoms disappear after some weeks; death is rare in healthy adults, but is more common in children and elderly (Rauber 1983; Peterson 2006; Shackleford et al. 2015).

Since the discovery in the 1930s that the active principles of the venom are proteins (D'Amour, 1936) acting on neurons (Sampayo 1944) and affecting neurotransmitter release (Frontali et al. 1976; Duchen, Gomez and Queiroz 1981), black widow spider venom (BWSV) became increasingly used as a scientific tool to uncover the mechanisms of neurotransmission.

The principal toxic components of BWSV are called latrotoxins (LTX), and to date seven of them have been isolated. Five of them, called latroinsectotoxins α, β, γ, δ and ε, specifically target insects (Grishin 1998; Rohou, Nield and Ushkaryov 2007); one, α-latrocrustatoxin, specifically targets crustaceans (Elrick and Charlton 1999); another, α-latrotoxin (α-LTX), is vertebrate-specific, and it is one of the best characterised (Frontali et al. 1976).

1.2.1 α-LTX as a secretogogue

Due to its ability to cause massive release of neurotransmitters and hormones in all secretory cells that have regulated exocytosis, α-LTX has been widely used as a tool to study secretion.

Starting from the 1970s, the effects of the toxin on secretion have been described in many neuronal and non-neuronal model systems such as frog NMJ, where α-LTX causes increased frequency of miniature end-plate potentials (MEPPs) and depletion of synaptic vesicles (Frontali et al. 1976); rat synaptosomes, where it causes a significant increase in the release of GABA (Grasso, Rufini and Senni 1978); mouse brain slices, where an increase in the frequency of exocytosis was described both for norepinephrine and for GABA

(Tzeng and Siekevitz 1978; Tzeng, Cohen and Siekevitz 1978); in chromaffin cells, where the toxin causes an increased secretion of adrenaline and noradrenaline (Picotti, Bondiolotti and Meldolesi 1982); in pancreatic β-cells cultures, where it stimulates insulin exocytosis (Lang et al. 1998); in primary cultures of cerebellar granule cells, where α-LTX causes an increase in the release of amino acid transmitters (Grasso and Mercanti-Ciotti 1993); in hippocampal organotypic cultures, where the toxin increases the frequency of miniature excitatory postsynaptic currents (mEPSCs) (Capogna, Gahwiler and Thompson 1996); in rat gonadotrophs, where it induces the release of luteinizing hormone (Tse and Tse 1999); and in neurohypophysis cells, where α-LTX causes the secretion of vasopressin and oxytocin (Hlubek, Tian and Stuenkel 2003).

One of the most surprising properties of α-LTX-evoked exocytosis is that it can happen both in the presence and in the absence of extracellular Ca^{2+}. The characteristics and modality of these two kinds of α-LTX-evoked secretion will be discussed in a further section (see 1.2.5).

The secretogogue action of α-LTX is very potent. In fact, whilst Ca^{2+}-independent release needs the classic exocytic machinery to occur, Ca^{2+}-dependent release can still occur in mice lacking the SNARE proteins VAMP2 and SNAP-25 and the active zone protein Munc-13 (Deak et al. 2009). It is possible, therefore, that in the presence of extracellular Ca^{2+} α-LTX uses an unknown pathway for exocytosis different from the classical one required instead in the absence of extracellular Ca^{2+} (Deak et al. 2009).

1.2.2 α-LTX structure

As described in several reviews (Ushkaryov 2002; Ushkaryov, Rohou and Sugita 2008; Silva, Suckling and Ushkaryov 2009), α-LTX is synthesized by free ribosomes in the cytosol of secretory epithelial cells in the black widow spider venom glands as an inactive precursor protein of 157 kDa. These cells then disintegrate, releasing the toxin, small molecules and proteases into the lumen of the venom gland. In order for the toxin to become active, the precursor has to be cleaved by a furin-like protease at two furin-like sites located in both N- and C-termini; the active toxin has a molecular mass of ≈ 131 kDa.

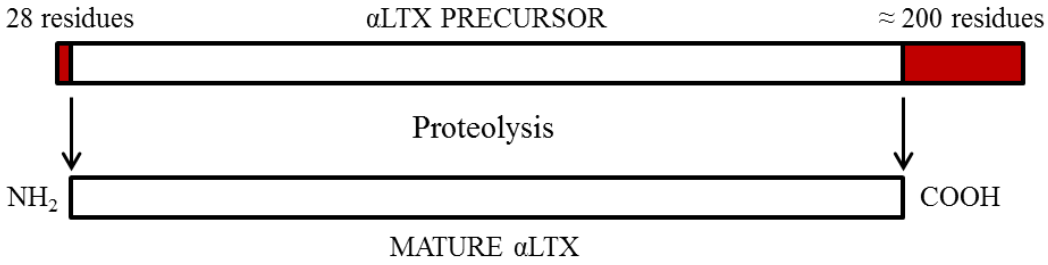

Figure 1.4. Schematic representation of αLTX processing in the venom gland. The precursor of αLTX is a protein of 157 kDa. It is then cleaved at furin-like sites both at the N- and the C-termini to produce the mature αLTX, with a molecular mass of 131 kDa.

The N-terminal part of α-LTX does not show significant homologies with other proteins. It consists of a large portion of α-helical structure and contains three conserved cysteines important for the structural stability and for the activity of the toxin (Kiyatkin et al. 1995). The C-terminal domain contains 22 ankyrin-like repeats (ALRs), a structure found in a wide variety of proteins that mediates intra- and inter-molecular interactions (Sedgwick and Smerdon 1999).

The three-dimensional (3D) structure of α-LTX was revealed by Orlova et al. (2000) using cryo-electron microscopy. It was shown that the monomeric α-LTX consists of three domains: the wing at the N-terminal domain, mainly composed of α-helices; the body, comprising the first 17 ALRs; the head at the C-terminal domain, consisting of 4.5 ALRs.

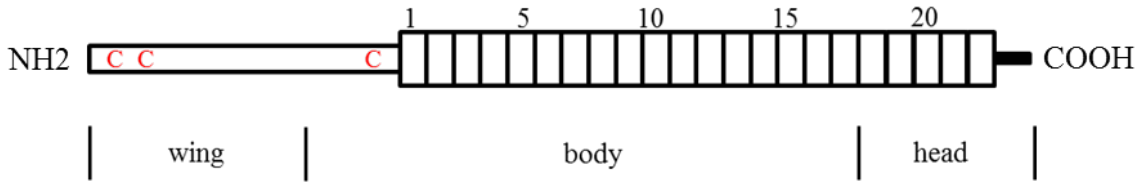

Figure 1.5. αLTX primary and domain structure. Letters C denote conserved cysteines at the N-terminal domain; boxes correspond to ankirin-like repeats. The identified 3D structure domains are indicated below.

However, the toxin does not exist as a monomer in nature, but as stable asymmetric dimers, in which two monomers are associated head-to-tail with the "horizontal" part of the body contacting the "vertical" part.

In the presence of divalent cations such as Ca^{2+} and Mg^{2+} (Ashton et al. 2000), the toxin is able to tetramerise into its active form. The tetramer, which resembles a bowl, has a C4 rotational symmetry, with the bottom formed by the horizontal parts of the bodies. The four heads form a central channel of about 3 nm in diameter; at one point, the channel is restricted to 1 nm. The wings extend on the side of the body perpendicularly to the tetramer's central symmetry axis (Orlova et al. 2000).

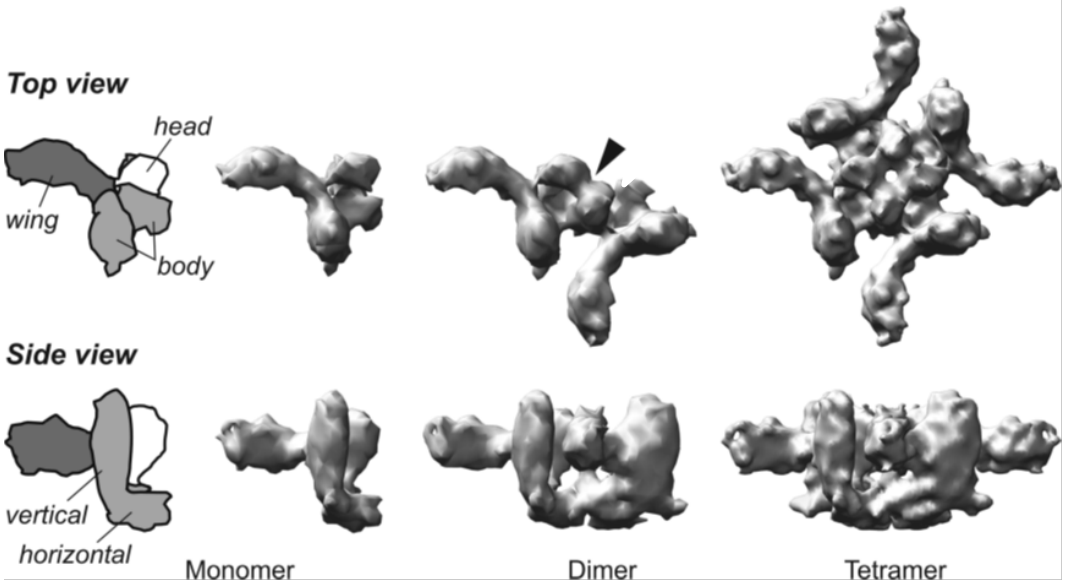

Figure 1.6. 3D reconstructions of the α-LTX monomer, dimer and tetramer, viewed from the top and side (Ushkaryov, Rohou and Sugita 2008).

1.2.3 Pore formation and receptor interactions

α-LTX is an amphipathic molecule; its bottom, being hydrophobic, is able to insert into cellular membranes, while the hydrophilic upper part remains above them. The insertion of the toxin is complete, and the central hole crosses the membranes from side to side, forming a pore that makes them permeable (Orlova et al. 2000).

The pore formed by α-LTX is pear-shaped, with a diameter of 2.5 nm at the bottom, 3.6 nm in the centre and 1 nm at the top. It is permeable to divalent and some monovalent cations (Volynski et al. 2000), and small molecules such as neurotransmitters and fluorescent dyes (Ashton et al. 2000; Davletov et al. 1998a), but not to trivalent cations, such as La^{3+} (Ashton et al. 2001).

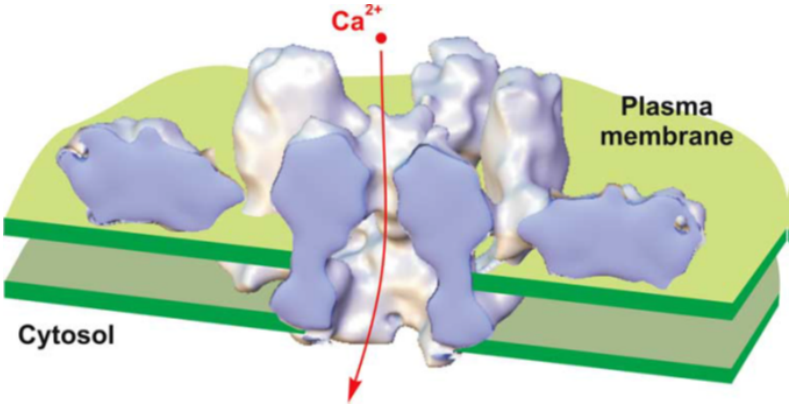

Figure 1.7. Section of α-LTX pore crossing the membrane and allowing cations into the cytosol (Ushkaryov, Volynski and Ashton 2004).

Although α-LTX is able to form pores in artificial lipidic bilayers (Finkelstein, Rubin and Tzeng 1976), biological membranes show resistance to the insertion of the toxin without the help of α-LTX receptors (Volynski et al. 2000; Hlubek et al. 2000).

Currently, three receptors are known to interact with α-LTX: neurexin Iα (NRX-Iα), protein tyrosine phosphatase σ (PTP-σ) and latrophilin 1.

NRX was the first α-LTX receptor to be isolated by affinity chromatography from bovine brain membranes (Petrenko et al. 1990). Six principal isoforms of NRX are expressed by three genes. These isoforms can be divided into two groups of three each, called α and β NRXs, with different domain structures. All of them consist of a single transmembrane region (TMR) and a short cytoplasmic tail; in α-NRXs, the N-terminal domain contains six laminin G/NRX/sex hormone-binding like (LNS) domains that, interspersed with epidermal growth factor-like (EGF-like) sequences, form three major repeats. In β-NRX, instead, the N-terminal is shorter and contains only one LNS domain and a unique N-terminal sequence (Ushkaryov et al. 1994; Ushkaryov et al. 1992).

Of the six isoforms of NRX, only NRX-Iα binds α-LTX with high affinity, and this interaction is Ca^{2+}-dependent (Petrenko et al. 1990; Davletov et al. 1995; Geppert et al. 1998).

NRXs are localised mainly in the brain (Ushkaryov et al. 1992; Ullrich, Ushkaryov and Südhof 1995), with some level of expression also in pancreas and lungs, heart, liver and kidney (Occhi et al. 2002).

PTP-σ is a receptor that, unlike NRX-Iα, is able to bind α-LTX also in the absence of Ca^{2+} (Krasnoperov et al. 2002). It is a member of the receptor-like PTPs family, and it consists of an extracellular ligand-binding domain, a single TMR, and a cytoplasmic phosphatase catalytic domain (Almo et al. 2007).

Although the binding to α-LTX is lower than the one observed for the other two receptors, the interaction between PTP-σ and the toxin has been demonstrated to be specific (Krasnoperov et al. 2002).

PTP-σ is mostly expressed in the brain, but it is also found in heart, kidney and placenta with lower expression (Pulido et al. 1995).

Latrophilin 1 (LPHN1) is the major receptor for α-LTX, able to bind it in a Ca^{2+}-independent manner. As this receptor is the main focus of the present work, its structure and function will be discussed in more detail in a following section (see section 1.3).

1.2.4 The recombinant LTX^{N4C}

Even before the isolation of the receptors that mediate α-LTX binding and function, it was clear that the toxin was able to trigger intracellular signalling; it was shown for example that binding of α-LTX led to the activation of phospholipase C (PLC), and to the subsequent production of IP_3 and release of Ca^{2+} from intracellular Ca^{2+} stores (Vicentini and Meldolesi, 1984). However, the formation of the pore made the study of the receptors' functions difficult.

The situation was resolved with the fortuitous construction of a mutant α-LTX containing a thrombin recognition site at the beginning of the ALR-containing domain. This recombinant toxin was named LTX^{N4C}, indicating the insertion of four amino acids between the N- and the C-termini (Ichtchenko et al. 1998).

This construct, having a defective folding, is still able to bind the receptors and to form dimers, but is unable to form tetramers and does not form membrane pores (Volynski et al. 2003).

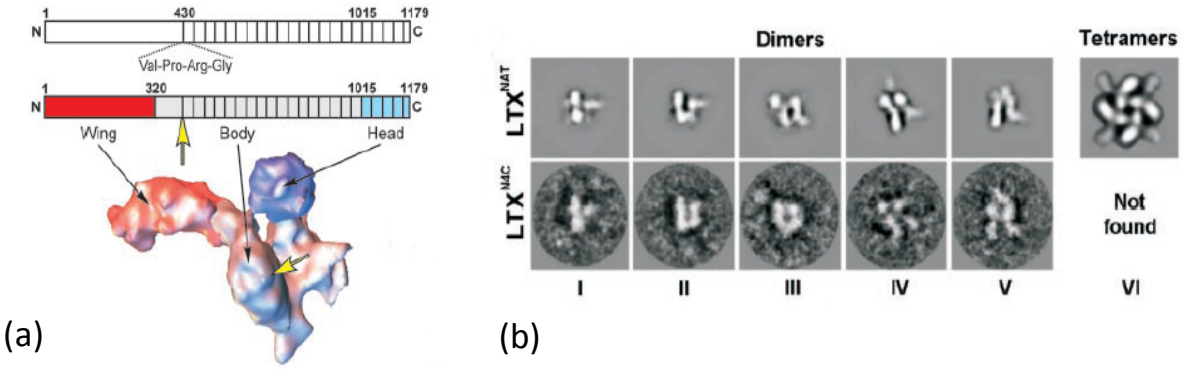

Figure 1.8. Structure of LTX^{N4C}. (a) Representation of the domain structure of LTX^{N4C}. The position of the insert is shown by an arrow. (b) Cryo-EM of native and mutant toxins showing that α-LTX, but not LTX^{N4C}, is able to form tetramers (Volynski et al. 2003).

1.2.5 Effects of α-LTX and LTX^{N4C} on exocytosis

As described in a previous section (see Section 1.2.1) starting from the 1970s data started to accumulate about the effects of α-LTX on neurotransmitter release in numerous neuronal systems such as the frog NMJ (Frontali et al. 1976), mouse cerebral cortex slices (Tzeng, Cohen and Siekevitz 1978), rat synaptosomes (Grasso, Rufini and Senni 1978), cerebellar granule cell cultures (Grasso and Mercanti-Ciotti 1993) and organotypic hippocampal cultures (Capogna, Gahwiler and Thompson 1996).

The exocytosis caused by α-LTX is, however, different from the typical Ca^{2+}-dependent exocytosis induced by action potentials; in fact, the toxin can induce exocytosis both in the presence and in the absence of extracellular Ca^{2+} (Tzeng, Cohen and Siekevitz 1978; Ceccarelli, Grohovaz and Hurlbut 1979).

The effects observed in the presence and absence of extracellular Ca^{2+} have different characteristics. First, in the presence of 1-2 mM Ca^{2+} a period of clonic release is initially observed, characterised by fast bursts of exocytosis, followed by a sustained tonic release that tends to decline and stop with time. In the absence of Ca^{2+}, instead, the secretion is only tonic, with the frequency that slowly rises, reaches a peak and then gradually decreases (Ceccarelli, Grohovaz and Hurlbut 1979; Ceccarelli and Hurlbut 1980; Fesce et al. 1986; Lelyanova et al. 2009).

Second, the total number of quanta released is roughly double in the presence of Ca^{2+} than in its absence. This is due to the role of Ca^{2+} in endocytosis, so that when Ca^{2+} is present vesicle recycling is still possible (Fesce et al. 1986).

Third, Mg^{2+} is required for the Ca^{2+}-independent action of the toxin (Misler and Hurlbut 1979), and Mg^{2+} fully supports α-LTX tetramerisation and pore formation. This suggests that tonic Ca^{2+}-independent exocytosis is caused by the pore that the toxin forms into the cellular membrane.

Given the knowledge that α-LTX requires the binding to receptors and that Ca^{2+}-independent exocytosis can be explained by the pore formation, it was necessary to find a tool to differentiate the role of receptors and pores. The appearance of LTX^{N4C} on the scene made this possibility an actuality. Unable to

form pores and strictly requiring extracellular Ca^{2+} for its activity (Ashton et al. 2001), LTX^{N4C} permits the study of the Ca^{2+}-dependent component of α-LTX effect alone, and also permits to delineate the role that the receptors have in this effect.

The effect of LTX^{N4C} on nerve terminals has been described for the first time in CA3 pyramidal neurons (Capogna et al. 2003) and later in mouse NMJ (Lelyanova et al. 2009). It was shown that binding of LTX^{N4C} to a receptor (thought to be latrophilin 1, see next section for details), lead to the mobilization of Ca^{2+} from internal stores (Capogna et al. 2003); furthermore, it was demonstrated that LTX^{N4C} causes clonic secretion of neurotransmitter for several hours, without the appearance of the tonic secretion observed with native α-LTX and without cessation of the effect, probably due to the lack of membrane disruption usually caused by the native toxin pores (Lelyanova et al. 2009). This strongly suggests that the clonic release is the component mediated by the receptor, which acts via mobilisation of intracellular Ca^{2+}.

1.3 Latrophilin 1

The major brain receptor for α-LTX is Latrophilin 1 (LPHN1), a presynaptic adhesion G protein-coupled receptor. It was isolated by two groups in 1996 from solubilised bovine brain using α-LTX affinity chromatography in the absence of Ca^{2+} (Davletov et al. 1996; Krasnoperov et al. 1996). Due to its high affinity for αLTX, it was named latrophilin by one group (Lelianova et al. 1997), whilst due to its ability to bind α-LTX in the absence of Ca^{2+} it was named CIRL (calcium-independent receptor of α-latrotoxin) by the other group (Krasnoperov et al. 1997).

As discussed in a previous section (see paragraph 1.2.3), LPHN1 is not the only receptor for α-LTX; therefore, the rise in exocytosis frequency could be attributed to the activation of the other receptors, for example, NRX-Iα. To distinguish the effects on exocytosis caused by α-LTX are due to the activation of LPHN1 only, experiments were made under conditions known to prevent the binding of α-LTX to NRX-Iα. LPHN1 is able to bind α-LTX in all ionic conditions; the interaction of NRX-Iα with the toxin, instead, is possible only in Ca^{2+}. Sr^{2+}, when replacing Ca^{2+}, fully supports α-LTX-mediated effects on exocytosis, but does not allow the interaction of the toxin with NRX-Iα (Davletov et al. 1998b). Therefore, the effect on exocytosis observed in at least this condition is due to the activation of LPHN1 only (Volynski et al. 2003).

1.3.1 G protein-coupled receptors: classification and signal transduction

G protein-coupled receptors are a large family of membrane proteins with different structures and functions. The ligands targeting these receptors are very diverse, ranging from ions, to peptides, proteins, nucleotides, lipids, photons to odorants (http://www.guidetopharmacology.org/GRAC/ReceptorFamiliesForward?type=GPCR).

Due to the diversity of this super-family, a classification is needed to group together proteins sharing common features and phylogenetic origin. Five main families have been identified (Fredriksson et al. 2003):

- Secretin receptor family
- Adhesion receptor family
- Glutamate receptor family
- Frizzled/Taste2 receptor family
- Rhodopsin family

The study of GPCRs is a prolific and intense field; many disorders, such as nephrogenic diabetes insipidus, colour blindness and hyperfunctioning thyroid adenoma, are due to abnormal GPCRs signalling and a great development in drugs targeting their functioning has risen (Karnik et al. 2003).

All GPCRs share the same basic features: an extracellular N-terminus domain, seven transmembrane regions (TMRs) linked by three extracellular and three intracellular loops, and a cytosolic C-terminus domain. The major constant factor between GPCRs is the TMRs, whilst the greatest diversity is found at the N-terminus domain.

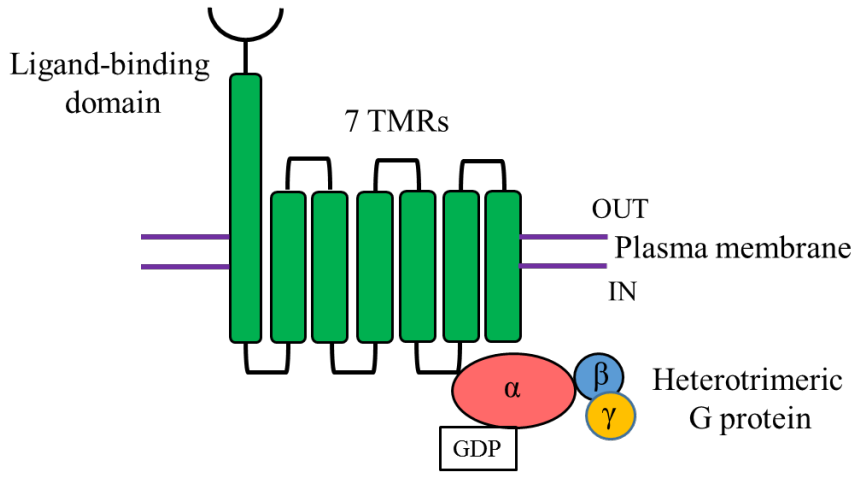

Figure 1.9. Schematic representation of a general heterotrimeric G protein-coupled receptor, composed of an extracellular N-terminal ligand binding domain, 7 TMRs connected by 3 intracellular and 3 extracellular loops, and an intracellular C-terminal domain attached to an heterotrimeric G protein. When inactive, the α subunit of the G protein is associated with GDP.

The seven stretches that form the TMRs are composed of 20-25 amino acids, forming α-helices of unequal length that cross the plasma membrane, organised in a barrel shape perpendicular to the membrane plane in a counter-clockwise manner from TMR I to TMR VII (when looking from the extracellular side). The TMRs are predominantly hydrophobic, but the strength of their hydrophobicity varies between them: TMR I, IV and VII, containing only one hydrophilic residue, are more hydrophobic than TMR II, III, V and VI, containing more neutral and ionic residues; this results in a different arrangement in the membrane, with the more hydrophobic TMRs exposed more to the lipidic bilayer (Ulloa-Aguirre et al. 1999).

Hydrogen bonds form between residues located in the same TMR and between residues belonging to different TMRs. These interactions exclude the possibility of a TMR pore in most GPCRs, and maintain the core tight in an inactive state (Ji, Grossmann and Ji 1998).

Disulphide bridges between Cys residues, mainly located in the N-terminus and extracellular loops I and II, are important for the stability of the ternary structure and binding properties of the receptor (Dixon et al. 1987). At the C-terminus, Cys residues can undergo palmitoylation, which creates a membrane anchor leading to the formation of a fourth intracellular loop. This process is vital for some GPCRs to maintain the functional coupling with G protein (O'Dowd et al. 1989; Qanbar and Bouvier 2003).

When a ligand binds the receptor, a signal is generated and transmitted to the intracellular G protein through the TMR core.

The specific binding site of the ligand is different depending on the class of GPCR involved and on the characteristics of the ligand. If the ligand is big, the correspondent GPCR usually exhibits a long N-terminus, where the binding site resides. For moderate size peptides, the binding site is usually located both in the N-terminus and extracellular loops; for small molecules, the ligand binding domain can be located in a pocket involving the middle and extracellular third of the TMs (such as for retinal chromophore), or in residues located in the first extracellular loop and several TMRs (such as for vasopressin) (Ulloa-Aguirre et al. 1999), or in the N-terminal domain alone (such as the metabotropic Glu and

GABA receptors). Once the agonist has bound the receptor, conformational changes of the TMRs transduce the signal and the activation of G protein occurs.

GPCRs are associated to heterotrimeric G proteins, composed of α, β and γ subunits. At least 28 G protein α subunits, 5 β subunits and 12 γ subunits have been identified, whose combinations are responsible for the diversity and specificity of the signalling. α subunits can be divided into four families according to their primary sequence similarities: G_s (G_s and G_{olf}); G_i (G_{tr}, G_{tc}, G_g, G_{1-3}, G_o and G_z); G_q (G_q, G_{11}, G_{14} and $G_{15/16}$); G_{12} (G_{12} and G_{13}) (Kristiansen 2004). The subunits β and γ form a tight complex dissociable only under denaturing conditions (Rens-Domiano and Hamm 1995).

Upon binding of an agonist, the activated receptor goes through conformational changes that increase its affinity for the GDP-bound form of a heterotrimeric G protein. This triggers the exchange of the GDP (associated with the α subunit) with GTP, and the dissociation of the βγ complex. Both the α and βγ subunits can then interact with specific effectors to start the intracellular signalling typical of the specific G protein involved. The GTP is finally hydrolysed back to GDP by the intrinsic GTPase activity of the α subunit or by GTPase activating proteins (GAPs) and the complex α+βγ reassociates going back to the inactive state.

The nature of the biological effects triggered by the activation of a receptor is very diverse, ranging from activation of ion channels, phospholipases and adenylyl cyclases, and depends from the specific G protein attached.

1.3.2 Latrophilins

Latrophilins are part of the Adhesion GPCR (aGPCR) family composed of three isoforms: latrophilin 1, 2 and 3 (Hamann et al. 2015). Their genes, denominated *lphn1*, *lphn2* and *lphn3*, are located respectively on chromosomes 19, 1 and 4 in humans and on chromosomes 8, 3 and 5 in mice. All latrophilins can bind α-LTX, with the affinity decreasing form LPHN1 to LPHN3, which shows almost no binding at all (Silva and Ushkaryov 2010).

Homologues forms of the three LPHNs are found in most chordates (Fredriksson and Schiöth 2005). LPHNs orthologues variants from distant vertebrates are more similar to each other than the homologues within one organism; this may indicate that the three LPHNs have different functions that have been strictly preserved in the evolutionary history of chordate animals (Silva and Ushkaryov 2010). The different pattern of expression of the three LPHN isoforms in various tissues further supports this explanation: whilst LPHN2 is ubiquitous, LPHN1 and 3 are expressed mainly in the brain (Ichtchenko et al. 1999; Matsushita, Lelianova and Ushkaryov 1999).

1.3.3 LPHN1 structure

As a member of the aGPCR family, LPHN1 is a large protein (185 kDa) whose primary structure comprises a large extracellular N-terminal domain, seven TMRs connected by three extracellular and three intracellular loops, and a cytoplasmic C-terminal domain. It undergoes an intracellular post translational cleavage that produces two functional parts: the N-terminal fragment (NTF) and the C-terminal fragment (CTF).

As described in Silva and Ushkaryov (2010) the NTF is a cell adhesion receptor-like domain of 120 kDa that begins with a hydrophobic signal peptide (SP). Following this, there is a 108 residues-long cysteine-rich region homologous to galactose-binding lectin (GBL); a 260 residues-long region homologous to olfactomedin; a 79 residues-long containing serines, theonines and prolines (STP); a 60 residues-long hormone-binding domain (characteristic of many adhesion GPCRs); a 180 residues-long Stalk region analogous to the one found in EMR3, another aGPCR. This region corresponds in LPH1 to the binding site for α-LTX; a 57 residues-long containing four cysteines called GPCR proteolysis site (GPS) motif, containing the site of post translational cleavage that generates the NTF and the CTF.

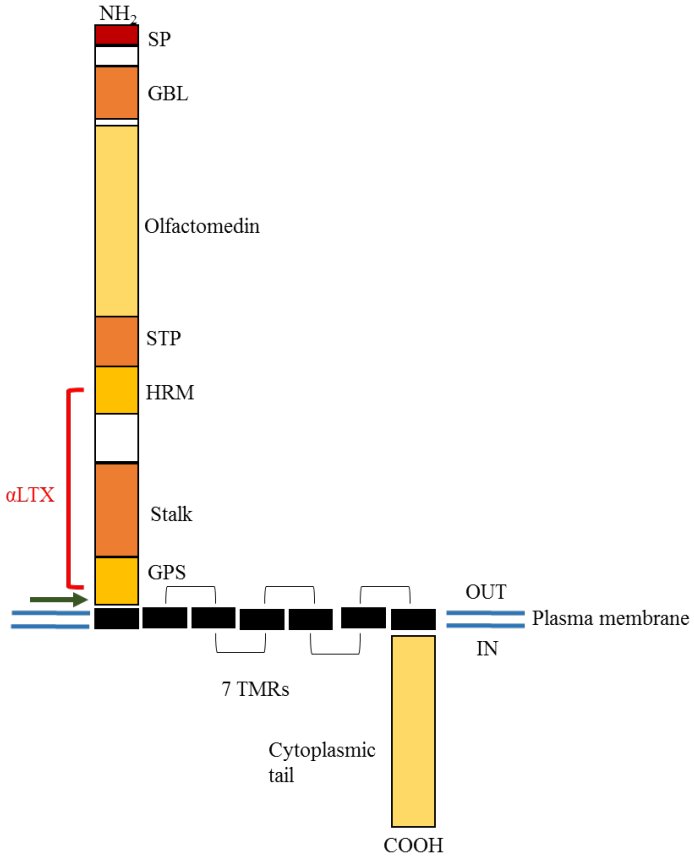

Figure 1.10. LPHN1 domain structure. SP, signal peptide; GBL, galactose-binding lectine; STP, Ser- Thr- and Pro-rich domain; HRM, hormone receptor motif; GPS, GPCR proteolysis site domain; 7 TMRs, seven transmembrane domains and correspondent loops; green arrow, cleavage site; red brackets, α-LTX binding site.

The CTF begins at the site of cleavage within the GPS motif, and it is composed of seven TMRs and a cytoplasmic tail, which is the least conserved domain among the latrophilin isoforms. The cytoplasmic tail contains five cysteine residues, three of which are positioned similarly to the ones in rhodopsin's cytoplasmic tail, and may be palmitoylated (Lelianova et al. 1997). The extracellular loops 1 and 2 contain two cysteines that can form an intramolecular disulphide bridge.

1.3.4 Interaction of LPHN1 fragments and intracellular signalling

The cleavage occurring in the GPS motif that give rise to the NTF and the CTF takes place in the endoplasmic reticulum (ER) and it is required for the delivery of the receptor to the cell surface (Volynski et al. 2004).

Once reached the cellular membrane, the two fragments behave independently as two distinct membrane proteins; the NTF, in fact, is not released into the medium, being attached to the membrane by a hydrophobic anchor, allowing it to stay on the membrane even without having any TMR (Volynski et al. 2004).

The association of NTF and CTF plays a crucial role in the function of the receptor; in fact, binding of a ligand occur at the NTF, whilst the intracellular signalling cascade at the CTF. The two functional parts must therefore be able to interact in order to generate the physiological effect of the receptor. Indeed, it has been demonstrated that upon binding of LTX^{N4C} NTF and CTF associate, forming ternary complexes LTX-NTC-CTF on the plasma membrane (Volynski et al. 2004).

This association does not necessarily occur between the same cleaved receptor molecules, but can either happen between two different LPHN molecules or between the NTF/CTF of LPHN with the NTF/CTF of another aGPCR, due to the highly conserved GPS motif in this receptor family (Silva et al. 2009).

As a GPCR, LPHN1 has been shown to interact with two types of Gα subunits: $G\alpha_o$ and $G\alpha_{q/11}$ (Lelianova et al. 1997; Rahman et al. 1999). The coupling of these G proteins with LPHN1 is functional: in fact, their association is stronger when GDP is present and weaker when an excess of GTP is added (Rahman et al. 1999). Furthermore, it has been shown that the activation of LPHN1 by α-LTX causes a rise in the concentration of IP_3 (Lelianova et al. 1997), whose production is triggered by the activation of PLC by a G protein. Indeed, the use of U73122, a drug that inhibits PLC activity, blocks the release of neurotransmitter caused by α-LTX in synaptosomes (Rahman et al. 1999).

Elevation of IP_3 leads to the release of Ca^{2+} from intracellular stores. Their role in LPHN1 activity has been investigated using thapsigargin (TG), a drug that

by irreversibly blocking the sarco/endoplasmic reticulum Ca^{2+} ATPase (SERCA) pumps causes the depletion of the stores. Stores depletion indeed inhibits the α-LTX-evoked release of neurotransmitter (Rahman et al. 1999).

1.3.5 Endogenous ligands

The first endogenous ligand of LPHN1 has been isolated by affinity chromatography and termed Lasso (LPHN1-associated synaptic surface organiser) (Silva et al. 2011).

Lasso belongs to the family of teneurins, brain specific cell surface proteins that play an important role in the development of the central nervous system, being involved in axon guidance and synaptogenesis (Tucker et al. 2007; Young and Leamey 2009). Its primary structure consists of a single TMR; the extracellular domain has eight EGF repeats, of which two possess unpaired cysteines that permit covalent homodimerisation of the molecule. The teneurin C-terminal associated peptide (TCAP) can be cleaved in vitro and possibly interact with LPHN1; when injected in the brain, TCAP affects behaviour linked to stress and anxiety (Wang et al. 2005). This would be in line with the implication of LPNH1 in attention deficit/hyperactivity disorder (ADHD), anxiety and schizophrenia. However no evidence of the TCAP cleavage exists in vivo so far (Silva et al. 2011).

Lasso is a postsynaptic protein that strongly and specifically binds LPHN1 on the presynaptic side, establishing a structural and functional interaction. Lasso is in fact able to activate LPHN1, initiating its signalling leading to an increase in the cytosolic Ca^{2+} concentration and to release of neurotransmitters (Silva et al. 2011).

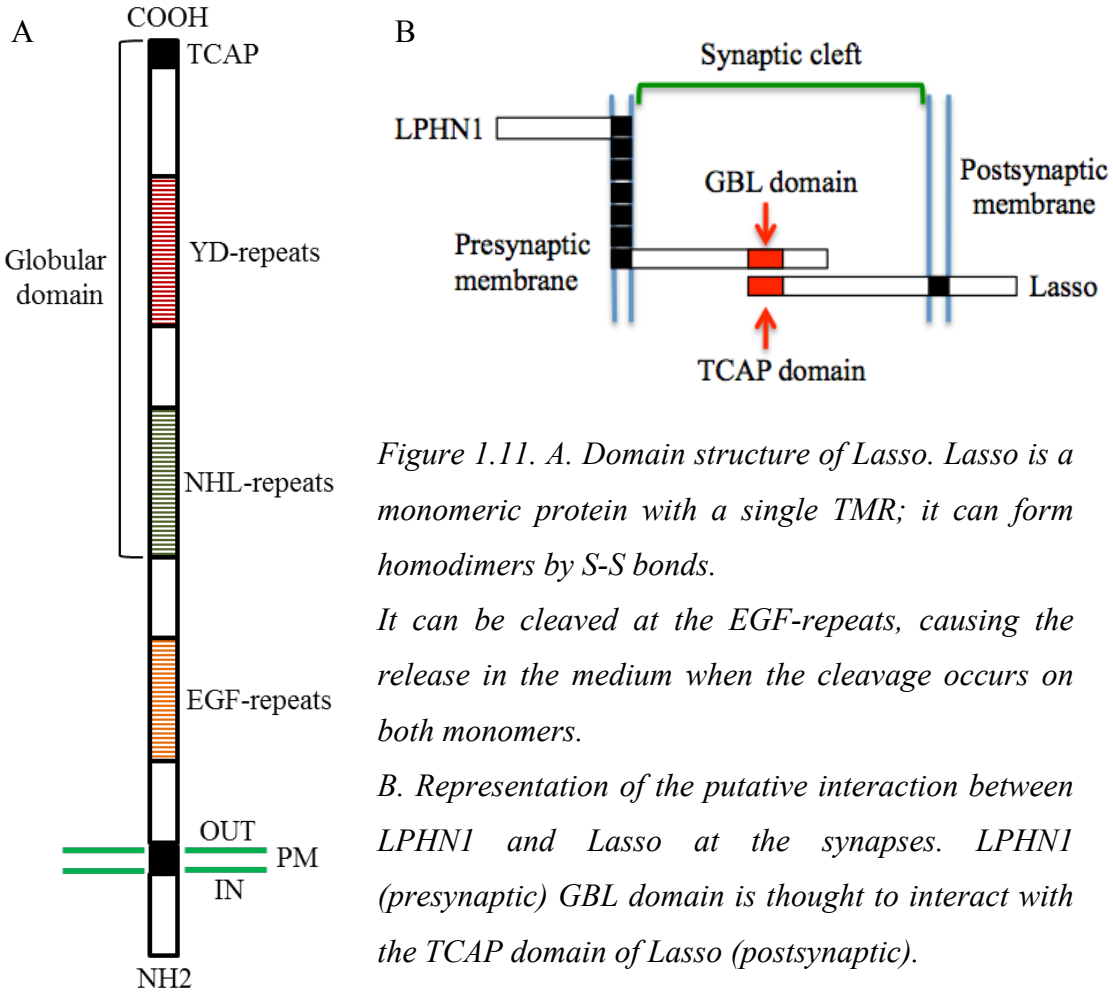

Figure 1.11. A. Domain structure of Lasso. Lasso is a monomeric protein with a single TMR; it can form homodimers by S-S bonds.

It can be cleaved at the EGF-repeats, causing the release in the medium when the cleavage occurs on both monomers.

B. Representation of the putative interaction between LPHN1 and Lasso at the synapses. LPHN1 (presynaptic) GBL domain is thought to interact with the TCAP domain of Lasso (postsynaptic).

More recently latrophilins, in particular LPHN3, has been found to interact with another molecule, fibronectin and leucine-rich transmembrane protein-3 (FLRT3) (O'Sullivan et al. 2012). This protein, whose levels of expression are high especially during the development of the nervous system (Robinson et al. 2004), acts as a repulsive cue in axon guidance and cell migration for neurons expressing the receptor Uncoordinated-5 (UNC-5) during embryonic development (Yamagishi et al. 2011), likely thanks to the ability of LPHN3, FLRT3 and UNC-5 to form trimeric complexes that are also involved in cell adhesion (Lu et al. 2015). In the adult nervous system, it can regulate neurite outgrow after peripherical nerve injury (Robinson et al. 2004).

The interaction between the extracellular domains of LPHN3 and FLRT3, forms a trans-synaptic complex that is able to regulate the number of excitatory synapses both in vitro and in vivo (O'Sullivan et al. 2012). Moreover, the interaction between the olfactomedin domain of LPHN3 and the leucine rich repeat (LRR) domain of FLRT3 contributes to the development of glutamatergic synapses (Ranaivoson et al. 2015).

1.4 Store-operated calcium entry

In response to the activation of GPCRs, Ca^{2+} is released from the stores and goes into cytosol, helping to increase the cytosolic Ca^{2+} concentration which can affect multiple cellular activities, including modulation of exocytosis. In eukaryotic cells, the ER functions as intracellular calcium store.

However, Ca^{2+} in the ER is needed for many cellular functions, such as correct protein folding and vesicle trafficking, and elevated Ca^{2+} concentration in its lumen is vital. In fact, depletion of Ca^{2+} from the ER for prolonged periods of time can lead to stress responses and apoptosis (Parekh and Putney 2005).

A decrease in the ER Ca^{2+} concentration leads to the opening of store operated calcium channels (SOCCs) on the plasma membrane, and it is believed that a major role of these channels is to provide extracellular Ca^{2+} influx for the replenishment of the intracellular Ca^{2+} stores. After replenishment SOCCs close and Ca^{2+} entry stops (Putney 2007). The current underlying store-operated calcium entry (SOCE) is called Ca^{2+} release-activated Ca^{2+} current (I_{CRAC}), with high Ca^{2+} selectivity and low single channel conductance.

1.4.1 Main proteins involved in SOCE

At least two classes of proteins are vital for the SOCE activation: stromal interaction molecules (STIMs) and Orai channels.

STIMs are proteins with a single TMR that are located in the ER membrane and function as sensors of intraluminal ER Ca^{2+} concentration. Two STIM isoforms are expressed in vertebrates, STIM 1 and STIM 2. These two molecules have different tissue distributions, with STIM 1 being ubiquitously expressed and STIM 2 being mostly expressed in neuronal tissues (Stathopulos and Ikura 2013). The major contributor to the activation of SOCE is STIM 1, which reacts to depletion of ER intraluminal Ca^{2+} by changing conformation and translocating to portions of the ER in close proximity with the plasma membrane (PM), the so called ER-PM junctions (Salido, Sage and Rosado 2009).

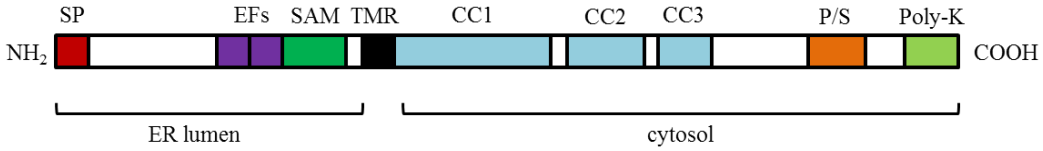

Figure 1.12. STIM 1 domain structure. SP, signal peptide; EFs, Ca^{2+}-binding EF-hand domains; SAM, sterile α motif; TMR, transmembrane region; CC1-3, cytosolic coiled-coil domains; P/S, Pro-Ser-rich region; Poly-K, poly-Lys rich domain

In Figure 1.12 the domain structure of STIM 1 is represented. The most important domains for the function of STIM 1 are the EFs and SAM located in the ER lumen, and the CC1-3 cytosolic domains. At basal ER Ca^{2+} concentration, the EFs domains form a hydrophobic pocket in which the binding of Ca^{2+} occurs. The presence of Ca^{2+} keeps the EFs and the adjacent SAM domains in a stable monomeric conformation. Upon depletion of Ca^{2+}, these domains destabilise and dimerization of EFs and SAM of two STIM 1 molecules is promoted. This leads to conformational changes that have repercussions on the cytosolic CC1-3 regions, and to the redistribution of STIM 1 in the ER-PM junctions, where it activates CRAC channels on the PM (Stathopulos and Ikura 2013).

As mentioned previously, two isoforms of STIM are expressed in vertebrates; it has been proposed that these two molecules have different functions, also dictated by their different affinities for Ca^{2+}: higher for STIM 1, whose equilibrium dissociation constant (K_d) is ≈ 400 μM, and lower for STIM 2, whose K_d is ≈ 700 μM. Thus, whilst STIM 1 gets activated by ER Ca^{2+} store depletion and plays a role in turning the SOCE ON and OFF, STIM 2 is in an activated state also in normal ER Ca^{2+} concentrations, playing a role in maintaining the basal intracellular Ca^{2+} concentration (Smyth et al. 2010; Stathopulos and Ikura 2013).

Orai proteins form the Ca^{2+} selective pore of CRAC channels. Three Orai isoforms are expressed in mammalian cells (Orai 1-3), with similar functions and ability to generate SOCE when co-expressed with STIM 1. However, Orai 1 seems to be the main isoform to mediate SOCE.

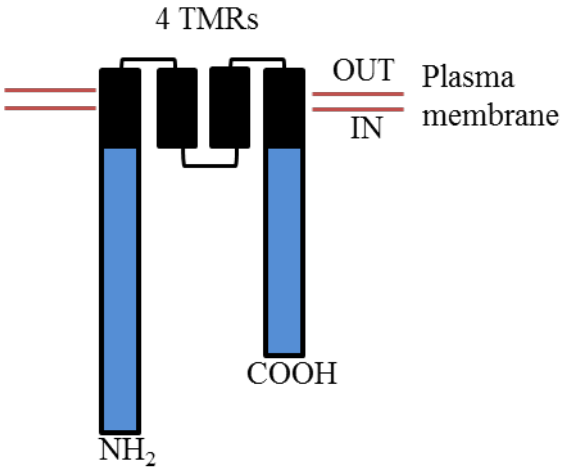

Figure 1.13. Orai 1 structure. The N- and C-terminal domains are both located in the cytosol, the four TMRs (transmembrane domains) are connected by two extracellular and one intracellular loops.

Orai 1 can bind calmodulin (CaM) in a Ca^{2+}-dependent manner in a portion of the N-terminal domain rich in proline and arginine; the interaction with STIM 1, instead, involves a coiled-coil sequence at the C-terminal domain (Berna-Erro, Redondo and Rosado 2012; Prakriya 2013).

Controversial evidence has been found on the involvement of transient receptor potential channels (TRPCs) in SOCE. In fact, to data that suggest an involvement of TRPCs, in particular TRPC 1, in SOCE, are counterposed results suggesting that TRPCs are more likely to function as receptor operated channels (ROCs).

TRPCs are a family of non-selective Ca^{2+} permeable channels. Mammas express seven isoforms of TRPCs, that are widely expressed in all tissues. They have six TMRs with cytoplasmic N- and C-terminal domains. The C-terminal domain contains a TRP signature motif (EWKFAR), whose function is still unclear, and a calmodulin/IP_3R-binding (CIRB) region, involved in the regulation of the channel activation (Salido, Sage and Rosado 2009; Smyth et al. 2010; Berna-Erro, Redondo and Rosado 2012).

1.4.2 Ca^{2+} stores depletion and opening of SOCCs

As mentioned previously, depletion of Ca^{2+} stores located in the ER leads to the activation of SOCCs and consequently the influx of Ca^{2+} ions into the cytosol; this mechanism is essential for the replenishment of the stores.

The mechanisms by which the depletion is communicated from the ER to the PM is complex and involves many proteins such as STIM 1, Orai channels and TRPC 1; however, this mechanism is still not completely understood, and there are suggestions that other proteins, such as SERCA and the microtubule end binding protein (EB 1), and also lipids might play a role in it (Vaca 2010).

STIM1 was previously described as a sensor for the ER Ca^{2+} concentration (Section 1.4.1). However, the role of this protein is much more complex due to its interactions with other proteins. It has been recently shown that STIM1 normally associates with EB 1 travelling continuously through the ER and functioning as a microtubule (MT) tracking protein with a role in ER remodeling (Grigoriev et al. 2008). Only upon upon ER Ca^{2+} depletion STIM1 dissociates form EB 1 and oligomerises at the ER-PM junctions, where first it associates with the SERCA pump (allowing the refilling of the stores in close proximity of the site of Ca^{2+} entry), and then with Orais channels and/or TRPC1, initiating SOCE (Sampieri et al. 2009). TRPC 1 can also work as a ROC in association with IP_3R (Vaca 2010). Once the refilling of the stores is complete, STIM1 dissociates from the SOCCs, then from the SERCA pump, and finally re-associates with EB 1 (Sampieri et al. 2009).

It appears that also lipids are important for SOCE: in fact, evidence suggests that both Orai and TRPC channels have to be localised in lipid rafts in order to exert their function as SOCCs (Pani and Singh 2009). Lipid rafts are sphingolipid and cholesterol-enriched domains on the PM that function as platforms for the grouping of signalling molecules, also allowing their interaction with channels and receptors. It appears that depletion of Ca^{2+} stores triggers the accumulation of SOCCs into lipid rafts, therefore facilitating the protein interactions needed to start the influx of calcium (Pani and Singh 2009).

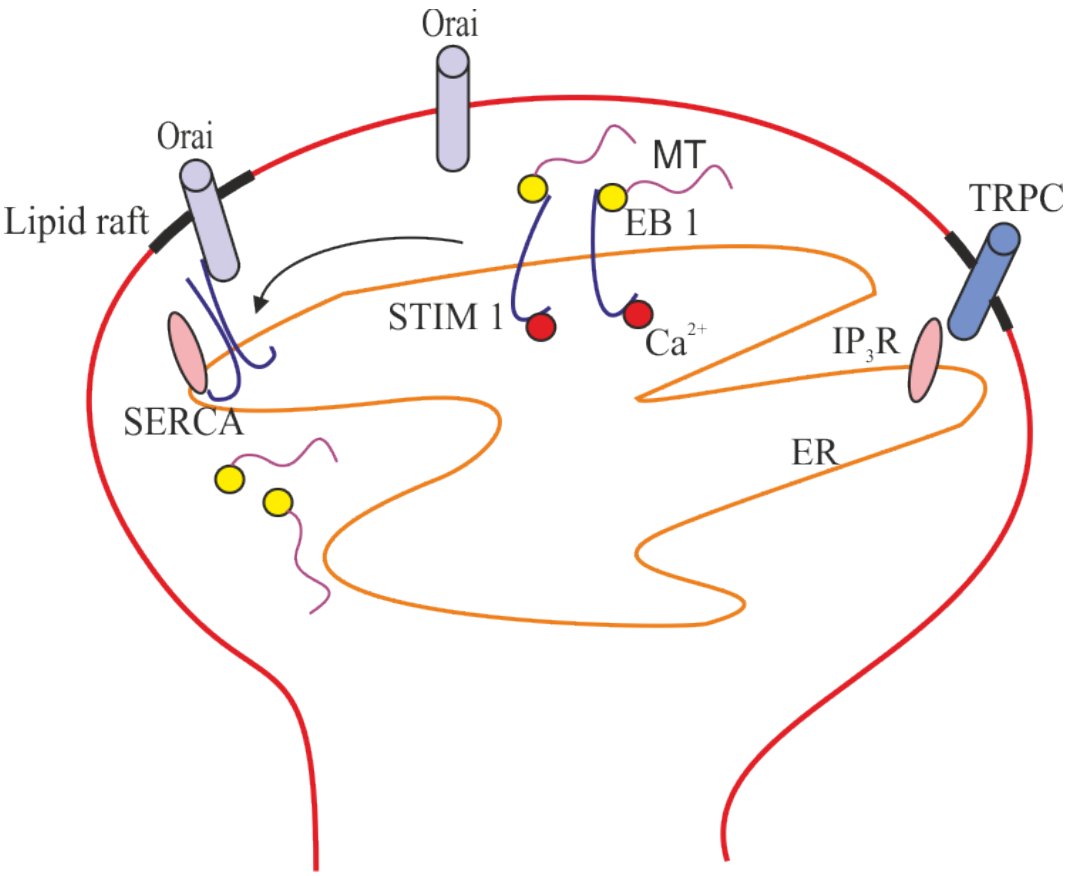

Figure 1.14. Components of SOCE. STIM 1 located at the ER is associated to EB 1 when intraluminal Ca^{2+} concentration is high enough to allow its binding to Ca^{2+}. Upon stores depletion STIM 1, unbound from Ca^{2+}, travels to puncta close to the PM, where associates with SERCA pump and SOCCs initiating Ca^{2+} influx. TRPC can function as a ROC, associated to IP_3R. Activated SOCCs are located in lipid rafts.

Another protein that participates in SOCE as a modulator of Ca^{2+} influx is SARAF. This protein, localised on the ER membrane, shares structure similarities with STIM proteins; it has a single TMR, with a luminal regulatory domain and a cytosolic functional domain. The exact mechanism by which SARAF senses the elevation in ER Ca^{2+} concentration is not clear, however, it is hypothesised that, upon refilling of the stores, it promotes the disaggregation of STIM dimers, therefore, stopping Ca^{2+} influx from Orai/TRPC channels and preventing the over-filling of the stores (Palty et al. 2012).

1.4.3 SOCE in neurons

The involvement of SOCE, and more broadly of Ca^{2+} released by presynaptic intracellular stores, in the modulation of spontaneous exocytosis is not well understood, and a limited number of studies have been carried out about this subject. Various studies from the 90's suggest that spontaneous release, although dependent from the extracellular Ca^{2+} concentration (as previously discussed in Section 1.1.3), is not controlled by VGCCs, as the addition of Cd^{2+} (a non-specific VGCCs blocker) in the presence of tetrodotoxin (TTX) does not change its frequency (for a review see Bouron 2001). The modulation of spontaneous exocytosis by intracellular stores has been first described in cerebellar interneurons and in hippocampal pyramidal neurons (Llano et al. 2000; Emptage, Reid and Fine 2001); here the authors described calcium transients occurring in presynaptic terminals upon stimulations of the stores that were not dependent on VGCCs. These waves of Ca^{2+} influx, that in the basket cells are coupled to bursts of GABA release, are probably mediated by SOCCs, known to be activated in response to the decreased Ca^{2+} concentration in the stores.

The function of the proteins involved in SOCE is not only limited to the refilling of the stores and to the possible regulation of spontaneous exocytosis: STIM 1 and Orai also participate in various signalling pathways (Majewski and Kuznicki 2015).

For example, SOCE is involved in the nuclear factor of activated T cells (NFAT)-dependent gene expression, vital for the nervous system development and function. The NFAT signalling pathways is activated upon Ca^{2+} influx, usually mediated by L-type VGCCs and NMDA receptors. Recently it has been shown that also SOCE regulates the NFAT mediated gene expression; in fact, treatment of neural stem/progenitor cells with thapsigargin (TG) induced a SOCE response and, subsequently, the stimulation of NFAT mediated gene expression, which was affected by SOCE inhibitors 2-APB, SKF96365 and BTP-2 and was completely abolished in mice containing a loss of function mutation to Orai channles (Majewski and Kuznicki 2015).

Another transcription factor regulated by SOCE is Sp4, whose activity is also regulated by Ca^{2+}: hyperpolarisation causes Sp4 polyubiquitinisation and degradation in cerebellar neurons, while depolarisation causes its increase. Treatment with SOCE inhibitors 2-APB and SKF96365 prevented the polyubiquitination and degradation of Sp4 in hyperpolarised cells, and increased its abundance under depolarising conditions (Lalonde, Saia and Gill 2014).

SOCE is also involved in guided axonal growth and regeneration, phenomena that are spatially and temporally regulated by Ca^{2+} signals. For example, TRPC channels are involved in BDNF-mediated growth cone guidance: inhibition of TRPC 3 channels impaired BDNF-induced Ca^{2+} elevation and growth cone turning (Li et al. 2005). Furthermore, growth cones responses to attractive guidance stimuli require the presence of STIM 1 and TRPC 1 (Shim, Zheng and Ming 2013).

There is evidence that STIM 1 suppresses the depolarisation-induced activation of $Ca_v1.2$ (L-type) VGCCs, and alters its surface expression by internalisation, leading to a complete loss of function (Park, Shcheglovitov and Dolmetsch 2010). The authors suggested that STIM 1 inhibits Ca^{2+} entry through $Ca_v1.2$, whilst promoting its entry through Orai channels. Another research group, despite observing the same inactivation of VGCCs by STIM 1, also reported that this effect does not require activation of Orai channels (Wang et al. 2010). What they postulate is that Orai channels enhance the recruitment of STIM 1 near $Ca_v1.2$ VGCCs by trapping STIM 1 in the puncta.

Together, all these results suggest that store depletion has a dual effect: on the one hand it activates SOCE; on the other it inhibits Ca^{2+} influx through -at least- $Ca_v1.2$ VGCCs (Moreno and Vaca 2011).

1.5 Voltage-gated calcium channels

Voltage gated calcium channels (VGCCs) are plasma membrane proteins that mediate Ca^{2+} influx in response to depolarisation of cells. They are widely expressed in many cell types, like neurons, muscle, cardiac and endocrine cells, and they initiate different cell events according to the cell type involved. In neurons, the opening of VGCC after an action potential is the trigger to initiate synaptic transmission (Dunlap, Luebke and Turner 1995).

1.5.1 VGCCs structure

VGCCs, purified for the first time from the skeletal muscle transverse tubules, are composed of four main subunits: α1, β, γ and α2δ.

The α1 subunit is a protein of about 2000 residues organised in four repeated domains (I-IV), each of one is formed of six TMRs (S1-S6) with a membrane-associated loop between the TMRs S5 and S6. It is the pore forming subunit, and its expression alone is sufficient to have functional channels. The S4 segment of each domain functions as the voltage sensor that promotes the channel activation: under the influence of the electric field, it rotates and initiates conformational changes that lead to the opening of the channel pore (Catterall 2000).

The β subunit is an intracellular protein with predicted α helices but no TMRs; the γ subunit is a glycoprotein with four TMRs; the α2δ subunit is a dimer connected to the plasma membrane by a TMR. This subunit, together with the β, helps to enhance the level of expression and to confer appropriate gating properties (Catterall 2011).

Differently from the VGCCs found in skeletal and cardiac muscles, the isolation of neuronal VGCCs revealed that these channels have all the subunits except the γ (Ahlijanian, Westenbroek and Catterall 1990; McEnery et al. 1991).

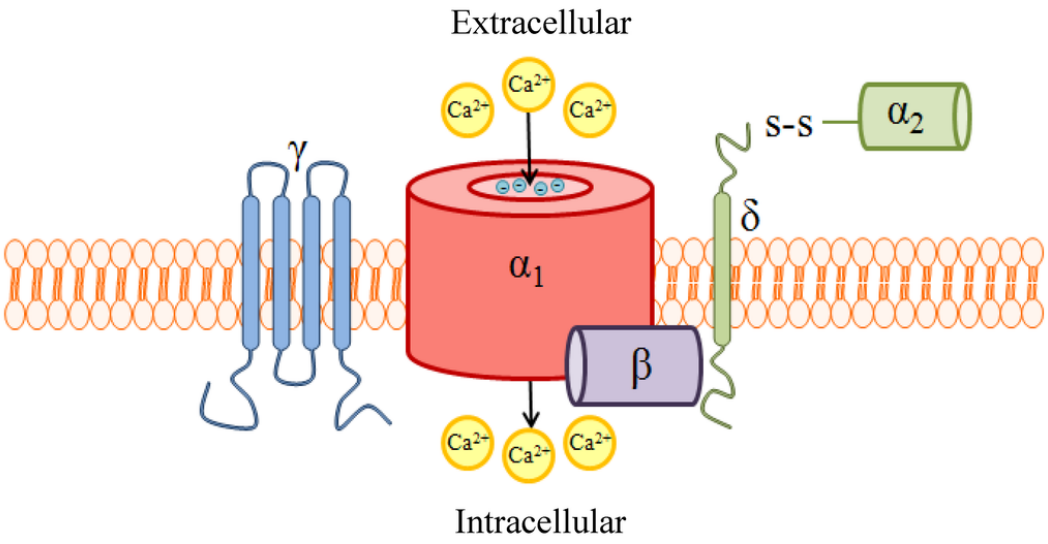

Figure 1.15. VGCCs quaternary structure and subunit composition. VGCCs are formed of a α1 pore forming subunit that determines the characteristics of the current; an intracellular β subunit and an extracellular α2δ subunits that confer appropriate gating properties; a transmembrane γ subunit. Neuronal VGCCs have all the subunit except the γ (Hannon and Atchison 2013).

1.5.2 Classes of VGCCs

Different α1 subunits generate different types of Ca^{2+} current through the channels, with distinctive physiological and pharmacological properties. The subunits can be divided into three families: Ca_v1, Ca_v2 and Ca_v3.

Ca_v1 (1 to 4) family generates L-type currents, so called because they are long lasting when Ba^{2+} is the current carrier; this type of current is activated at high voltages, has low voltage-dependent inactivation, large single channel conductance, and is regulated by cAMP-dependent protein phosphorylation pathways. It can be inhibited by Ca^{2+} antagonist drugs like benzothiazepines and dihydropyridines. This type of current can be found in skeletal and cardiac muscles, endocrine cells, neurons and retina.

Ca_v2 (1 to 3) family generates different types of currents: $Ca_v2.1$ conducts P/Q-type currents, blocked by ω-agatoxin IVA; $Ca_v2.2$ conducts N-type currents,

blocked by ω-conotoxin GVIA; $Ca_v2.3$ conducts R-type currents, blocked by the peptide SNX-482. These three types of currents are mostly found in neurons.

Ca_v3 (1 to 3) family generates T-type currents, so called because of their transient opening; unlike L-type currents, this type activates at more negative membrane potentials, inactivates rapidly, deactivates slowly, and has a small single channel conductance. This type of current can be found in skeletal and cardiac muscles and in neurons (Catterall 2011).

Table 1.1 Classes of VGCCs.

Current type	**Pore-forming subunit**	**Primary localisation**
L	$Ca_v1.1$	Skeletal muscle
L	$Ca_v1.2$	Cardiac muscle, endocrine cells, neurons
L	$Ca_v1.3$	Endocrine cells, neurons
L	$Ca_v1.4$	Retina
P/Q	$Ca_v2.1$	Nerve terminals, dendrites
N	$Ca_v2.2$	Nerve terminals, dendrites
R	$Ca_v2.3$	Nerve terminals, dendrites, cell bodies
T	$Ca_v3.1$	Cardiac and skeletal muscles, neurons
T	$Ca_v3.2$	Cardiac muscle, neurons
T	$Ca_v3.3$	Neurons

1.5.3 $Ca_v2.1$ channels

As mentioned previously, $Ca_v2.1$ subfamily of Ca^{2+} channels conducts P/Q-type currents. These channels are localised presynaptically in the central nervous system, where they are abundant especially in the cerebellum (Purkinje and granule cells), hippocampus, visual cortex, spinal cord and dorsal root ganglia (Mintz, Adams and Bean 1992).

These channels are responsible (along with $Ca_v2.2$ channels) for fast release of neurotransmitters, such as GABA, glutamate and acetylcholine. They interact with synaptotagmin through a specific synaptic protein interaction site located in the intracellular loop connecting the domains II and III, and they can be regulated by G protein-coupled receptors, more specifically by the βγ subunit that shifts the activation of the channels to more positive membrane potentials (Catterall 2011).

Several toxins act on P/Q Ca^{2+} channels, blocking them. Among them, ω-agatoxin IVA and ω-agatoxin IVB from the American funnel web spider *Agelenopsis aperta* specifically block P/Q-type channels; ω-conotoxin MVIIC and ω-conotoxin CVIB from the marine cone snail block P/Q channels, along with N-type channels; ω-grammotoxin from the tarantula spider *Grammostola spatulata* blocks both P/Q and N-type channels; ω-PnTx3-3 from the South American "armed" spider *Phoneutrica nigriventer* blocks P/Q, N and L-type channels (Nimmrich and Gross 2012).

1.6 Aims and objectives

This work aims to give new insight on the regulation of spontaneous exocytosis operated by G protein-coupled receptors, in particular LPHN1, using the mouse neuromuscular junction (NMJ) as a model system.

As extensively discussed previously, LPHN1 is an adhesion G protein coupled receptor whose activation causes a massive increase in spontaneous neurotransmitter release (Capogna et al. 2003; Lelyanova et al. 2009); it has been shown that LPHN1 is functionally associated to $G\alpha_o$ and $G\alpha_q$ (Rahman et al. 1999), and that its stimulation causes activation of PLC and elevation of intracellular IP_3 (Ichtchenko et al. 1998).

With this in mind, we hypothesize that LPHN1 has a role in regulating spontaneous exocytosis most likely by modulating the cytosolic $[Ca^{2+}]$ via the release of Ca^{2+} from intracellular stores and/or the opening of plasma membrane channels. This modulation should already give some effect when LPHN1 is at rest, but would be more prominent upon activation. At that point, we suggest that LPHN1 develops its effects by activating the $G\alpha_q$ protein intracellular pathway, which includes stimulation of PLC, subsequent production of IP_3 and stimulation of IP_3 receptors on the ER. This in turn causes the efflux of Ca^{2+} from intracellular Ca^{2+} stores and, consequently, the opening of store-operated Ca^{2+} channels (SOCCs) on the plasma membrane, whose activation causes a Ca^{2+} influx that further increases the cytosolic $[Ca^{2+}]$ allowing the refilling of the stores.

Therefore, objectives of this work are:

- To investigate the influence of LPHN1 on spontaneous exocytosis by studying LPHN1 KO mice;
- To give evidences in favour of the hypothesis that LPHN1 is the receptor responsible for the elevation in exocytosis upon stimulation by LTX^{N4C};
- To analyse the characteristics of LPHN1-mediated increase in spontaneous exocytosis;
- To delineate the molecular mechanisms underpinning the effects observed upon LPHN1 activation, with particular attention to the $G\alpha_q$ signalling pathway and SOCCs.

CHAPTER 2
MATERIALS AND METHODS

2.1 Materials

All chemicals were from Sigma-Aldrich (Sigma-Aldrich Company Ltd, Dorset, UK) unless otherwise stated.

2.1.1 Bacterial strains

Escherichia coli Rosetta-gami 2^{TM} strain competent cells were purchased from Novagen (Millipore UK Limited, Hertfordshire, UK); *E. coli* DH5α^{TM} strain competent cells were purchased from Invitrogen (Life Technologies Ltd, Paisley, UK).

2.1.2 Bacteria culture media

For bacterial cultures, media were prepared in distilled water and autoclaved at 121°C. 2-XYT medium contained, per litre: 16 g Trypton, 10 g yeast extract and 5 g NaCl (pH 7.5). 1.2-1.5% agar was added to the above medium to prepare agar plates. When needed, chloramphenicol (34 μg/ml), kanamycin (50 μg/ml), tetracycline (25 μg/ml) and/or ampicillin (100 μg/ml) were added. Antibiotics were purchased from Calbiochem (Millipore UK Limited, Hertfordshire, UK). SOC medium contained 0.5% yeast extract, 2% Trypton, 10 mM NaCl, 2.5 mM KCl, 10 mM $MgCl_2$, 10 mM $MgSO_4$, and 20 mM glucose.

2.1.3 DNA plasmids

LTX^{N4C}, Lasso and LPHN-42 plasmids were kindly donated by Vera Lelyanova.

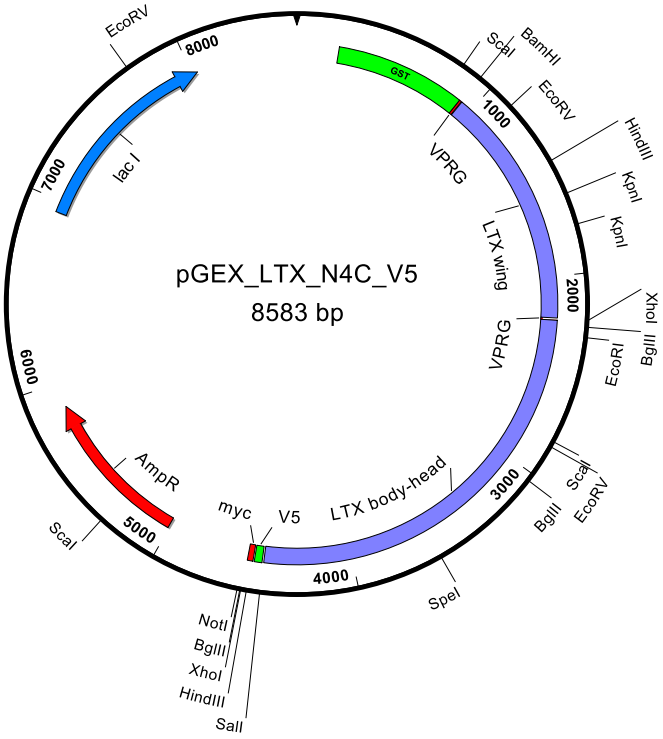

Figure 2.1. Plasmid for expression of recombinant LTX^{N4C}.

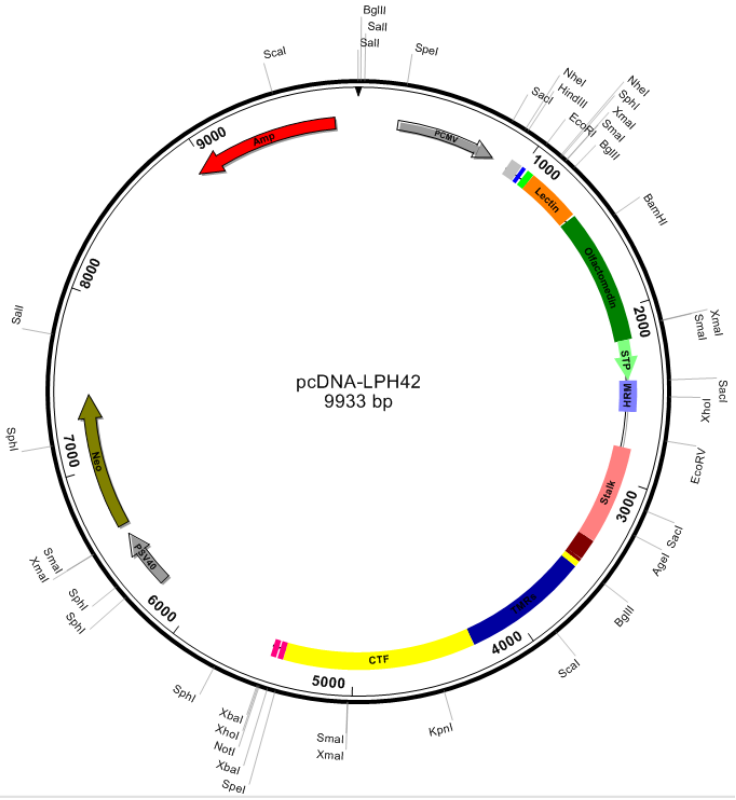

Figure 2.2. Plasmid for expression of LPHN1 on the basis of pcDNA3.1.

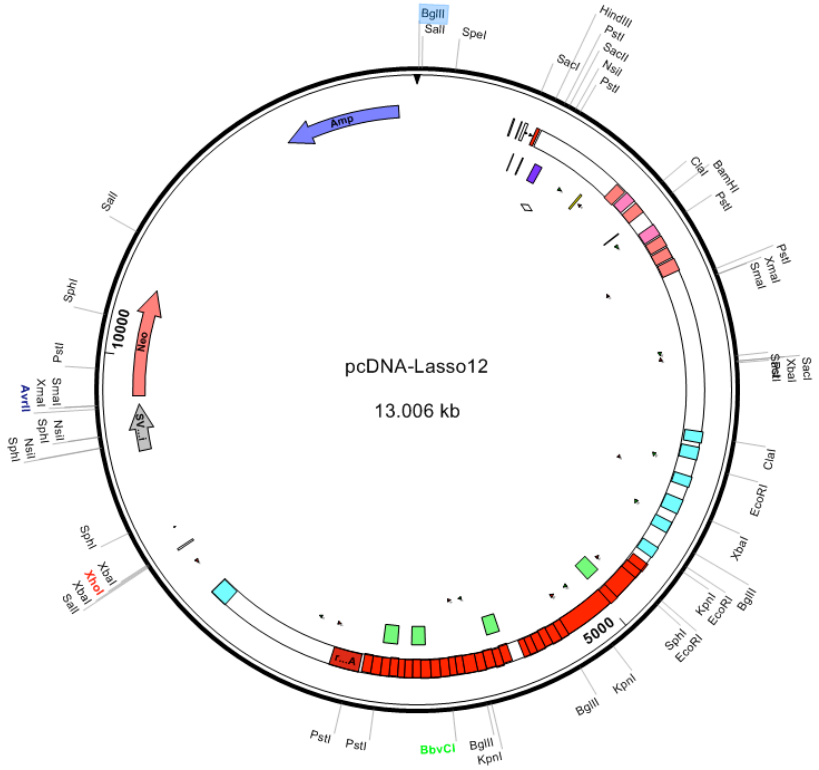

Figure 2.3. Plasmid for expression of GST-Lasso.

2.1.4 Cell lines

Mouse neuroblastoma NB2a cells wild type (WT) and NB2a clones stably expressing LPHN-42 or LPHN-72 were from Professor Yuri Ushkaryov (University of Kent and Greenwich, Chatham Maritime, UK).

2.1.5 Cell culture media

Dulbecco's MEM (supplemented with GlutaMAX^{TM}) and Trypsin-EDTA (0.25%, phenol red) were from Gibco (Life Technologies Ltd, Paisley, UK). Sterile water was from PAA (PAA Cell Culture Company, Cambridge, UK). Fetal bovine serum, Dulbecco's PBS and G418 (200 µg/ml) were used.

2.1.6 Transfection

Lipofectamine 2000 transfection reagent was from Invitrogen (Life Technologies Ltd, Paisley, UK). Superfect^{R} transfection reagent was from Quiagen (QIAGEN Ltd., Manchester, UK).

2.1.7 Mice

1-2 days old C57BL/6J WT and LPHN1 knock out (KO) (AG148) newborn mice were used for hippocampal neurons primary cultures; 21-28 days old C57BL/6J WT and LPHN1 KO mice were used for electrophysiological experiments on neuromuscular junctions (NMJs).
LPHN1 KO mice (AG148) were from Professor Yuri Ushkaryov (University of Kent and Greenwich, Chatham Maritime, UK); other mice were from Charles River (Charles Rivers Laboratories, Margate, UK).

2.1.8 Neuronal culture media

Hibernate A® (HA) and hibernate A® minus calcium (HA – Ca^{2+}) were purchased from BrainBits (BrainBits LLC, Springfield, US); Hank's BSS without Ca^{2+} and Mg^{2+} and sterile water EP grade were from PPA (PPA Cell Culture Company, Cambridge, UK); Neurobasal A®, B27® supplement and GlutaMAX™ were from Gibco (Life Technologies Ltd, Paisley, UK). Papain, laminin and poly-D-lysine were also used.

2.1.9 Whole-cell patch clamp buffers

External solution: 2 mM $CaCl_2$, 3 mM CsCl, 11 mM glucose, 4.8 mM HEPES, 160 mM NaCl. pH was adjusted to 7.2-7.5 with NaOH; glucose was added just before use and the solution was filter sterilised. Internal pipette solution: 150 mM CsCl, 10 mM EGTA, 5 mM HEPES, 10 mM NaCl, 4.5 mM ATP-Mg, 0.1 mM GTP. pH was adjusted to 7.2-7.5 with KOH.

2.1.10 Current clamp buffers

Buffer A (Ca^{2+} buffer): 137 mM NaCl, 5 mM KCl, 2 mM $CaCl_2$, 1 mM $MgCl_2$, 10 mM HEPES, 5.6 mM glucose. Glucose was added just before use and the solution was filter sterilised. Buffer B (Ca^{2+} -free buffer): 137 mM NaCl, 5 mM KCl, 0.2 mM EGTA, 1 mM MgCl2, 10 mM HEPES, 5.6 mM glucose. Glucose was added just before use and the solution was filter sterilised. Variations to the buffers will be stated in the text as appropriate. Sharp electrodes manufactured from borosilicate glass (Harvard Biosciences, Inc., USA) were filled with a 5 M ammonium acetate solution.

2.1.11 Pharmacological agents

1-2-(4-methoxyphenyl)-2-[3-(4-methoxyphenil)propoxyethyl-1H-imidazole (SKF96365), 2-Aminoethyl diphenylborinate (2APB), BAPTA-AM, cadmium, gadolinium, nimodipine, prefluooctanoic acid (PFOA), ryanodine, tetrodotoxin, thapsigargin (TG), U73122 and U73343 were used. UBO-QIC was from the Institute of Pharmaceutical Biology, University of Bonn, Germany. ω-Agatoxin IVA, ω-conotoxin GVIA and ω-conotoxin MVIIC were from Alomone (Alomone Labs, Jerusalem, Israel).

2.1.12 SDS-PAGE

Sodium dodecyl sulphate polyacrylamide gel electrophoresis (SDS-PAGE) running buffer was prepared as a 10X (250 mM Tris, 2.5 M glycine, 10% SDS) and diluted to 1X when needed. 6X sample buffer was prepared with 0.375 M Tris (pH 6.8), 12% SDS, 60% glycerol, 0.6 M DTT and 0.06% bromophenol blue. 1X sample buffer was prepared with: 0.0625M Tris (pH 6.8), 2% SDS, 10% glycerol, 0.1M DTT, 0.01% bromophenol blue. Coomassie Blue R dye contained 0.1 % Coomassie Brilliant Blue R-250, 50% methanol and 10 % glacial acetic acid.

2.1.13 Western blotting

Western blot transfer buffer, containing 25 mM Tris, 192 mM Glycine, 10% methanol, was cooled to 4°C before use and used several times before discarding.

2.1.14 Immunofluorescence

Antibodies used in immunofluorescence experiments are shown in Table 2.1. TBS-T buffer contained 137 mM NaCl, 2.7 mM KCl, 19 mM Tris, 0.1% triton-X. Blocking buffer contained TBS-T supplemented with 1% BSA.

Table 2.1. Antibodies used for immunofluorescence experiments

Antibody	**Species**	**Concentration**	**Manufacturer**
Anti GST	mouse	1:1000	Abcam
Anti GST	rabbit	1:1000	Abcam
Anti V5	mouse	1:1000	AbdSerotec
Anti LTX	rabbit	1:2000	Obtained by immunisation of rabbits
Anti LPHN1	rabbit	1:500	Obtained by immunisation of rabbits
Anti mouse 680 nm	donkey	1:1000	Li-Cor
Anti mouse 800 nm	donkey	1:1000	Li-Cor
Anti rabbit 680 nm	donkey	1:1000	Li-Cor
Anti rabbit 800 nm	donkey	1:1000	Li-Cor
Anti rabbit-HRP conj.	goat	1:5000	Santa Cruz Biotecnology

2.1.15 Other materials

Phosphate buffer saline (PBS) buffer contained 137 mM NaCl, 2.7 mM KCl, 10 mM Na2HPO4, 1.8 mM KH2PO4. pH was adjusted to 7.4 using HCl. TE was prepared with 10 mM Tris-HCl and 1 mM EDTA (pH 8), and autoclaved at 121°C. Glutathione-S-transferase (GST)-bind™ kit for column affinity chromatography was purchased from Novagen (Millipore UK Limited, Hertfordshire, UK).

2.2 Methods

2.2.1 Transformation of competent bacteria

The heat shock method was used for transformation. Different amounts of DNA (from 1 to 10 ng) were added to 20 µl of cells, briefly mixed, and incubated for 30 min on ice. Cells were then heated at 42°C in a water bath for 30 s, and re-placed on ice for 2 minutes. Subsequently, 80 µl of SOC medium was added to each tube, and the mixture was incubated for 1 h at 37°C, with shacking. 50 µl of the transformed cells were then plated on 2XYT-agar plates supplemented with 100 µg/µl ampicillin, 34 µg/µl chloramphenicol, 25 µg/µl tetracycline (*E. coli* Rosetta-gami 2^{TM}) or with 100 µg/µl ampicillin (*E coli* DH5α^{TM}) and incubated overnight at 37°C, with vigorous shaking.

2.2.2 Protein expression and extraction

A single colony of bacteria was selected and cultured in 2 ml 2XYT containing 100 µg/µl ampicillin, 34 µg/µl chloramphenicol, and 25 µg/µl tetracycline overnight shacking at 37°C. The next day the culture was diluted 1:50 with the fresh medium and left growing until the desired optical density was reached (0.25 – 1). The culture was induced with 50 mM Isopropyl β-D-1-thiogalactopyranoside (IPTG) and expression was carried out for 16 – 20 h at room temperature (RT).
The culture was then centrifuged at 4°C at 5000 x g for 10 min. The pellet was then resuspended in 50 µl of ice cold PBS and sonicated 3 times for 30 s. The mixture was centrifuged again under the same conditions and the supernatant containing the soluble protein was collected. The pellet containing the insoluble protein was resuspended in PBS.

2.2.3 Affinity chromatography

The 10X GST bind/wash buffer provided in the kit (Novagen) was diluted to 1X with water. 10X elution buffer containing 100 mM reduced glutathione was prepared and aliquots were kept at -20°C. When needed, the elution buffer was diluted to 1X with dH2O. The column was prepared with 1.5 ml of GST bind resin consisting of an agarose matrix with attached reduced glutathione (GSH).
Protease inhibitor cocktail for bacterial cells (Sigma-Aldrich) was added to the supernatant from the protein extraction procedure. The supernatant was then loaded into the column and incubated for 1 h, at 4°C, with end-over-end rotation.
The extract was then passed through a plastic column supplied with a porous polythene filter, and fractions of the flow through were collected and stored for analysis. The column was then washed with 10 column volumes of GST wash buffer, and samples were taken for analysis. The bound protein was then eluted with 3 volumes of GST elution buffer, and the elution fractions were collected.

2.2.4 LTX binding experiment

Different concentrations of LTX were used (2 – 50 nM) in order to identify the best condition for binding. Cells expressing LPHN-42 or LPHN-71 were incubated with the toxin for 20 min in an Eppendorf tube. They were then centrifuged at 9000 rpm for 2 min at RT and the supernatant containing the unbound toxin was collected. Cells were then washed with PBS briefly (with a 10-s centrifugation of individual tubes) and the supernatant was removed. After lysis for protein extraction (see Section 2.2.7), cells were centrifuged at 9000 rpm for 10 min, at 4°C.

2.2.5 Cell culture

Cell cultures were performed under sterile conditions in a laminar air flow cabinet. Neuroblastoma NB2a cells WT were grown in DMEM medium containing GlutaMAX supplemented with 10% FBS. The same medium was used for NB2a cells stably transfected with LPHN-42 or LPHN-71 with the addition of G418 for selection of the cells containing the LPHN1 plasmids. Cells were plated in T75 flasks and grown at 37°C, 5% CO_2.

Passaging of the cells was performed after a confluence of 80-90 % was reached (normally, 2-3 times a week); for this, cells were washed with PBS, detached from the flask using Trypsin-EDTA for 1 min, and diluted with fresh complete DMEM at a ratio from 1:6 to 1:12 for further plating.

2.2.6 Transient transfection

The day before transfection, cells were counted using a haemocytometer and plated in 35-60 mm dishes (depending on the experiment) so that they would be 80-90% confluent at the time of transfection.

For transfection using Lipofectamine® 2000, the Lipofectamine® complex was prepared using serum-free medium, incubated at RT for 5 min, and then added to the DNA mixed with serum-free medium (4 μg DNA for transfections using a 35 mm dish, 8 μg DNA for transfections using a 60 mm dish). After a further incubation of 20 min at RT the DNA-Lipofectamine complex was added to the cells and then incubated under usual conditions for 24-48 hours.

For transfection using Superfect®: DNA and Superfect were diluted in serum-free medium and incubated for 5-10 minutes at RT to allow complex formation. The complex was then further diluted with serum-free medium, and transferred onto the cells after the growth medium in the plates was removed. After a 3-h incubation at 37°C, the transfection complex was removed from the plates and replaced with complete DMEM. The cells were then incubated under usual conditions for 24-48 hours.

2.2.7 Protein extraction

Plates with transfected cells were placed on ice, cells were washed with PBS containing 5 mM EDTA (to loosen cell attachment), scraped off the plates and transferred into 15 ml centrifuge tubes. Cells were then counted using a haemocytometer, centrifuged at 800 x g for 5 minutes at 4°C and diluted in PBS containing 1% Triton X-100 to a concentration of > 600,000 cells/100 µl. Cells were incubated on ice for 20 min, centrifuged, and the supernatant containing the solubilised proteins was collected.

2.2.8 Chloroform/methanol precipitation

One volume of methanol was added to the supernatant obtained from protein extraction and mixed well; 1 volume of chloroform was then added and mixed. The mixture was centrifuged at 10,000 rpm for 10 min, at RT. The supernatant was removed and discarded, the pellet containing proteins was left to air-dry for approximately 5 min and then resuspended in 1X SDS-PAGE loading buffer.

2.2.9 SDS-PAGE

SDS-PAGE was carried out using a Bio-Rad apparatus. The concentration of the resolving gels was chosen according to the protein size, from 6 to 10%. The mixture (water, 30% polyacrylamide-Bis, Tris-HCl, pH 8.8, 10% SDS, 10% APS, TEMED) was poured into gel plates, overlaid with water and let polymerise overnight at 4°C. The 5% stacking gel mixture (dH2O, 30% polyacrylamide-Bis, Tris-HCl, pH 6.8, 10% SDS, 10% APS, TEMED) was poured on top of the resolving gel and let polymerise with a 10 or 15-wells comb. After polymerisation, the comb was removed and the wells washed with 1X SDS-PAGE running buffer.

After addition of the sample buffer, samples were either boiled for 3 minutes at 100°C or heated for 20 minutes at 50°C for samples containing LPHN1, briefly centrifuged and loaded into the wells.

The gel was then placed into the gel tank filled with 1X running buffer; electrophoresis was carried out at a constant voltage of 120 V for ~ 90 minutes. The gel was then stained with Coomassie Blue R dye or used for western blot transfer.

2.2.10 Western blotting

After SDS gel electrophoresis, the proteins were transferred onto a polyvinylidene fluoride (PVDF) membrane at a constant current of 180 mA for 70 min using the wet method. The transfer tank (Sigma) was filled with 1X transfer buffer cooled down to 4°C using a water-circulating cooling incubator, with continuous stirring. Blotting paper and PVDF membrane were cut to fit the transfer cassette; the PVDF membrane was activated in methanol and pre-equilibrated with 1X transfer buffer.

The cassette was assembled as follows: 1X sponge, 1X blotting paper, PVDF membrane, gel, 1X blotting paper, 1X sponge. Air bubbles were removed by carefully rolling a pipette over the surface.

The blot cassette was placed in the transfer tank so that the gel was on the negative pole side, and the PDVF membrane was on the positive pole side.

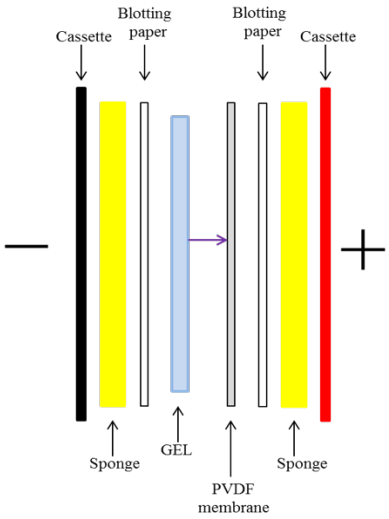

Figure 2.4. Western blot transfer cassette assembly.

2.2.11 Immunostaining

After the transfer was complete, the PVDF membrane was placed into a 50 ml centrifuge tube containing ~4 ml of blocking buffer and incubated on a rotator overnight.

The following day, the blocking buffer was replaced with blocking buffer containing the primary antibody. After an incubation of 1 h, the membrane was washed (3 times for 5 min) with TBS-T, and then incubated with blocking buffer containing the secondary antibody for 1 hour. The membrane was then washed (3 times for 5 min) and the blot was visualised using the Odyssey detection system.

2.2.12 Neuronal cell cultures

Hippocampi from 1-2 days old mice were dissected under a binocular microscope in aseptic conditions, placed into vials with HAB buffer (Hibernate A, 2% B27, 0.5 mM GlutaMAX) and kept at 4°C until plating (no more than 10 days after dissection).

Working under a sterile cell culture hood, cells were placed in dissociation buffer (HA – Ca^{2+} containing 2 mg/ml papain) and incubated 10 min at 37°C. The dissociation buffer was then removed and replaced with HAB buffer. The tissue was triturated using a silanised Pasteur pipette. The undispersed pieces were let to settle for 1 min, the supernatant containing the dispersed cells was transferred into a 15 ml tube and centrifuged at 700 rpm for 2 min. The pellet was resuspended in Neurobasal A medium supplemented with 2% B27 and 0.5 mM GlutaMAX, and the cells were plated on coverslips coated with 50 µg/ml poly-D-lysine and 10 µg/ml laminin in a 24 wells plate (10,000 cells/well).

Neurons were kept in an incubator at 37°C, 5% CO_2 and half of the medium was changed every 3-4 days. The cultures were left growing for 14 – 21 days until used for electrophysiological recordings.

2.2.13 Recordings of spontaneous postsynaptic currents in hippocampal neurons

Experiments on central synapses were carried out on primary cultures of hippocampal pyramidal neurons, 21 days after plating.

Coverslips with neurons were transferred into a perfusion chamber (Harvard Biosciences, Inc.) mounted on top of an inverted microscope and perfused at RT with external solution (see Section 2.1.9) at a flow rate of 1 ml/min. Borosilicate glass pipettes were pulled using a Flaming-Brown-type pipette puller (P97, Sutter, USA) to show a resistance of 3 – 7 MΩ, filled with the internal solution (see Section 2.1.9), and manipulated using a PatchStar motorised micromanipulator (Scientifica).

The cells were observed on a computer screen using a C-mount colour video camera attached to the trinocular microscope head. The cell chosen for the patch was approached to obtain a cell-attached GΩ seal (resistance of the pipette of at least 1 GΩ). The recorded neurons were voltage-clamped at -70 mV, and a short suction was applied by mouth to break through the membrane to accomplish the whole cell patch.

Excitatory postsynaptic currents (EPSC) and inhibitory postsynaptic currents (IPSC) were amplified (10 mV/pA), filtered (2.9 kHz), and digitised (5 kHz) using the recording equipment which consisted of a patch-clamp amplifier (Model 2400, A-M Systems, Inc., USA), a two-channel 8-pole Bessel high-frequency filter/amplifier (LPF202A , Warner Instruments), a HumBug harmonic frequency quencher (Quest Scientific), and Digidata 1322A digital transformer (Axon Instruments). The data were acquired using pClamp software (Axon Instruments) and analysed with MiniAnalysis 6.0 software (Synaptosoft).

2.2.14 Recordings of spontaneous postsynaptic potentials at the NMJs

Experiments on NMJ were carried out on preparations of *flexor digitorum brevis* from the mouse hind paws (21-28 days old male mice, C57BL/6J). The mice were euthanized by cervical dislocation. The hind paws were removed and pinned to petri dishes coated with Silgard silicone polymer filled with Ca^{2+}-containing buffer (see Section 2.1.10) using entomological pins; the muscle was removed and cleaned from the connective tissue under a dissection microscope. The preparations were then moved to the recording rig and observed using a C-mount video camera attached to a binocular microscope (SMZ-645, Nikon, Japan) and dark-field illumination. Presynaptic activity was evaluated by postsynaptic registration of miniature end plate potentials (MEPPs) using a sharp electrode (tip diameter < 0.5 μm, resistance 30 – 40 MΩ) prepared using a Sutter pipette puller (P97) and filled with a solution containing 5 M ammonium acetate. Electrodes were inserted into the muscle fibres using a PatchStar motorised micromanipulator (Scientifica) and the membrane potentials were recorded in the current clamp mode using Axoclamp 2B pre-amplifier (Axon Instruments), LPF202A amplifier with high frequency filter (Warner Instruments), Hum Bug harmonic frequency quencher (Quest Scientific), and Digidata 1322A digital transformer (Axon Instruments).

Resting membrane potentials of recorded cells varied from -70 to -20 mV; only cells with membrane potentials between – 70 and -40 mV were considered for analysis.

Preparations were bathed at room temperature in a static buffer containing 137 mM NaCl, 5 mM KCl, 2 mM $CaCl_2$, 1 mM $MgCl_2$, 10 mM HEPES and 5.6 mM glucose, unless specified otherwise.

Membrane potentials were acquired using Axoscope 10.2 software (Axon Instruments), the recorded traces were adjusted to baseline using Clampfit (pCLAMP 10 software) and analysed using MiniAnalysis 6.0 software (Synaptosoft). Frequency histograms of MEPPs were created in MiniAnalysis plotting the number of events per second.

To test the effects of different pharmacological agents on the LTX^{N4C}-induced increase in miniature end-plate potentials (MEPPs) the specified drugs were added to the NMJ preparations bathed in Ca^{2+} buffer (unless specified otherwise) for 15 – 20 min prior to the addition of the toxin: PFOA (0.2, 1, 10, 50 and 100 μM), TTX (1 μM), UBO-QIC (1 μM), U73122 (10 μM), U73343 (10 μM), Gd^{3+} (1 mM), nimodipine (10 μM), ω-Con MVIIC (1 μM), ω-Con GVIA (50 nM), ω-Aga IVA (200 nM). Recordings of MEPPs were taken immediately, after 10 min and just before the addition of LTX^{N4C} to evaluate possible changes in the basal frequency. BAPTA-AM was incubated for 40 min in Ca^{2+} -free buffer before the the toxin was added. Afetr the addition of 0.25 nM LTX^{N4C} the recordings continued for an average of 60 min. If the effect of LTX^{N4C} did not develop at the expected time (20 min after addition) the recordings continued for up to 90 min. In other experiments, drugs (100 μM PFOA, 1 μM UBO-QIC, 10 μM U73122, 10 μM U73343, 50 μM 2APB, 100 μM ryanodine, 50 μM SKF96365, 100 μM YM58483, 10 μM TG, 10 μM nimodipine, 1 μ ω-Con MVIIC) were added 30 min after LTX^{N4C} addition, i.e. when the toxin's effect was already developed and recordings of increased activity from several cells were made.

To test depolarisation-induced release, 20 mM KCl were used in containing a buffer containing 122 Mm NaCl, 0.2 mM EGTA, 1 mM $MgCl_2$, 10 mM HEPES, 5.6 mM Glucose, with or without 2 mM $CaCl_2$. In the presence of 100 μM PFOA, the concentration of KCl used was 40 mM.

2.2.15 Data analysis

To ensure the presence of internal and external independent controls, recordings were collected from several fibres of the same preparation (n = 5 – 15) as well as from different paws (N = 2 – 3) for each experimental condition.

The data were collected using MiniAnalysis 6.0 software (Synaptosoft) and validated using One-way ANOVA or non-parametric tests (Mann-Whitney U test) with significance set at $P < 0.05$ using GraphPad Prism 6.0. Graphs were created using GraphPad Prism 6.0; figures represent mean ± SEM unless otherwise specified.

CHAPTER 3
RESULTS I. Expression of LTX^{N4C} in a bacterial system

3.1 Introduction

The expression of active αLTX and LTX^{N4C} is necessary in order to study the toxin-evocked effects due to the binding to LPHN1. Different methods have already been used to express LTX, using both baculovirus (Kiyatkin et al. 1995; Volynski et al. 1999) and bacterial (Dulubova et al. 1996) systems. However, both of these systems have been proven to be inadequate for the purpose. The baculovirus vectors used by Kiyatkin and collaborators (1995) proved to produce mostly insoluble and inactive αLTX; this problem was overcame by Volynski et al. (1999), who successfully optimised a method to express functional αLTX. However, several factors such the high cost of the reagents needed, the long time needed for expression, the difficulty of the procedure and the low yield make this procedure not ideal.

Bacterial expression, which partially overcomes the limitations mentioned above for the baculovirus system, has also been used to produce active αLTX (Dulubova et al. 1996); although being cheap, fast and easy, this system did not solve the low yield problem, and the toxin produced was mostly insoluble due to incorrect protein folding.

Here, I attempted to optimise a method for bacterial expression of LTX^{N4C} in order to overcome the problems encountered before.

Expression of recombinant proteins using bacterial cells as a host is a widely used strategy due to its simplicity and speed, and the high yield of protein expressed.

Different methods are available for bacterial transformation. In the present work, the method chosen was the heat shock, where bacterial cells are first incubated with the plasmid DNA at low temperature in the presence of divalent cation (Ca^{2+}); this is followed by a sudden increase in temperature that causes the incorporation of the DNA plasmid into the bacterial cells.

Despite the simplicity of the procedure and the high yield achieved with bacterial expression, problems can arise when expressing eukaryotic proteins in prokaryotic hosts, because (1) bacteria do not use some of the codons necessary for the translation of eukaryotic proteins and therefore lack the corresponding tRNAs; (2) bacteria lack the exocytotic secretory system and protein translation in bacteria occurs inside the cytosol, where the reductive environment and the lack of appropriate chaperones can prevent the proper post-translational modifications and folding of eukaryotic proteins; (3) in bacteria proteins destined for secretion are transported across the membrane by protein transport systems, which often fail to recognise eukaryotic proteins; (4) even if foreign proteins are transported through the inner membrane of the Gram negative bacteria, they may not readily escape from the bacterial periplasm and into the medium due to the relatively small size of the outer membrane pores.

Different strategies can help overcome these problems and therefore improve the expression of the target protein (Khow and Suntrarachun 2012):

- Modification of the bacteria strain so that the target protein finds a proper environment for its correct assembly;
- Modification of the growth media, such as supplement of cofactors to help the correct protein folding;
- Modification of the temperature in which the expression takes place, to slow down protein synthesis and therefore decrease protein aggregation and formation of inclusion bodies;
- Co-expression of molecular chaperons to guide the folding of the recombinant protein in the appropriate way.

In the present work I overcame some of these issues (codon preference and reducive cytosolic environment) by using a particular strain of *E. coli*, Rosetta-Gami 2, which combines the features of Rosetta and Origami strains. The Rosetta strain facilitates the expression of eukaryotic proteins because it contains the pRARE plasmid that supplies tRNAs for codons rarely used in *E. coli* (AUA, AGG, AGA, CUA, CCC and GGA). The Origami 2 strain contains mutations in the thioredoxin reductase (*trxB*) and glutathione reductase (*gor*) genes, which

creates an oxidative environment and thus enhances disulphide bond formation in the cytoplasm, leading to the expression of correctly folded and active proteins.

LTX^{N4C} cDNA was previously subcloned in our laboratory into a GST-fusion system. The gene of interest was inserted into a pGEX vector in-frame with the GST sequence, which therefore becomes fused to the protein of interest at the N-terminal. Expressing a recombinant protein as a GST-fusion protein gives some advantages: after translation, the GST protein rapidly folds into a stable and soluble protein; GST can be therefore used to guide the correct folding of the protein of interest, enhancing its expression and solubility. Furthermore, GST allows a simple and quick purification of the fusion protein by affinity chromatography using immobilised glutathione.

The expression in the pGEX vector is controlled by a *tac* promoter, which can be induced by the lactose analogue isopropyl b-D thiogalactoside (IPTG); to control the expression of the insert more strictly, the vector also contains a *lacI*^{q} repressor that binds to the operator region of the *taq* promoter and prevents the expression until IPTG is added.

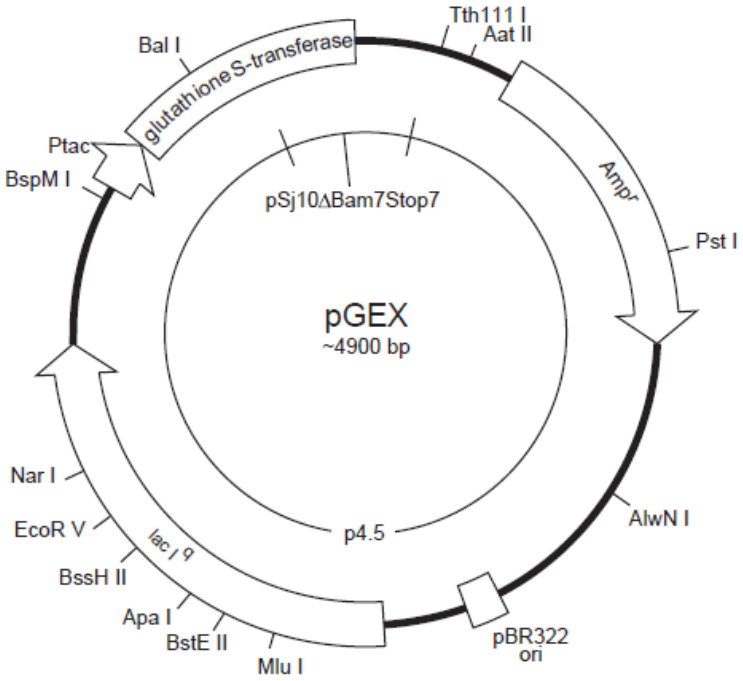

Figure 3.1. Map of the pGEX GST-fusion vector

3.2 Results

3.2.1 Plasmid purification

The plasmid encoding GST-LTX^{N4C} fusion protein had been previously prepared in our lab.

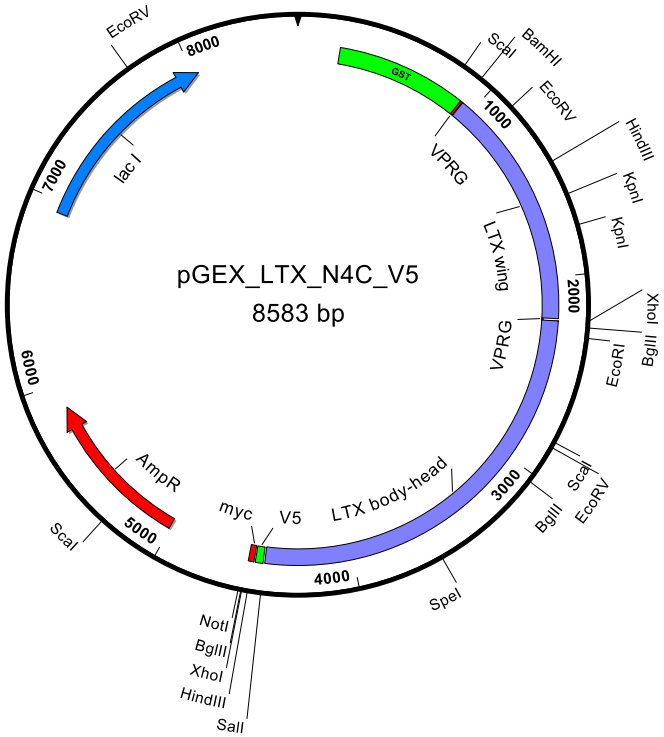

Figure 3.2. Map of the GST-LTX^{N4C} plasmid used for bacterial expression. The toxin cDNA carried additional modifications: GST is attached at the N-terminal and V5 and Myc epitopes are attached at the C-terminal. These modifications allow the recognition of both the N- and C-termini of the recombinant fusion protein in order to identify and isolate the full size protein.

The GST-LTX^{N4C} plasmid was transformed into Rosetta-Gami 2 cells and the culture was grown in the presence of ampicillin, chloramphenicol, kanamycin and tetracyclin in order to maintain the pGEX_LTX^{N4C}_V5-myc and the pRARE plasmids.

To verify that the plasmid retained its structure and did not undergo any recombination in this bacterial strain, the plasmid was then isolated and analysed by restriction mapping and Agarose-gel electrophoresis (Figure 3.3).

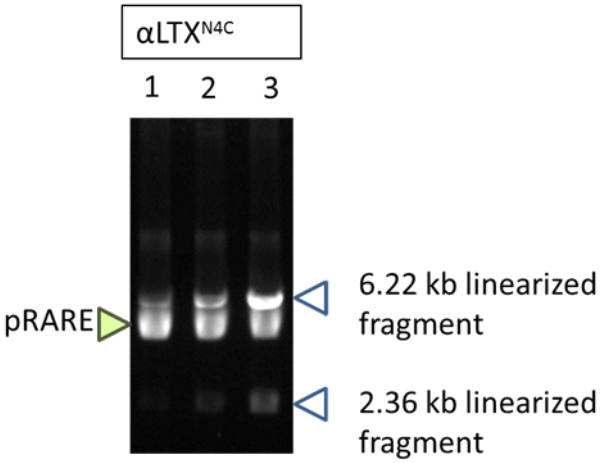

Figure 3.3. Restriction analysis of α-LTX^{N4C}. Plasmid containing the GST-LTX^{N4C} cDNA insert was cleaved with Xho I restriction enzyme. The reactions were analysed on a 1 % agarose gel at a constant voltage of 120V for 1 hour to yield the expected fragments. Lanes 1-3 contain plasmid preparations from three test cultures. Blue arrows indicate the position of the 6.22 kb and 2.36 kilobase-pair (Kbp) fragments as determined using the DNA size markers. The green arrow represents the position of the pRARE plasmid endogenously present in the Rosetta-Gami 2 cells.

The plasmid isolated from the Rosetta-Gami-2 cells appeared to be cleaved into two fragments (6.22 kb and 2.36 Kbp), as expected from the map. However, the presence of the pRARE plasmid not only made it difficult to purify sufficient amounts of the pGEX_LTX^{N4C}_V5-myc plasmid, but also precluded its detailed restriction mapping. Therefore, the plasmid DNA isolated from the Rosetta-Gami-2 cells (and containing both plasmids) was re-transformed into XL-1 Blue bacterial cells for further analysis, amplified in the presence of ampicillin, but in the absence of chloramphenicol, kanamycin and tetracycline that are required for the survival of cells containing the pRARE plasmid. The plasmid DNA isolated

from the recipient strain was then isolated and analysed by cleavage with restriction nucleases Xho I and Pst I, and their combination. As demonstrated by Figure 3.4, only the target plasmid was amplified in the recipient strain, and its restriction fragments fully corresponded to the theoretical map, indicating that the Rosetta-Gami cells did not alter the structure of pGEX_LTX^{N4C}_V5-myc. Thus, it could be used for expression of GST-LTX^{N4C}.

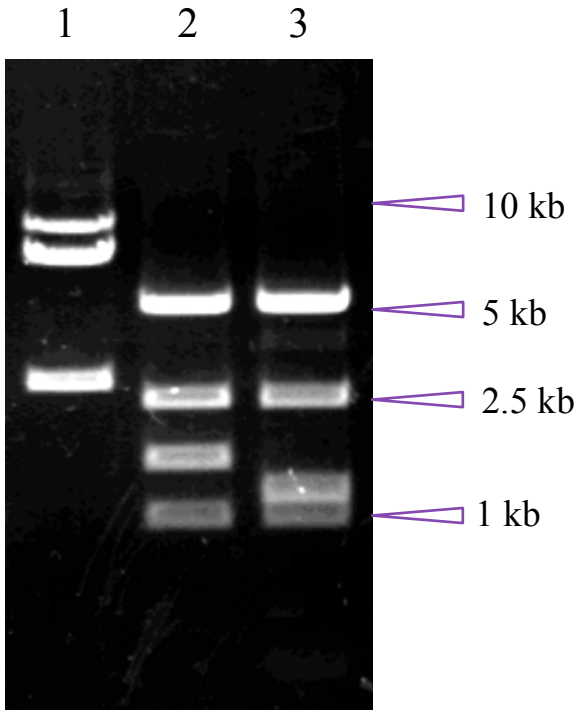

Figure 3.4. Restriction analysis of α-LTX^{N4C}. Individual plasmid containing GST-LTX^{N4C} cDNA insert were cleaved Xho I (lane 1), Pst I (lane 2) and the combination of Xho I and Pst I (lane 3) restriction enzymes. The reactions were analysed on a 1 % agarose gel at a constant voltage of 120V for 1 hour to yield the expected fragments. The restriction fragments corresponds to the theoretical map.

3.2.2 GST-LTX^{N4C} expression

Several conditions were tested in order to optimise the expression of LTX^{N4C} in the bacterial strain chosen. Because induction at different optical densities (OD) leads to different yields of expression (generally with the yield decreasing at increasing ODs), the cutures were grown up to different ODs (0.25, 0.50, 0.70 and 1) to determine the optimal point of induction. After induction, the cultures were left expressing the protein at RT in order to slow both bacterial growth and protein expression; other cultures where treated in the same way but without induction by IPTG. Leaky expression was also optimised by growing bacteria at 37°C for 16 h or at RT fr 20 h without induction.

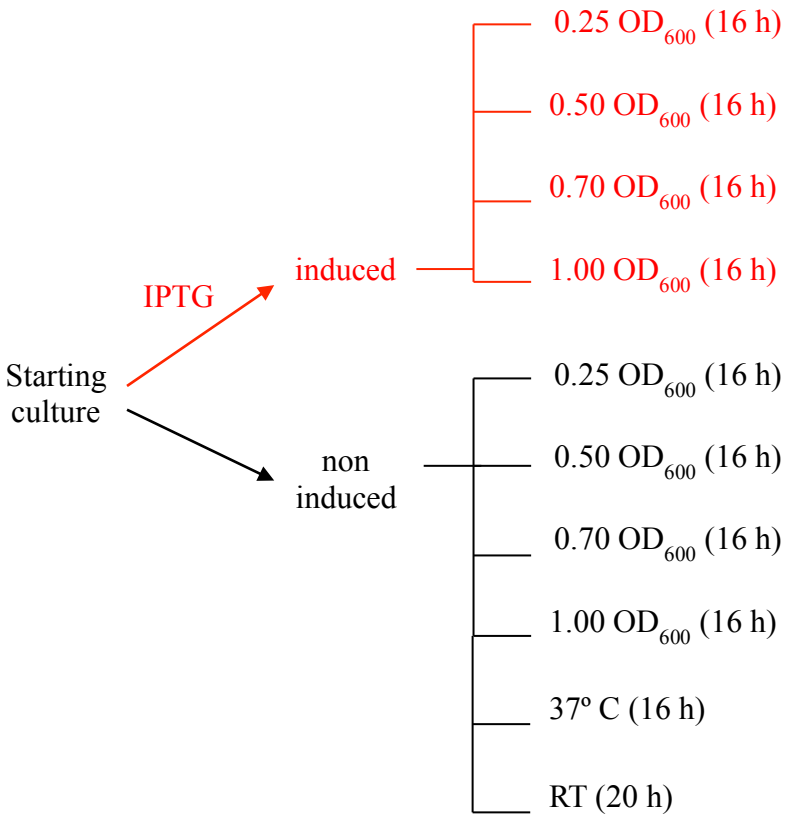

3.2.2.1 Leaky expression analysis

To determine the presence and the extent of leaky expression of GST-LTX^{N4C}, I first carried out an experiment when a culture of Rosetta-Gami cells transformed with the pGEX-LTX^{N4C} plasmid was grown to 0.25 OD_{600} to achieve exponential growth and then allowed to grow at RT for 16 hours without induction. In parallel, a similar culture was grown under the same conditions, but was induced by adding IPTG at 0.25 OD600. In addition, a control culture of non-transfected Rosetta-Gami cells was grown under the same regime, with or without IPTG induction.

The expression of LTX^{N4C} was analysed by SDS-PAGE and Coomassie staining (Figure 3.5 A). As visible on the gel, a protein band of the size predicted for the GST-LTX^{N4C} fusion is present in the transformed cells, but not in the control (position of the protein pointed by the arrow). The protein is expressed in both conditions, both induced and non-induced. It is evident that the induction leads to a large overall increase of the expression (about 7.5 times more than non-induced), but the majority of the protein produced is insoluble and precipitates in the pellet (with approximately 98.4 % of the protein produced in the pellet and 1.6 % in soluble form, Figure 3.5 B and C). Although with the leaky expression the amount of recombinant toxin is much lower, the proportion of the soluble protein increases, while LTX^{N4C} content in the pellet decreases (with 89 % in the pellet and 11 % in the supernatant, Figure 3.5 B and C).

Given the result of this experiment, suggesting that the greatest amount of functional protein is expressed without induction, this condition was always used as a benchmark in subsequent experiments, where the induction conditions were optimised.

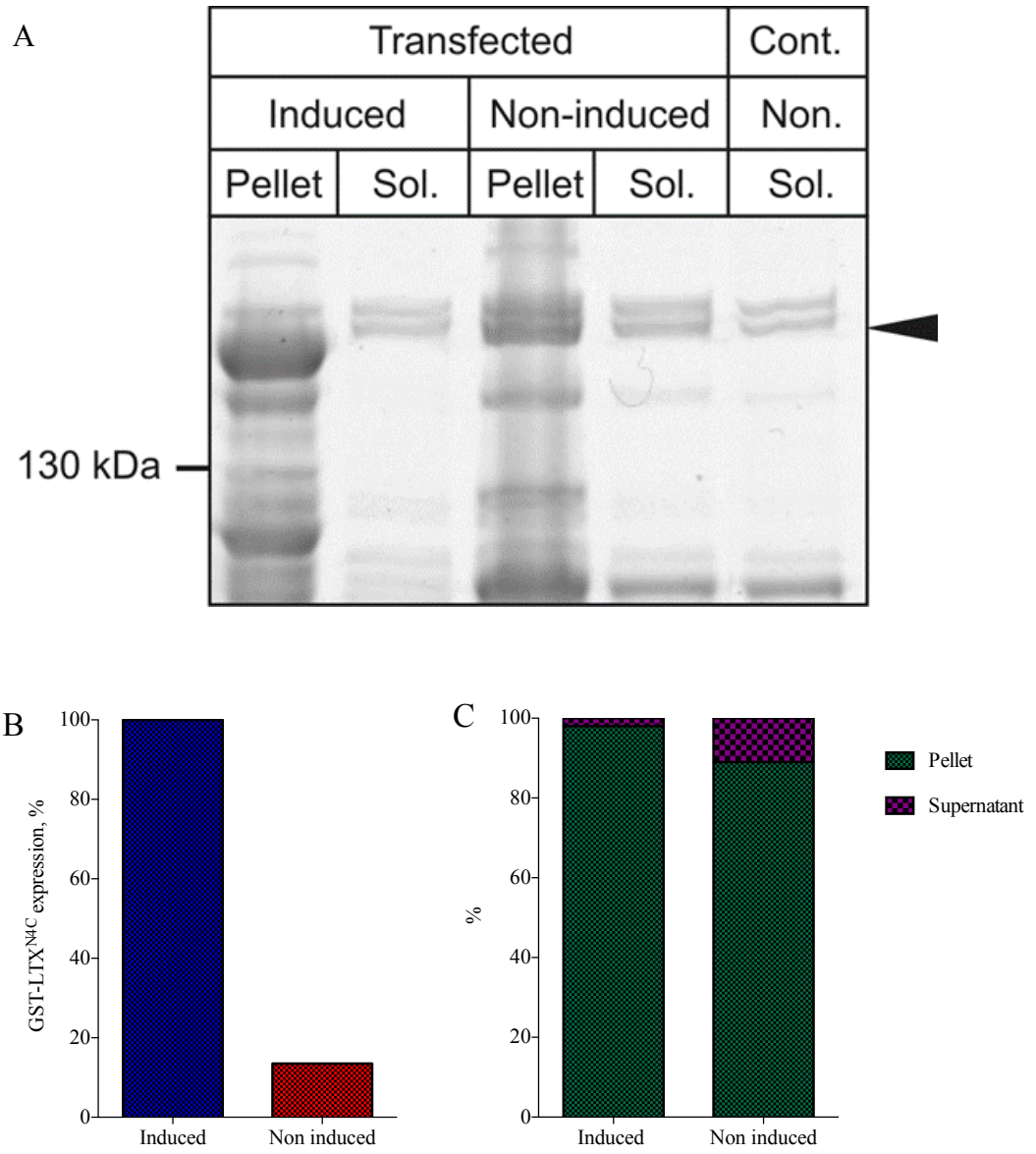

Figure 3.5. Analysis of the leaky expression of the GST-LTX^{N4C} fusion protein. A. Coomassie staining of GST-LTX^{N4C} expression. The position of the protein of interest is shown by the arrow. B. Comparison of total GST-LTX^{N4C} expression in induced and non induced cultures. Leaky expression is present, however the induced culture expresses approximately 7.5 times more protein than the non-induced. C. Comparison of the amount of protein going in the pellet or in solution in the two conditions considered. Whilst only 1.6 % of the total fusion protein expressed is soluble in induced cultures, in non induced cultures approximately 11 % of protein is soluble.

3.2.2.2 Optimisation of induction

One way to optimise the production of the soluble fusion protein is to find an optimal time for induction of expression. This is because the exponentially growing bacterial cells undergo changes to their physiological state, which affect the amount of chaperones available, the activity of transcription and translation and therefore may affect the cell's ability to synthesise a properly folded protein. The expression of GST-LTX^{N4C} in cultures induced at different OD_{600} was analysed. Cultures were grown under usual conditions and separately induced at different OD_{600}. They were then left for expression at RT for ≈ 16 hours. Control, non-induced cultures were grown at the exactly same growing conditions, but were not induced.

The expression of GST-LTX^{N4C} was analysed using SDS-PAGE and Western blotting using an anti-GST antibody. As can be observed on the blot (Figure 3.6 A), a large quantity of soluble GST-LTX^{N4C} is expressed in the condition where the culture was induced at 0.5 OD_{600}. The soluble fraction of expressed protein tends to decrease when the induction is made at a later stage, with the respective insoluble fraction increasing in the pellet. When not induced, the expression of LTX^{N4C} is overall lower, but most of the protein expressed is in a soluble form. No traces of LTX^{N4C} are detectable in the negative control.

Given these observation, I concluded that the best condition of expression for LTX^{N4C} in our bacterial system is with induction at 0.5 OD_{600}.

A

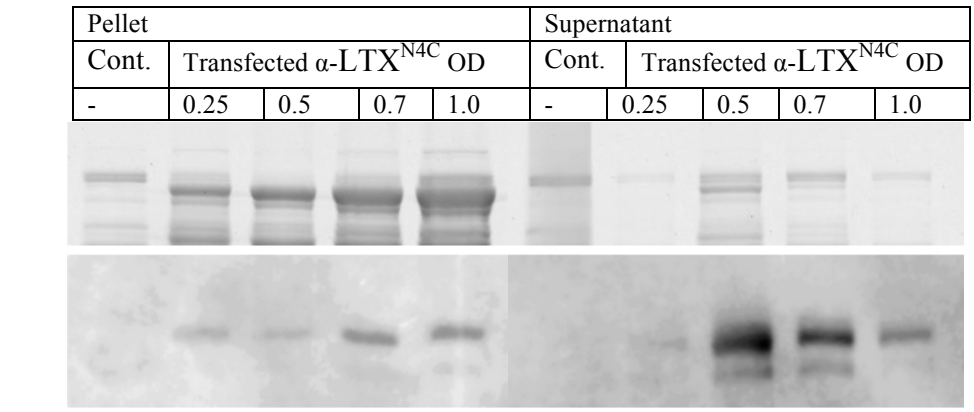

B

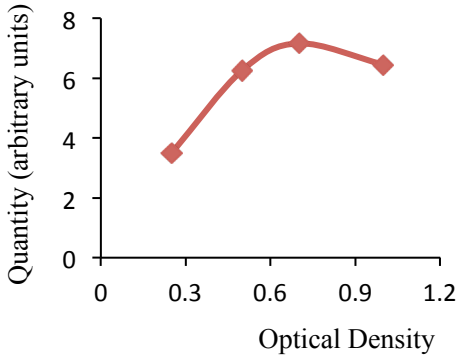

C

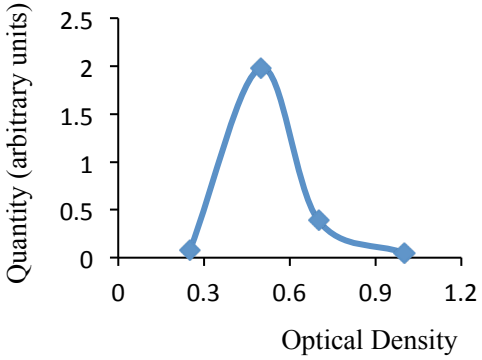

Figure 3.6. Optimisation of the time of induction of GST-LTX^{N4C} expression. A. Coomassie staining of the gel (top) and a respective Western blot (bottom) showing the amount of LTX^{N4C} expressed in the cultures induced at different OD_{600}, in induced and non induced conditions. Note that sample loading on the gel was proportionate to the volumes of the soluble and insoluble fractions, while 10-fold lower amounts of cell pellets were loaded on the blot. B-C. Quantification of the expression of soluble LTX^{N4C} in induced cultures. In the induced conditions, with increasing OD_{600} at induction, the amount of fusion protein in the pellet greatly increases (B), while the amount of soluble protein increases and then falls (C).

3.2.2.3 Optimisation of the leaky expression

As previously shown, a high amount of soluble protein is expressed without induction. To explore the possibility of further enhancing the leaky expression, I experimented with time and temperature of growth to allow cultures to express LTX^{N4C} without induction. One culture was left expressing for 20 hours at RT, while another was left for 16 hours at 37°C.

The expression of LTX^{N4C} was analysed using SDS-PAGE and Coomassie staining (Figure 3.7). As in the previous experiments, leaky expression produced a detectable amount of soluble protein and a relatively small amount of insoluble fusion protein in the pellet. Between the two different growing temperatures, expression at RT appeared to be more optimal.

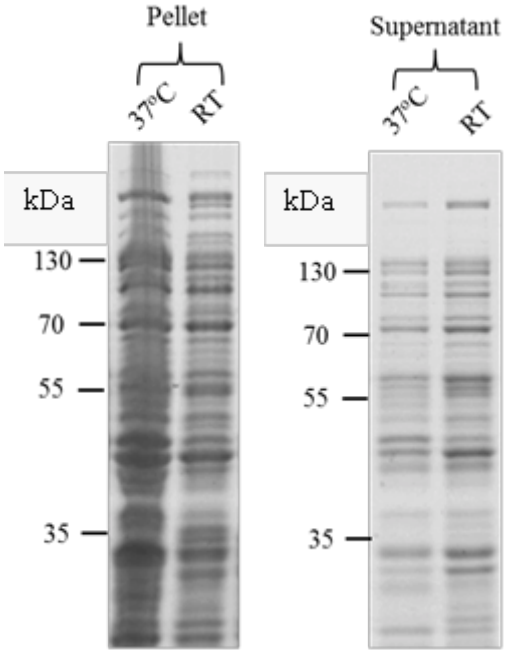

Continued on the next page

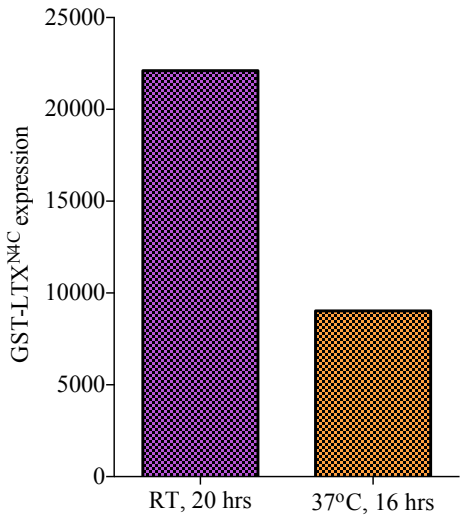

Figure 3.7. Optimisation of the leaky expression. A high amount of soluble protein is expressed without induction in both experimental conditions. The best condition to express LTX^{N4C} without induction seems to be at RT for 20 hours.

A detectable amount of soluble GST-LTX^{N4C} protein was produced by leaky expression. However, the comparison between the expression after induction of an exponential culture at 0.5 OD_{600} (grown subsequently at 16°C) and the expression without induction after 20 h growth at RT, shows that a much larger amount of soluble fusion protein is produced when the culture is induced (Figure 3.8).

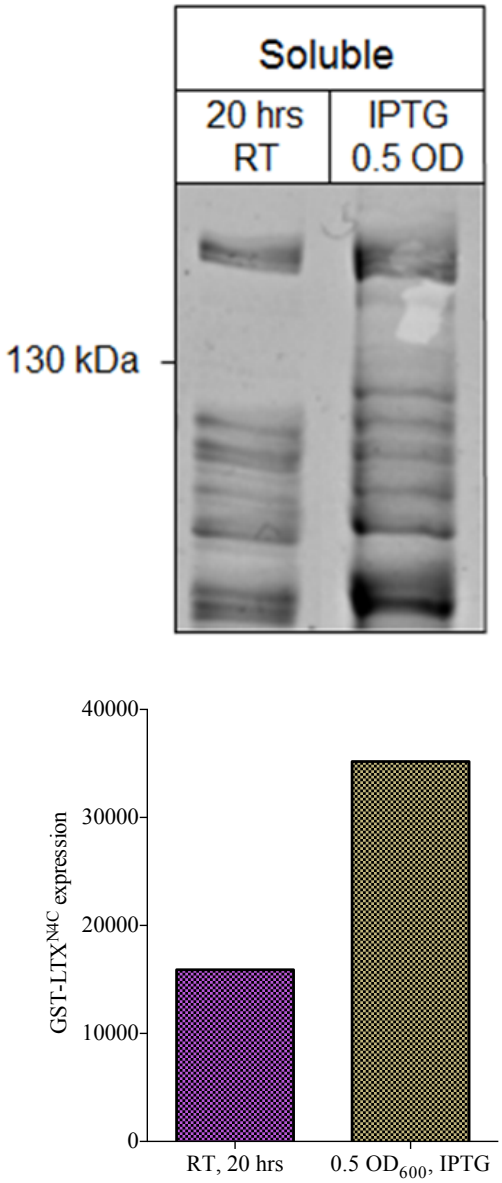

Figure 3.8. Comparison between the best conditions of expression without and with induction. The condition producing the larger amount of soluble LTX^{N4C} is the one with induction at 0.5 OD$_{600}$.

3.2.3 Purification of GST-LTX^{N4C}

Purification of the expressed GST-LTX^{N4C} was performed using GSH-column affinity chromatography and analysed by SDS-PAGE and western blot using an anti α-LTX antibody (Figure 3.9). A large amount of protein is visible in the load. After passing the load through the column a substantial amount of protein remained bound to the GST-bind resin, as in the flow through the quantity of LTX^{N4C} was visibly diminished. After extensive washes the column was eluted, and the majority of the purified protein is detectable in the third elution. Given the amount of protein that did not bind to the column, further affinity chromatographies of the flow through were performed in order to exhaust it. The presence of the protein in the washes suggests that the binding to the beads is not strong.

Degradation of the protein is present. The upper band (≈160 kDa) represents the full size LTX^{N4C}-GST construct; the lower (≈ 130 kDa) represent the full size LTX^{N4C} without the GST insert. Minor degradation is also detectable producing fragments of ≈ 150 kDa.

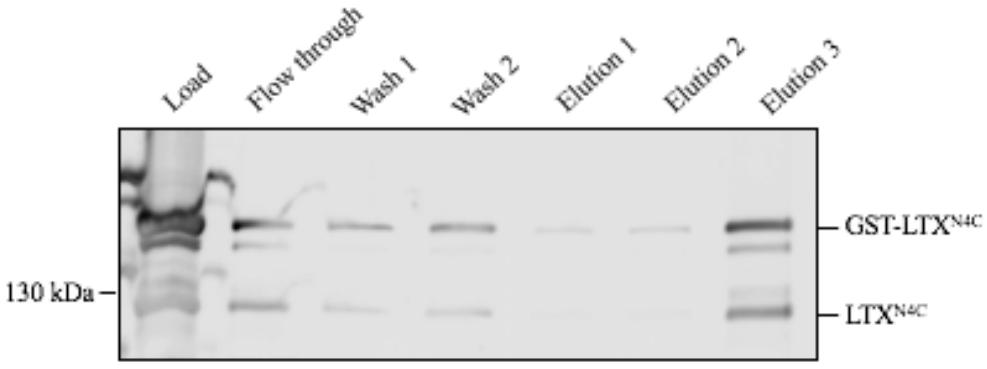

Figure 3.9. GSH-column affinity chromatography of LTX^{N4C}. The purified protein presents signs of degradations. The protein is also visible in the flow through and in the washes.

3.2.4 Biological activity of GST-LTX^{N4C}

The functional activity of the purified LTX^{N4C} was tested using neuroblastoma NB2a cells expressing LPHN1. Wild type NB2a cells were used as a negative control. Different concentrations of GST-LTX^{N4C} were added to establish the best condition for binding. Binding was analysed by SDS-PAGE and Western blot using an anti V5 antibody (Figure 3.10).

The N-terminal fragment of LPHN1 stained with the anti-V5 antibody was only visible in transfected cells. However, the binding of the toxin was detectable also in the negative control, suggesting some non-specific binding. It is notable that at 2, 5 and 20 nM GST-LTX^{N4C}, the LPHN1-expressing cells bind a higher amount of fusion protein than the control cells. However, at 50 nM GST-LTX^{N4C}, LPHN1 N-terminus seems to be strongly affected by the bound toxin, which is no longer detectable. This may be caused by the detrimental effect of the very high concentration of LTX^{N4C} that may overstimulate latrophilin, causing cell death, which leads to membrane disruption with consequent loss of bound protein and/or to protein degradation. Further optimisation of the isolation procedure is clearly necessary.

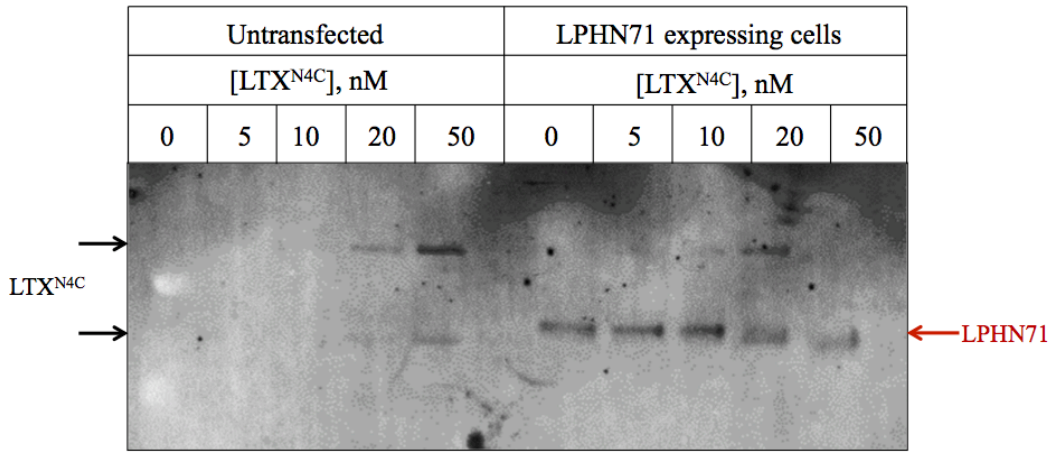

Figure 3.10. GST-LTX^{N4C} biological activity. Bound LTX^{N4C} is present to also in untransfected cells, suggesting that the a large proportion of binding is non-specific. However, with the exception of 50 nM fusion protein, LTX^{N4C} binds the LPHN1-expressing cells better.

3.3 Discussion

Having chosen to express LTX^{N4C} in a bacterial system, I tried to overcome the problems associated with the incorrect protein folding by using the Rosetta-Gami 2 *E. coli* strain. The optimisation procedure included the induction of fusion protein expression at different stages of culture growth and subsequent incubation at different temperatures. It has been found that a very high proportion of soluble GST-LTX^{N4C} is expressed when the culture is induced at 0.5 OD and then grown at 16°C. The induction under these specific conditions also produces better yield of the fusion protein compared to its leaky expression without induction. However, the yield of soluble protein is much lower at optical densities of 0.25 and 0.7, which creates only a very narrow window of culture density at which the successful expression can be expected.

The GST-LTX^{N4C} fusion protein can be relatively easily and inexpensively purified using GSH-column affinity chromatography, although this process is also rather inefficient, with a large proportion of fusion protein appearing in the flow-through fractions and only a small amount being eluted from the column. The fusion protein has a relatively low biological activity as tested by its binding to the toxin receptor LPHN1.

When expression of GST-LTX^{N4C} was repeated using the same conditions as described above, very little soluble protein was produced, and its purification was unsuccessful. This suggests that the selected conditions are not robust for reliable production of GST-LTX^{N4C}.

Given the large amounts of GST-LTX^{N4C} that can be produced in a preparative bacterial culture, the losses described above could still make bacterial expression worthwhile. However, the biological activity of the bacterially produced protein remains uncertain, and requires more research. In addition, further optimisation of expression and the use of cooling incubators are required.

For these reasons, we conclude that the expression of LTX^{N4C} in a bacterial system is not optimal. Alternative methods for its expression could be using yeast or baculovirus systems.

The LTX^{N4C} used in the experiments described further on in this work was expressed in a baculovirus system.

CHAPTER 4
RESULTS II. Spontaneous exocytosis: control by LPHN1 and effects of LTX^{N4C}.

4.1 Introduction

As extensively discussed in the first chapter (see Chapter 1, Sections 1.2 and 1.3), Latrophilin-1 (LPHN1) is a presynaptic G-protein-coupled receptor whose function has been investigated using α-latrotoxin, a component of Black Widow spider venom, in its native (α-LTX) and mutant (LTX^{N4C}) forms. The native α-LTX is a tetramer that binds presynaptic receptors and inserts itself into the cellular membrane, forming pores permeable to divalent cations. In contrast, LTX^{N4C} is unable to form pores, but still binds the same receptors, and it can be used to study the functions of the receptors alone (Ushkaryov, Volynski and Ashton 2004). When bound to LPHN1, both α-LTX and LTX^{N4C} cause a dramatic increase in the frequency of neurotransmitter release, suggesting a role of this receptor in the regulation of exocytosis (Capogna et al. 2003; Lelyanova et al. 2009).

There are two endogenous ligands of LPHN1: Lasso/teneurin-2 (Silva et al. 2011) and FLRT3 (Boucard et al. 2014). As argued in Discussion (Section 4.3), only Lasso, but not FLRT3, binds to neuronally-expressed LPHN1. However, in any case the role of these interactions in LPHN1 signalling is unclear, and therefore I used the exogenous agonist of LPHN1, LTX^{N4C}.

Here, I investigated the role of LPHN1 in spontaneous release of neurotransmitter at neuromuscular junction (NMJ) and in central synapses, by comparing the frequency of spontaneous (miniature) synaptic events in wild type (WT) and LPHN1 knockout (KO) mice. Furthermore, the effects that LTX^{N4C} exerts on exocytosis in NMJ were analysed using different bathing buffers.

4.2 Results

4.2.1 Basal frequency of exocytosis at the mouse NMJ

Given the known role of extracellular Ca^{2+} in LTX-induced exocytosis, I first determined the basal rate of neurotransmitter release by recording MEPPs in a buffer containing 2 mM Ca^{2+} or no added Ca^{2+}, without any other experimental manipulation. Recordings were collected from several fibres of the same paw as well as from different paws in order to ensure the presence of internal and external independent controls.

In Ca^{2+}-containing buffer, spontaneous release of neurotransmitter had a frequency of 0.36 ± 0.03Hz (approximately 1 vesicle released every 3 seconds) (Figures 4.1 and 4.3).

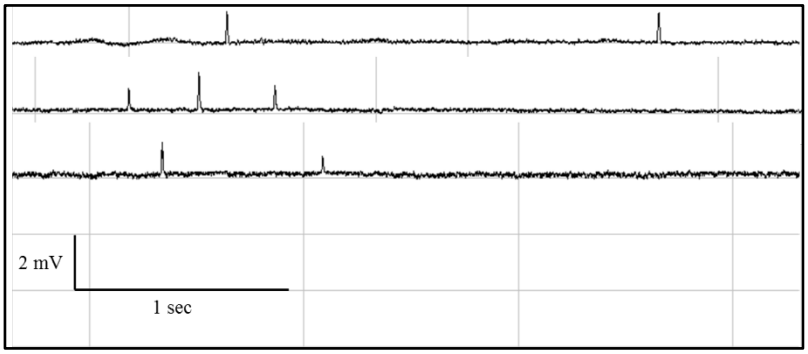

Figure 4.1. Examples of representative individual traces of MEPPs recorded at the mouse NMJ in the presence of 2 mM extracellular Ca^{2+} (Ca^{2+}_e).

Removal of Ca^{2+} form the extracellular buffer caused a decrease in the neurotransmitter release of about 3.5 fold, with a frequency of 0.10 ± 0.01 Hz (approximately 1 vesicle released every 10 seconds) (Figures 4.2 and 4.3). The MEPPs amplitude did not change between the two experimental conditions (0.82 ± 0.11 mV in Ca^{2+} vs. 0.87 ± 0.17 mV in Ca^{2+}-free buffer).

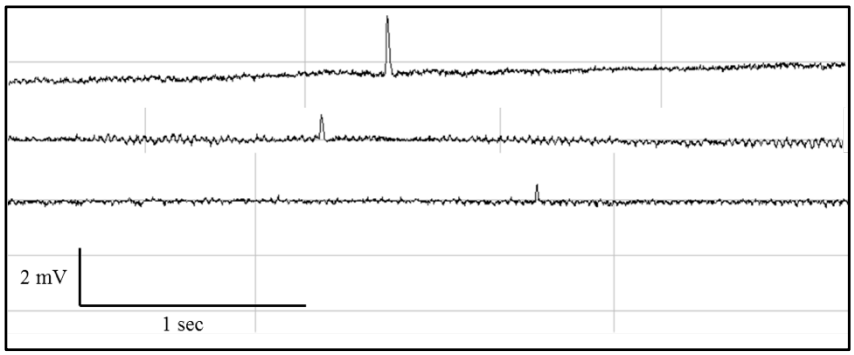

Figure 4.2. Single traces of MEPPs recorded at the mouse NMJ in the absence of 2 mM $Ca^{2+}_{e.}$

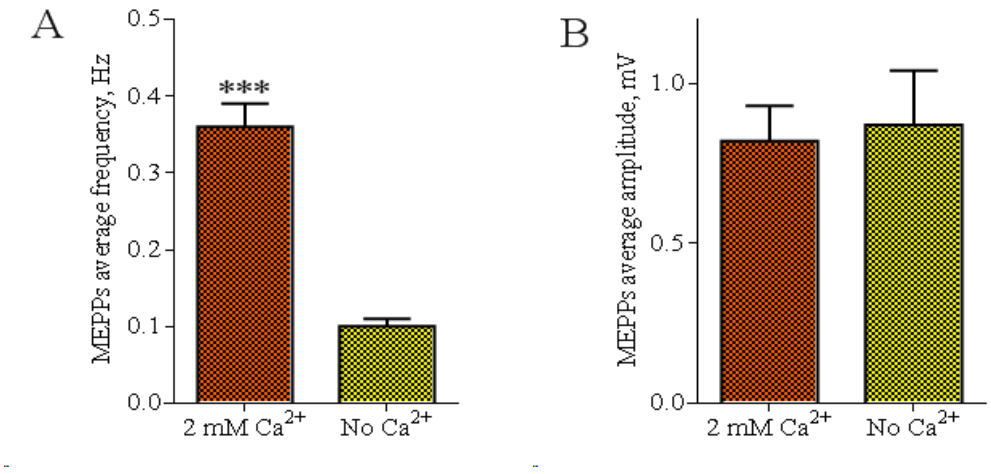

Figure 4.3. A. Average frequencies of MEPPs in the presence and absence of Ca^{2+}_{e} *(2 mM). B. Average amplitude of MEPPs with and without the presence of 2 mM* Ca^{2+}_{e}*. The difference between the conditions is not statistically significant (n = 23 individual cells with* Ca^{2+} *and 12 without* Ca^{2+}*; ***, P < 0.001, Mann – Whitney U test).*

4.2.2 Basal frequency of exocytosis at the NMJ as a function of LPHN1 expression

To investigate the involvement of LPHN1 in the spontaneous release of neurotransmitter, MEPPs were recorded in LPHN1 WT ($^{+/+}$), heterozygous ($^{+/-}$) and KO ($^{-/-}$) mice. Recordings were made both in Ca^{2+}-containing and in Ca^{2+}-free buffers to determine the Ca^{2+} dependence of the process on all genetic backgrounds.

Results show a progressive increase of neurotransmitter release with the decreasing dose of the LPHN1 gene: in Ca^{2+}-containing buffer, the average frequency of exocytosis was of 0.36 ± 0.03 Hz in LPHN1$^{+/+}$ mice; in LPHN1$^{+/-}$ mice I determined an increase in the frequency that went up to an average of 0.56 ± 0.14 Hz; finally, in LPHN1$^{-/-}$ mice the frequency reached an average of 1.68 ± 0.44 Hz (Figure 4.4 A).

The MEPPs average amplitudes are not significantly different between the experimental conditions (0.82 ± 0.11 mV in WT; 0.79 ± 0.31 mV in Het; 0.85 ± 0.24 mV in KO, Figure 4.4 B).

Removal of Ca^{2+} from the extracellular buffer caused a decrease in the frequency on all genetic backgrounds. However, the tendency of increased frequency going from LPHN1$^{+/+}$ to $^{+/-}$ and $^{-/-}$ was still present. The average frequency of exocytosis was 0.10 ± 0.01 Hz in $^{+/+}$ mice; in $^{+/-}$ mice the average frequency rose to an average of 0.24 ± 0.13 Hz; finally, in $^{-/-}$ mice the average frequency of release went up to 0.61 ± 0.19 Hz (Figure 4.4 A).

The MEPPs average amplitudes were not significantly different between the experimental conditions (0.87 ± 0.17 mV in LPHN1$^{+/+}$; 0.86 ± 0.22 mV in $^{+/-}$; 0.81 ± 0.19 mV in $^{-/-}$, Figure 4.4 B).

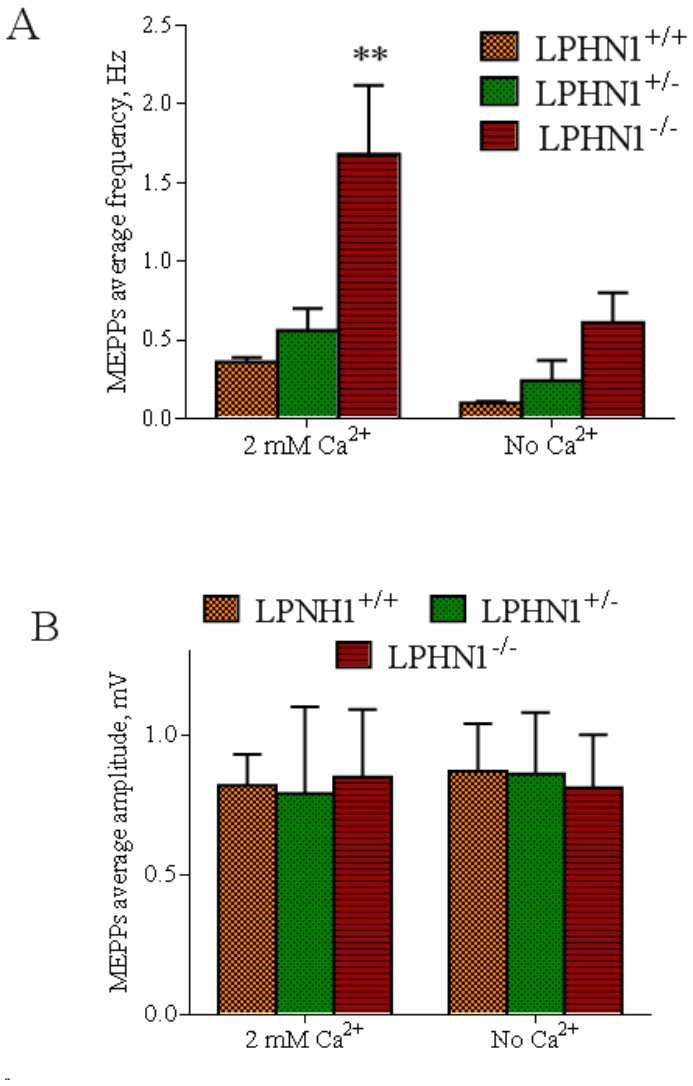

*Figure 4.4. Average frequencies of MEPPs in LPHN1$^{+/+}$, $^{+/-}$, and $^{-/-}$ mice. Recordings were done in the presence and absence of 2 mM Ca^{2+}_e. The difference between the WT and KO frequency is statistically significant (n = 25 LPHN1$^{+/+}$, 41 $^{+/-}$ and 28 $^{-/-}$ individual cells in the presence of Ca^{2+}_e, and 34 LPHN1$^{+/+}$, 14 $^{+/-}$ and 29 $^{-/-}$ individual cells in Ca^{2+}-free buffer. **, P < 0.01, One-way ANOVA). The difference in the average amplitudes between the conditions is not statistically significant (B).*

4.2.3 Basal frequency of exocytosis in LPHN1$^{+/+}$ and $^{-/-}$ hippocampal neuronal cultures

Hippocampi from 1-2 days old mice were dissected and plated on coverslips following the protocol described in Chapter 2, Section 2.2.12. The cultures were then grown for several days/weeks and compared in terms of cells' viability and physiological parameters.

After 1 day, the LPHN1$^{+/+}$ and $^{-/-}$ cultures did not significantly differ in the number of cells per field of view ($^{+/+}$: 434 ± 37.56 cells/field of view, n = 7; $^{-/-}$: 430 ± 35.2 cells/field of view, n = 7, see Figure 4.5 C).

However, after 14 days it was possible to observe that LPHN1$^{+/+}$ and $^{-/-}$ cultures grew in very different ways, with the $^{+/+}$ neurons being healthy, dense and connected, while the $^{-/-}$ cultures were very sparse and with few connections, with many neurons dead (Figure 4.6 A and B).

Spontaneous synaptic activity in LPHN1$^{+/+}$ and $^{-/-}$ neurons was determined by recording miniature excitatory and inhibitory postsynaptic currents using the whole-cell voltage clamp approach (see Chapter 2, Section 2.2.13 for details).

LPHN1$^{+/+}$ neurons showed a significantly higher average frequency of EPSCs and IPSCs than LPHN1$^{-/-}$ neurons (0.21 ± 0.05 Hz in LPHN1$^{+/+}$ neurons vs. 0.10 ± 0.02 Hz in $^{-/-}$ neurons, see Figure 4.7 A).

The average amplitudes were not statistically different in the two conditions considered (1.28 ± 0.04 nA in LPHN1$^{+/+}$ and 1.39 ± 0.07 nA in $^{-/-}$ neurons, see Figure 4.7 B).

A. LPHN1$^{+/+}$ pyramidal neuron culture

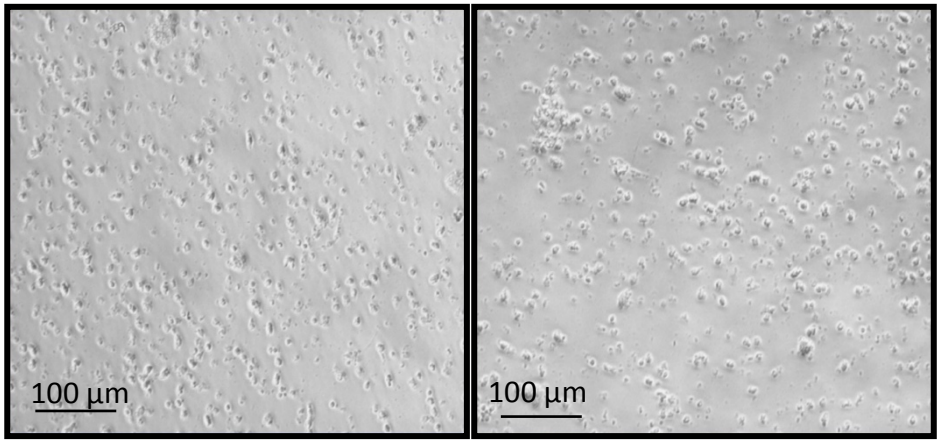

B. LPHN1$^{-/-}$ pyramidal neuron culture

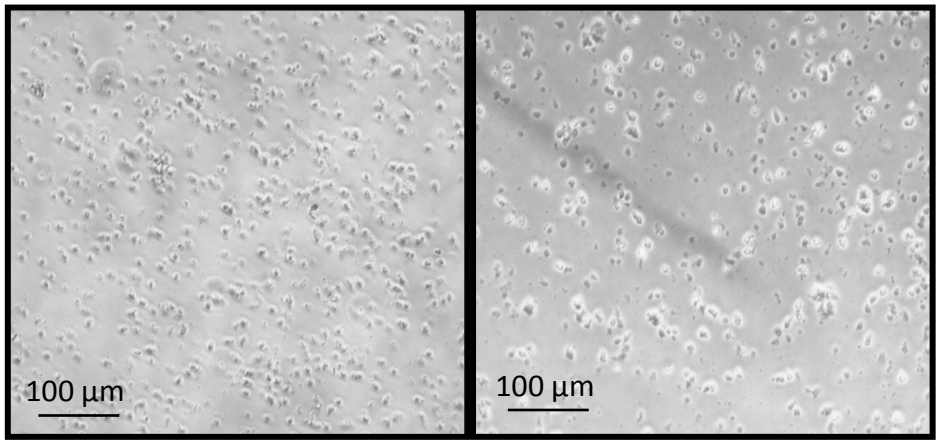

C

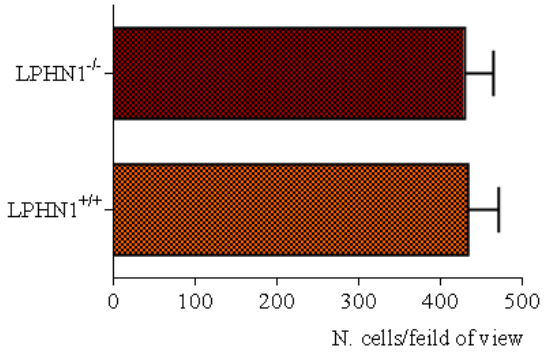

Figure 4.5. Primary cultures of LPHN1 WT (A) and KO (B) pyramidal neurons on day 1 of culture. Cells were plated with an average of 10-25 x 10^3 cells per well. The difference in number between the two cultures is not statistically significant (C).

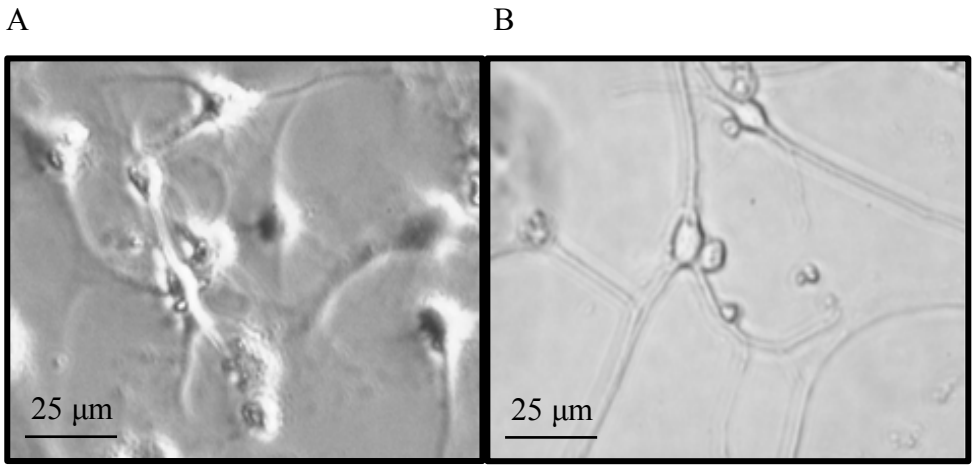

Figure 4.6. Primary cultures of WT (A) and LPHN1 KO (B) pyramidal neurons after 14 days in culture.

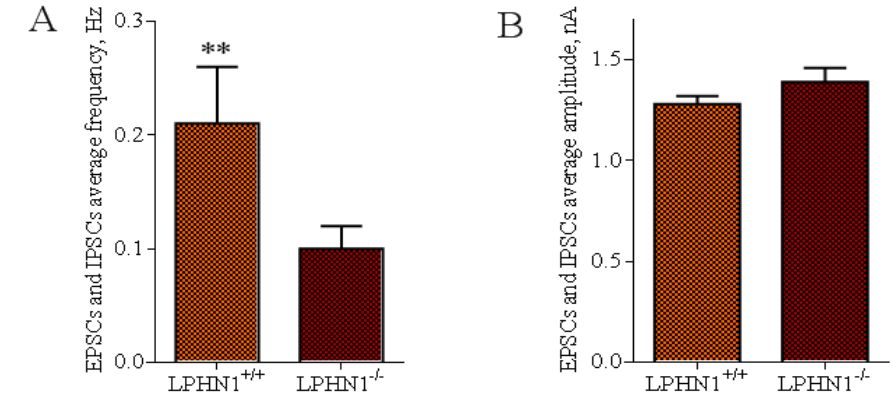

*Figure 4.7. A. Average frequency of ESPCs and ISPCs in LPHN1$^{+/+}$ and $^{-/-}$ pyramidal neurons primary cultures. B. Average amplitude of ESPCs and ISPCs in LPHN1$^{+/+}$ and $^{-/-}$ pyramidal neurons primary cultures. The difference between the conditions is not statistically significant (n = 25 and 26 cells for WT and KO cultures; **, P < 0.01, Mann – Whitney U test).*

The analysis of the ESPCs and ISPCs separately shows that upward-going inhibitory currents (IPSCs) were predominant in both LPHN1$^{+/+}$ and $^{-/-}$ cultures. In both cases, however, the frequency was higher in LPHN1$^{+/+}$ neurons (Figures 4.8, 4.9 and 4.10).

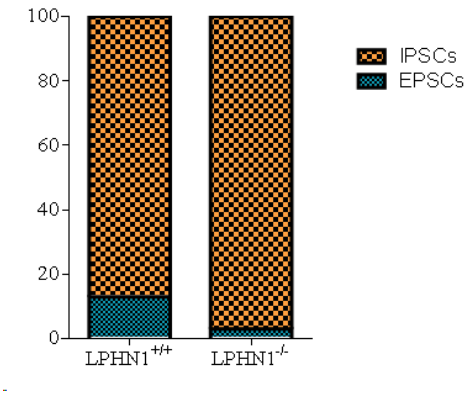

Figure 4.8. ESPCs and ISPCs analysis. In both cultures, the majority of the postsynaptic currents recorded were upward-going inhibitory currents (87% ISPCs and 13% ESPCs in WT neurons, 97% ISPCs and 3% ESPCs in LPHN1 KO neurons).

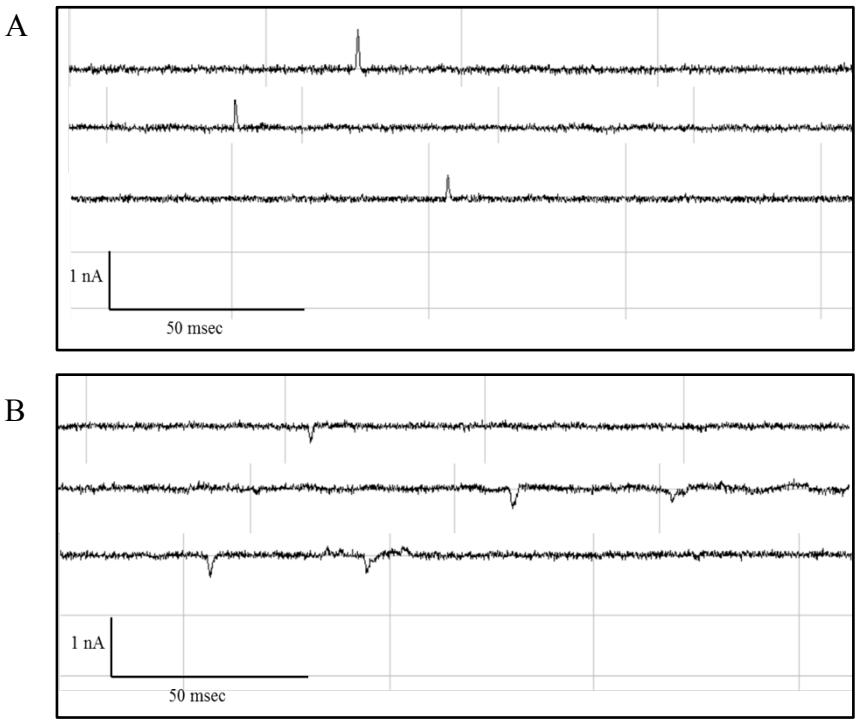

Continued on the next page

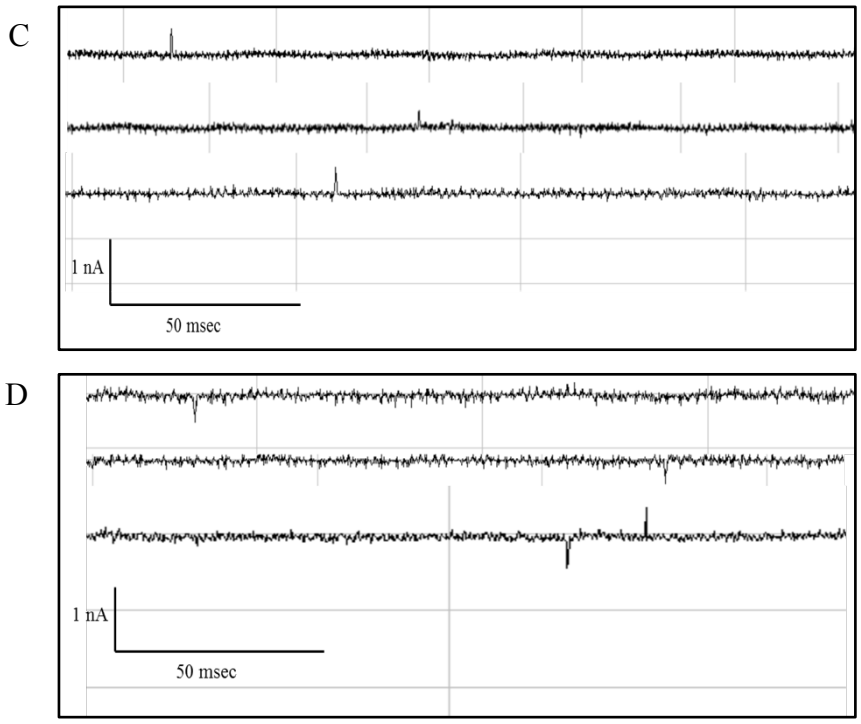

Figure 4.9. Individual traces of IPSCs (A, C) and EPSCs (B, D) recorded in WT (A, B) and KO (C, D) pyramidal neuron primary cultures. Note the presence of an IPSC in D.

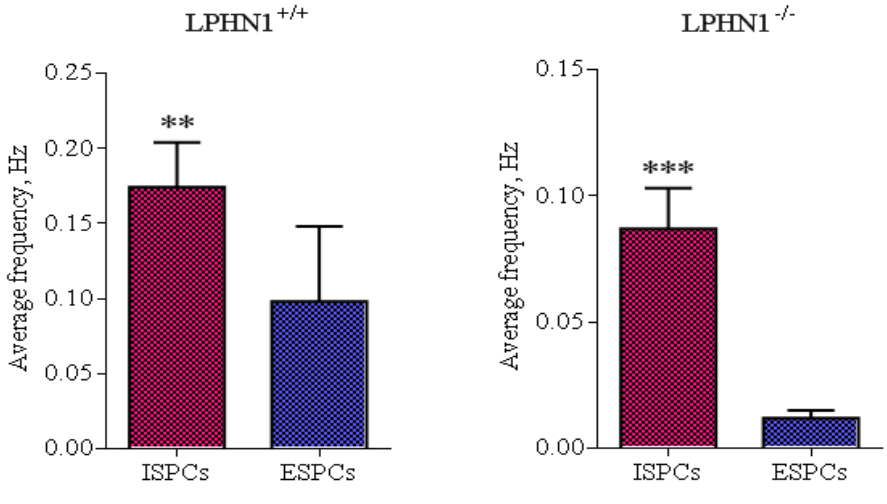

*Figure 4.10. Average frequencies of ISPCs and ESPCs in LPHN1$^{+/+}$ and $^{-/-}$ hippocampal primary cultures (n = 25 LPHN1$^{+/+}$ cells and 26 $^{-/-}$ cells. **, P<0.010; ***, P < 0.001, Mann Whitney U test).*

The amount of recorded spontaneous synaptic activity in dissociated neuronal cultures may depend on the number of synaptic connections made by adjacent neurons onto the recorded cell. Given that LPHN1 KO mice spontaneously released 4.7 times more acetylcholine at the NMJs (Section 4.2.2 above) and 3 times more glutamate and GABA at central synapses (A. Ashton, Y. Ushkaryov; unpublished data) than WT animals did, the results described in this Section indicate that synaptic connectivity in the 14 days-old hippocampal cultures from KO mice was at least 6 times poorer than in such cultures from WT animals.

4.2.4 Stimulation of spontaneous exocytosis by LTX^{N4C} at the NMJ

In order to investigate the effects of the activation of LPHN1 on spontaneous neurotransmitter release recordings of MEPPs were performed on neuromuscular preparations stimulated using LTX^{N4C}.

The response to the toxin was examined in the absence and in the presence of extracellular Ca^{2+} (2mM). In a Ca^{2+}-free environment, LTX^{N4C} is known to bind to LPHN1, and therefore it should be able to activate the machinery that brings about an increase in neurotransmitter release. However, under this condition, LTX^{N4C} was not able to elicit this effect, and the frequency of exocytosis showed only a small non-significant increase (0.19 ± 0.05 Hz).

Upon the addition of 2 mM Ca^{2+}, the effect of the toxin immediately started, and the frequency of neurotransmitter release increased up to 160 times compared to the basal frequency without extracellular Ca^{2+} (15.50 ± 7.07 Hz).

It is clear from the results shown in Figure 4.11 (A) that LTX^{N4C} requires extracellular Ca^{2+} to exert its effects on exocytosis. However, these effects do not develop immediately after the toxin is added to preparations in a buffer containing 2 mM Ca^{2+}. In this case, a delay of about 17 ± 2.5 minutes (n = 5) is always observed, likely due to the fact that LPHN1 needs time to activate the intracellular pathways involved in its activity. After this time, the cells start to fire with the increased frequency described above (Figure 4.12).

The average amplitude of MEPPs before and after the addition of LTX^{N4C} was not significantly different (0.82 ± 0.11 mV in Ca^{2+} buffer, 0.96 ± 0.04 mV after the addition of LTX^{N4C}).

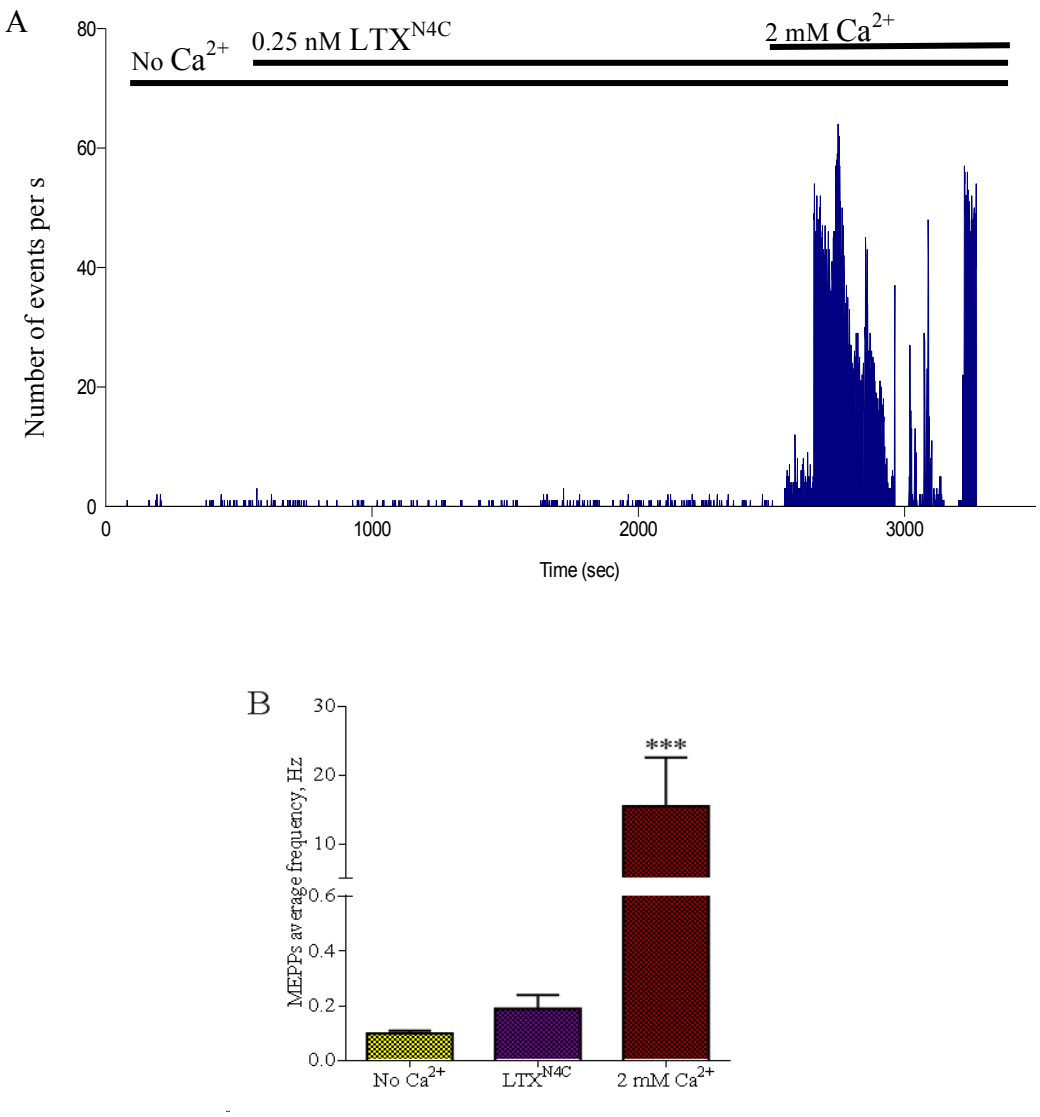

*Figure 4.11 A. The frequency of MEPPs in Ca^{2+}-free buffer, after the addition of LTX^{N4C}, and subsequent addition of 2 mM Ca^{2+}. LTX^{N4C} was only able to induce and increase in the frequency of exocytosis when $Ca^{2+}{}_e$ was present. B. Average frequency of MEPPs in Ca^{2+}-free buffer, after the addition of LTX^{N4C} and Ca^{2+} (n = 5 cells in Ca^{2+}-free buffer, 5 cells after the addition of LTX^{N4C}, and 4 cells after further addition of 2 mM Ca^{2+}; ***, P < 0.001, Mann – Whitney U test).*

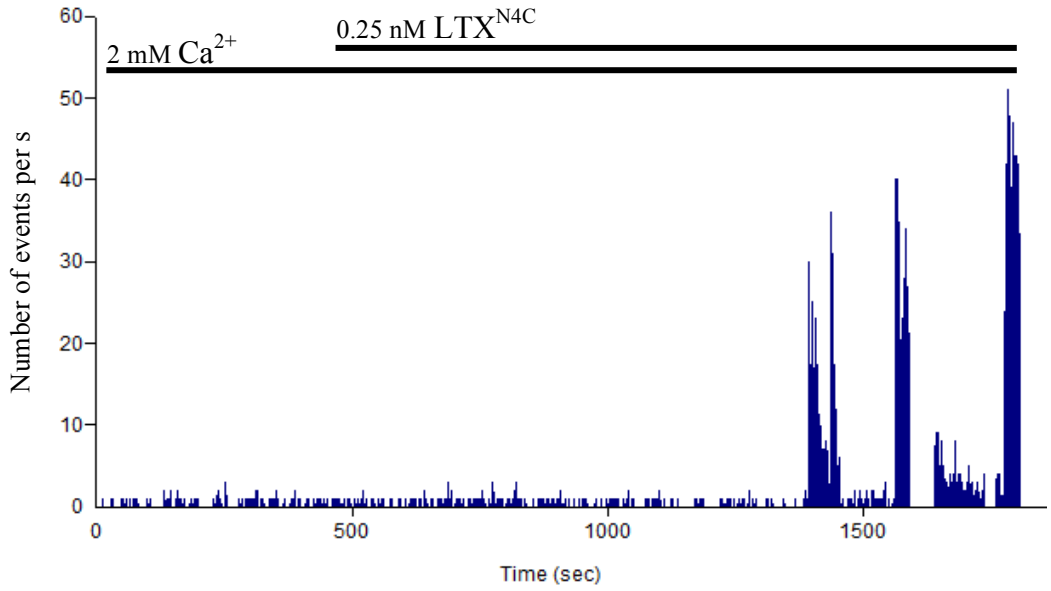

Figure 4.12. Frequency of MEPPs in the presence of 2 mM Ca^{2+}_e and after the addition of LTX^{N4C}. The effects of LPHN1 stimulation do not develop immediately after the addition of LTX^{N4C}, but after 17 minutes on average.

4.2.5 Bursts analysis

One peculiar characteristic of the increased frequency of exocytosis induced by LTX^{N4C} in Ca^{2+}-containing buffer was that it was not uniform. The terminals went through bursts of increased exocytosis, in which the frequency could reach close to 100 Hz, and periods of moderate activity, where the rate of release was significantly lower than that observed in the bursts, but about 2.5 times higher than the basal frequency (Figure 4.13). The averaged frequency of neurotransmitter release was 47.37 ± 4.09 Hz during bursts and 0.75 ± 0.10 Hz during the interburst intervals (Figure 4.14 A).

The MEPPs amplitude during bursts and interburst intervals was not significantly different (0.69 ± 0.01 Hz during bursts and 0.65 ± 0.02 Hz during interburst intervals, Figure 4.14 B).

When compared to the frequencies that appear in 2 mM Ca^{2+} only (ranging from 0 to 1 Hz), when LTX^{N4C} is added we have three groups of frequencies: a group, similar to the one observed in Ca^{2+}-containing buffer, representing interburst intervals; and a group, whose frequency ranges from 10 to 100 Hz (representing the bursts); and a third group, whose frequencies range from 1 to 3 Hz, that I termed undefined bursting activity to indicate that in such instances it was not possible to identify clearly the beginning or end of a burst (Figure 4.15).

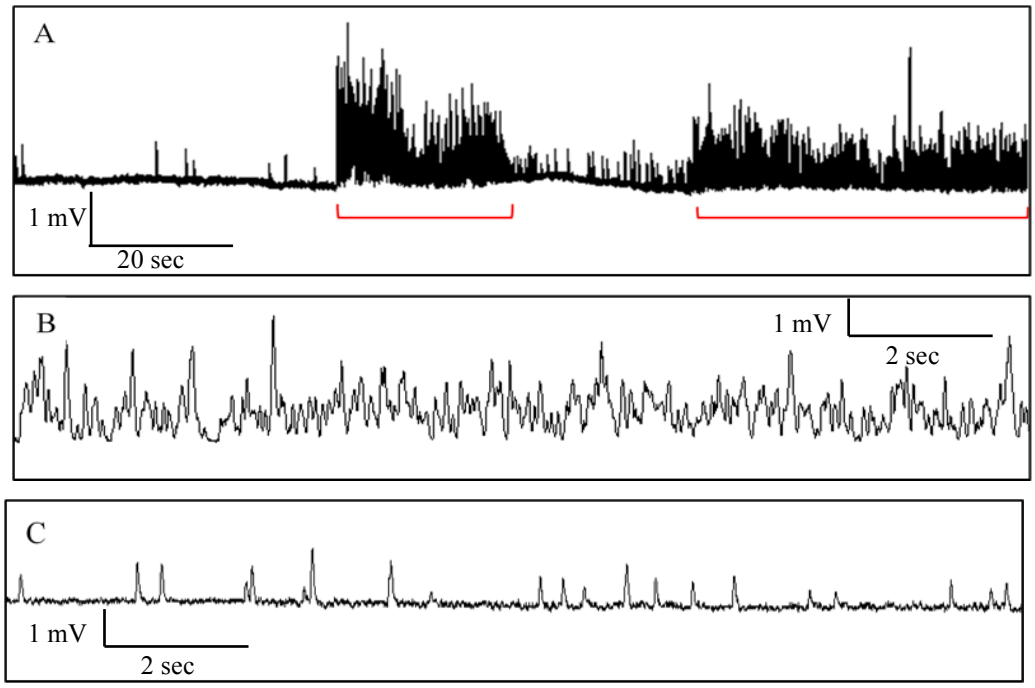

Figure 4.13. Individual traces of MEPPs recorded at the mouse NMJ after the addition of 0.25 nM LTX^{N4C}*. The frequency of spontaneous neurotransmitter release dramatically increased compared to the frequency in* Ca^{2+} *only. Characteristic of the effect of* LTX^{N4C} *in* Ca^{2+} *is the appearance of bursts of release (underlined in red) that can reach frequencies of 100 Hz, interspersed with periods of moderate activity where the frequency goes back closer to control. B. A magnified section of a MEPPs recording in a burst. C. A magnified section of an interburst interval.*

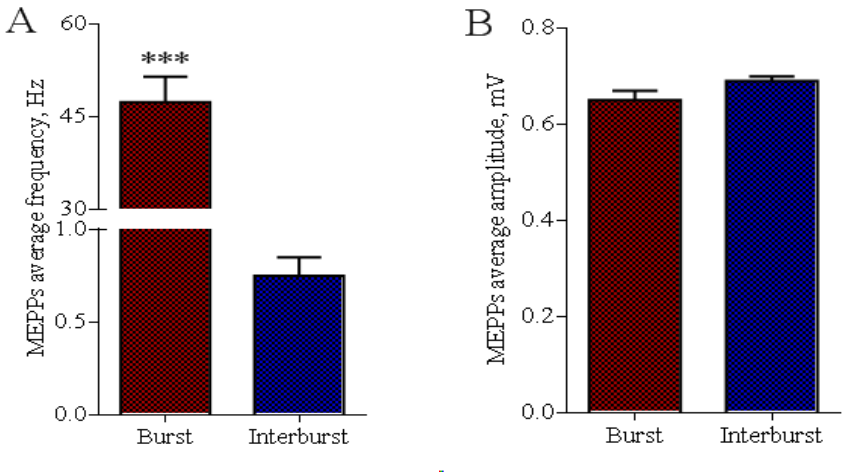

*Figure 4.14. Average frequency of MEPPs during bursts and interburst intervals. B. Average amplitude of MEPPs in bursts and interburst intervals. The difference between the conditions is not statistically significant (n = 14 bursts, 13 interburst intervals; ***, P < 0.001, Mann – Whitney U test).*

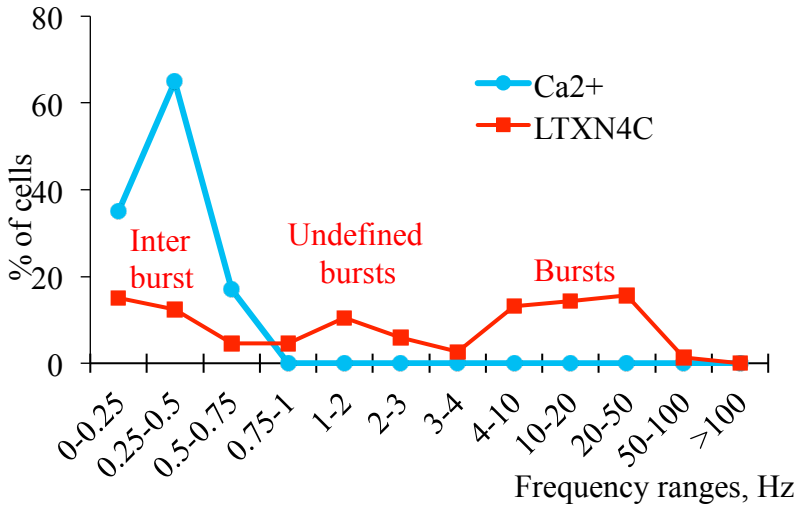

Figure 4.15. Distribution of frequencies in Ca^{2+} buffer and after the addition of LTX^{N4C}. In Ca^{2+}, the majority of events are concentrated between 0 and 1 Hz. After the addition of LTX^{N4C}, instead, due to the bursting behaviour I have three groups of frequencies: one corresponding to the interburst periods (0 – 0.75 Hz), one to corresponding to the bursts (10 – 100 Hz), and one corresponding to undefined bursts where the limits of the bursts were not completely clear (1 – 3 Hz).

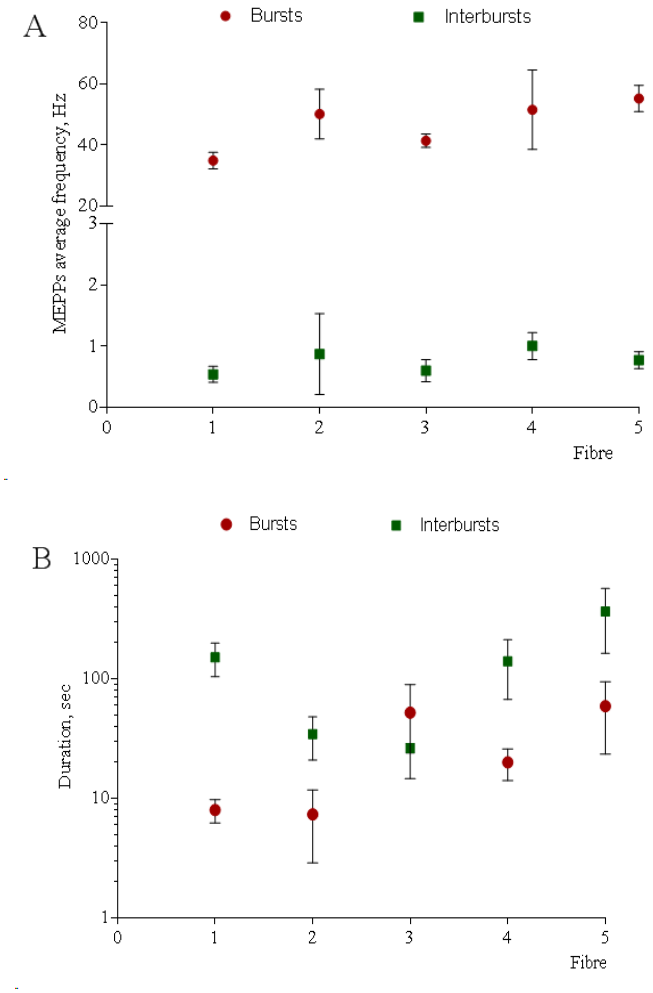

Figure 4.16. Representation of the frequency (A) and duration (B) of the bursts and interburst intervals measured in five individual single fibres.

4.2.6 Influx of extracellular Ca^{2+} is crucial for the effects of LPHN1

I showed in my previous experiments that extracellular Ca^{2+} is needed to cause the increase in exocytosis due to the activation of LPHN1 after addition of LTX^{N4C}.
However, from these experiments it was not possible to determine if the extracellular Ca^{2+} was simply needed outside the cell, for example to enhance the binding of the toxin to the receptor, or if Ca^{2+} needed to enter into the nerve terminals in order to cause these effects.
To address this issue, I performed experiments using BAPTA-AM, a Ca^{2+} chelator able to penetrate inside cells and bind two Ca^{2+} ions.
When 500 μM BAPTA-AM was incubated with the muscle preparations, the frequency of exocytosis underwent a small decrease (from 0.10 ± 0.01 Hz to 0.07 ± 0.04 Hz).
Under this conditions, 0.25 nM LTX^{N4C} was not able to elicit a significant increase in exocytosis even after the addition of Ca^{2+} (0.12 ± 0.04 Hz and 0.22 ± 0.04 Hz before and after the addition of Ca^{2+}, respectively,), suggesting that the influx of Ca^{2+} and consequent elevation in cytosolic Ca^{2+} concentration is needed to see the effects of LPHN1 activation (Figures 4.17 and 4.18).

A

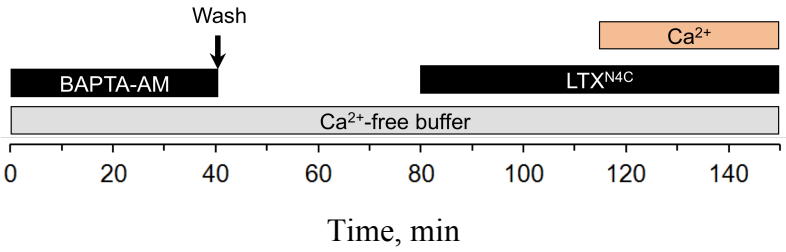

B

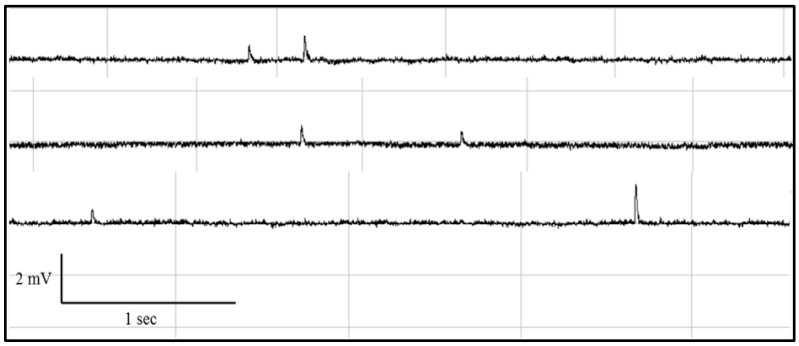

C

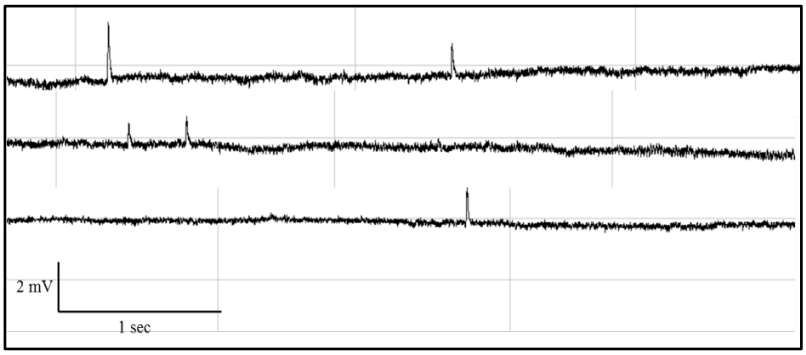

Figure 4.17. A. Representation of the protocol used in the experiments using BAPTA-AM. B. Single traces of MEPPs after the addition of LTX^{N4C} in Ca^{2+}-free buffer treated with BAPTA-AM and after Ca^{2+} was added to the buffer (C). The addition of LTX^{N4C} is not able to elicit its effects when intracellular Ca^{2+} is chelated.

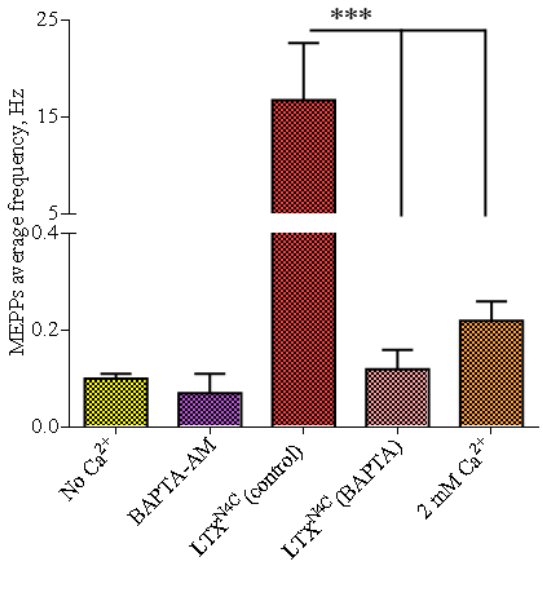

*Figure 4.18. Average frequency of MEPPs induced by LTX^{N4C} in terminals filled with BAPTA-AM. Ca^{2+} influx is needed to elicit the increase in exocytosis typical of the activation of LPHN1, as chelation of intracellular Ca^{2+} fully inhibits exocytosis even when the cation is added to the extracellular buffer. A control treated with LTX^{N4C} but not with BAPTA-AM is shown (n = 5 cells in Ca^{2+}-free buffer, 8 cells in Ca^{2+}-free buffer after the addition of BAPTA-AM, 4 cells after subsequent addition of LTX^{N4C} and 12 cells after addition of 2 mM Ca^{2+}. 7 cells have been used for the control with LTX^{N4C}; ***, P < 0.001, Mann – Whitney U test).*

4.2.7 Stimulation of spontaneous exocytosis using GST-Lasso

Lasso is the main endogenous ligand known for LPHN1. To investigate the effects that this protein could have in exocytosis, current clamp experiments were carried out following the same procedure used with LTX^{N4C}.

Recombinant fragment of Lasso fused to glutathione-S-transferase (GST), GST-Lasso, was purified from *Escherichia coli* by affinity chromatography using a glutathione column (for details see Chapter 2, Section 2.2.3), and dialysed in a buffer containing 2 mM Ca^{2+}.

Upon addition of 100 nM GST-Lasso, the frequency of exocytosis was increased by about 3 times only in one of the experiments, whilst in the other cases the frequency decreased about 2 times; overall, it was not possible to observe a significant change in the rate of neurotransmitter release (0.45 ± 0.3 Hz, Figure 4.20 A).

The average amplitudes are not statistically different in the two conditions considered (0.79 ± 0.02 in buffer A vs. 0.89 ± 0.07 mV after the addition of GST-Lasso, figure 4.20 B).

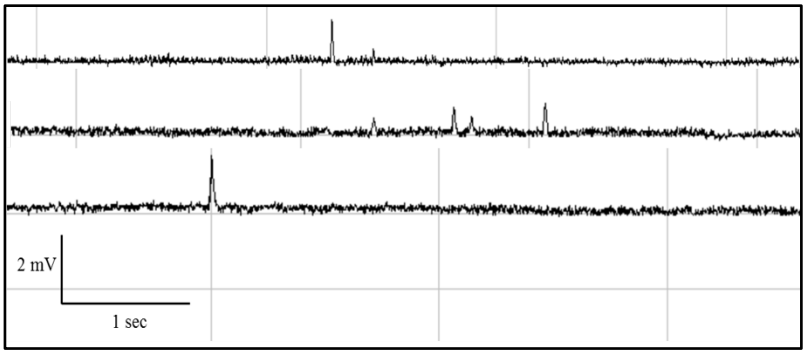

Figure 4.19. Individual traces of MEPPs in Ca^{2+}-containing buffer after the addition of GST-Lasso. This stimulation was not able to significantly change the rate of spontaneous exocytosis.

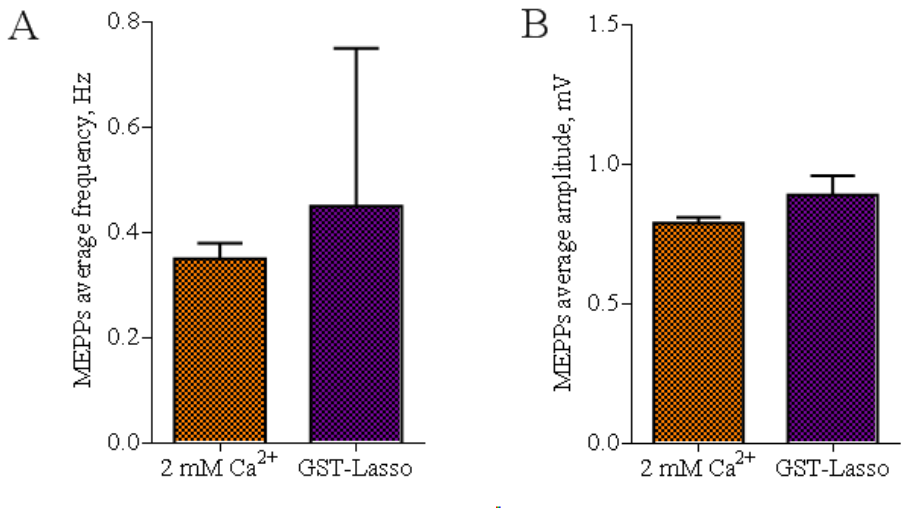

Figure 4.20. A. Average frequency of MEPPs in Ca^{2+}-containing buffer before and after the addition of 100 nM GST-Lasso. The difference is not statistically significant. B. Average amplitude of MEPPs before and after the addition of GST-Lasso in Ca^{2+}-containing buffer. The difference is not statistically significant (n = 19 cells in Ca^{2+} buffer, 31 cells after the addition of GST-Lasso; N = 3).

4.2.8 The effects of LTX^{N4C} are present in Ba^{2+}- and Sr^{2+}-containing buffers

As shown above, LTX^{N4C} in Ca^{2+}-containing buffer causes a 160-fold increase in exocytosis, characterised by bursting behaviour. Previous data suggest that this effect is not due to pore formation and must be mediated by a receptor (Volynski et al. 2003). However, LPHN1 is not the only receptor that binds LTX^{N4C}; neurexin Iα (NRX-Iα) and PTP-σ also bind to LTX^{N4C}, although NRX requires Ca^{2+} for the binding (see Chapter 1, Section 1.2.3).

A way to ascertain that the effects on exocytosis observed upon addition of LTX^{N4C} can be ascribed to the activation of LPHN1 only is to replace the Ca^{2+} in the extracellular buffer with Ba^{2+} or Sr^{2+}. In fact, in the presence of these divalent cations LTX^{N4C} binds well to LPHN1, but the binding to NRX-Iα is not possible (Davletov et al. 1998).

The neuromuscular preparations were incubated in buffers containing 2 mM Ba^{2+} or 2 mM Sr^{2+} and MEPPs were recorded in order to measure the basal frequency of exocytosis in the presence of these cations. Compared to the basal frequency of exocytosis in Ca^{2+} buffer (0.36 ± 0.03 Hz), the average frequency in these conditions was not significantly different (0.34 ± 0.29 Hz and 0.58 ± 0.20 Hz respectively).

Upon the addition of 0.25 nM LTX^{N4C}, the frequency of exocytosis increased significantly, and cells showed the bursting behaviour typical of the activation of LPHN1; bursts reached an average frequency of 41.05 ± 3.02 Hz in Ba^{2+}-containing buffer and 37.45 ± 17.94 Hz in Sr^{2+}-containing buffer (Figures 4.21 and 4.22 respectively). Interburst intervals had a frequency of 0.88 ± 0.19 Hz in Ba^{2+}-containing buffer and 0.84 ± 0.16 Hz in Sr^{2+}-containing buffer (Figures 4.21 and 4.22 respectively). These values do not significantly differ from the values obtained in Ca^{2+} buffer.

The average amplitude of MEPPs was not significantly different in the presence of extracellular Ca^{2+}, Ba^{2+} or Sr^{2+}, both in unstimulated NMJs (0.82 ± 0.11 mV in Ca^{2+}, 0.90 ± 0.06 mV in Ba^{2+} and 1.01 ± 0.04 mV in Sr^{2+}) and in NMJs treated with LTX^{N4C} (0.69 ± 0.01 mV in Ca^{2+}, 0.93 ± 0.02 mV in Ba^{2+} and 0.90 ± 0.06 mV in Sr^{2+}).

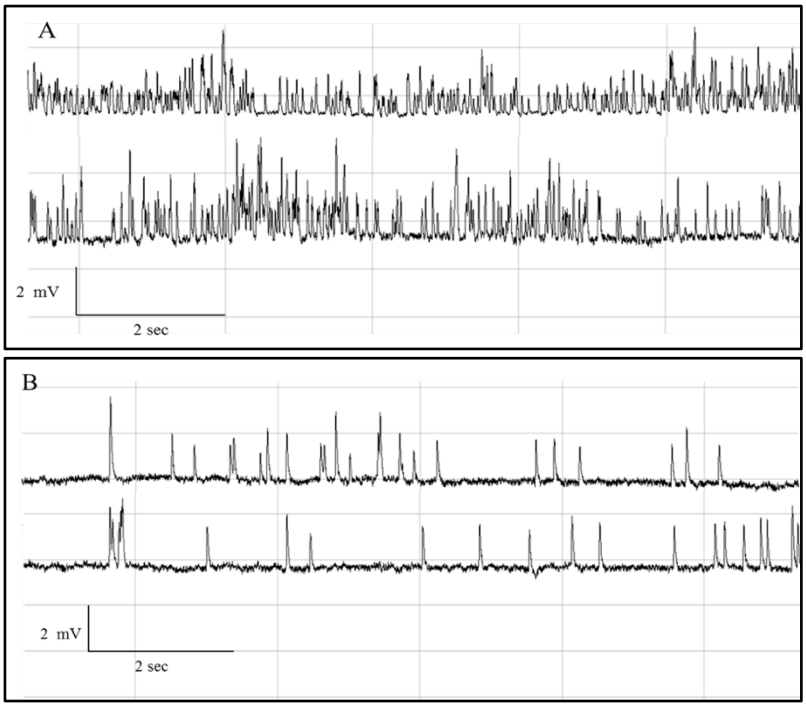

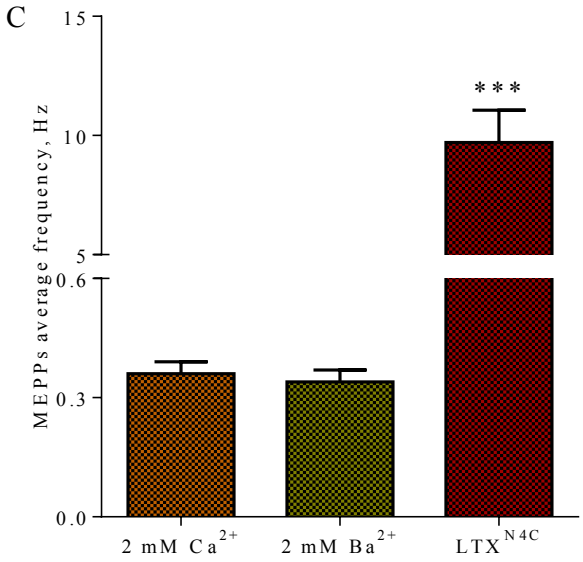

*Figure 4.21. Individual traces of MEPPs in Ba^{2+} buffer after the addition of LTX^{N4C}. A burst (A) and an interburst interval (B) are shown. C. Average frequency of MEPPs in Ca^{2+} buffer, Ba^{2+} buffer without Ca^{2+}, and after the addition of LTX^{N4C} (N = 2, n = 11 cells recorded in Ca^{2+} buffer, 16 cells in Ba^{2+} buffer, and 70 cells after the addition of LTX^{N4C}; ***, P < 0.001, Mann – Whitney U test).*

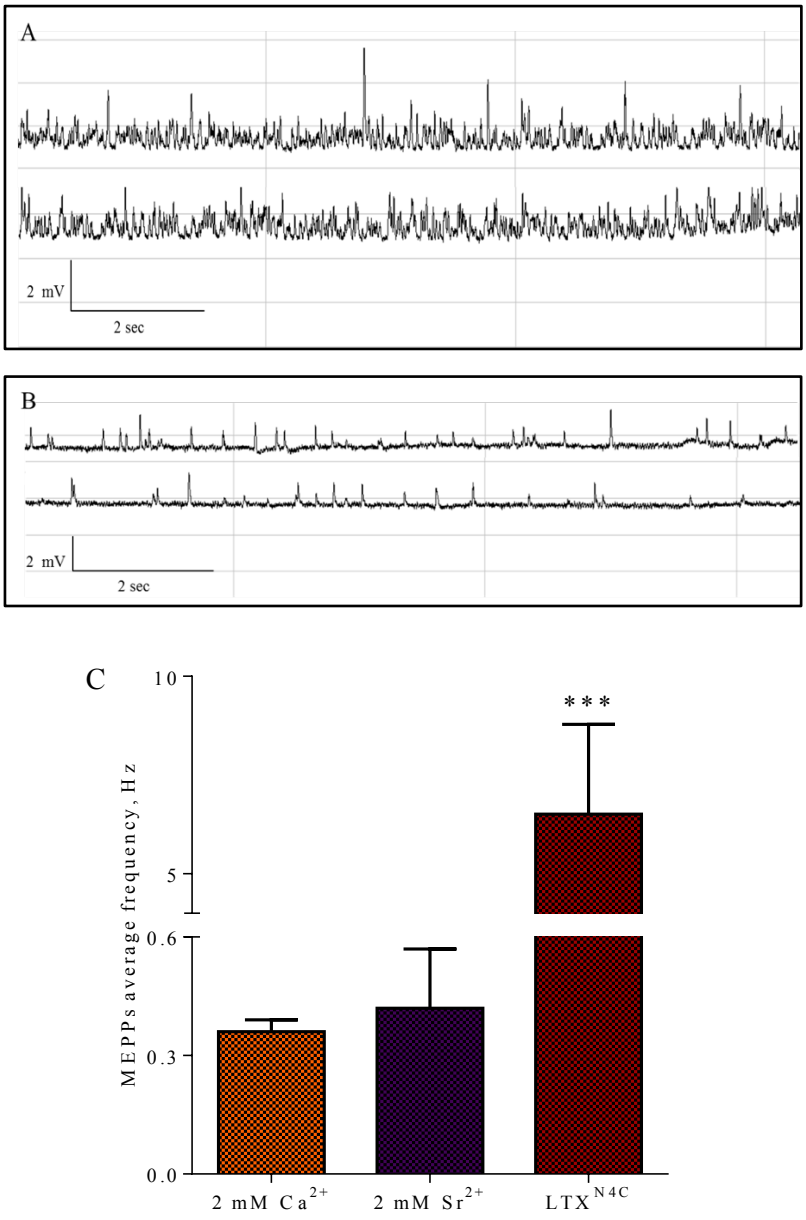

*Figure 4.22. Individual traces of MEPPs in Sr^{2+} buffer after the addition of LTX^{N4C}. A burst (A) and an interburst interval (B) are shown. C. Average frequency of MEPPs in Ca^{2+} buffer, Sr^{2+} buffer without Ca^{2+}, and after the addition of LTX^{N4C} (N = 2, n = 8 cells recorded in Ca^{2+} buffer, 5 cells in 2 mM Sr^{2+}, and 45 cells after the addition of LTX^{N4C}; ***, P < 0.001, Mann – Whitney U test).*

These results indicate that LTX^{N4C} does not require neurexins to stimulate exocytosis and suggest that LPHN1 plays a crucial role in toxin's effect. However, in the absence of Ca^{2+} the toxin can still interact with PTPσ (Krasnoperov et al. 2002), and although the toxin triggers a signalling cascade inconsistent with the stimulation of PTPσ (activation of Gαq, PLC and release of intracellular Ca^{2+}), some involvement of PTPσ in the massive exocytosis observed here could not be excluded.

4.2.9 LPHN1$^{-/-}$ neurons do not respond to LTX^{N4C}

To exclude the possibility that the effects on exocytosis described here are caused by the binding of LTX^{N4C} to either NRX or PTPσ, LPHN1$^{-/-}$ mice were used. LTX^{N4C} (0.1 nM) was added to the NMJ preparations in Ca^{2+}-containing buffer, and the frequency of MEPPs was recorded. As a confirmation of the results described earlier in this chapter (Section 4.2.2) the basal frequency of exocytosis in LPHN1$^{-/-}$ was significantly higher than in LPHN1$^{+/+}$ preparations (1.7 ± 0.3 Hz). Addition of LTX^{N4C} to LPHN1$^{-/-}$ preparations did not significantly change the frequency of exocytosis (1.8 ± 0.5 Hz). The same concentration of LTX^{N4C} was instead sufficient to cause an increase of exocytosis in $^{+/+}$ preparations, which went from a basal frequency of 0.37 ± 0.2 Hz to a frequency of 4.9 ± 0.8 Hz after the addition of LTX^{N4C} (Figures 4.23 and 4.24 A).

As expected, no bursts were found in the absence of LTX^{N4C} in both LPHN1$^{+/+}$ and $^{-/-}$ preparations; upon addition of 0.1 nM LTX^{N4C}, the bursts increased to 14/h in LPHN1$^{+/+}$ and 0.7/h in $^{-/-}$ cells (Figure 4.24 B).

The findings described here support the conclusions from the experiments with Ba^{2+} and Sr^{2+} and strongly suggest that the effects of LTX^{N4C} on exocytosis are mediated by the activation of LPHN1 rather than the other two toxin receptors (NRX and PTPσ).

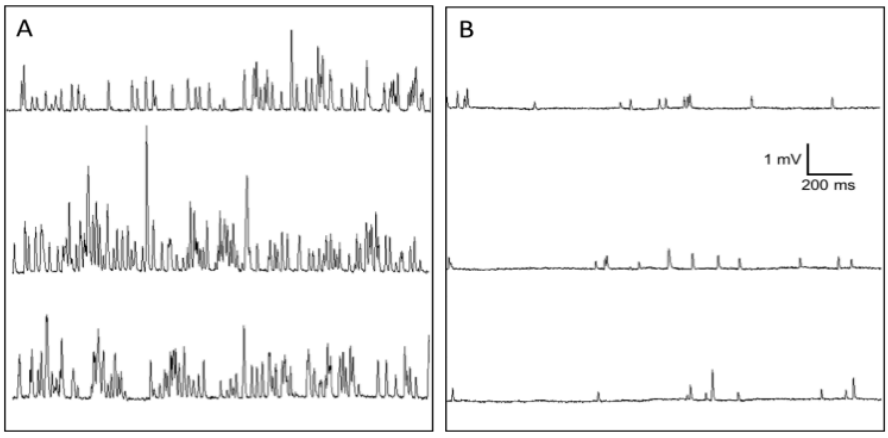

Figure 4.23. Individual traces of MEPPs after the addition of 0.1 nM LTX^{N4C} in LPHN1$^{+/+}$ (A) and $^{-/-}$ (B) NMJ preparations.

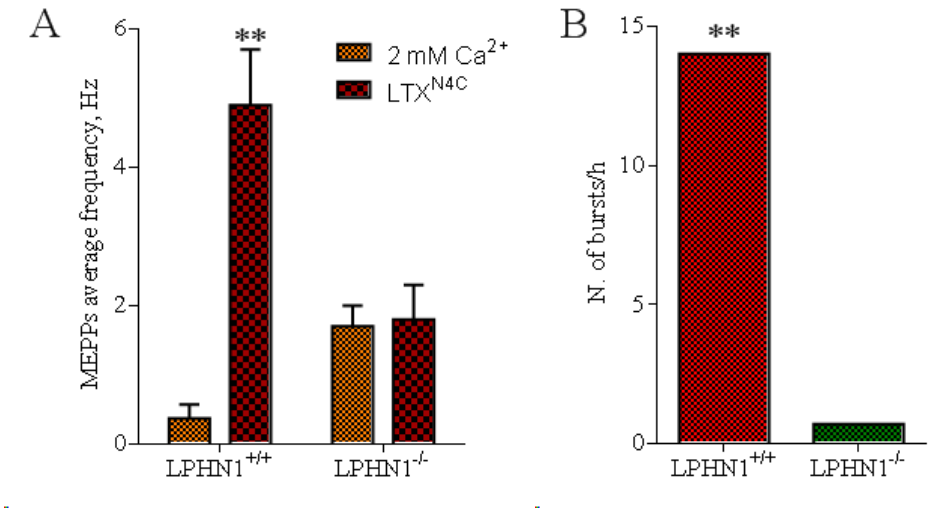

*Figure 4.24. A. Average frequency of MEPPs in LPHN1$^{+/+}$ and $^{-/-}$ NMJ preparations before and after the addition of 0.1 nM LTX^{N4C} in Ca^{2+}-containing buffer (n = 19 LPHN1$^{+/+}$ and 3 $^{-/-}$; **, P < 0.01). B. Number of bursts per hour in LPHN1$^{+/+}$ and $^{-/-}$ NMJs after the addition of 0.1 nM LTX^{N4C} in Ca^{2+} buffer (n = 3 LPHN1$^{+/+}$ and 3 $^{-/-}$; **, P < 0.01, Mann – Whitney U test).*

4.2.10 The dissociation of LPHN1 NTF and CTF impairs the response of LPHN1 to LTX^{N4C}

LPHN1 is composed of two functional parts, the extracellular N-terminal fragment (NTF) and the intramembrane C-terminal fragment (CTF), that need to interact in order to induce intracellular cascade that produce the effects on exocytosis described throughout this chapter.

Perfluorooctanoic acid (PFOA) is a weak detergent that can be used to solubilise multi-subunit protein without dissociating them into individual subunits. PFOA was used to study the interaction of the NTF and CTF of LPHN1 in rat brain synaptosomes by comparing its ability to solubilise the fragments with that of Thesit (Lubrol). While Thesit solubilised both fragments in parallel, by obviously disrupting the membrane (see Figure 4.25 A), PFOA solubilised the NTF and CTF differentially. In fact, at RT exposure of synaptosomes to increasing concentrations of PFOA caused the complete solubilisation of the NTF at 0.5% (12 mM) PFOA, together with a small amount of the CTF, and of both the NTF and CTF at much higher concentrations (>1%, 24 mM) (see Figure 4.25 B). The differential solubilisation was even more prominent at 4° C: in this case, while the NTF was removed from the membrane at PFOA concentration of 0.5%, the CTF did not get solubilised at any of the PFOA concentrations tested (see Figure 4.25 C) (Rahman, Ushkaryov, data not published).

An important conclusion could be made on the basis of these findings: although PFOA is a weak detergent and does not readily solubilise the cell membrane, it still breaks up the association between the NTF and CTF. The interaction of the two LPHN1 fragment is vital for the receptor to transduce its signal inside the cell, where the G protein initiates the intracellular cascade that in turn leads to the increase in exocytosis described. It is therefore possible that, if PFOA were able to dissociate NTF and CTF without disrupting the membrane and solubilising the NTF, the activation of LPHN1 by LTX^{N4C} would not have the usual outcomes on exocytosis. In fact, PFOA at concentrations below 300 μM is not toxic to cultured cells (Choi et al. 2013) and thus should not damage the plasma membrane, but could inhibit the NTF-CTF interaction.

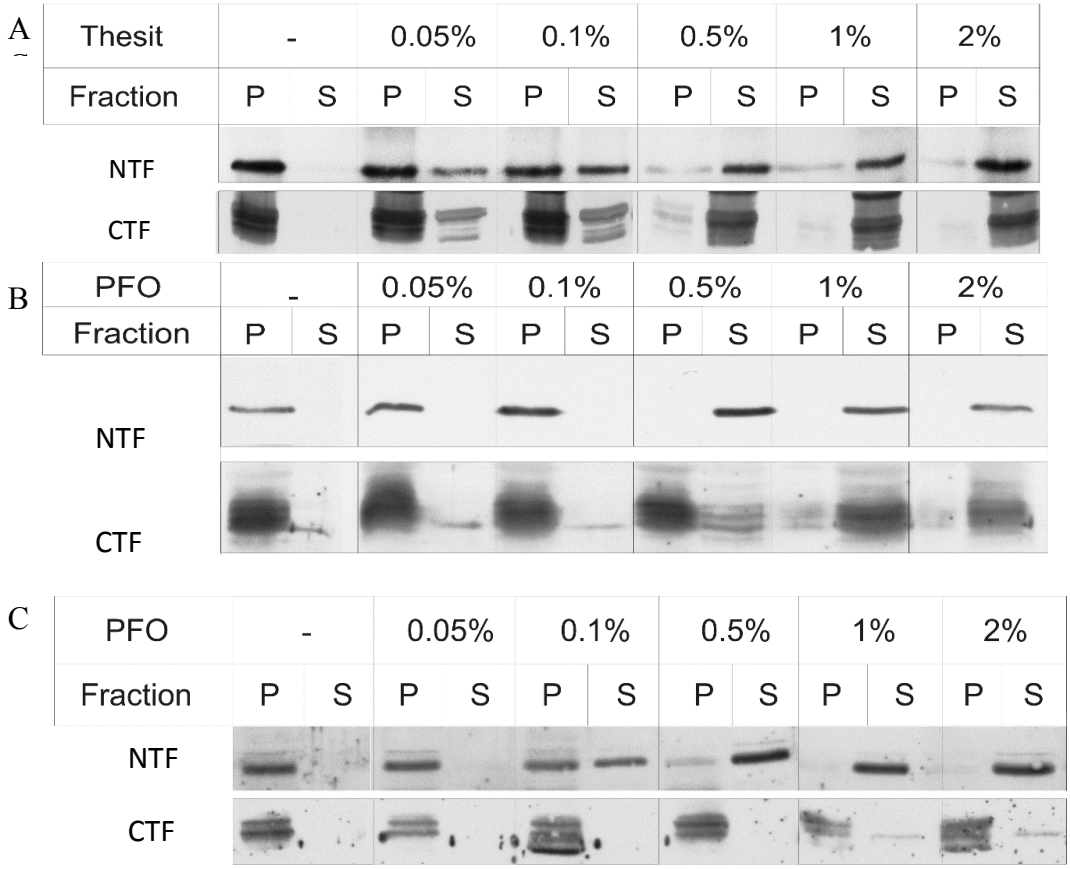

Figure 4.25. Solubilisation of LPHN1 NTF and CTF from rat brain synaptosomes by different concentrations of Thesit and PFOA. A. Thesit removes both fragments from the membrane equally (4 °C); both NTF and CTF start to go in solution at 0.05% and are completely solubilised at 0.5% Thesit. PFOA differentially solubilises NTF and CTF at RT (B) and at 4 °C (C). At both temperatures the NTF goes in solution at 0.5% PFOA; the CTF is solubilised at 1% PFOA at RT, but never at 0° C.

To test this hypothesis, the preparations were incubated with different concentrations of PFOA (0.2 – 100 µM) and LPHN1 was stimulated with LTX^{N4C} in order to investigate the possible changes in its activity.

A non-significant rise in the frequency of neurotransmitter release was observed after the addition of PFOA at all concentrations tested (0.69 ± 0.38 Hz). This rise in frequency, similar to the one observed in $LPHN1^{+/-}$ mice (0.56 ± 0.14 Hz), may

suggest that LPHN1 was already deregulated to some extent by PFOA, and that this deregulation is causing an increase in neurotransmitter release. The lack of statistical significance might be due to type II statistical error, which could be overcome by increasing the number of recordings in these conditions.

After the addition of PFOA, the LTX^{N4C}-induced rate of exocytosis was affected in a PFOA concentration-dependent manner. At increasing concentrations of PFOA the number of cells responding with bursting behaviour to LPHN1 stimulation by LTX^{N4C} decreased significantly, and the time for the toxin to develop its effects greatly increased. AT 100 μM PFOA the toxin was unable to cause any effect. (see Table 4.1 and Figure 4.26).

Table 4.1. Percentage of cells bursting, time to burst (min) and overall frequency (Hz) in the presence of different concentrations of PFOA after the addition of LTX^{N4C}.

[PFOA], μM	Cells bursting (%)	Time to burst (min)	Overall frequency (Hz)	N, number of muscles	n, number of fibres
0	89	17	15.50	2	38
0.2	82	23	13.72	2	28
1	40	24.5	7.66	2	25
10	21.5	21	1.87	2	27
50	12.5	59.5	1.56	2	32
100	0	∞	0.84	3	44

In all conditions where the cells responded to LTX^{N4C} bursting behaviour was present, and the average frequency of exocytosis inside the burst did not significantly differ from the control condition (Ca^{2+} buffer without the presence of PFOA), suggesting that although the activity of LPHN1 was impaired by the presence of PFOA, when the signalling was able to start to produce its effects the mechanism was fully functional and only its triggering was affected.

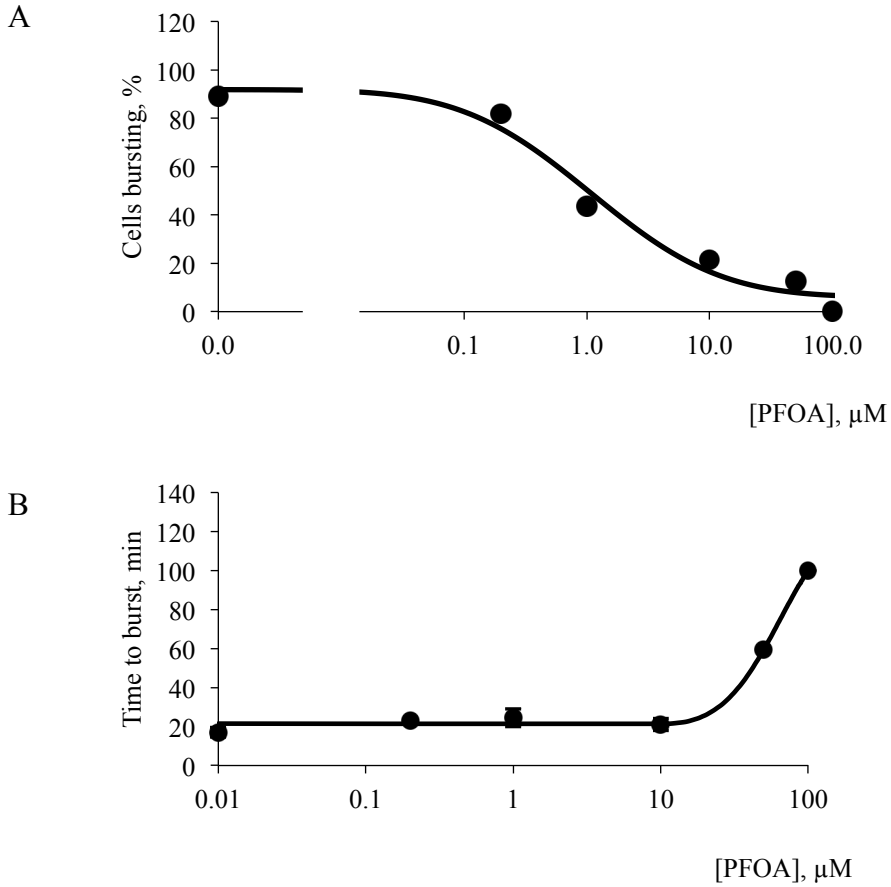

Figure 4.26. The percentage of cells bursting after the addition of LTX^{N4C} (A) and the time elapsed from the addition of the toxin and the observed effect (B) were plotted against the concentration of PFOA.

Exocytosis during bursts of activity showed a small, non-significant decrease with increasing PFOA concentration (Figure 4.27 A). However, because the number of cells responding to the stimulation of LPHN1 constantly fell with the increase in PFOA concentration, the overall frequency of neurotransmitter release consistently decreased going from 0 to 100 µM PFOA (Table 4.1 and Figure 4.27 B).

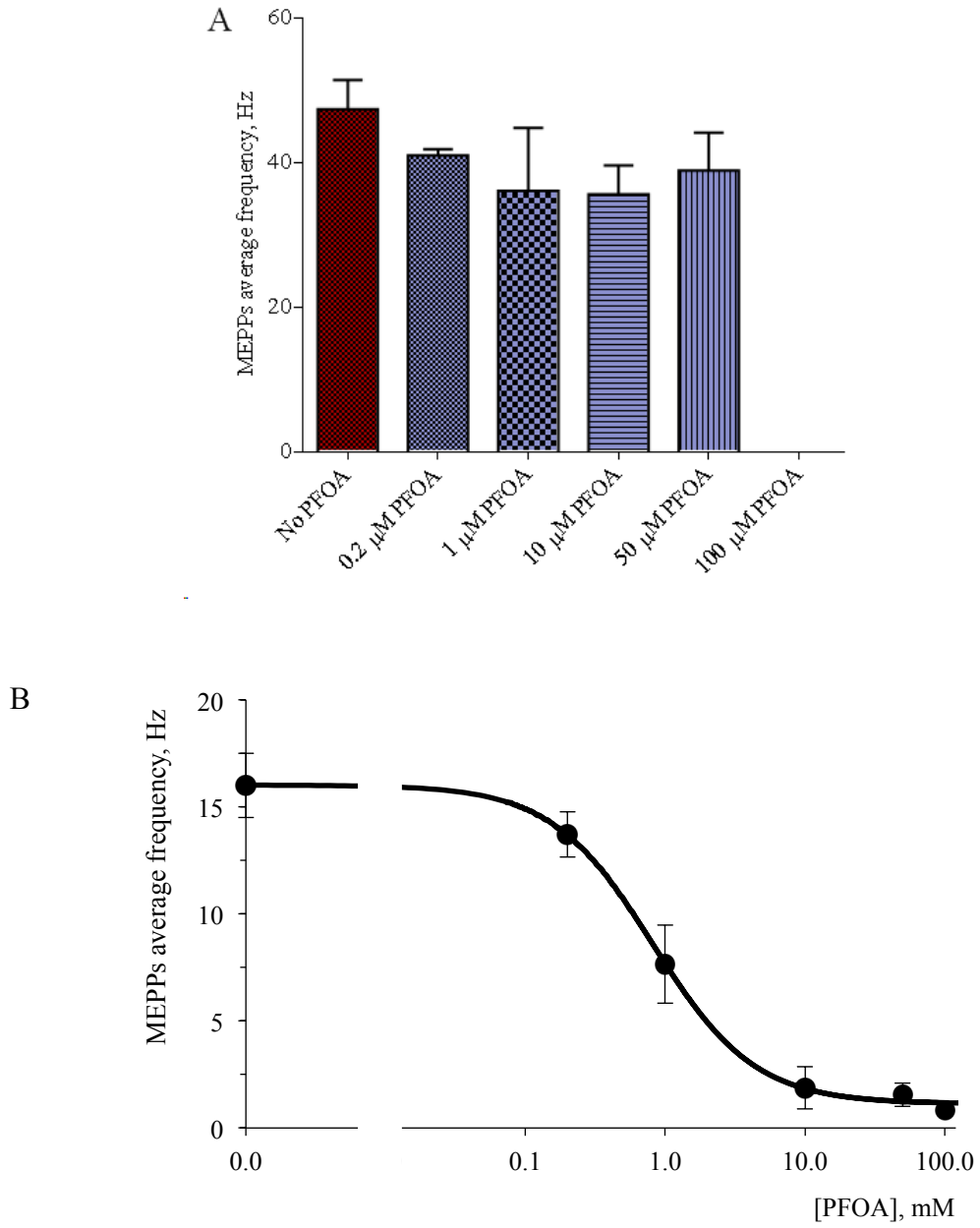

Figure 4.27. A. Average frequency of MEPPs during bursts at different concentrations of PFOA. The difference between the conditions is not statistically significant (n = 33 bursts in Ca^{2+} buffer, 22 in 0.2 µM PFOA, 11 in 1 µM PFOA, 6 in 10 µM PFOA and 4 in 50 µM PFOA). B. Overall average frequency of exocytosis after the addition of LTX^{N4C} at different concentrations of PFOA (n = 38 cells in Ca^{2+} buffer, 28 in 0.2 µM PFOA, 25 in 1 µM PFOA, 27 in 10 µM PFOA, 32 in 50 µM PFOA and 44 in 100 µM PFOA).

In a reverse experiment, 100 µM PFOA added after the increase of exocytosis caused by the activation of LPHN1 had already started was able to stop this effect almost completely. In fact, the overall frequency of exocytosis dropped from 15.50 ± 7.07 Hz observed after the addition of LTX^{N4C} in control conditions to 1.12 ± 0.52 Hz in the presence of 100 µM PFOA. The inhibition in the effects of LPHN1 activations happened in approximately 2 minutes. Of the 16 cells recorded, only 3 were still reacting to the toxin, one of them showing bursting behaviour (22 Hz during the burst) and the other two having an overall increased frequency of 2 and 6 Hz (Figure 4.28).

The presence of PFOA in the extracellular buffer did not cause any significant changes in the average MEPPs amplitude compared to the control in Ca^{2+} buffer (0.82 ± 0.11 mV in Ca^{2+}, 0.98 ± 0.05 mV in the presence of PFOA), nor did the subsequent addition of LTX^{N4C} (0.75 ± 0.03 mV in 0.2 µM PFOA, 0.76 ± 0.06 mV in 1 µM PFOA, 1.05 ± 0.04 mV in 10 µM PFOA, 1.06 ± 0.01 mV in 50 µM PFOA, and 0.77 ± 0.05 mV in 100 µM PFOA.

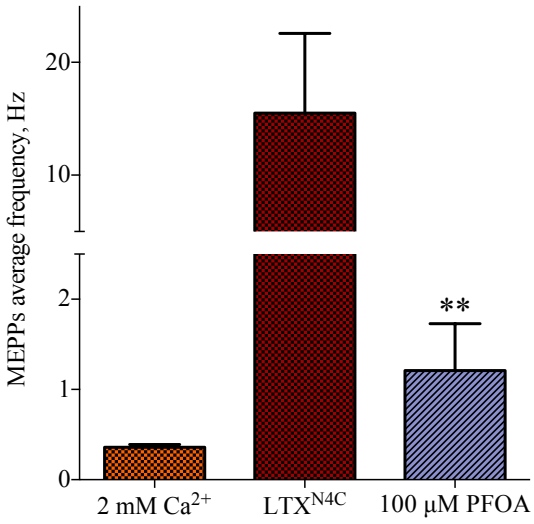

*Figure 4.28. Average frequency of MEPPs in Ca^{2+} buffer and after the addition of LTX^{N4C} and 100 µM PFOA. PFOA significantly inhibits the effects on exocytosis caused by the activation of LPHN1 (n = 19 cells recorded after the addition of LTX^{N4C} and 18 after subsequent addition of PFOA; **, P < 0.01, Mann – Whitney U test).*

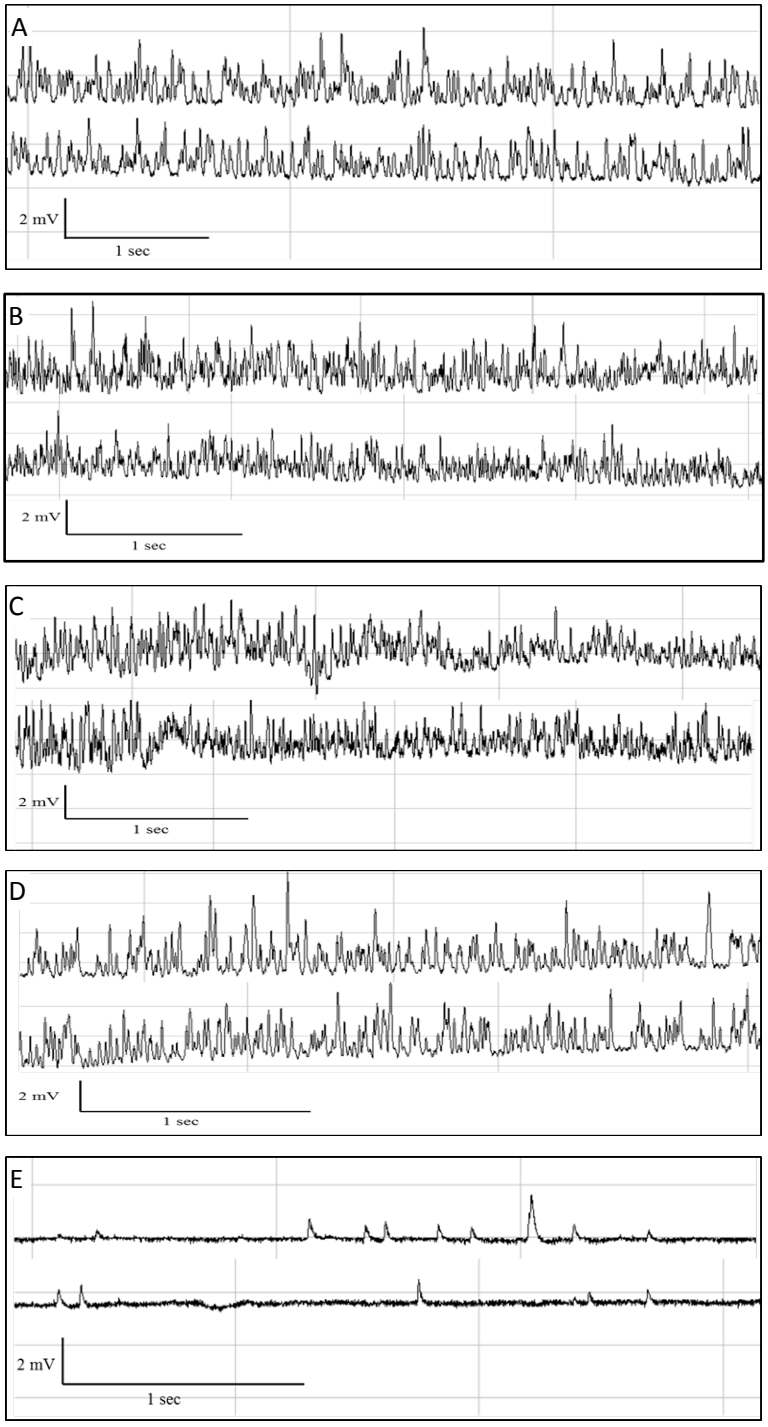

Figure 4.29. Single traces of MEPPs during bursts after the addition of LTX^{N4C} in 0.2 (A), 1 (B), 10 (C), and 50 (D) µM PFOA. The frequency of MEPPs inside the burst does not change between these conditions. No bursts develop in 100 µM PFOA (E).

To exclude the possibility that PFOA prevented the binding of the toxin to the receptor and therefore reduced or fully blocked LPHN1 activation by LTX^{N4C}, a binding experiment was performed under the same conditions used in the experiments described earlier. LPHN1-expressing neuroblastoma (Nb2a) cells were incubated with 5 nM αLTX in the presence of several PFOA concentrations (0.2, 50 and 100 µM). Nb2a cells not expressing LPHN1 were used as a control. Following incubation with the toxin, the amount of bound and unbound LTX^{N4C} was determined by Western blotting (see Chapter 2, Section 2.2.4 for details).
As shown in Figure 4.30, the concentrations of PFOA I used in the experiments on NMJ did not prevent the binding of LTX to LPHN1. This interaction was specific, as demonstrated by in a control experiment with WT neuroblastoma cells not expressing LPHN1.

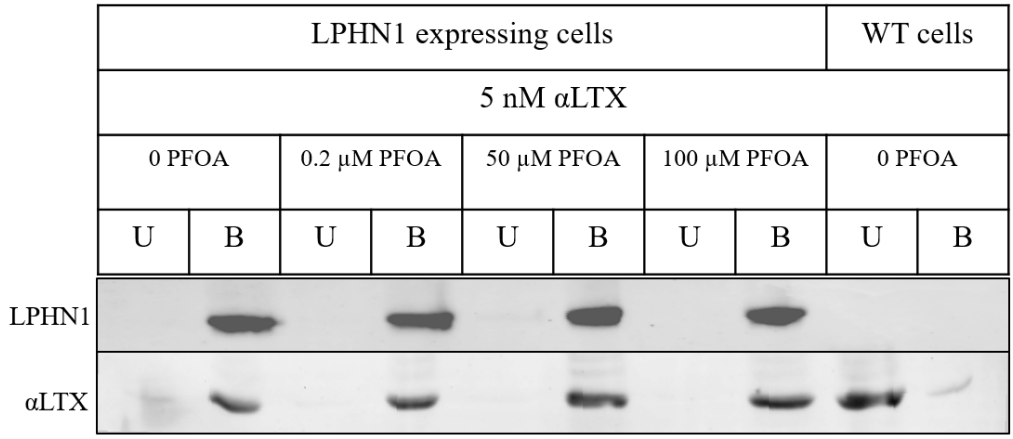

Figure 4.30. Western blot analysis of unbound (U) and bound (B) samples of αLTX to LPHN1 expressing cells. In LPHN1 expressing cells, αLTX band is visible only in the pellets containing the cells. By contrast, in WT cells most αLTX is present in the supernatant. As the purpose of this experiment was not to compare the amount of binding of the toxin to LPHN1 in the presence of different concentrations of PFOA, but only its presence or absence, a loading control was not included.

Interestingly, PFOA also affected depolarisation-induced exocytosis. One way to study spontaneous, asynchronous exocytosis is to increase the extracellular KCl concentration to depolarise cells. In our control experiments the NMJ preparations were initially incubated in Ca^{2+}-free buffer; subsequently 20 mM KCl and 2 mM Ca^{2+} were added to the buffer (as shown at the top of panel A in Fig. 4.31), and MEPPs were recorded in order to evaluate the changes in the frequency of exocytosis. No significant changes in exocytosis were detectable when KCl was added in the absence of Ca^{2+} (0.10 ± 0.01 Hz in Ca^{2+}-free buffer vs. 0.11 ± 0.05 Hz after the addition of 20 mM KCl); addition of Ca^{2+} caused a gradual but fast increase of neurotransmitter release (time from the addition to start, 22 ± 8 seconds) that reached an average of 16.13 ± 5.34 Hz, and then slowly decreased and fully seized in approximately 40 minutes (Figure 4.31). In both conditions (with/without extracellular Ca^{2+}) the resting membrane potential of the muscle fibres became more positive upon addition of KCl.

To investigate whether PFOA affects only LPHN1-mediated exocytosis or depolarisation-induced exocytosis as well, KCl was used to depolarise the membrane in the presence of different concentrations of PFOA. The concentrations used were 10 µM PFOA (the concentration at which LPHN1-mediated exocytosis showed strong impairment) and 100 µM PFOA (the concentration at which LPHN1-mediated exocytosis was completely blocked).

The presence of 10 µM PFOA to the buffer did not bring about any significant changes either in the frequency of exocytosis (11.63 ± 1.23 Hz, Figure 4.32, A) or to the time necessary to elicit the increase of exocytosis (67.5 ± 53 seconds, Figure 4.32, B).

With 100 µM PFOA, instead, the addition of 20 mM KCl was not able to cause any increase in the frequency of exocytosis (0.33 ± 0.28 Hz). To have an effect, it was necessary to increase the concentration of KCl to 40 mM (Figure 4.32 A), and also in this case the effect developed about 7 minutes after the addition of KCl (420 ± 60 seconds, Figure 4.32, B). At that point, no significant differences were observed in the frequency of exocytosis (17.56 ± 3.08 Hz).

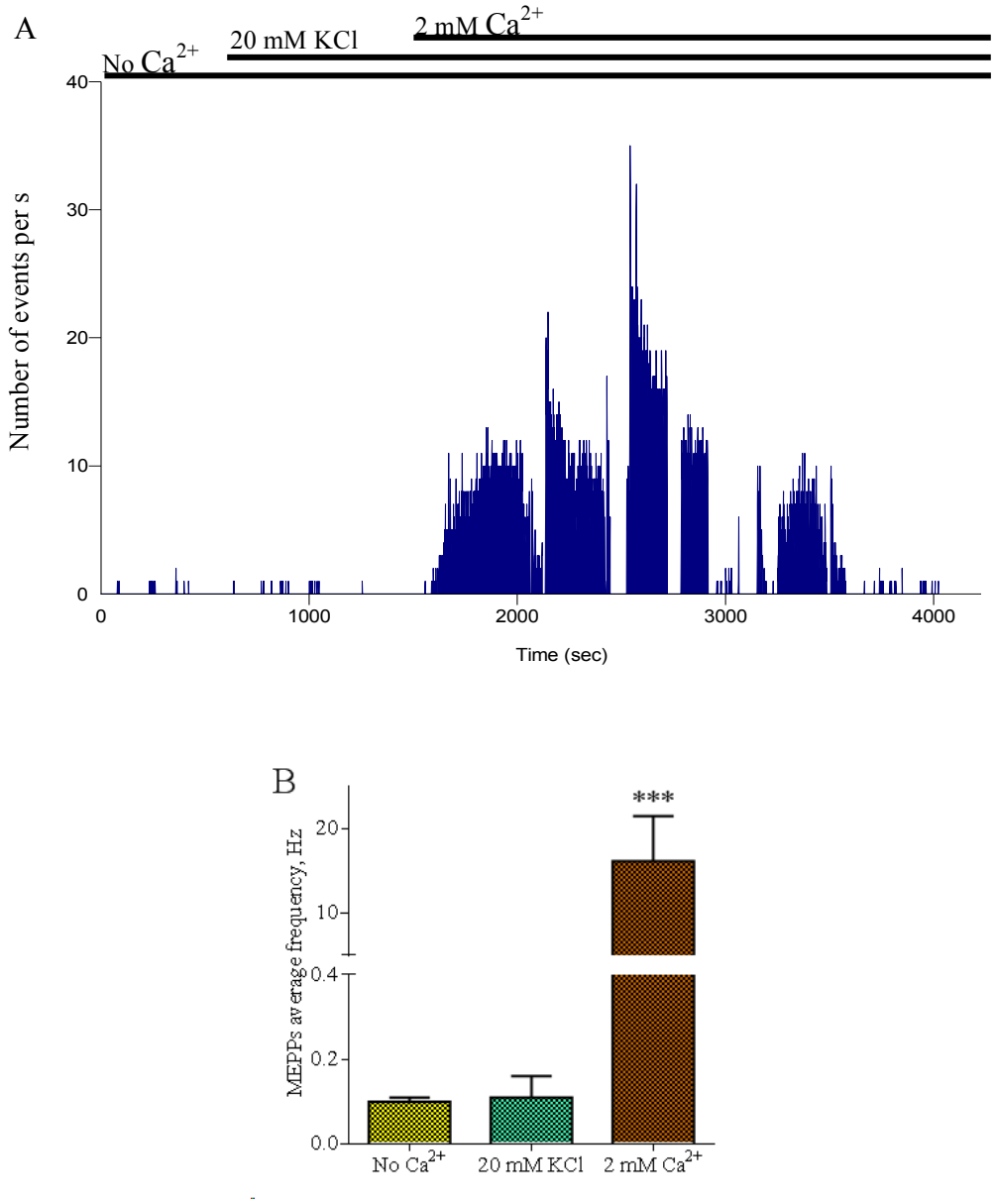

*Figure 4.31. Changes in the frequency of MEPPs after the sequential addition of 20 mM KCl and 2 mM Ca^{2+}. Recordings were made on multiple individual fibres as indicated by the breaks in the otherwise continuous data. Addition of KCl slightly depolarised the muscle fibres, causing an increased resting membrane potential. B. Average frequency of MEPPs in Ca^{2+}-free buffer, and after the sequential addition of 20 mM KCl and 2 mM Ca^{2+} (n = 10 cells recorded in Ca^{2+}-free buffer, 21 cells after addition of KCl, and 38 cells after subsequent addition of Ca^{2+}; ***, P < 0.001, Mann – Whitney U test).*

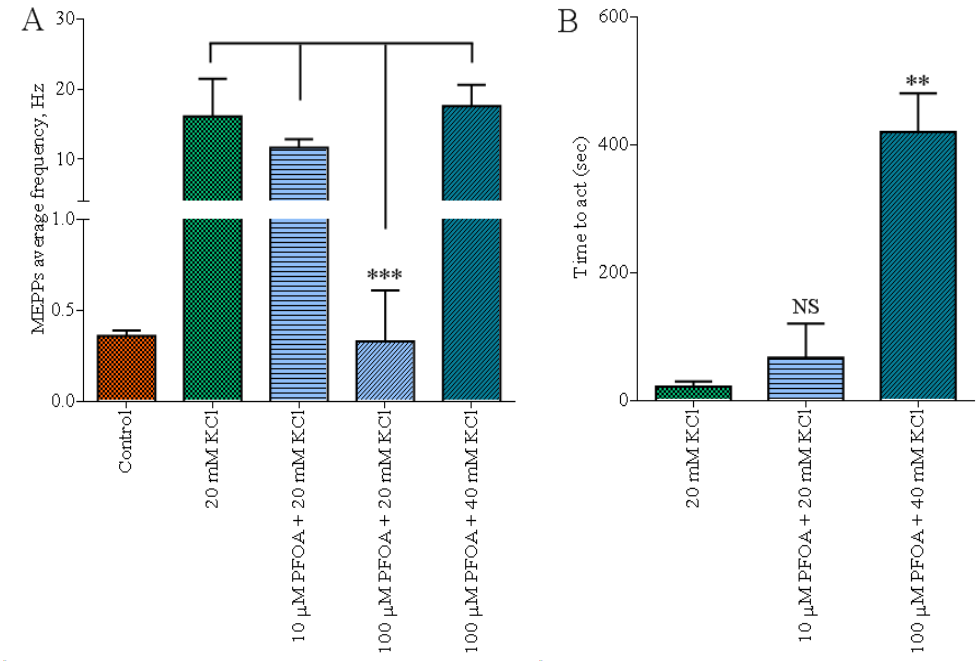

*Figure 4.32. A. Average frequency of MEPPs after the addition of 20 mM KCl in the presence of different concentrations of PFOA. To elicit a response in the presence of 100 µM PFOA it was necessary to double the amount of KCl used (n = 55 cells recorded in the presence of 20 mM KCl in Ca^{2+} buffer, 33 in 10 µM PFOA, 11 cells in 100 µM PFOA; 9 cells were recorded in the presence of 40 mM KCl in 100 µM PFOA; ***, P < 0.001, One-way ANOVA). The resting membrane potential was slightly increased after the addition of KCl. B. Time from the addition of KCl to the start of increased exocytosis. With 100 µM PFOA and 40 mM KCl, the difference is statistically significant (n = 2 experiments using 20 mM KCl in 10 µM PFOA and 2 experiments using 40 mM KCl in 100 µM PFOA; **, P < 0.01, Mann – Whitney U test).*

4.2.11 TTX-sensitive voltage-gated sodium channels and membrane depolarisation are not required for LPHN1-mediated increase in exocytosis

Due to some similarities in the behaviour of LTX^{N4C} and KCl-induced exocytosis and based on earlier reports that LTX^{N4C} can inhibit voltage-gated potassium channels (Lang et al. 1998; Lajus et al. 2006), there remained a possibility that LTX^{N4C} acted by depolarising the membrane. To investigate whether voltage-gated Na^+ channels and cell depolarisation are involved in the activity of LPHN1, I used tetrodotoxin (TTX). Produced by endosymbiotic bacteria and found principally in fish belonging to the *Tetraodontiformis* family, this potent neurotoxin is able to block voltage-gated Na^+ channels, by binding to and closing their pore domain, and thus inhibit the formation of action potentials.

NMJ preparations were bathed in Ca^{2+}-containing buffer (2 mM) and 1 μM TTX was added; no significant changes in the frequency of exocytosis were detectable between this two conditions (0.36 ± 0.03 Hz in Ca^{2+} buffer vs. 0.57 ± 0.17 Hz after the addition of TTX). Subsequent addition of 0.25 nM LTX^{N4C} was able to elicit an increase in exocytosis, in all features comparable with the increase obtained in control conditions, showing bursting behaviour. The overall frequency of exocytosis was 18.78 ± 4.52 Hz, and the frequency during the burst was of 33.48 ± 4.42 Hz (Figures 4.33 and 4.34 A).

The presence of TTX in the buffer did not significantly change the average amplitude of MEPPs (0.81 ± 0.07 mV), neither did the addition of LTX^{N4C} (1.04 ± 0.01 mV, Figure 4.34 B).

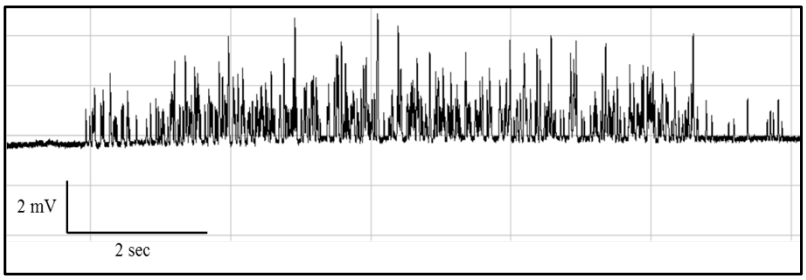

Figure 4.33. Single trace of a MEPPs recording showing a burst in the presence of 1 μM TTX.

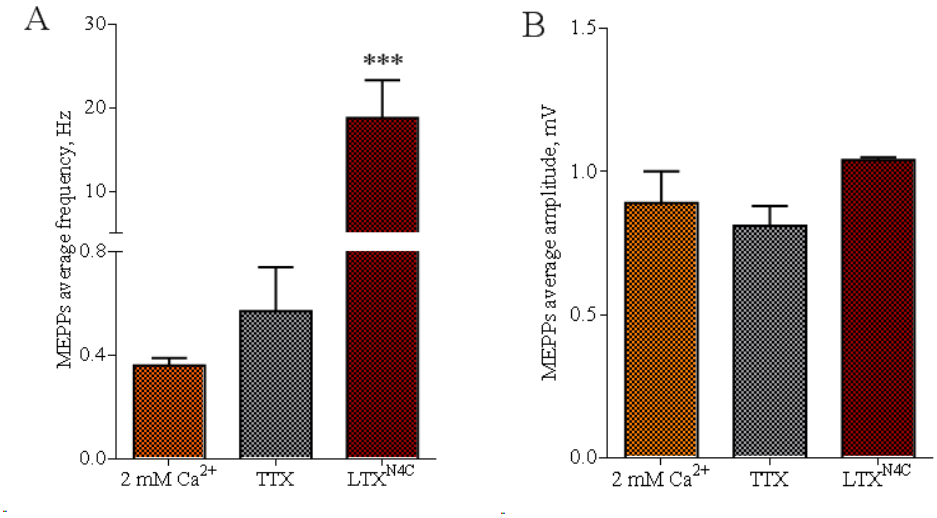

*Figure 4.34. A. Average frequency of MEPPs in Ca^{2+}-containing buffer and after the addition of TTX and LTX^{N4C}. 1 μM TTX does not inhibit the increase in exocytosis caused by the activation of LPHN1 by LTX^{N4C}. B. Average amplitude of MEPPs in Ca^{2+} buffer and after the addition of TTX and LTX^{N4C}. The difference between the conditions is not statistically significant (n = 6 cells in Ca^{2+} buffer, 5 cells after addition of TTX and 12 cells after addition of LTX^{N4C}; ***, P < 0.001, Mann – Whitney U test).*

4.3 Discussion

The purpose of the experiments described in this chapter was to analyse spontaneous neurotransmitter release and the role that LPHN1 plays in this process. To do so, the basal frequency of exocytosis was studied in LPHN1 WT, Het and KO mice, using as a model system either the neuromuscular junction (NMJ) and primary cultures of pyramidal neurons.

The NMJ is a well establish model system to study the physiological mechanisms of synaptic transmission. Its structure has been extensively studied since the early 20th century, using gold or silver staining techniques and visualised with light microscopes. Later on in the 1950s, electron microscopy studies showed the high density of synaptic vesicles in the presynaptic terminals and the folding of the postsynaptic membranes at motor endplates associated with the postsynaptic densities (De Robertis 1958; Heuser 1989; Ribchester 2009) .

Studies at the frog NMJ demonstrated that muscular contraction happens in response to electrical stimulation of the innervating neuron and that acetylcholine (ACh) is the neurotransmitter used in these synapses. Moreover, NMJ studies gave strong support to one of the central neurobiological dogmas, that is that neurotransmitters are released from presynaptic vesicles by Ca^{2+}-dependent exocytosis, followed by endocytosis and refilling of the vesicles with ACh (del Castillo and Katz 1956; Ceccarelli and Hurlbut 1980a; Ceccarelli and Hurlbut 1980b; Heuser 1989; Ribchester 2009) .

To study neurotransmitter release at the NMJ I used sharp electrodes and the current clamp approach. This is an intracellular recording technique used to record spontaneous MEPPs. This approach, developed in the 1950s by Bernard Katz on the frog NMJ (Fatt and Katz 1952), consists in applying an electrical current to a cell using a microelectrode, and recording the fluctuations in the membrane voltage of that cell through an amplifier. In this method (such as in the voltage clamp method, used in the experiment in central synapses and discussed later), the changes in the postsynaptic membrane potential are recorded to evaluate the presynaptic release of vesicles filled with neurotransmitter.

As well as in the peripheral nervous system (PNS), I examined neurotransmitter release also in the central nervous system using as a model the pyramidal neurons of the hippocampus.

In central neurons, excitatory responses are mediated by glutamate acting on AMPA and NMDA receptors (Hestrin et al. 1990), while inhibitory responses are mediated by GABA acting on $GABA_A$ and $GABA_B$ receptors (Isaacson, Solis and Nicoll 1993).

To study neurotransmitter release at central synapses I used the whole-cell voltage clamp approach. In this technique, the membrane potential is held to a desired voltage, and by doing so it is possible to measure the flow of current through the membrane of cells and thus directly detect the opening of ion channels (Cole 1949).

At the mouse NMJ, the basal rate of spontaneous exocytosis in Ca^{2+}-containing buffer is of about 1 vesicle every 3 seconds. Removal of Ca^{2+} from the extracellular buffer causes a significant decrease in the rate of neurotransmitter release, that drops to 1 vesicle released approximately every 10 seconds.

This result supports the observation that spontaneous asynchronous release is dependent on the extracellular Ca^{2+} concentration ($[Ca^{2+}]_e$) (Glitsch 2008; Ermolyuk et al. 2013), whilst it seem to contradict other findings according to which $[Ca^{2+}]_e$ would only weakly influence this kind of exocytosis, especially at the NMJ (Smith et al. 2012; Ramirez and Kavalali 2011).

Things change when the basal frequency of release is analysed in LPHN1 Het and KO mice. At the NMJ, the frequency of exocytosis consistently increases going from LPHN1 WT, Het and KO: as I already mentioned, in LPHN1 WT mice 1 vesicle is released every 3 seconds when Ca^{2+} is present in the extracellular buffer; in Het mice the rate goes up with 1 vesicle released every 2 seconds and in KO mice there is a further increase to 2 vesicles every 1.2 seconds.

When Ca^{2+} is removed from the extracellular buffer, I find the same tendency of increased exocytosis between the three genetic backgrounds. In LPHN1 WT mice, the rate of spontaneous release is of 1 vesicle released every 10 seconds; in Het mice the rate goes up to 1 vesicle released every 4 seconds, and in KO mice it goes further up to 1 vesicle released every 1.6 seconds.

These results strongly support the hypothesis that LPHN1 has a role in the control and regulation of spontaneous exocytosis. The involvement of LPHN1 in this process was already previously demonstrated by the fact that its activation by α-LTX or LTX^{N4C} leads to a dramatic increase in the frequency of neurotransmitter release both at the mouse NMJ and in central synapses (Davletov et al. 1998; Capogna et al. 2003; Lelyanova et al. 2009). However, our experiments conducted using LPHN1 KO models show that LPHN1 controls exocytosis not only upon its activation, but also in resting conditions, when LPHN1 seems to have a role in restricting Ca^{2+} influx and thus reducing the rate of spontaneous neurotransmitter release.

Other suggestions about the physiological role of LPHN1 come from the experiments conducted on cultured pyramidal neurons. Initially designed to investigate spontaneous exocytosis in the same way as in the NMJ, results in central synapses showed an inverse trend, with the frequency of release observed in LPHN1 KO neurons being lower than that in WT neurons. However, LPHN1 WT cultures had a significantly higher cell density and, consequently, a larger number of synaptic connections than LPHN1 KO cultures. This played an important role in the recorded synaptic activity and, therefore, further experiments using equal-density cultures (or pairs of cultured neurons forming monosynaptic connections) should be conducted. Nonetheless, these results suggest that LPHN1 may be important for neuronal survival and connectivity (a view supported by Boucard et al. 2014).

Another thing to notice is that the majority of PSCs recorded in both WT and KO neurons were inhibitory in nature. This suggests that the connections present in the cultures were mostly due to interneurons connected to the pyramidal cells, rather than being the pyramidal cells communicating between them. This suggests a bigger role of LPHN1 in the survival of pyramidal neurons compared to interneurons.

Experiments were conducted on mouse NMJ in order to investigate the effects that the stimulation of LPHN1 using LTX^{N4C} has on the release of neurotransmitter. The results collected confirm previous studies that showed how the activation of LPHN1 led to an increase in exocytosis (Capogna et al. 2003;

Lelyanova et al. 2009). However, due to the difficulties in maintaining a good seal in the patch-clamp recordings in the absence of Ca^{2+}e, Ca^{2+} was never completely removed in that work (Capogna et al., 2003). In the present work, LTX^{N4C} was added to the preparations in the presence or in the total absence of extracellular Ca^{2+}. Being still able to bind LPHN1 in the absence of extracellular Ca^{2+} (Davletov et al. 1996b) , LTX^{N4C} should be able to activate the receptor and start the intracellular signalling also in this condition. However, when Ca^{2+} is not present in the extracellular buffer, no increase in exocytosis is observed. The effect starts as soon as Ca^{2+} is added to the buffer (within 1 minute), leading to an increase of about 160 times compared to the basal frequency observed in the absence of Ca^{2+}. When LTX^{N4C} is added directly in Ca^{2+}-containing buffer, however, its effects do not develop immediately, but always after a delay of about 17 minutes. This suggests that LPHN1 needs time to activate the molecular pathways that lead to the increased exocytosis.

An interesting characteristic of the LTX^{N4C}-evoked neurotransmitter release is that it goes through waves of increased activity (bursts of exocytosis) interspersed with periods of moderate activity, where the frequency is only slightly higher than that observed in resting conditions. Depending on LTX^{N4C} concentration, the frequency of MEPPs in these bursts can reach 100 to 200 Hz, while the bursts are quite irregular both in pattern and in length, ranging from a few seconds to a couple of minutes. The interburst intervals have an average MEPPs frequency closer to control conditions and their length can also vary from 10 seconds to several minutes. This behaviour suggests that LPHN1 causes waves of increased intracellular Ca^{2+} concentration, which in turn lead to waves of increased exocytosis. Whether the Ca^{2+} responsible for this elevation comes from intracellular Ca^{2+} stores or from the opening of some Ca^{2+} channels on the plasma membrane is not determined yet, and will be investigated in details in further chapters.

Extracellular Ca^{2+} seems to be crucial for the effects of LPHN1 activation by LTX^{N4C} to start manifesting. At least two possibilities could explain this dependency: either (1) Ca^{2+} is needed outside the cells, for example, to enhance the binding of LTX^{N4C} to LPHN1 and/or LPHN1 activation, or (2) Ca^{2+} needs to

enter the nerve terminals and thus increase neurotransmitter release. The Ca^{2+}-independency of the binding of LTX^{N4C} to LPHN1 has been demonstrated previously (Davletov et al. 1996a) . Furthermore, our experiments using intracellular Ca^{2+} chelator BAPTA-AM strongly suggest that the mutant LTX^{N4C} is unable to cause increased neurotransmitter release even in the presence of extracellular Ca^{2+}, when Ca^{2+} is chelated within the cytosol. This suggests that specifically cytosolic Ca^{2+} is required for LTX^{N4C}-stimulated LPHN1 to trigger exocytosis.

So far, two endogenous ligands for LPHN1 have been described (Silva et al. 2011; O'Sullivan et al. 2012). The first was isolated by affinity chromatography of solubilised rat brain on the N-terminal domain of LPHN1 and termed Lasso. It is a postsynaptic protein belonging to the Teneurin family, but its function and the role of its interaction with LPHN1 are still unclear (Silva et al. 2011). The second, FLRT3, a protein with roles in axon guidance and cell migration for Uncoordinated-5-expressing neurons during the development of the CNS, was identified by low-stringency immunoprecipitation with the N-terminus of LPHN3, whose structure is only partially homologous to that of LPHN1 (O'Sullivan et al. 2012).

The interaction of both Lasso (teneurin-2) and FLRT3 with LPHN1 in low-stringency conditions were subsequently confirmed by cell-expression experiments (Boucard et al. 2014). However, the FLRT3 did not bind LPHN1 in affinity chromatography (Silva et al. 2011). This can be explained by the use of LPHN1 constructs expressing in different cell lines: Silva et al. (2011) used neuroblastoma NB2a cells, while all other authors used HEK293 cells.

Our laboratory has studied the ability of different cell lines to produce native LPHN1 and determined that the protein expressed in neurons or neuron-like cells, such as NB2a differs in its secondary structure from LPHN1 expressed in non-neuronal cells, such as HEK293 and CHO. Moreover, only the neuronal/NB2a-expressed LPHN1 retains the ability to bind αLTX and mediate its effect (Y. Ushkaryov, personal communication). This promiscuity of LPHN1 interactions, dependent on the site of LPHN1 synthesis, may be a rather significant observation from the point of view of the role that LPHN1 plays in the

brain as opposed to other tissues, where it is expressed in small amounts (Ichtchenko et al. 1999; Matsushita, Lelianova and Ushkaryov 1999). However, importantly for our findings, all LPHN1 used this project was produced in NB2a cells or in native neurons and therefore was most likely linked to Lasso.

Experiments were therefore conducted using a recombinant fragment of Lasso which had been shown to induce presynaptic Ca^{2+} signals in central synapses (Silva et al. 2011). In the instance of mouse NMJs, however, no significant changes in the frequency of exocytosis were observed (Figure 4.20). This observation may indicate that LPHN1-Lasso interaction does not directly regulate exocytosis, or at least not under the conditions tested in this work. Lasso is a member of the teneurin family, a class of proteins involved in neuronal development, axon guidance and synaptogenesis (Tucker et al. 2007; Young and Leamey 2009). This could suggest that LPHN1-Lasso interaction is involved in the synapses formation and survival. Such a conclusion is consistent with the LPHN1 KO cultures demonstrating poor synaptic connectivity and neuronal survival rate compared to WT ones.

My experiments also, for the first time, have addressed the possibility that LTX^{N4C} effects could be mediated not only by LPHN1, but also by other receptors able to bind LTX^{N4C}, mainly NRX Iα. Exploiting the ability of LPHN1 to bind LTX^{N4C} in any ionic condition and the strict requirement of Ca^{2+} for LTX^{N4C}-NRX Iα interaction (Petrenko et al. 1990; Davletov et al. 1995; Geppert et al. 1998), the replacement of Ca^{2+} in the extracellular buffer by Ba^{2+} and Sr^{2+} (Figure 4.21 and 4.22) confirms that LTX^{N4C} does not require NRX Iα (or any other neurexins, which all need Ca^{2+}, Geppert et al. 1998). Even more importantly, the use of NMJ preparations from mice lacking LPHN1 strongly support the hypothesis that LPHN1 is the only receptor that mediates the effect of LTX^{N4C} (Figure 4.24).

Another suggestion that LPHN1 is responsible for mediating the effects on exocytosis observed upon addition of LTX^{N4C} comes from our experiments using PFOA. When synaptosomes are incubated with PFOA, the NTF and CTF of LPHN1 are differentially solubilised; this can suggest that PFOA is able to prevent the interaction between the two LPHN1 fragments, with potential

repercussions for the LPHN1-mediated signalling and exocytosis. Indeed, at any PFOA concentration higher than 0.2 μM LPHN1-mediated exocytosis was impaired in a concentration-dependent manner and completely blocked by 100 μM PFOA (Figure 4.26), a concentration that does not disrupt LTX^{N4C}-LPHN1 interaction (Figure 4.30) nor causes any cytotoxic effects (Choi et al. 2013). Thus, the interaction between NTF, which binds LTX^{N4C}, and CTF, which mediates intracellular signalling, is essential for LTX^{N4C}-induced exocytosis.

Very interestingly, at higher concentrations, PFOA also retards the depolarisation-induced neurotransmitter release and requires higher concentration of KCl to stimulate exocytosis (Figure 4.32). This result suggests that the dissociation of NTF and CTF of LPHN1 impairs the ability of presynaptic terminals to respond to depolarisation. This observation is comparable to the one obtained when hippocampal neuronal cultures were treated with a soluble form of LPHN1 (Ushkaryov, data not published). When the soluble ectodomain of LPHN1 was added to the cultures at an early stage of synapse development, the interaction between endogenous LPHN1 and its postsynaptic ligand (most likely Lasso) was perturbed, leading to the loss of LPHN1 from presynaptic nerve terminals. As a result, the synapses formed in this culture were largely insensitive to moderate depolarisation. This synaptic inactivity could be overcome by a stronger or longer-lasting depolarisation. The conclusion from that work is that LPHN1 contributes to the ability of presynaptic terminals to respond to depolarisation by enabling Ca^{2+} influx. This may be due to a decreased activity of VGCCs or their inappropriate localisation in the active zone. In this case, the loss of presynaptic LPHN1 could be compared to the dissociation (and inhibition) of LPHN1 by PFOA, which also leads to synaptic insensitivity to depolarisation. Both experiments suggest that LPHN1 plays a central role in Ca^{2+} maintenance at the presynaptic terminal.

Taken together, these results confirm the involvement of LPHN1 in the regulation of exocytosis, and show that the activation of this receptor by LTX^{N4C} causes waves of exocytosis, which most likely follow the waves of increased intracellular Ca^{2+} concentration. However, the molecular mechanisms underlying the effects of LPHN1 signalling remain unclear. The purpose of the next chapters

is to investigate which intracellular pathways are induced on LPHN1 activation and the source of the Ca^{2+} responsible for the intracellular oscillations that lead to the bursting exocytosis.

CHAPTER 5
RESULTS III. The intracellular pathways of LPHN1 signalling

5.1 Introduction

As discussed in Chapter 4, LPHN1 is involved in the control of spontaneous exocytosis: LPHN1 KO and, to a lower degree, Het mice show deregulations in the rate of spontaneous neurotransmitter release at the NMJ. Experiments on central synapses also suggest a role of LPHN1 in neuronal survival and connectivity.

My results from experiments using LTX^{N4C} confirm previous studies that showed how the activation of LPHN1 leads to a dramatic increase in the rate of exocytosis (Capogna et al. 2003; Lelyanova et al. 2009); I showed that in order for this increase to happen extracellular Ca^{2+} is needed. In fact, in Ca^{2+}-free buffer the frequency of exocytosis does not significantly change compared to the baseline.

Although the effects of the activation of LPHN1 have now been confirmed in the current project, little has been known about the molecular mechanisms that cause them. In this chapter I explore the intracellular pathways involved in this activation.

First, I investigated what Gα protein subunit is activated by LPHN1; I then interfered with the intracellular molecular components of the pathway activated by the G protein in order to ascertain whether these are responsible for the effects observed when LPHN1 is activated.

5.2 Results

5.2.1 $G\alpha_q$ is involved in the activity of LPHN1

Previous studies showed that LPHN1 is coupled to G proteins; in particular, affinity chromatography of solubilised rat brain membranes using an αLTX column showed that $G\alpha_o$ and $G\alpha_{q/11}$ are associated with LPHN1, which was isolated on the toxin column (Rahman et al. 1999).

To ascertain that the effects observed when LPHN1 is activated are mediated by one of these G proteins, I performed LTX^{N4C}-induced stimulation of the mouse NMJ in the presence of an inhibitor specific for the $G\alpha_{q/11}$. This molecule, called UBO-QIC, is an analogue of YM254890; extracted from the plant *Ardisia crenatasims*. UBO-QIC is an acyclic depsipeptide that inhibits the $G\alpha_{q/11}$ signalling by directly binding to this G protein and inhibiting the release of GDP (Bernard et al. 2014).

When added in Ca^{2+}-containing buffer (2 mM) at the beginning of the recordings, UBO-QIC prevented the LPHN1-mediated activity by interfering with its molecular signalling pathway. In fact, when 0.25 nM LTX^{N4C} was added after 1 μM UBO-QIC, the toxin was not able to produce the typical effects I described in the previous chapter (see Chapter 4, Sections 4.2.4 and 4.2.5). The MEPPs frequencies were 0.33 ± 0.08 Hz in Ca^{2+} buffer with UBO-QIC, 2.28 ± 1.99 Hz in Ca^{2+} buffer with UBO-QIC and LTX^{N4C} (Figure 5.2 A, B, C).

No differences in the average amplitude were present between the experimental conditions considered (0.82 ± 0.11 mV in Ca^{2+} buffer, 0.81 ± 0.06 mV in the presence of UBO-QIC, and 0.92 ± 0.01 mV after the addition of LTX^{N4C}, Figure 5.2, D).

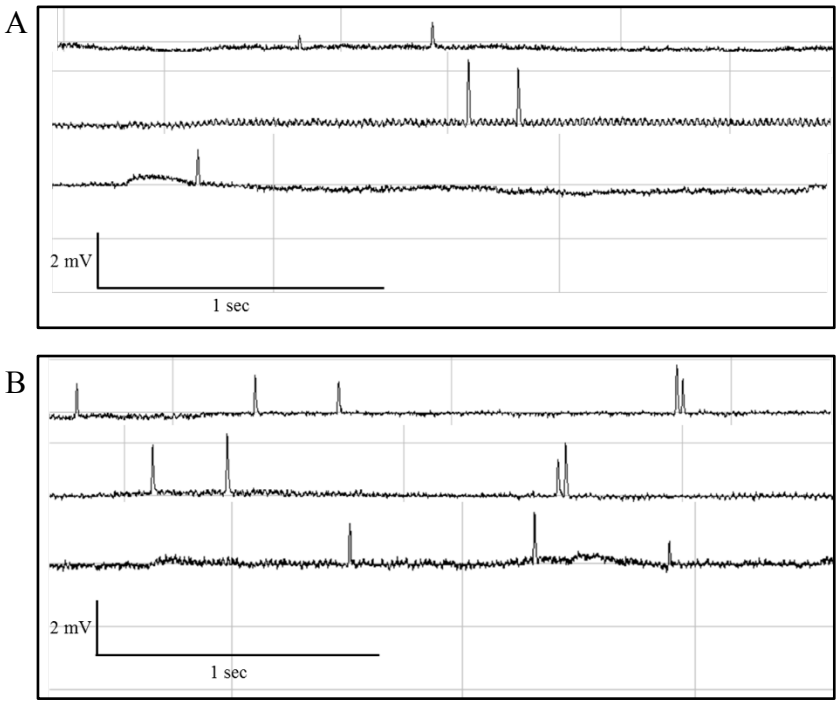

Figure 5.1. Single traces of MEPPs recordings in Ca^{2+} buffer after the addition of UBO-QIC (A) and LTX^{N4C} (B). The addition of LTXN4C does not cause increased exocytosis in the presence of UBO-QIC.

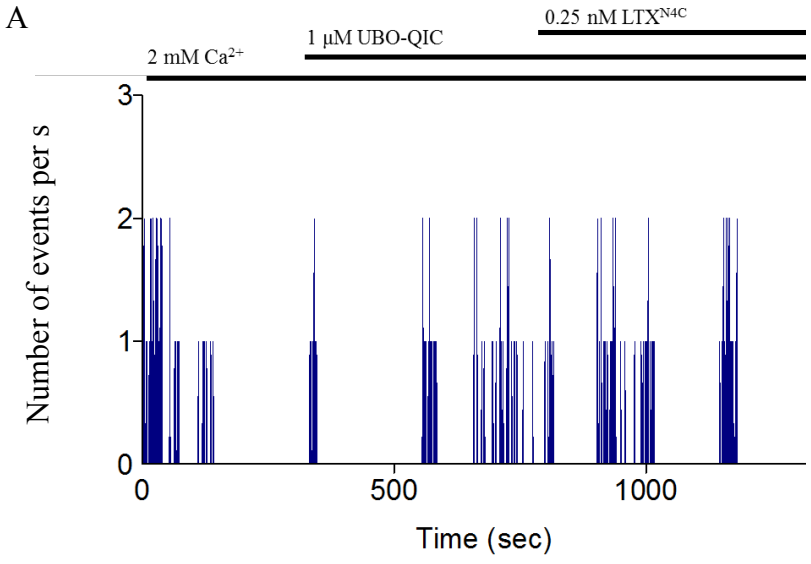

Continued on the next page

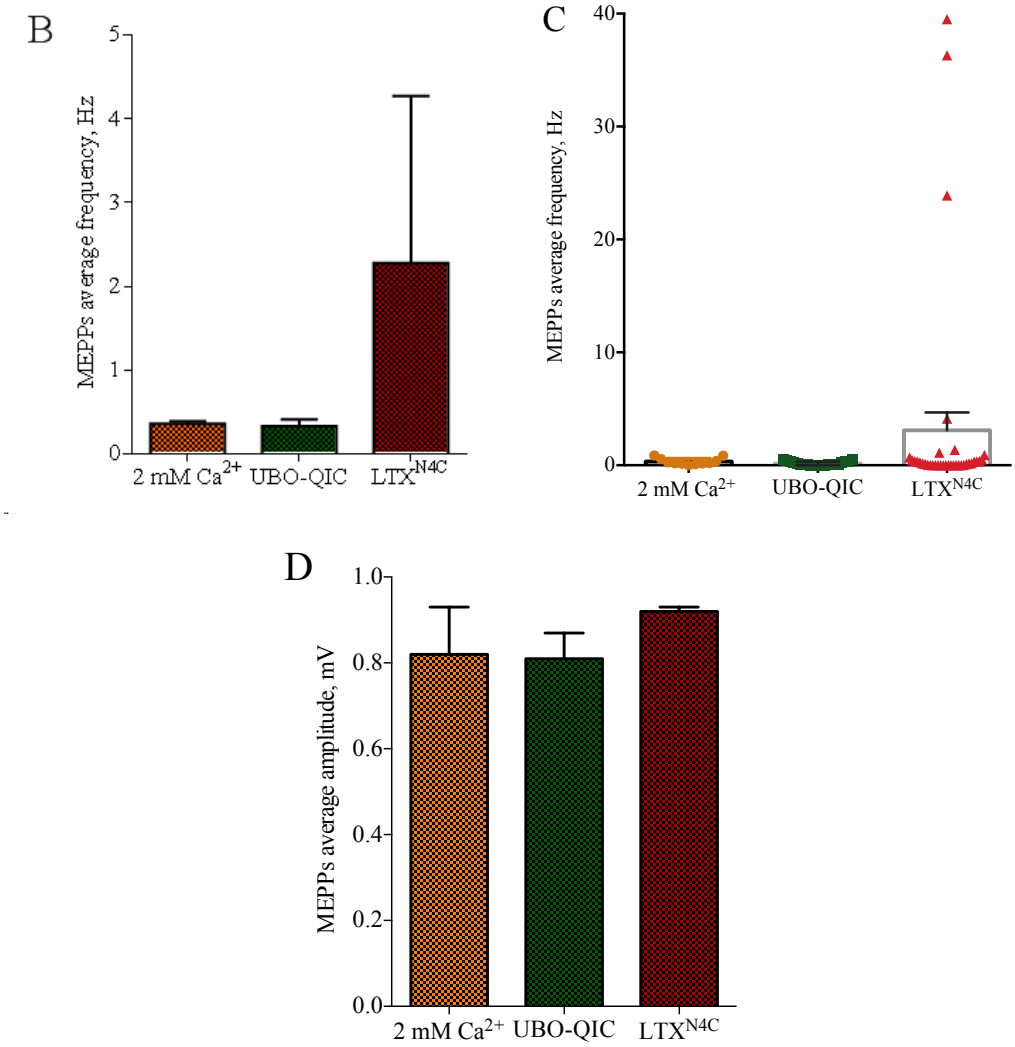

Figure 5.2. A. Frequency plot of a recording of MEPPs in Ca^{2+} buffer (2 mM), after the addition of UBO-QIC and LTX^{N4C}. The presence of UBO-QIC in the buffer prevents the activation of $G\alpha_{q/11}$ protein and the effects usually observed upon addition of LTX^{N4C} do not develop. B. Average frequency of MEPPs in Ca^{2+} buffer, after the addition of UBO-QIC and of LTX^{N4C}. The difference between the conditions is not statistically significant. C. Scatter plot of the data summarised in B. Each point represents the frequency of a single fibre recorded under the given condition. Note that about 30% of the recorded cells still respond to the toxin with increased frequency. D. Average amplitude of MEPPs in Ca^{2+} buffer, after the addition of UBO-QIC and LTX^{N4C}. The difference between the conditions is not statistically significant (N = 3, n = 20 cells recorded in Ca^{2+}, 24 after the addition of UBO-QIC and 36 after addition of LTX^{N4C}).

In a reverse experiment, when added after 0.25 nM LTX^{N4C} and when the effects of the activation of LPHN1 were already manifested, UBO-QIC (1 μM) was able to significantly reduce the frequency of exocytosis (15.50 ± 7.07 Hz LTX^{N4C} vs 2.76 ± 1.35 Hz LTX^{N4C} and UBO-QIC, Figure 5.4 A and B). The fall in the frequency of neurotransmitter release is observed after approximately 6 minutes from the addition of UBO-QIC.

The differences in the average amplitudes between the experimental conditions were not significant (0.82 ± 0.11 mV in Ca^{2+} buffer, 1.14 ± 0.02 mV after the addition of LTX^{N4C}, and 0.78 ± 0.04 mV after the addition of UBO-QIC, Figure 5.4 C).

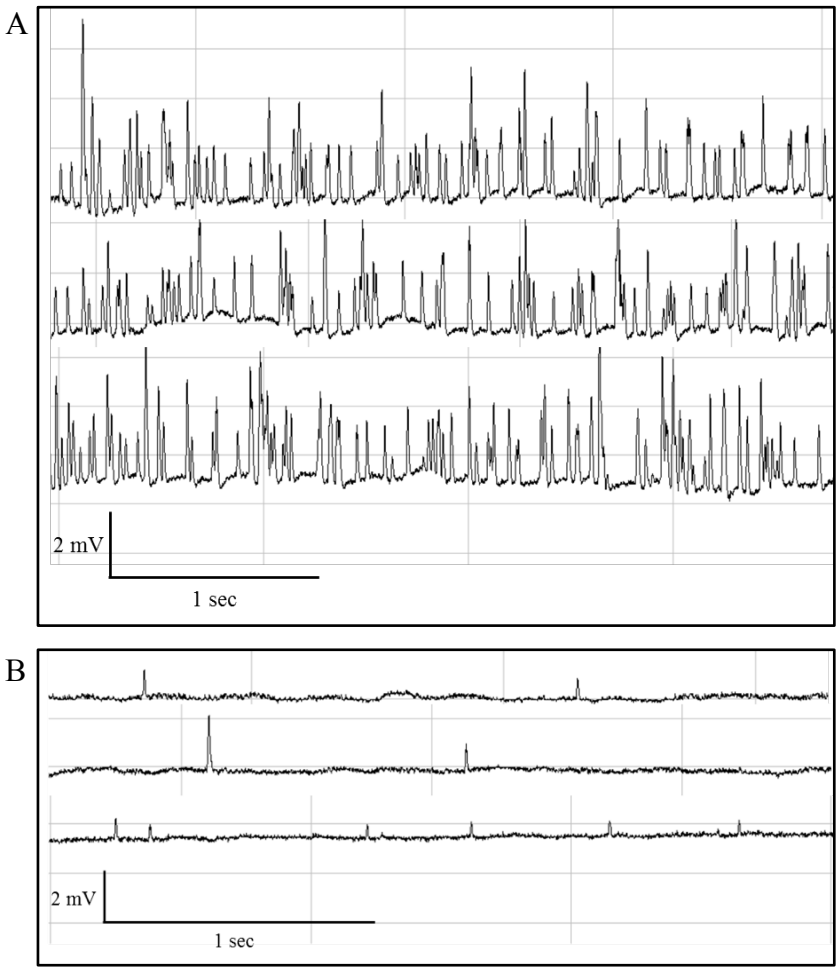

Figure 5.3. Single traces of MEPPs recordings in Ca^{2+} buffer after the addition of LTX^{N4C} (A) and UBO-QIC (B). UBO-QIC is able to stop the increased exocytosis caused by the stimulation of LPHN1.

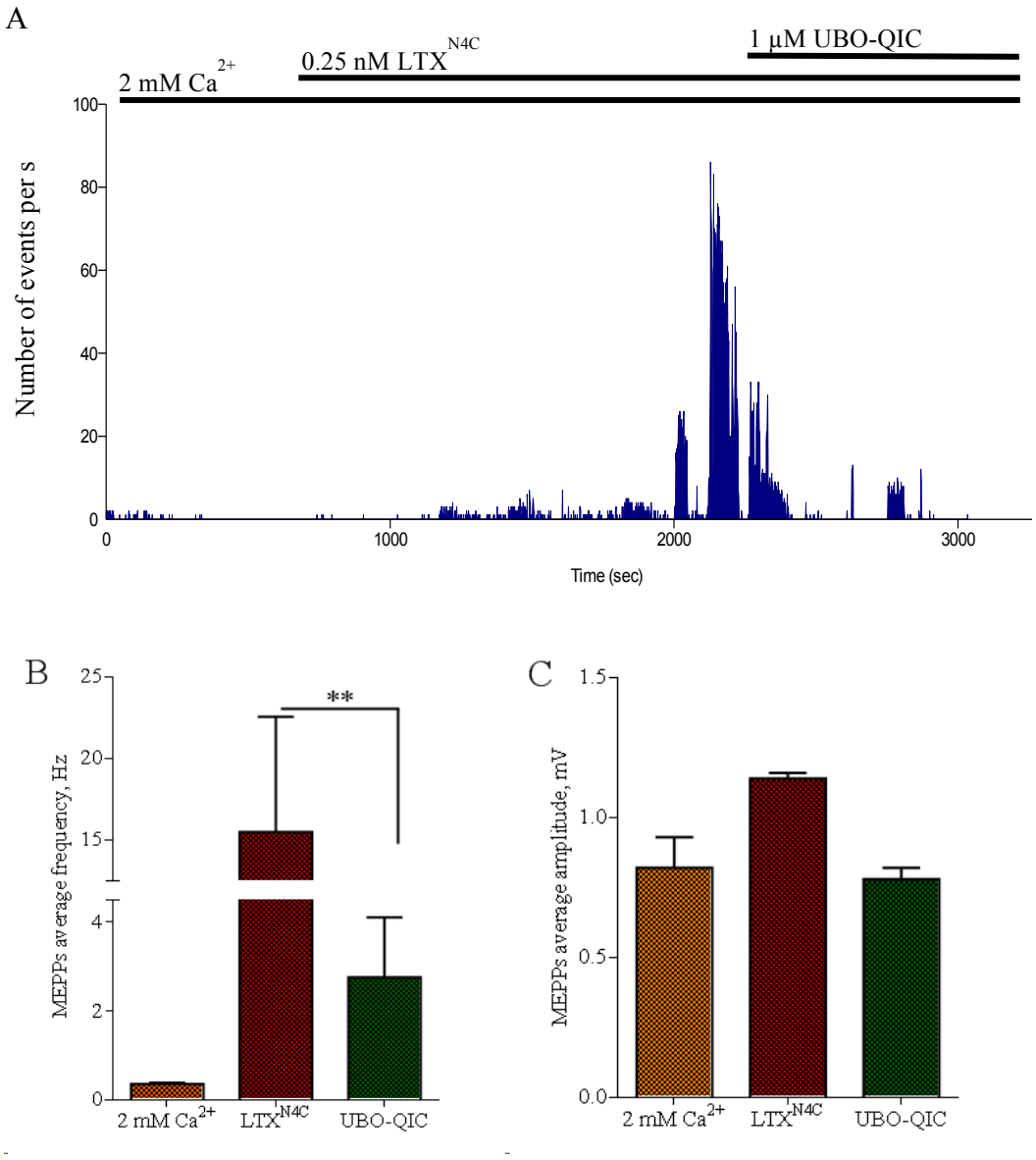

*Figure 5.4. A. Frequency plot of a recording of MEPPs in Ca^{2+}-containing buffer (2 mM) where UBO-QIC was added once LTX^{N4C} already started to exert its effect. UBO-QIC is able to significantly reduce the frequency of exocytosis due to the activation of LPHN1. B. Average frequency of MEPPs in Ca^{2+} buffer, after the addition of LTX^{N4C} and subsequent addition of UBO-QIC. C. Average amplitude of MEEPs in Ca^{2+} buffer and after the addition of LTX^{N4C} and UBO-QIC. The difference between the conditions is not statistically significant (N = 3, n = 19 cells recorded in Ca^{2+} buffer, 36 after the addition of LTX^{N4C}, and 29 after the addition of UBO-QIC; **, P <0.010, Mann – Whitney U test).*

5.2.2 PLC is needed for LPHN1 activity

After determining that $G\alpha_{q/11}$ was responsible for LPHN1 activity, it was important to further investigate the molecular pathway involved in the effects observed upon LPHN1 activation. PLC is a known downstream intracellular target of activated $G\alpha_{q/11}$. The involvement of PLC in αLTX Ca^{2+}-dependent release and the ability of PLC inhibitors to attenuate LTX^{N4C} effects on exocytosis were already described in model systems such as synaptosomes and cultured pyramidal neurons (Davletov et al. 1998; Rahman et al. 1999; Capogna et al. 2003). Here, I interfered with PLC in NMJ preparations using its well-known inhibitor, U73122. This compound has a double action that in turn leads to decreased intracellular Ca^{2+} concentration: it both inhibits the coupling of PLC with the G protein and prevent the hydrolysis of PIP2 to IP_3 (Bleasdale et al. 1990; Smith et al. 1990; Bleasdale and Fisher 1993). The inactive analogue of U73122, U73343 was used as a control.

When added in Ca^{2+}-containing buffer at the beginning of the recordings, 10 μM U73122 inhibited the effects of LPHN1 activation. In fact, when 0.25 nM LTX^{N4C} was subsequently added, the toxin was not able to fully produce its effects (0.34 ± 0.12 Hz Ca^{2+} buffer with U73122 vs. 2.39 ± 1.81 Hz Ca^{2+} buffer with U73122 and LTX^{N4C} Figure 5.6 A and B).

The differences in the average amplitudes between the conditions studied were not statistically significant (0.82 ± 0.11 mV in Ca^{2+} buffer, 0.77 ± 0.06 mV in the presence of U73122, and 0.96 ± 0.06 mV after the addition of LTX^{N4C}, Figure 5.6 C).

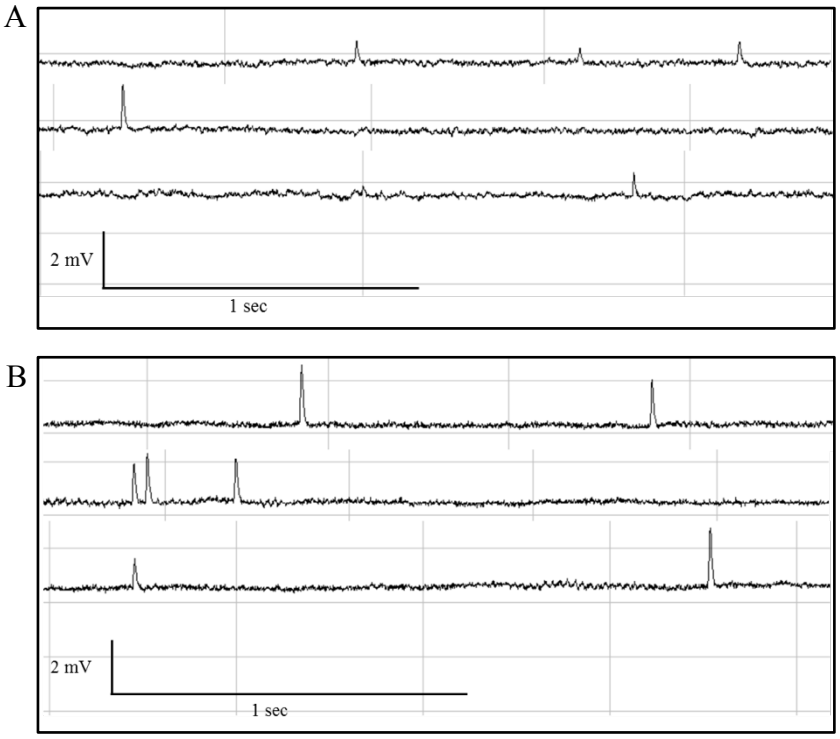

Figure 5.5. Single traces for MEPPs recordings in Ca^{2+} buffer in the presence of U73122 (A) and after the addition of LTX^{N4C} (B). Stimulation of LPHN1 by LTXN4C is not able to produce the typical increase in spontaneous exocytosis when U73122 is present.

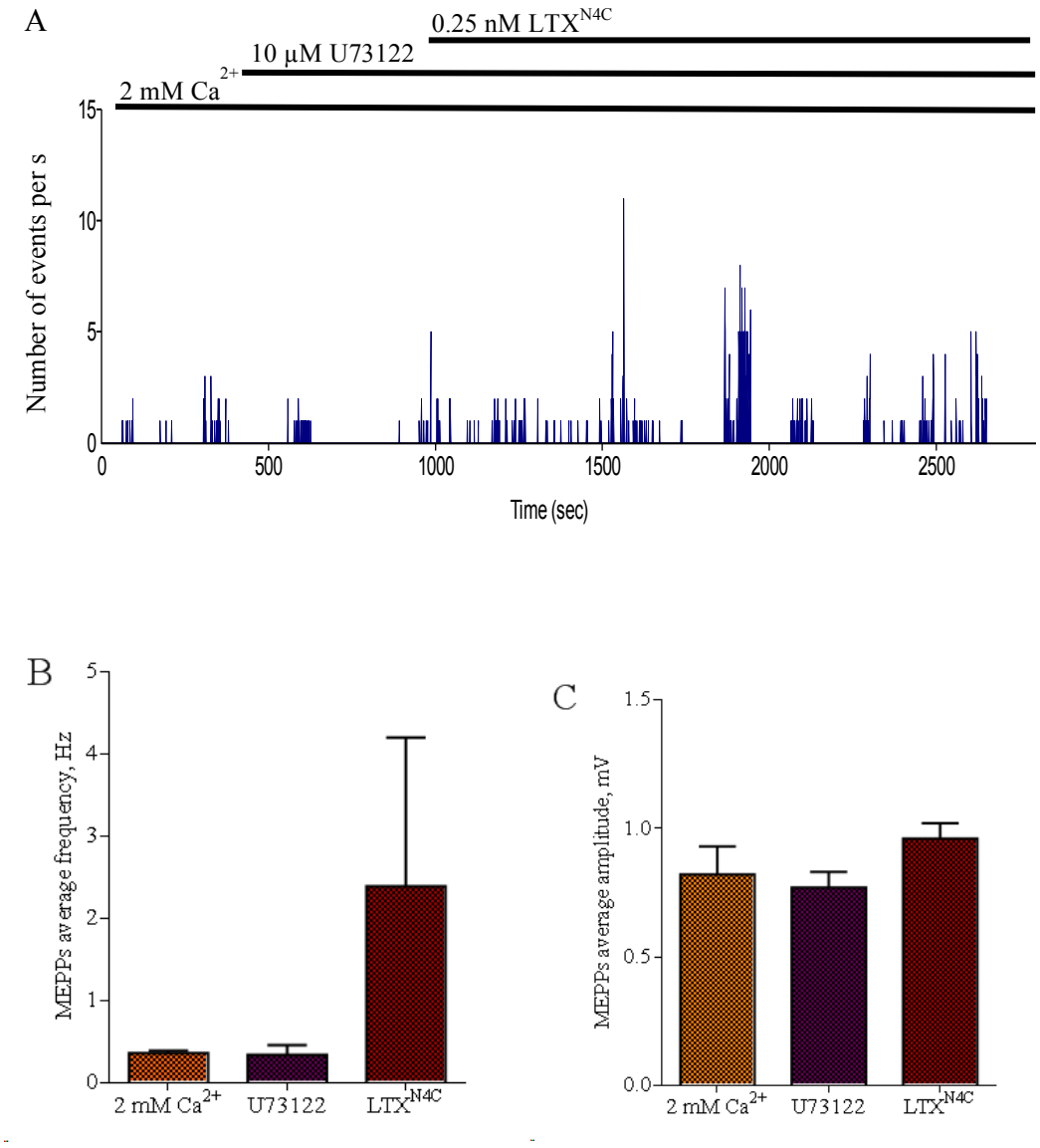

Figure 5.6. A. Frequency plot of a MEPPs recording in Ca^{2+} buffer (2 mM), after the addition of U73122 and of LTX^{N4C}. The presence of U73122 in the buffer successfully inhibits the activation of LPHN1. B. Average frequency of MEPPs in buffer A, after the addition of U73122 and subsequent addition of LTX^{N4C}. The difference between the conditions is not statistically different. C. Average amplitude of MEPPs in Ca^{2+} buffer, and after the sequential addition of U73122 and LTX^{N4C}. The difference is npt statistically significant (N = 2, n = 9 cells recorded in Ca^{2+}, 12 after the addition of U73122, and 22 after the addition of LTX^{N4C}).

The blockade of LPHN1 effects was also observed when PLC is inhibited after LPHN1 already started to act. In fact, adding U73122 after LTX^{N4C} already started to exert its effects led to a significant decrease in the MEPPs frequency (22.85 ± 3.87 Hz in Ca^{2+} buffer with LTX^{N4C} vs. 3.68 ± 2.37 Hz in Ca^{2+} buffer with LTX^{N4C} and U73122, Figure 5.8 A and B). The decrease in neurotransmitter release was observed after approximately 20 minutes from the addition of U73122.

The average amplitudes did not significantly change between the experimental conditions considered (0.82 ± 0.11 mV in Ca^{2+} buffer, 0.80 ± 0.03 mV after the addition of LTX^{N4C}, and 1.25 ± 0.03 mV after the addition of U73122, Figure 5.8 C).

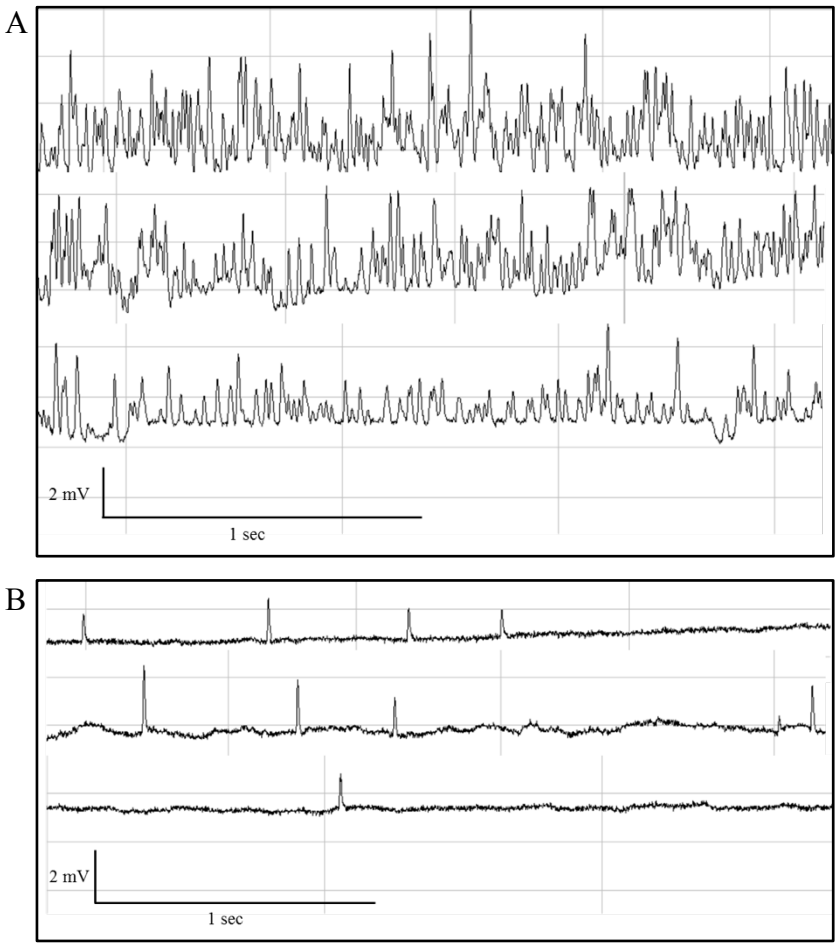

Figure 5.7. Single traces of MEPPs recordings in Ca^{2+} buffer after the addition of LTX^{N4C} (A) and subsequent addition of U73122 (B). U73122 is able to abolish the effects of LPHN1 activation.

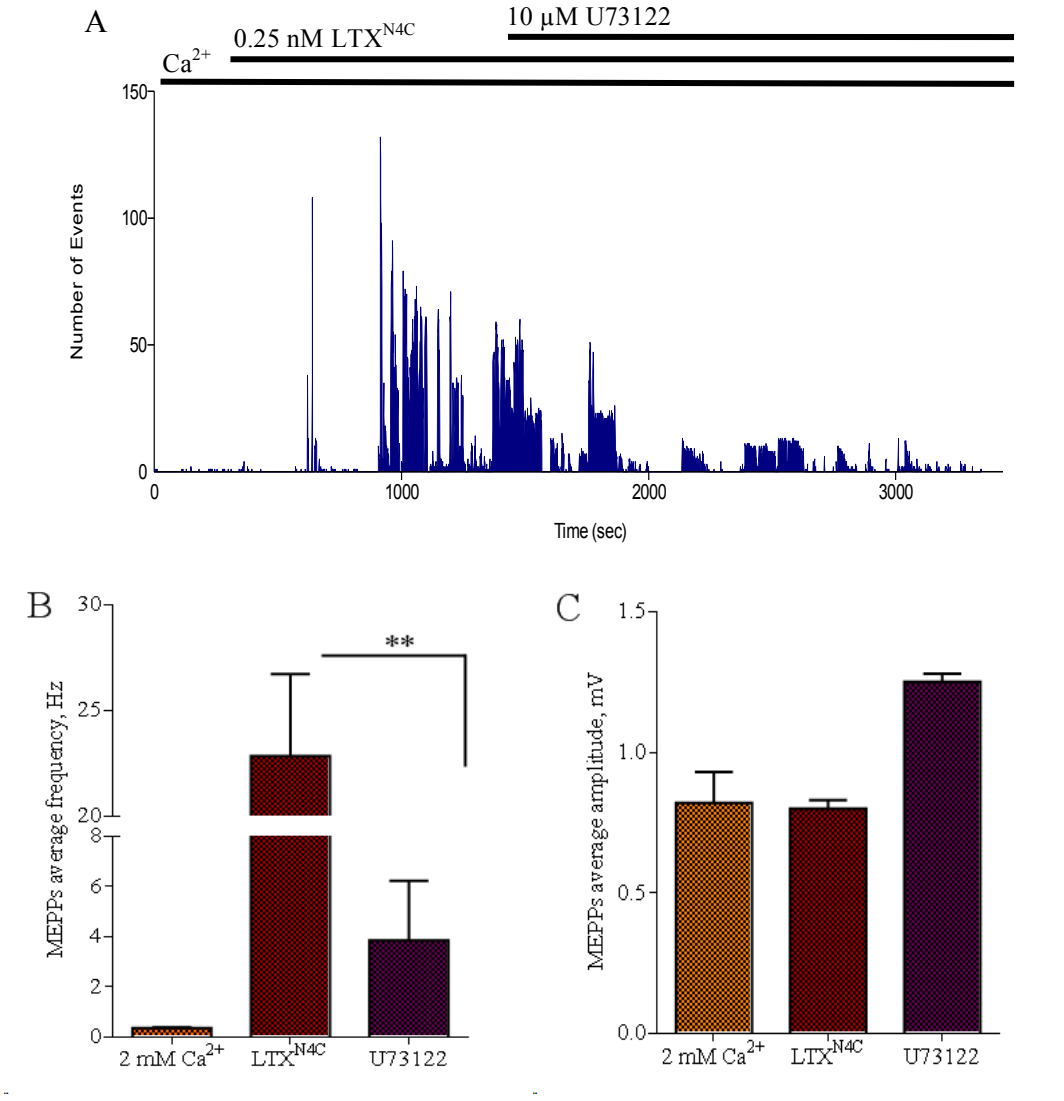

*Figure 5.8. A. Frequency plot of a MEPPs recording in Ca^{2+} buffer (2 mM), after the addition of LTX^{N4C} and of U73122. U73122 successfully reduces the increase in exocytosis caused by LTX^{N4C}. B. Average MEPPs frequency in Ca^{2+} buffer, after the addition of LTX^{N4C} and subsequent addition of U73122. C. Average amplitude of MEPPs in Ca^{2+} buffer, and after the sequential addition of LTX^{N4C} and U73122. The difference between the conditions is not statistically significant (N = 2, n = 13 cells recorded in Ca^{2+} buffer, 19 after the addition of LTX^{N4C}, and 38 after the addition of U73122; **, P < 0.010, Mann – Whitney U test).*

U73343 was used in the same kind of experiments, as a negative control and to make sure that the PLC inhibitor U73122 did not have off-target activities. In this case, LPHN1 was able to fully activate and develop the usual effects when U73343 (10 μM) was added either before or after LTX^{N4C} (Figure 5.9).

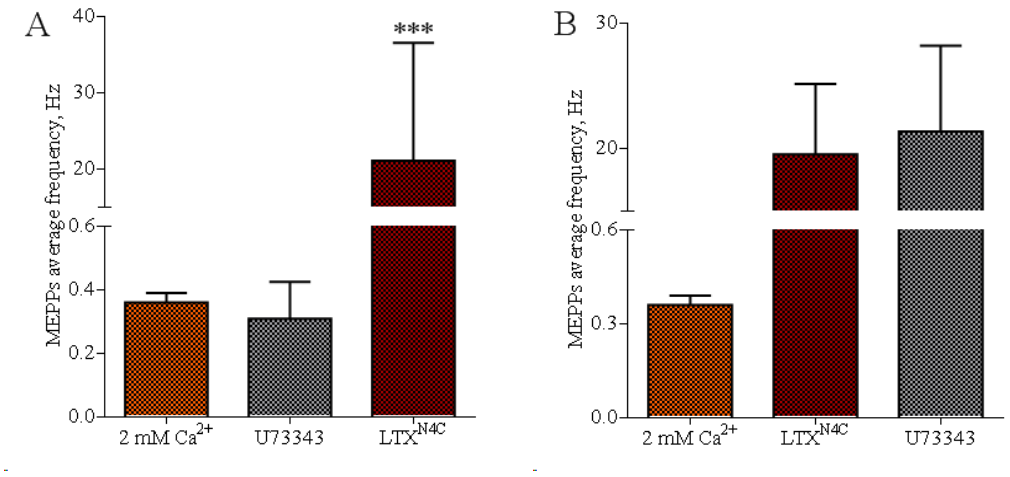

*Figure 5.9. A. Average frequency of MEPPs in Ca^{2+} buffer (2 mM) and after the sequential addition of U73343 and LTX^{N4C} (N = 1, n = 6 cells recorded in Ca^{2+} buffer, 6 after addition of U73343,and 12 after addition of LTX^{N4C}; ***, P < 0.001, Mann – Whitney U test) . B. Average frequency of MEPPs in Ca^{2+} buffer (2 mM) and after the sequential addition of LTX^{N4C} and U73343. The difference between the conditions is not statistically significant (N = 1, n = 5 cells recorded in Ca^{2+} buffer, 10 afetr addition of LTX^{N4C}, and 9 after addition of U73343, Mann – Whitney U test).*

5.2.3 Role of intracellular Ca^{2+} stores in the activity of LPHN1

The experiments described in the previous sections confirm that the molecular pathway involving Gαq/11 protein and the subsequent activation of PLC is necessary for the LPHN1-mediated effect. The final target of the molecular pathway investigated here is the intracellular Ca^{2+} stores: PLC leads to the production of IP_3 (and DAG) from PIP_2, and IP_3 in turn activates IP_3 receptors (IP_3R) on the endoplasmic reticulum (ER); this causes the release of Ca^{2+} from the intracellular Ca^{2+} stores and consequent elevation in the cytosolic Ca^{2+} concentration.

In previous works, LTX^{N4C} was shown to cause hydrolysis of PIP_2 (and consequent production of IP_3) in synaptosomes (Ichtchenko et al. 1998), and the block of IP_3 receptors caused inhibition of the effects on exocytosis operated by LTX^{N4C} in cultured hippocampal neurons (Capogna et al. 2003). To verify that intracellular Ca^{2+} stores are involved in My model system, the NMJ, I used 2-Aminoethoxydiphenyl borate (2APB), a blocker of IP_3R (IC_{50} = 42 μM).

When added after the addition of 0.25 nM LTX^{N4C}, i.e. after the effects due to the activation of LPHN1 were already fully developed, 50 μM 2APB was able to reduce (and almost fully arrest) the rate of exocytosis (15.50 ± 7.07 Hz in Ca^{2+} buffer with LTX^{N4C} vs 0.18 ± 0.13 Hz in Ca^{2+} buffer with LTX^{N4C} and 2APB, Figure 5.11 A and B). The decrease in neurotransmitter release was observed after approximately 20 minutes from the addition of 2APB.

The average amplitude between the conditions considered was not significantly different (0.82 ± 0.11 mV in Ca^{2+} buffer, 0.91 ± 0.01 mV after the addition of LTX^{N4C}, and 0.77 ± 0.03 mV after the addition of 2APB, Figure 5.11 C).

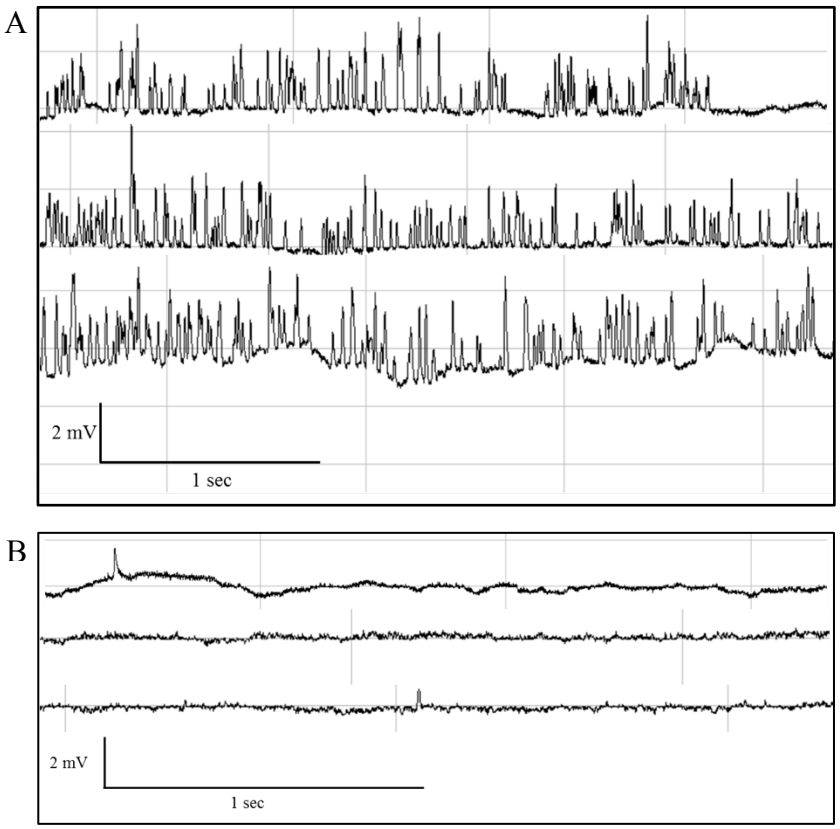

Figure 5.10. Single traces of MEPPs recordings in Ca^{2+} buffer after the addition of LTX^{N4C} (A) and 2APB (B). Addition of 2APB fully stops the effects due to the activation of LPHN1.

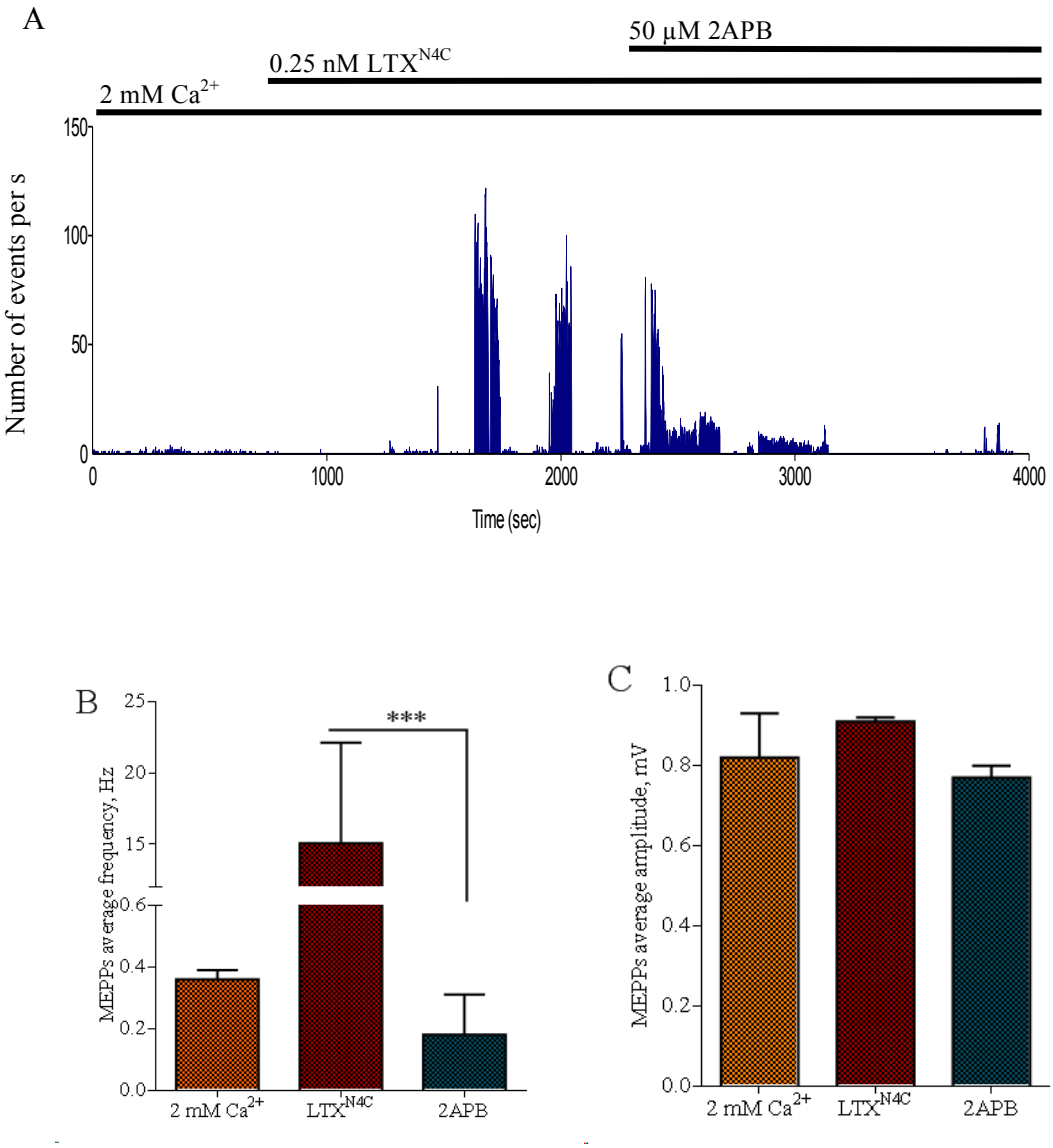

*Figure 5.11. A. Frequency plot of a MEPPs recording in the presence of 2 mM Ca^{2+}, after the addition of LTX^{N4C} and of 2APB. 2APB is able to significantly reduce the elevation in exocytosis caused by LTX^{N4C}. B. Average frequency of MEPPs in Ca^{2+} buffer, after the addition of LTX^{N4C} and subsequent addition of 2APB. C. Average amplitude of MEPPs in Ca^{2+} buffer and after the sequential addition of LTX^{N4C} and 2APB. The difference is not statistically significant (N = 2, n = 6 cells recorded in Ca^{2+} buffer, 13 after addition of LTX^{N4C} and 11 after the addition of 2APB; ***, P < 0.001, Mann – Whitney U test).*

However, 2APB also blocks TRPC channels. In research, this compound is used to manipulate intracellular release of calcium ions and modify TRPC channel activity (it stimulates SOCE at low concentration and inhibits it at higher concentrations), although its lack of specific effects calls for caution when interpreting the results under certain circumstances (Maruyama et al. 1997; Bootman et al. 2002).

Therefore, to confirm the crucial role of the intracellular Ca^{2+} stores in the downstream signalling medated by LPHN1, I used a very specific blocker of the Ca^{2+} ATPase involved in the refilling of intracellular Ca^{2+} stores, thapsigargin (TG). This drug elevates the cytosolic Ca^{2+} concentration by stimulating the release of Ca^{2+} from IP_3- and ryanodine sensitive stores, and at the same time blocking the sarco/endoplasmic reticulum Ca^{2+} ATPase (SERCA) pump, causing the depletion of the stores (Thastrup et al. 1990; Lytton, Westlin and Hanley 1991; Treiman, Caspersen and Christensen 1998).

TG alone caused a large increase in spontaneous neurotransmitter release when added to the NMJ preparartions (as described in Chapetr 6, section 6.2.2); in Ca^{2+}-free buffer, this increase ceases once the elevation in intracellular Ca^{2+} subsides.

When added after the peak in exocytosis caused by TG in Ca^{2+}-free buffer had subsided, LPHN1 activation by LTX^{N4C} was unsuccessful to elicit the increase in exocytosis typically observed, also after the addition of 2 mM Ca^{2+} to the extracellular buffer (0.10 ± 0.01 Hz in Ca^{2+}-free buffer, 8.85 ± 1.28 Hz after the addition of TG, 0.16 ± 0.09 Hz after the addition of LTX^{N4C} and 0.02 ± 0.01 Hz after the addition of Ca^{2+}, Figure 5.13). This result strongly supports the hypothesis that intracellular stores are crucial for LPHN1-mediated increase in spontaneous exocytosis.

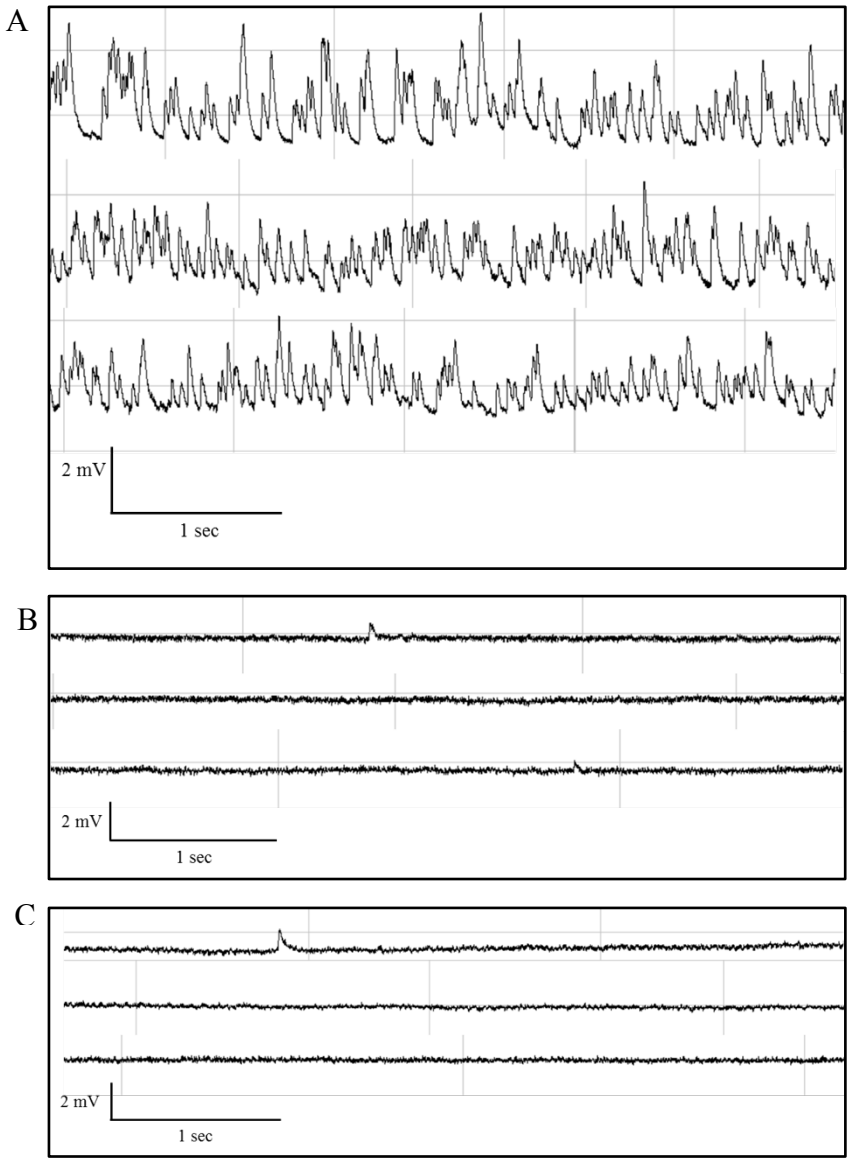

Figure 5.12. Individual traces of MEPPs recordings in Ca^{2+}-free buffer after the addition of TG (A), and after the addition of LTX^{N4C} (B) and 2 mM Ca^{2+} (C) once the effects of TG had ceased. In the presence of LTX^{N4C}, the addition of Ca^{2+} after the effects of TG subsided is not able to restore the increase in exocytosis.

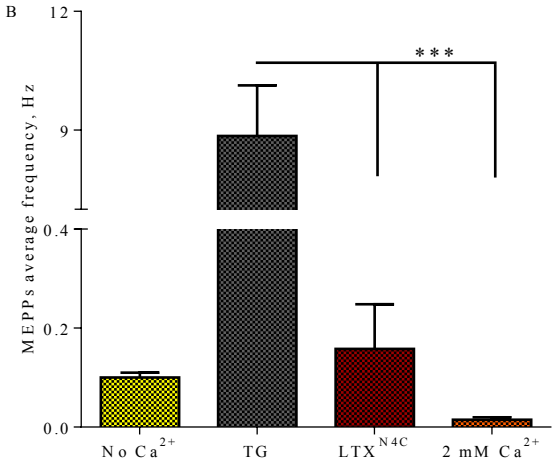

*Figure 5.13. Average frequency of MEPPs in Ca^{2+}-free buffer and after the sequential addition of TG, LTX^{N4C}, and 2 mM Ca^{2+} (N = 2, n = 5 cells recorded, in Ca^{2+}-free buffer, 5 after the addition of TG, 5 after the addition of LTX^{N4C} and 9 after the addition of Ca^{2+}; ***, P < 0.001, Mann – Whitney U test).*

Furthermore, to ascertain whether IP_3 sensitive stores are the only ones involved in the action of LPHN1, ryanodine was used to block ryanodine sensitive Ca^{2+} release.

The neuromuscular preparations were treated with 100 µM ryanodine and subsequently LTX^{N4C} was added in order to see if the effects of the activation of LPHN1 were still able to develop. The presence in the buffer of ryanodine did not prevent the development of the effects of LTX^{N4C}, and cells showed increased exocytosis and bursting behaviour. However, under these conditions the overall increase was slightly less than in Ca^{2+} buffer alone (9.45 ± 2.59 Hz in the presence of ryanodine vs. 15.50 ± 7.07 Hz in Ca^{2+} buffer, Figure 5.14). The average frequency during the bursts was of 25.80 ± 2.13 Hz, a value that is not significantly different from the one observed in Ca^{2+} without the addition of the drug.

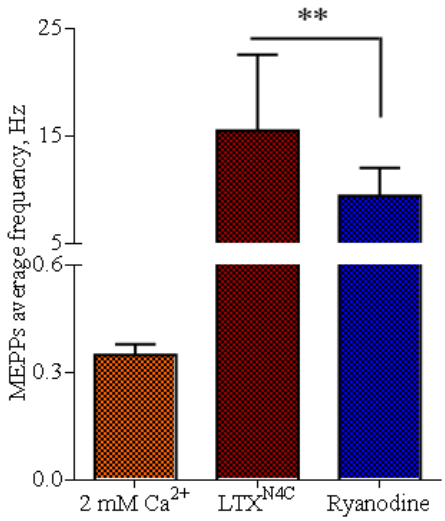

*Figure 5.14. Comparison between the average frequency of MEPPs in Ca^{2+}-containing buffer (2 mM) after the addition of LTX^{N4C}, and in Ca^{2+}-containing buffer with ryanodine after the addition of LTX^{N4C} (N = 1, n = 7 cells recorded in Ca^{2+} buffer, 5 cells after the addition of LTX^{N4C}, and 11 cells after the addition of LTX^{N4C} in the presence of ryanodine; **, P < 0.010, Mann – Whitney U test).*

5.3 Discussion

The purpose of the experiments described in this chapter was to delineate the intracellular molecular pathway that LPHN1 activates in order to develop its effects.

As discussed previously, LPHN1 is a G protein coupled receptor, most likely associated with $G\alpha_o$ and $G\alpha_{q/11}$ proteins (Rahman et al. 1999).

$G\alpha_o$ is the most abundant G protein in the CNS and in the PNS, where it plays a major role in neuronal development and axonal regeneration, being associated with GAP-43 protein and representing about 10% of the proteins present in growth cones. The association of $G\alpha_o$ with Alzheimer's amyloid-β (A4) precursor protein (APP) suggests a role for this protein in the pathogenesis of Alzheimer's disease. It also has a role in visual signal transduction and olfactory reception (for a review see Kasahara and Ui, 2011).

The GPCRs that are associated with $G\alpha_o$ are mostly neurotransmitter receptors, such as muscarinic ACh receptors (M2 subtype), dopamine D2 receptors, α2A adrenergic receptors, and $GABA_A$ receptors. The target molecule for this G protein is adenylate cyclase: activation of $G\alpha_o$ inhibits its activity, therefore reducing the production of cAMP. Furthermore, $G\alpha_o$ is known to inhibit neurotransmitter release by inhibiting the action potential-evoked opening of P/Q and N-type Ca^{2+} channels (for a review see Kasahara and Ui, 2011).

By contrast, activation of $G\alpha_{q/11}$ leads to an increase in cytosolic $[Ca^{2+}]$ by activating PLC, which in turn hydrolyses PIP_2 which releases IP_3 and DAG. IP_3 will then activate IP_3R on the ER leading to the release of Ca^{2+} from intracellular Ca^{2+} stores, whilst DAG activates protein kinase C (PKC).

Similarly to $G\alpha_o$, GPCRs associated with $G\alpha_{q/11}$ are neurotransmitter receptors, such as muscarinic Ach receptors (M1, M3 and M5), and serotonin 5-HT_2 receptors.

Because the activation of LPHN1 causes an increase in neurotransmitter release, I tested the functional involvement of $G\alpha_{q/11}$ in this effect. To do so, I used a selective inhibitor of $G\alpha_{q/11}$, UBO-QIC, which inhibits the $G\alpha_{q/11}$ signalling by

directly binding to this G protein and inhibiting the exchange of GDP with GTP (Bernard et al. 2014).

My experiments support the hypothesis that $G\alpha_{q/11}$ is the G protein involved in the increase of neurotransmitter release observed upon activation of LPHN1. The evidence for this is that inhibition of this G protein prevented the increase in MEPPs due to LPHN1 activation when added before LTX^{N4C} (see Figure 5.2), and significantly reduces the frequency of exocytosis when added after the effects of LPHN1 activation were already present (see Figure 5.4).

To further evaluate whether the molecular pathway initiated by LPHN1 activation involves $G\alpha_{q/11}$, I conducted further experiments using drugs interfering with the downstream molecular elements of the $G\alpha_{q/11}$ pathway. Previous studies already showed an involvement of these molecules in the effects on exocytosis caused by both αLTX and LTX^{N4C} in different model systems. First, PLC, an enzyme found in the cytoplasm that acts by cleaving phospholipids (in this case PIP_2) at the phosphate group, was shown to completely inhibit αLTX Ca^{2+}-dependent exocytosis in synaptosomes (Davletov et al. 1998; Rahman et al. 1999), and to significantly reduce LTX^{N4C} effects in cultured hippocampal neurons (Capogna et al. 2003).

Second, PIP_2 hydrolysis and consequent production of IP_3 was shown to be involved in the effects of LTX^{N4C} in synaptosomes (Ichtchenko et al. 1998), and the block of IP_3R was demonstrated to significantly reduce the effects of the mutant toxin on exocytosis in hippocampal neurons (Capogna et al. 2003).

In the present experiments using NMJ preparations, the effect of LPHN1 activation was blocked by U73122, a well-known inhibitor of PLC, whose effects contribute to the decrease of cytosolic [Ca^{2+}] by inhibiting the coupling between $G\alpha_{q/11}$ and PLC, while at the same time preventing the hydrolysis of PIP_2. These experiments further suggest the involvement of PLC in the downstream effects of LPHN1 and, therefore, support the hypothesis that this is the pathway used by this receptor. Indeed, U73122 inhibits the development of the LTX^{N4C} effects via the activation of LPHN1 when added before (Figure 5.6) or after (Figure 5.8) LTX^{N4C}. This effect was specifically caused by the PLC inhibition (see Figure 5.9).

Finally, I have confirmed the involvement of the IP_3-sensitive intracellular calcium stores as a final target of the downstream molecular pathway of LPHN1. Thus, blocking IP_3R with 2APB blocked the effect of LTX^{N4C} via LPHN1. Although caution is needed when using 2APB due to its relatively poor specificity, at least some of the effects observed can still be attributed to the blockade of IP_3R. First, 2APB-induced inhibition of the effects of LPHN1 stimulation is in line with the rest of the experiments revealing the downstream mechanism of this receptor. Second, the depletion of the calcium stores using TG also blocks the LTX^{N4C} actions.

2 APB was more effective than UBO-QIC and U73122 in reducing the frequency of neurotransmitter release. This can be due to the fact that TRPC channels, that open in response to intracellular Ca^{2+} store depletion, are also blocked by 2APB, causing a further drop in the cytosolic [Ca^{2+}]. This mechanism is further discussed in the next Chapter (Chapter 6). However, at least part of the effect of 2APB can be attributed to the blockade of IP_3R, because the effect of this drug did not develop immediately, which would be expected if it blocked influx of extracellular Ca^{2+} via a channel.

Interestingly, although IP_3-sensitive stores appear to be most important for the action of LTX^{N4C}, the ryanodine experiments demonstrate the possible additional involvement of Ryanodine sensitive stores in the effects of LPHN1 activation. However, the contribution of the ryanodine-sensitive stores is relatively small, causing only a slight decrease in the frequency of neurotransmitter release (see Figure 5.14) and failing to inhibit the bursting behaviour typical of the activation of LPHN1.

Taken together, the results of these experiments support the involvement of $G\alpha_{q/11}$ protein and of its intracellular signalling pathway in the effects that develop in response to the activation of LPHN1. The subsequent activation of PLC, hydrolysis of PIP_2 in IP_3 and consequent opening of IP_3R are essential for the increase in spontaneous exocytosis observed after addition of LTX^{N4C}. The resulting mobilisation of Ca^{2+} from the IP_3-sensitive intracellular Ca^{2+} stores appear therefore to be a crucial element for LPHN1 to be able to fully develop its effects (Figure 5.15).

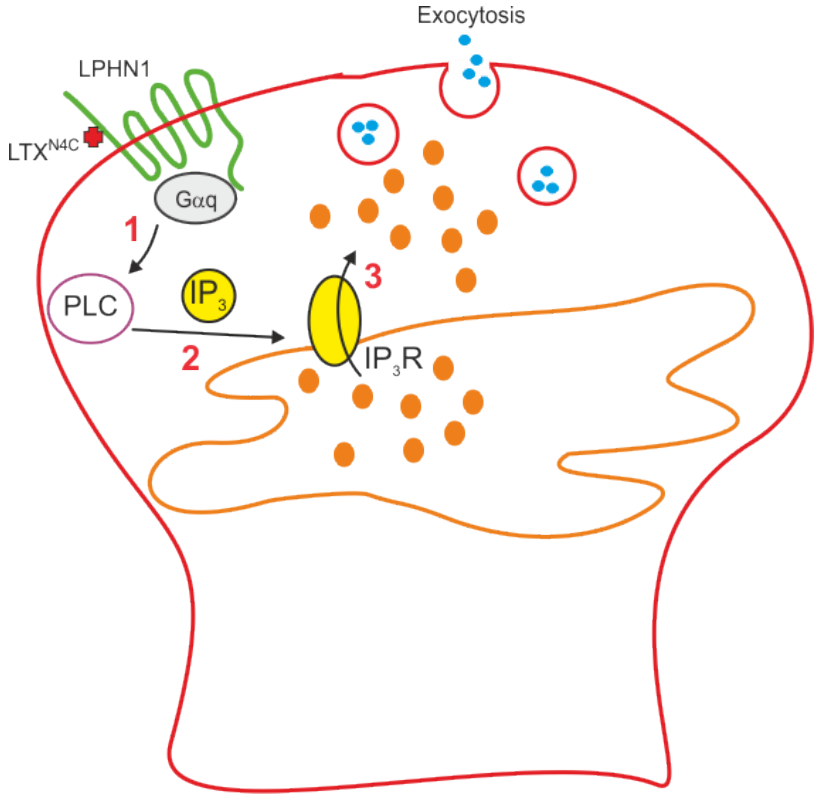

Figure 5.15. Schematic representation of the intracellular pathway activated by LPHN1. Upon binding of LTX^{N4C}, LPHN1 activates Gα$_q$ protein, which in turns activates PLC on the plasma membrane (arrow 1). PLC then promotes the cleavage of PIP$_2$ in DAG and IP$_3$ (arrow 2); whilst the first activates PKC, the latter binds to IP$_3$Rs on the ER, causing the release of Ca^{2+} from intracellular Ca^{2+} stores into the cytosol (arrow 3). The elevation in cytosolic Ca^{2+} concentration in turn starts the machinery that ultimately leads to increased exocytosis of neurotransmitter.

One important aspect of these findings is that cytosolic Ca^{2+} plays a critical role in the effect of LTX^{N4C}-induced activation of LPHN1. Thus, My experiments using BAPTA-AM (see Chapter 4, Section 4.2.6) directly indicate that chelation of cytosolic Ca^{2+} completely blocks LTX^{N4C} effects. However, the increase in cytosolic Ca^{2+} concentration caused by LPHN1 signalling leading to Ca^{2+} release from intracellular stores does not seem to be in itself sufficient to increase exocytosis.. In fact, as we discussed in Chapter 4, LTX^{N4C} does not cause

any significant increase in exocytosis in the absence of extracellular Ca^{2+}. This suggests that Ca^{2+} influx is needed in order to observe the increase in exocytosis typical of the activation of LPHN1. This aspect needs further investigation, and the next chapters of this work will address this issue.

CHAPTER 6
RESULTS IV. LPHN1 and calcium entry

6.1 Introduction

I reported in the previous chapter that the intracellular molecular pathway activated by LPHN1 involves $G\alpha_{q/11}$ protein, PLC, and IP_3R that ultimately causes an increase in intracellular [Ca^{2+}] due to the efflux of Ca^{2+} from the intracellular Ca^{2+} stores located at the ER (see Chapter 5).

However, the rise in intracellular [Ca^{2+}] caused by this mechanism is not sufficient to elicit the increase in the frequency of neurotransmitter release typical of the activation of LPHN1, as the addition of LTX^{N4C} in the absence of extracellular Ca^{2+} does not cause any significant change in the rate of exocytosis.

Furthermore, I demonstrated that extracellular Ca^{2+} is needed to enter the cells in order to allow the effects of the activation of LPHN1 to develop (see Chapter 4, section 4.2.6).

In this chapter I investigated the nature of the channels involved in this mechanism. Based on the crucial involvement of the intracellular calcium stores in the effect of LTX^{N4C}, I hypothesised that the toxin-evoked signal, via activation of LPHN1 and depletion of the stores stimulates the process called store-operated calcium entry (SOCE). The channels involved in SOCE, the store-operated Ca^{2+} channels (SOCCs), are a class of channels present at the plasma membrane that become activated in response to the decrease in [Ca^{2+}] in the intracellular Ca^{2+} stores (Putney 2007). The exact nature of these channels is still being investigated, but evidences suggest that SOCCs include Orai channels (Orai 1 – 3) and TRPC channels (TRPC 1 – 7). The opening of SOCCs is regulated by STIM protein (STIM 1 – 2), an ER Ca^{2+} sensor that detects a decrease in the stored [Ca^{2+}] and causes the opening of Orais and TRPCs (for a review see Chapter 1, Section 1.4.1).

6.2 Results

6.2.1 SOCE is involved in the activity of LPHN1

To test the involvement of SOCCs in the increase in exocytosis caused by the activation of LPHN1 I used several blockers known to affect these channels:

Gadolinium

Gadolinium is a trivalent cation known to act as a blocker of many cation channels including TRPCs. More specifically, Gd^{3+} is known to inhibit Ca^{2+} entry through TRPC 1, TRPC 2, TRPC3, TRPC 6 and TRPC 7, whilst it has an opposite effect on TRPC4 and TRPC 5, which can be stimulated by Gd^{3+} and in general by trivalent cations (Schaefer et al. 2000).

The neuromuscular junction preparations were incubated in a buffer containing 2 mM Ca^{2+}; Gd^{3+} (1 mM) was subsequently added to the preparations and MEPPs were recorded in order to test its effects on the basal frequency of neurotransmitter release. No significant changes were detected in the frequency of exocytosis with the addition of Gd^{3+} alone (0.42 ± 0.13). Upon addition of LTX^{N4C} no significant changes were recorded in the frequency of MEPPs; out of 16 cells recorded only one cell showed a slight increase in exocytosis to 3.21 Hz, suggesting that the block of SOCE induced by Gd^{3+} was not complete in all cells. However, the overall frequency of exocytosis did not significantly differ from the frequency recorded in the other conditions (0.28 ± 0.15 Hz, Figure 6.2 A and B).

The average amplitude did not show any significant difference between the conditions tested (0.82 ± 0.11 mV in Ca^{2+} buffer, 0.87 ± 0.18 mV in the presence of Gd^{3+} and 1.12 ± 0.04 after the addition of LTX^{N4C}, figure 6.2 C).

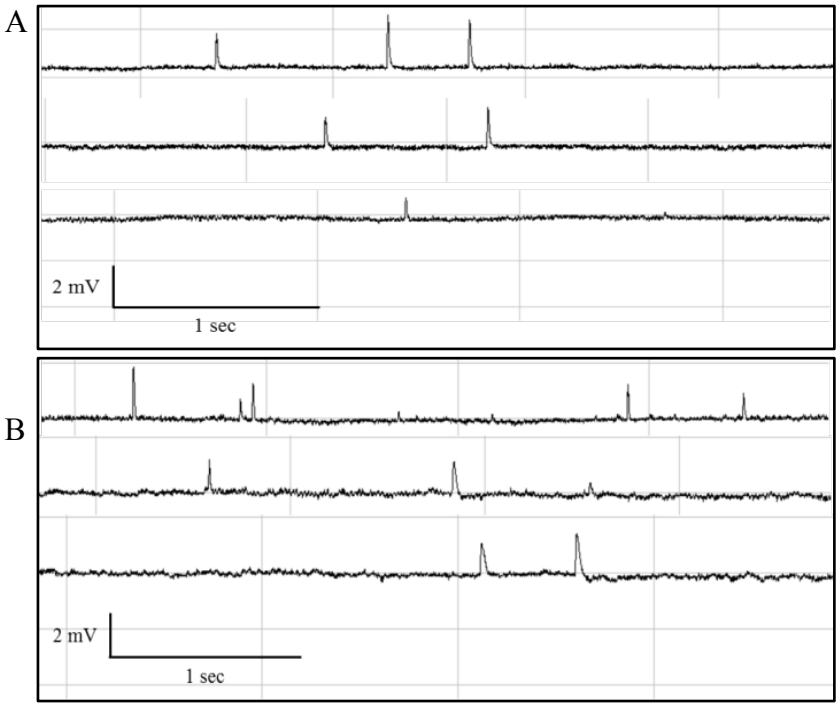

Figure 6.1. Single traces of MEPPs recordings in the presence of Gd^{3+} (A) and after the addition of LTX^{N4C} (B). Addition of LTX^{N4C} in the presence of Gd^{3+} does not elicit the typical effects of LPHN1 activation.

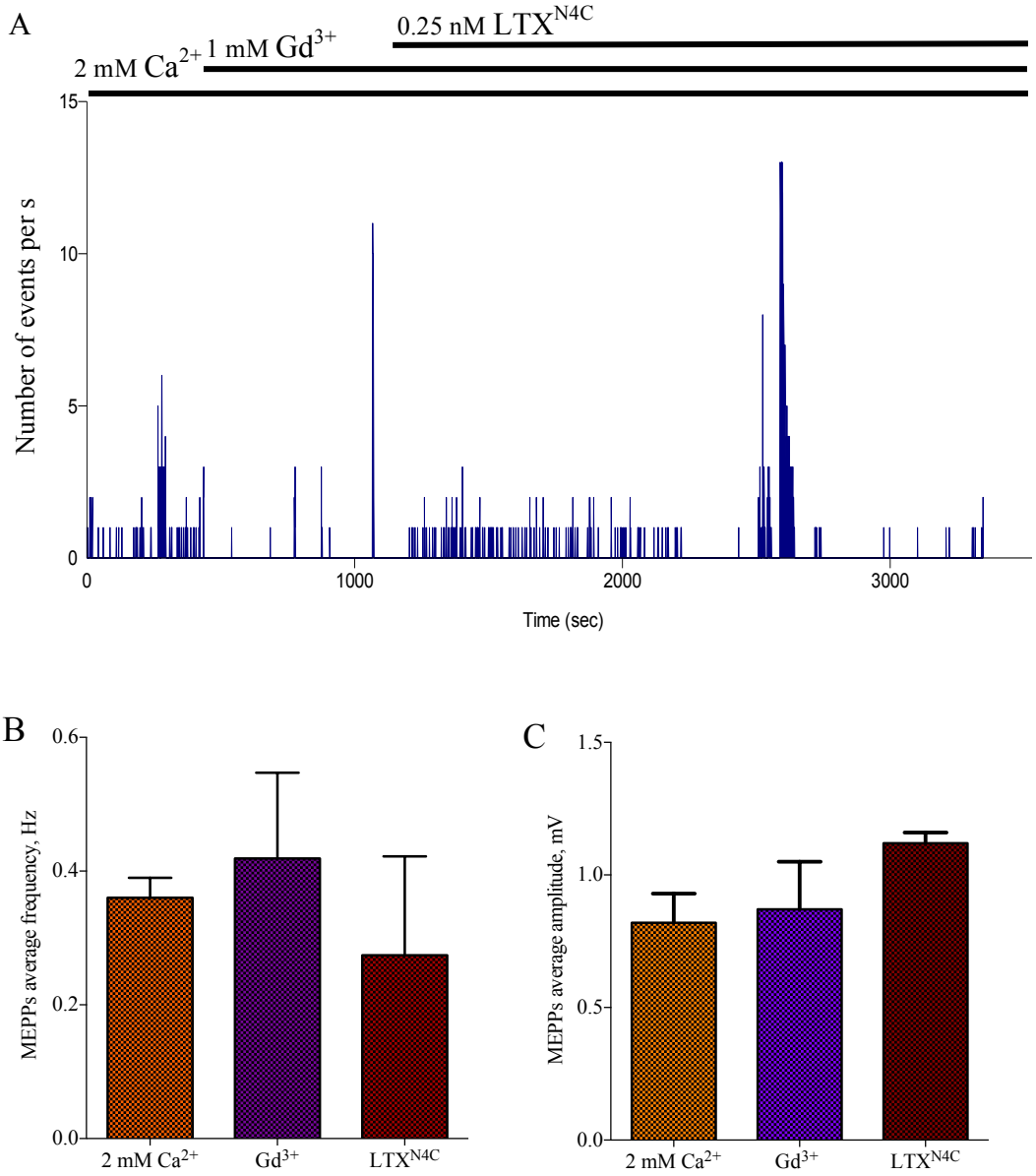

Figure 6.2. A. Frequency plot of a MEPPs recording in the presence of 2 mM Ca^{2+}, and after the addition of Gd^{3+} and LTX^{N4C}. Gd^{3+} inhibits the development of LPHN1-mediated ACh release. B. Average frequency of MEPPs in Ca^{2+} buffer, after the addition of Gd^{3+} and subsequent addition of LTX^{N4C}. The difference between the conditions is not statistically significant. C. Average amplitude of MEPPs in Ca^{2+} buffer and after the addition of Gd^{3+} and LTX^{N4C}. The difference is not statistically significant (N = 2, n = 7 cells recorded in Ca^{2+} buffer, 9 cells with Gd^{3+}, and 15 cells after the addition of LTX^{N4C}).

2APB

As discussed in a previous section (see Chapter 5, Section 5.2.3), this compound has the double effect of blocking IP_3R and TRPC channels (Bootman et al. 2002). In addition, low concentrations of 2APB may even stimulate Ca^{2+} influx via SOCCs. However, I used a high concentration of 2APB. Therefore, the effects observed when using 2APB in my experiments can be at least partially attributed to its inhibitory action on SOCCs, in particular TRPC 3, TRPC 6 and TRPC 7 (Lievremont, Bird and Putney 2005).

Addition of 50 μM 2APB to the preparations after the LPHN1-mediated effects had already started caused a significant decrease in the frequency of neurotransmitter release (13.93 ± 5.08 Hz Ca^{2+} buffer with LTX^{N4C} vs 0.18 ± 0.13 Hz Ca^{2+} buffer with LTX^{N4C} and 2APB, Figure 6.4 A and B). This decrease in observed after approximately 20 minutes from the addition of 2APB.

The average amplitude between the conditions considered was not significantly different (0.82 ± 0.11 mV in Ca^{2+} buffer, 0.91 ± 0.01 mV after the addition of LTX^{N4C}, and 0.77 ± 0.03 mV after the addition of 2APB, Figure 6.4 C).

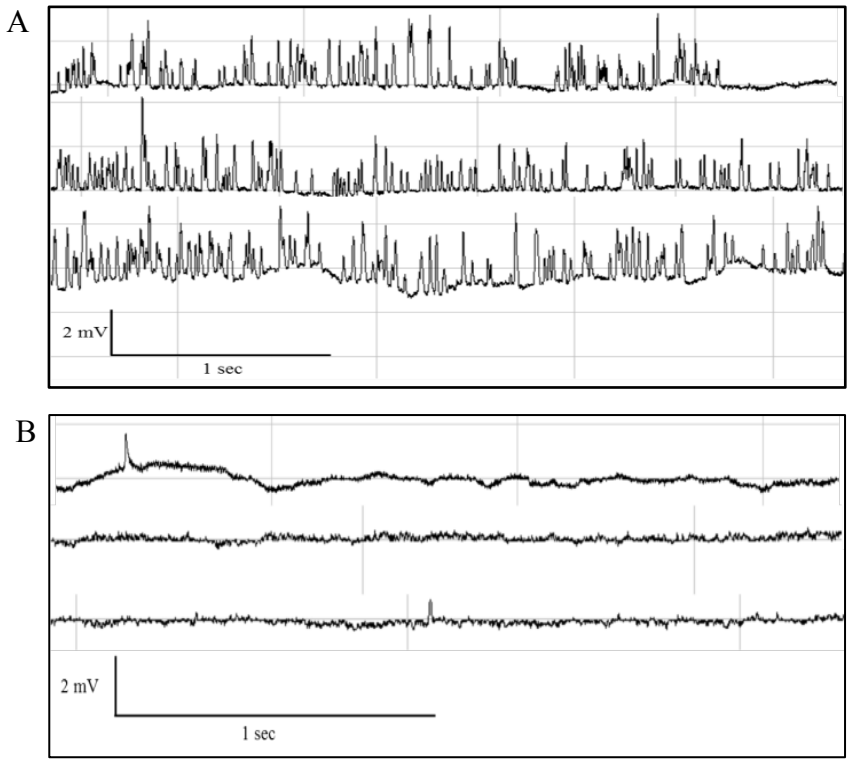

Figure 6.3. Single traces of MEPPs recordings in Ca^{2+} buffer after the addition of LTX^{N4C} (A) and 2APB (B). 2APB is able to stop the elevation in exocytosis that follows activation of LPHN1.

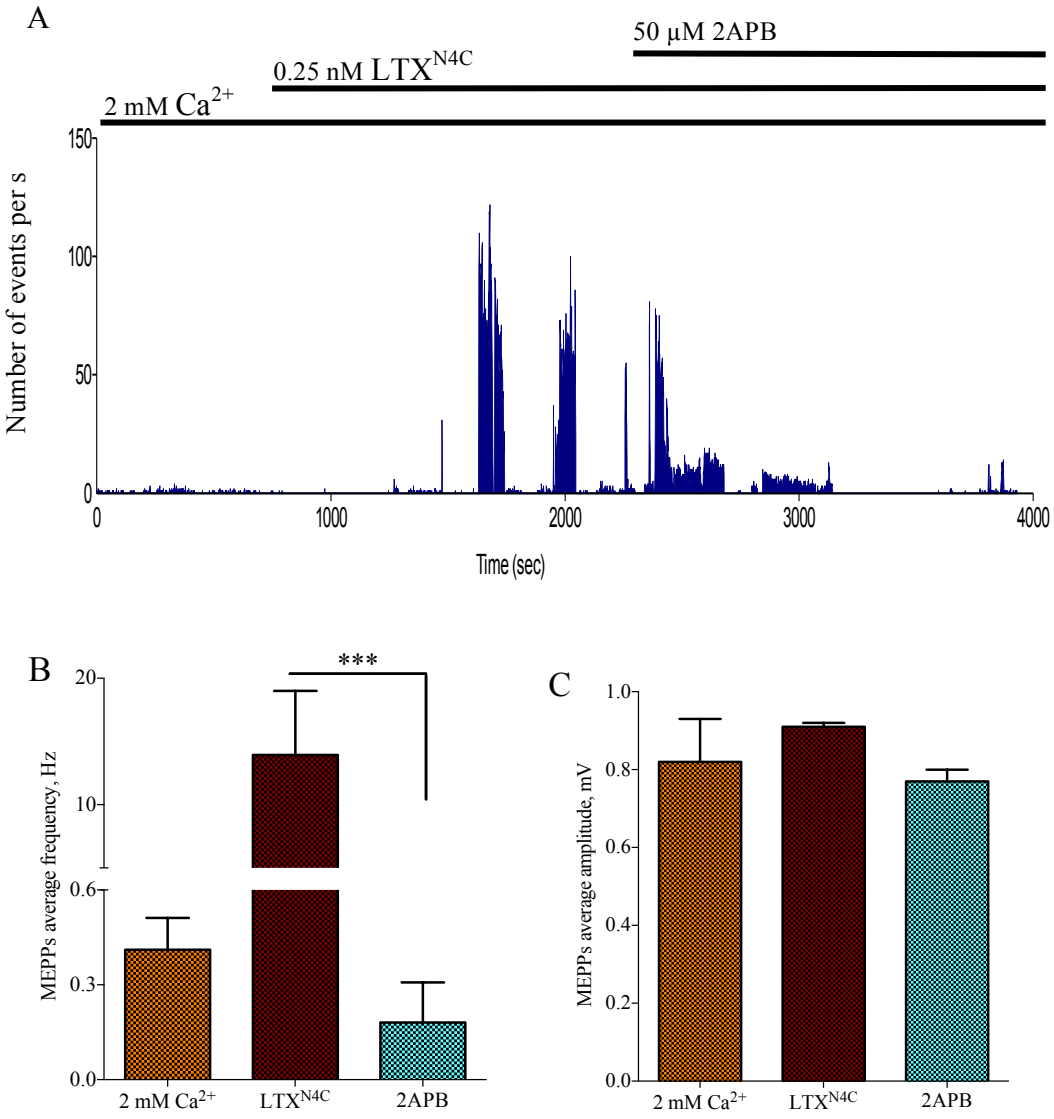

*Figure 6.4. A. Frequency plot of a MEPPs recording in the presence of 2 mM Ca^{2+}, after the addition of LTX^{N4C} and subsequent addition of 2APB. 2APB significantly reduced the elevation in exocytosis caused by LTX^{N4C}. B. Averaged frequency of MEPPs in Ca^{2+} buffer, after the addition of LTX^{N4C} and 2APB. C. Average amplitude of MEPPs in Ca^{2+} buffer and after the sequential addition of LTX^{N4C} and 2 APB. The difference between the conditions is not statistically significant (N = 2, n = 6 cells recorded in Ca^{2+} buffer, 13 cells after addition of LTX^{N4C}, and 11 cells after addition of 2APB; ***, P < 0.001, Mann – Whitney U test).*

SKF96365

1-[2-(4-Methoxyphenil)-2-[3[(4-methowyphenyl)propoxy]ethil-1H-imidazole hydrochloride (SKF96365) is an imidazole compound that inhibits SOCE by blocking TRPCs channels and by interfering with the STIM – Orai 1 association after Ca^{2+} store depletion (Varnai, Hunyady and Balla 2009). Furthermore, SKF96365 blocks T-type VGCCs (Singh et al. 2010) and K^+ channels (Schwarz, Droogmans and Nilius 1994).

SKF96365 (50 μM) was added to the neuromuscular preparations after the effects of LPHN1 had already started to manifest upon the addition of 0.25 nM LTX^{N4C}. The decrease in exocytosis started after approximately 1 minute from the drug addition, with some cells becoming quiet and others still under the effects of toxin, although with a lower frequency. The block of exocytosis was complete, with no cells reacting to LTX^{N4C}, after approximately 10 minutes from the addition of SKF96365. On average the frequency of exocytosis dropped from 20.26 ± 6.12 Hz to 1.46 ± 0.67 Hz (Figure 6.6 A and B).

The average amplitude was not significantly different between the conditions considered (0.82 ± 0.11 mV in Ca^{2+} buffer, 0.96 ± 0.04 mV after the addition of LTX^{N4C}, and 1.14 ± 0.02 mV after the addition of SKF96365, Figure 6.6 C).

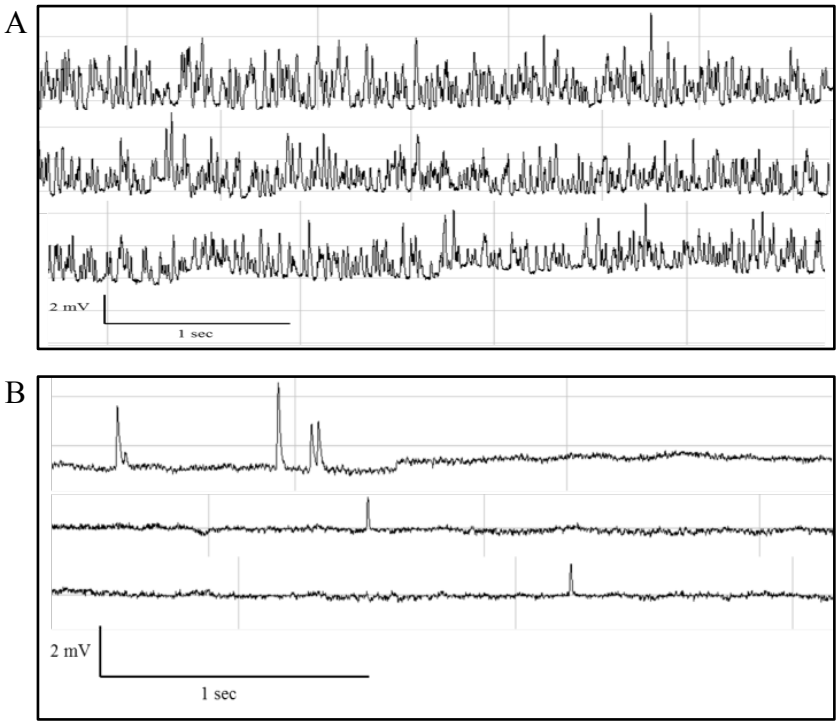

Figure 6.5. Single traces of MEPPs recordings in Ca^{2+} buffer after the addition of LTX^{N4C} (A) and of SKF96365 (B). Addition of SKF96365 is able to fully stop the effects due to the activation of LPHN1.

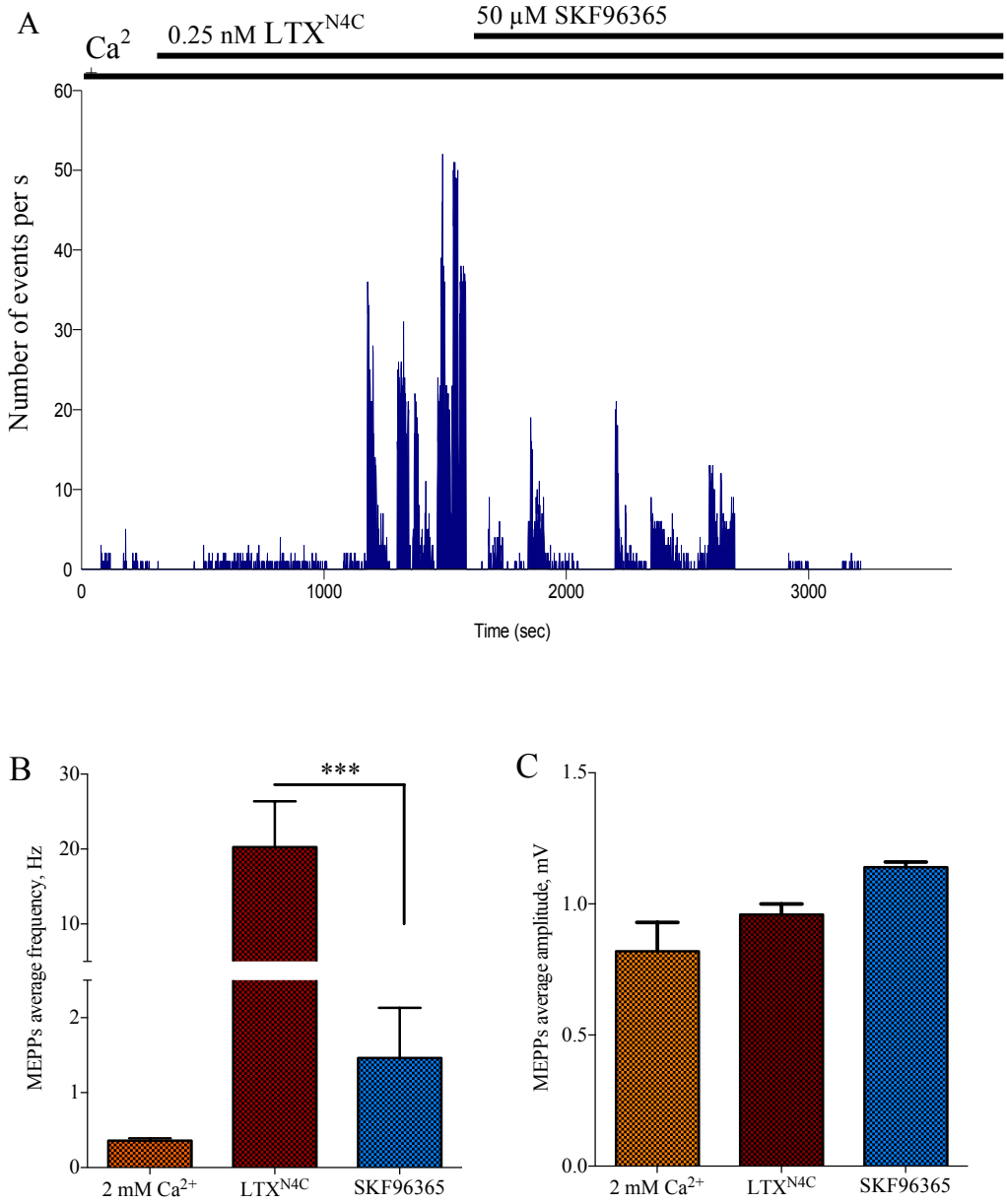

*Figure 6.6. A. Frequency plot of a MEPPs recording in the presence of 2 mM Ca^{2+}, and after the addition of LTX^{N4C} and SKF96365. SKF96365 successfully inhibits the increase in exocytosis caused by LPHN1 activation. B. Average frequency of MEPPs in buffer A, and after the addition of LTX^{N4C} and SKF96365. C. Average amplitude of MEPPs in Ca^{2+} buffer and after sequential addition of LTX^{N4C} and SKF96365. The difference is not statistically significant (N = 1, n = 5 cells recorded in Ca^{2+} buffer, 7 cells after addition of LTX^{N4C} and 17 cells after addition of SKF96365; ***, P < 0.001, Mann – Whitney U test).*

YM58483

This compound, a pyrazole derivate, is a potent inhibitor of SOCE, as it has been shown to block TG-induced Ca^{2+} influx (Ishikawa et al. 2003; Zitt et al. 2004). YM58483 (100 μM) was added once the activation of LPHN1 already manifested its effects upon the addition of 0.25 nM LTX^{N4C}. The cells recorded continued to burst for approximately 15 minutes after the addition of YM58483, but with a lower overall frequency; the spontaneous activity subsequently stopped almost completely. The calculated averaged frequency of exocytosis after addition of YM58483 was 2.92 ± 1.62 Hz (Figure 6.8 A and B).

The average amplitude of MEPPs did not significantly change between the experimental conditions considered (0.82 ± 0.11 mV in Ca^{2+} buffer, 1.01 ± 0.01 mV after the addition of LTX^{N4C}, and 0.74 ± 0.02 mV after the addition of YM58483, Figure 6.8 C).

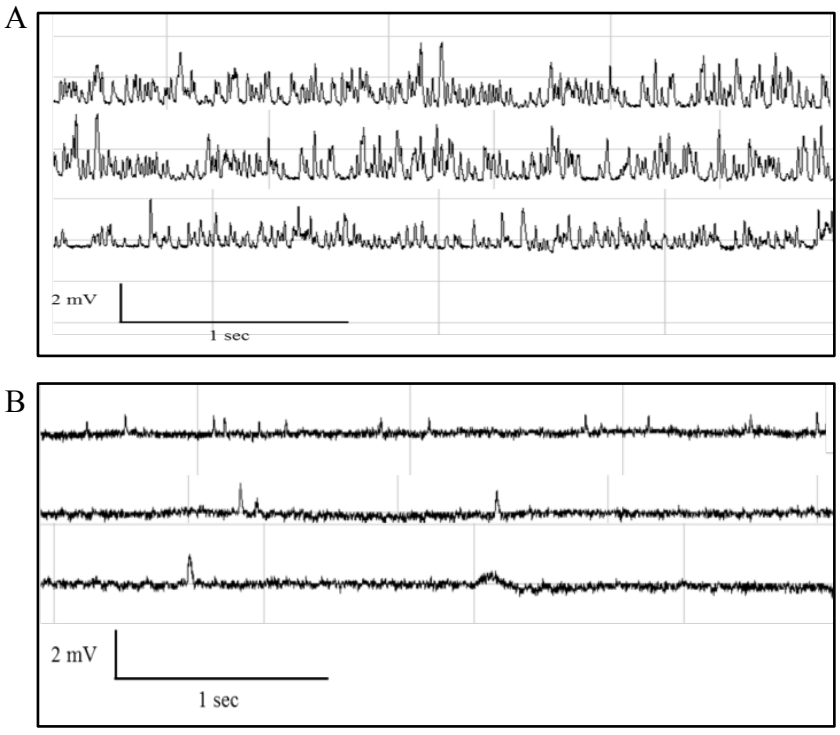

Figure 6.7. Single traces of MEPPs recordings in Ca^{2+} buffer after the addition of LTX^{N4C} (A) and of YM58483 (B). YM58483 is able to inhibit the effects due to LPHN1 activation when added after stimulation by LTX^{N4C}.

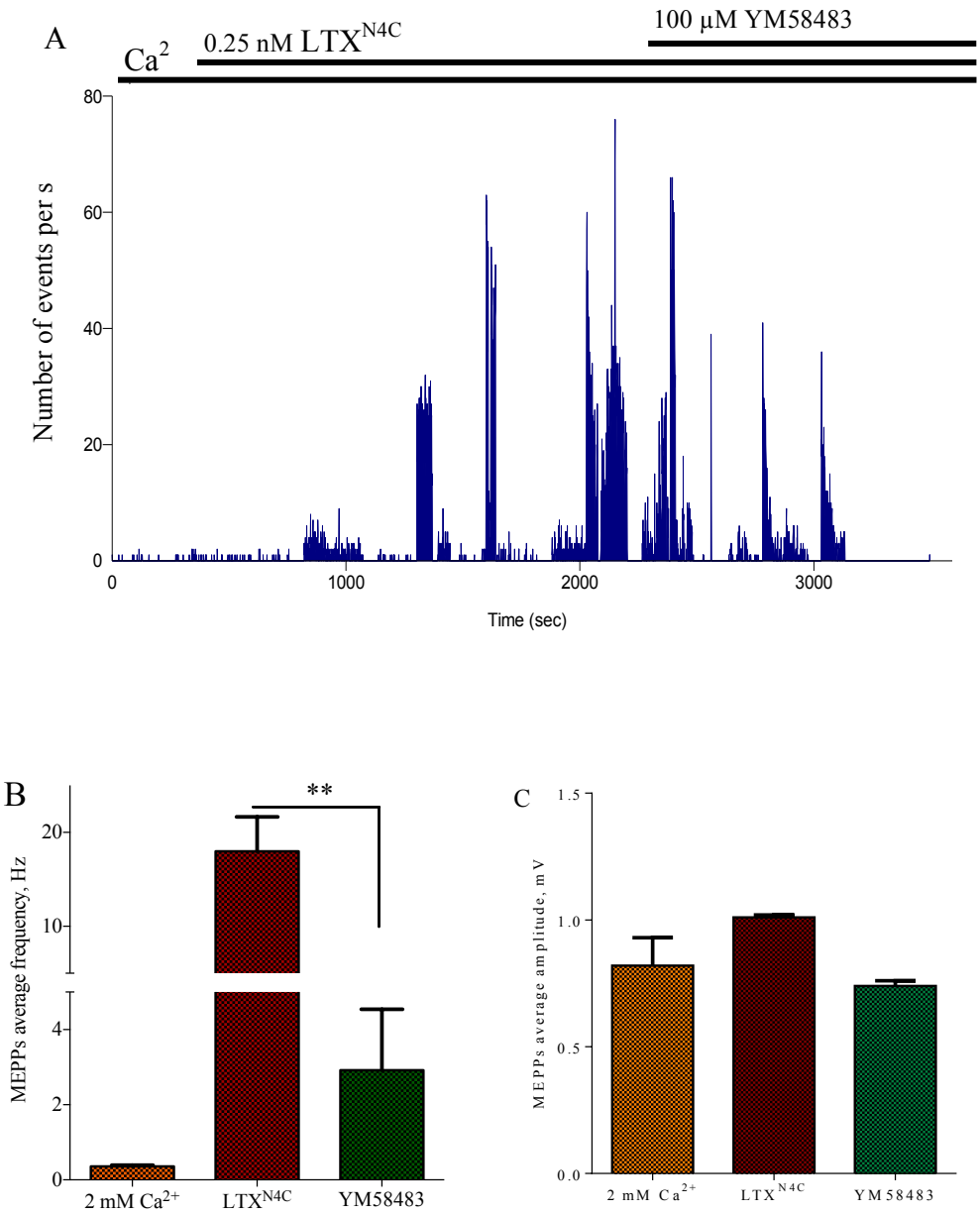

*Figure 6.8. A. Frequency plot of a MEPPs recording in buffer containing 2 mM Ca^{2+}, and after the addition of LTX^{N4C}, and YM58483. YM58483 significantly reduced the frequency of exocytosis caused by LPHN1 activation by LTX^{N4C}. B. Average frequency of MEPPs in Ca^{2+} buffer, and after the addition of LTX^{N4C}, and YM58483. C. Average amplitude of MEPPs in Ca^{2+} buffer, and after the sequential addition of LTX^{N4C} and YM58483. The difference between the conditions is not statistically significant (N = 1, n = 6 cells recorded in Ca^{2+} buffer, 15 cells after addition of LTX^{N4C}, and 11 after addition of YM58483; **, P < 0.010, Mann – Whitney U test).*

To summarise, all the drugs used directed to block or inhibit different components of the SOCE successfully acted against the activation of LPHN1 and, although not completely, they were effective in decreasing significantly the frequency of exocytosis (Figure 6.9).

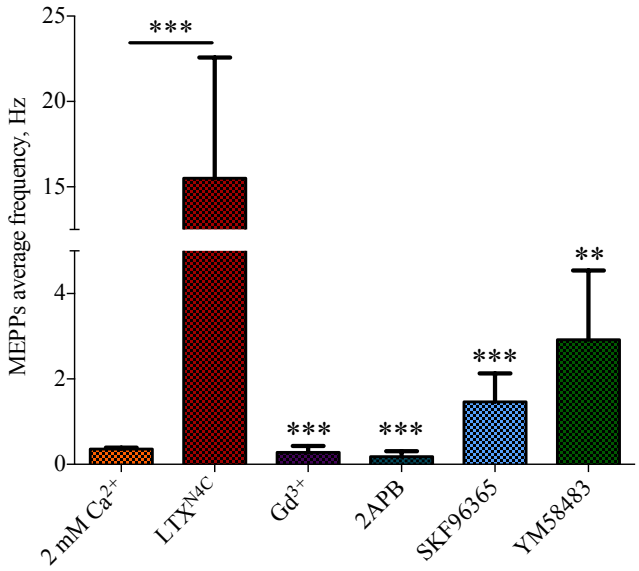

*Figure 6.9. Summary of the average frequency of MEPPs upon addition of drugs directed to inhibit or block components of the SOCE (Gd^{3+}, 2APB, SKF96365, and YM58483). The values of MEPPs frequency in each condition were compared to the effects of LTX^{N4C} using the Mann – Whitney U test (**, $P < 0.01$; ***, $P < 0.001$). The graph shows the results of four independent series of experiments, where the effects of LTX^{N4C} under treatment conditions were compared to their own negative and positive control values, recorded on the same preparations prior to the treatments. The graph does not attempt to compare each treatment to an average control value, but only serves to illustrate the scale of effects of different treatments (note, however, that the control values are remarkably similar in all experiments). For these reasons, no correction for multiple pairwise comparisons has been applied.*

6.2.2 Depletion of intracellular Ca^{2+} stores using thapsigargin

As I determined in the experiments described in the previous sections of this chapter, the activation of LPHN1 ultimately leads to the influx of Ca^{2+}, which presumably occurred due to the opening of SOCCs in response to the depletion of the intracellular Ca^{2+} stores. To confirm the critical role of the intracellular Ca^{2+} stores in the LPHN1 signalling pathway, I used thapsigargin (TG), an inhibitor of the sarco/endoplasmic reticulum Ca^{2+} ATPase (SERCA) pump. Extracted from the plant *Thapsia garganica*, this compound raises the cytoplasmic Ca^{2+} concentration by stimulating the release of Ca^{2+} from IP_3 and GTP-sensitive intracellular stores, and at the same time irreversibly blocking the refilling of these stores by the SERCA pump (Thastrup et al. 1990; Lytton, Westlin and Hanley 1991; Treiman, Caspersen and Christensen 1998).

In a Ca^{2+}-containing buffer (2 mM), the effects caused by the elevation of intracellular [Ca^{2+}] caused by TG were remarkably similar to the effects of LPHN1 activation by LTX^{N4C}. However, as the $G\alpha_q$ – PLC – IP_3 pathway was not stimulated by TG, its effects were apparently due to the opening of SOCCs. This suggested that the burst-like release of ACh caused by LTX^{N4C} is indeed associated with the activity of SOCCs.

Upon the addition of 10 μM TG, the frequency of neurotransmitter release had a ~ 35 fold increase compared to the basal frequency of release in Ca^{2+} buffer (0.36 ± 0.03 Hz in Ca^{2+} buffer vs 12.12 ± 2.56 Hz after the addition of TG). This increase occurred within 1 minute from the addition of the drug, and it could continue for a long time (> 1 hour) without attenuation (Figure 6.11 A and B).

Addition of TG caused a significant increase in the average amplitude of MEPPs (0.82 ± 0.11 mV in Ca^{2+} buffer, 2.5 ± 0.02 mV after the addition of TG, Figure 6.11 C).

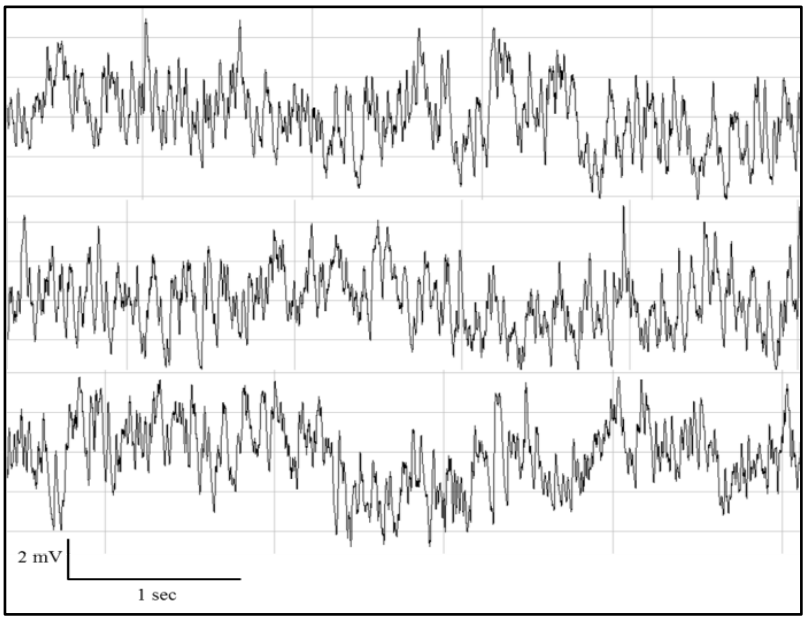

Figure 6.10. Single traces of MEPPs recorded in Ca^{2+} buffer after the addition of 10 µM TG. This drug caused a 35 fold increase in neurotransmitter release, that lasted > 1 hour without attenuation.

A

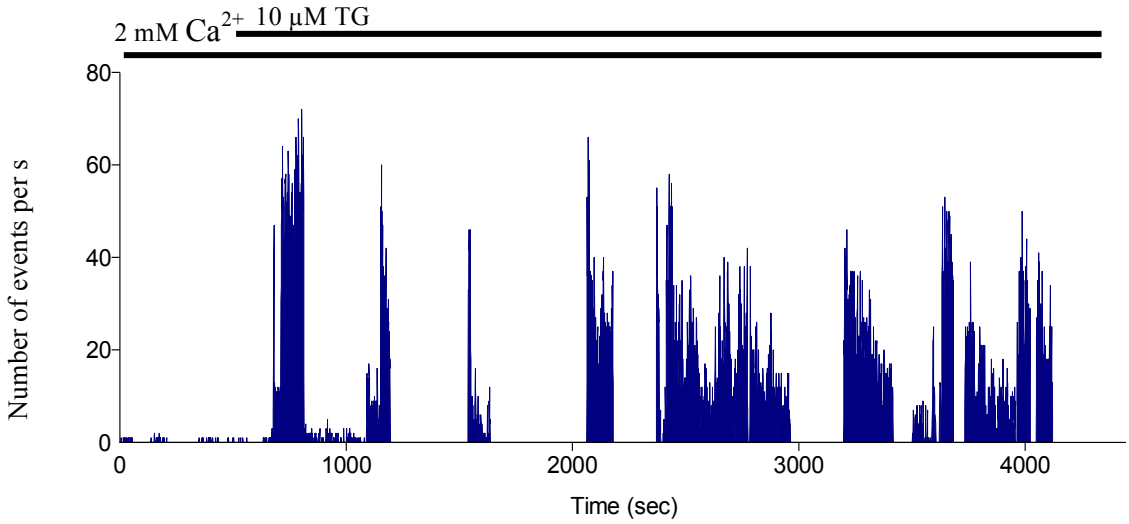

Continued on the next page

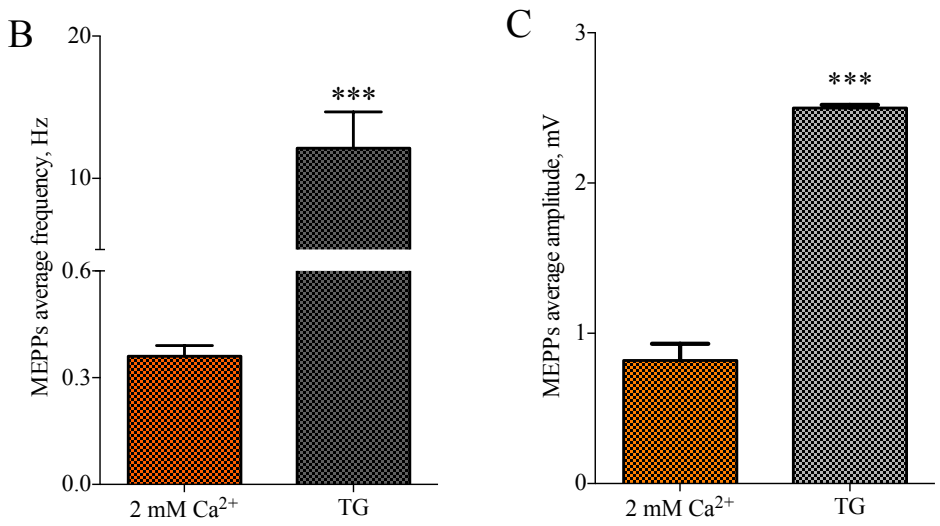

*Figure 6.11. A. Frequency plot of a MEPPs recording in 2 mM Ca^{2+} and after the addition of TG. B. Average frequency of MEPPs in Ca^{2+} buffer and after the addition of TG. C. Average amplitude of MEPPs in Ca^{2+} buffer and after the addition of TG (N = 3, n = 25 cells in Ca^{2+} buffer, 27 cells after addition of TG; ***, P < 0.001 Mann – Whitney U test).*

In a Ca^{2+}-free buffer, the addition of TG caused a temporary increase in neurotransmitter release that ceased after ~ 10 minutes. The features of this increase were not significantly different from that observed in the presence of extracellular Ca^{2+} (11.25 ± 4.98 Hz in Ca^{2+}-free buffer vs 12.12 ± 2.56 Hz in Ca^{2+} buffer). After the cessation of exocytosis, if Ca^{2+} was added to the extracellular buffer, the frequency of exocytosis went back up to the previous levels (13.49 ± 1.19 Hz), and again continued for a long time (Figure 6.13 A and B).

Also in this case the average amplitude of MEPPs in TG (both in the presence and in the absence of Ca^{2+}) was significantly higher than the amplitude in Ca^{2+} buffer; the amplitude with and without Ca^{2+} in the presence of TG was not statistically significant (2.08 ± 0.03 mV and 2.17 ± 0.03 mV respectively, Figure 6.13 D).

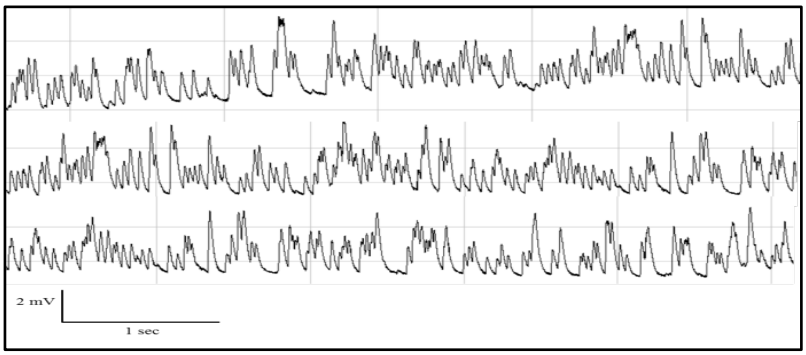

Figure 6.12. Single traces of a MEPPs recording in Ca^{2+}-free buffer after the addition of TG. The elevation in frequency of exocytosis in the absence of Ca^{2+} in the extracellular buffer is the same as in the presence of Ca^{2+}. In this case, however, the elevation stops after about 10 minutes.

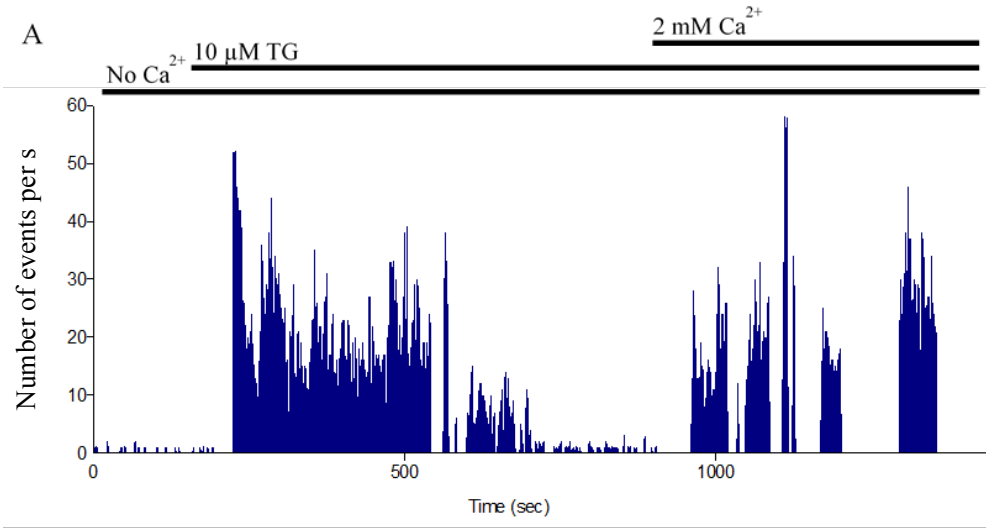

Continued on the next page

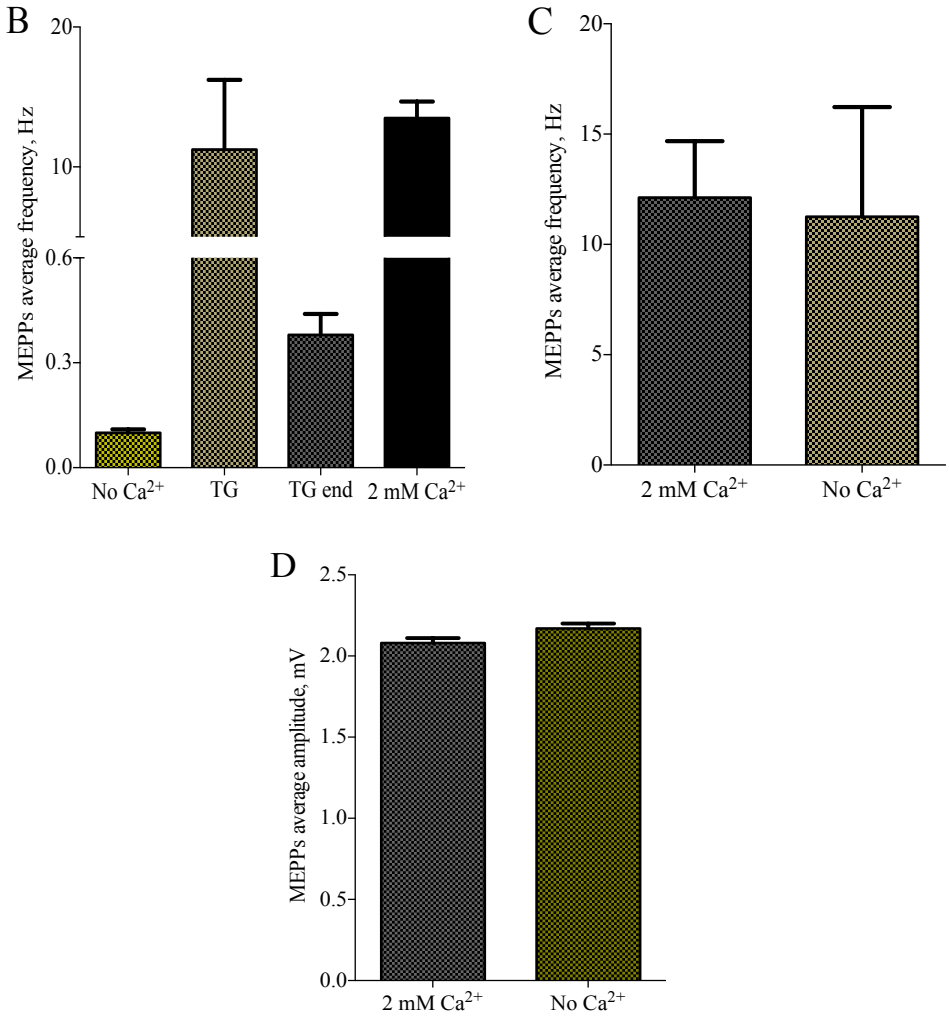

Figure 6.13. A. Frequency plot of a MEPPs recording in Ca^{2+}-free buffer, after the addition of TG and subsequent addition of 2 mM Ca^{2+}. B. Average frequency of MEPPs in a Ca^{2+}-free buffer, after the addition of TG and subsequent addition of 2 mM Ca^{2+}. C. Comparison between the average frequency of MEPPs induced by 10 μM TG in the presence and in the absence of extracellular Ca^{2+}. The difference is not statistically significant. D. Average amplitude of MEPPs caused by TG in the presence and in the absence of extracellular buffer. The difference is not statistically significant (N = 2, n = 15 cells recorded after the addition of TG in Ca^{2+}buffer, and 18 cells in Ca^{2+} free buffer).

Interestingly, when TG (10 μM) was added in Ca^{2+}-containing buffer after LTX^{N4C} (0.25 nM), and after the effects of LPHN1 activation had already developed, the exocytosis stopped completely within seconds of the addition of TG (0.05 ± 0.03 Hz, Figure 6.15).

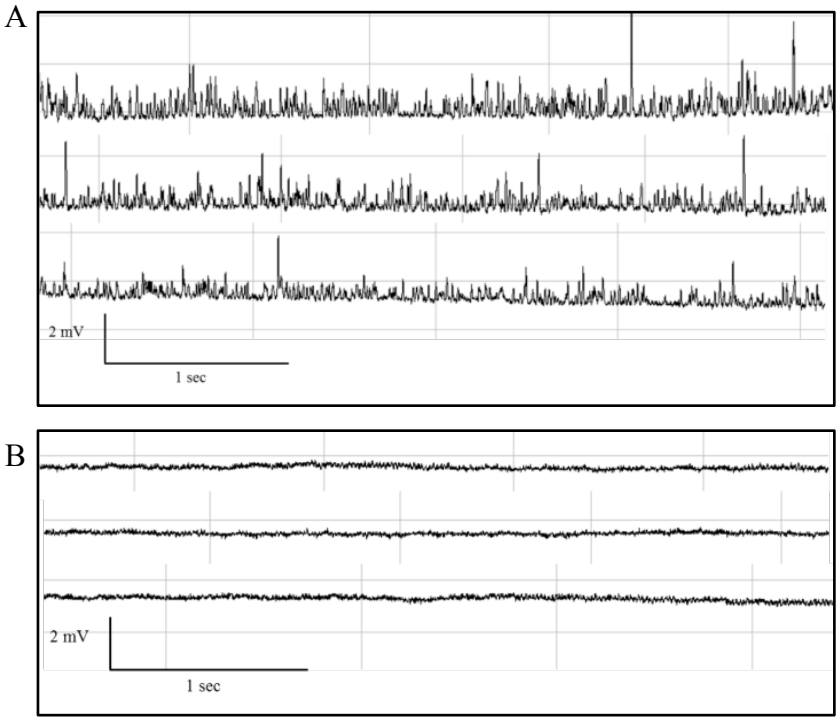

Figure 6.14. Single traces of MEPPs in Ca^{2+} buffer after the addition of LTX^{N4C} (A) and after the addition of TG (B). TG is able to stop LPHN1-mediated increase in exocytosis within seconds from addition.

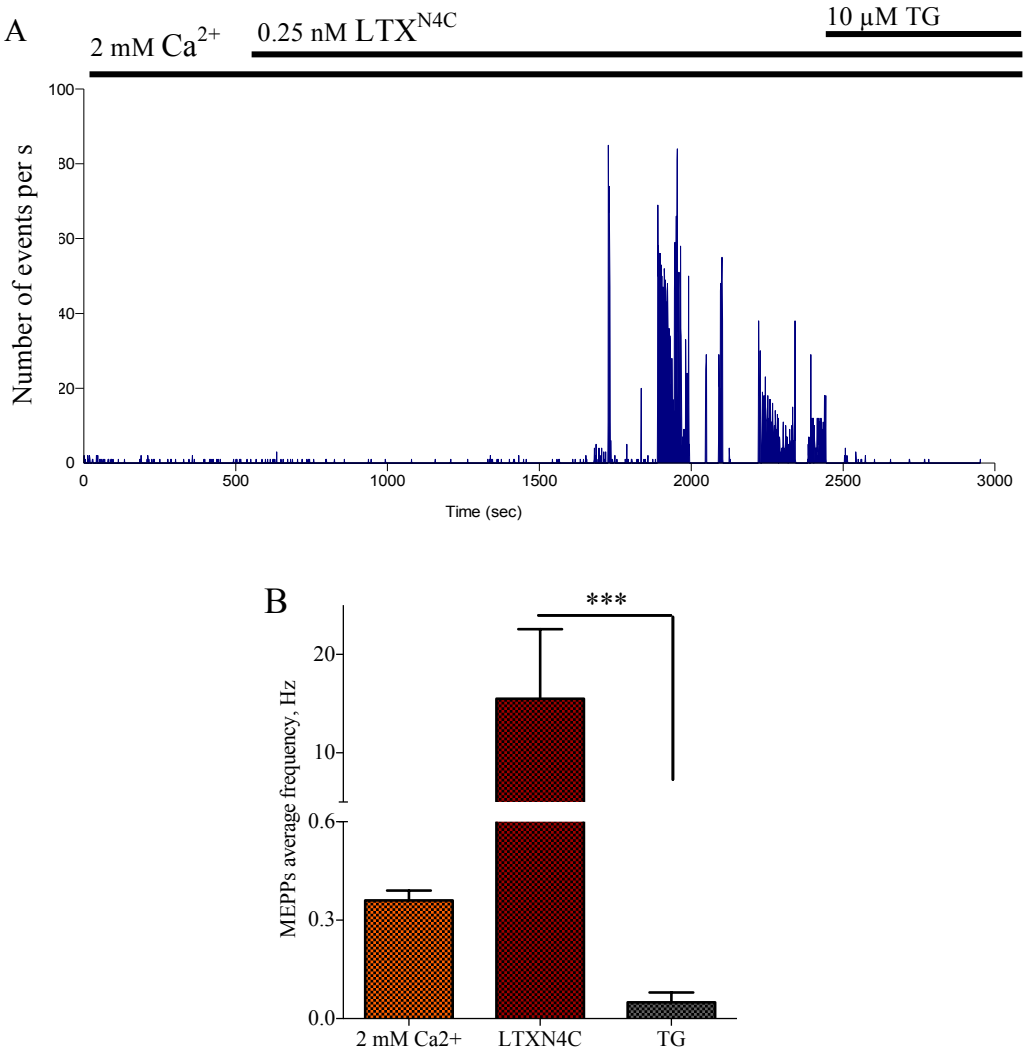

*Figure 6.15. A. Frequency plot of a MEPPs recording in the presence of 2 mM Ca^{2+}, and after the sequential addition of LTX^{N4C} and TG. Addition of TG, after LTX^{N4C} had triggered an increase in exocytosis, caused a sudden cessation of neurotransmitter release. B. Average frequency of MEPPs in Ca^{2+} buffer, after the addition of LTX^{N4C} and TG (N = 3, n = 12 cells recorded in Ca^{2+} buffer, 15 cells after the addition of LTX^{N4C}, and 17 cells after the addition of TG; ***, P < 0.001, Mann – Whitney U test).*

In a specular experiment, when LTX^{N4C} (0.25 nM) was added in Ca^{2+}-free buffer after the peak of exocytosis caused by TG (10 μM) has ceased, I did not observe any increment in the frequency of neurotransmitter release, not even when 2 mM Ca^{2+} was added to the extracellular buffer at a later stage (0.16 ± 0.09 Hz after the addition of LTX^{N4C} in Ca^{2+}-free buffer + TG, and 0.02 ± 0.01 Hz after the addition of Ca^{2+}, Figure 6.17). This data suggested that intact intracellular Ca^{2+} stores were critical for the toxin-induced influx of extracellular Ca^{2+} and likely mediated the toxin's effect.

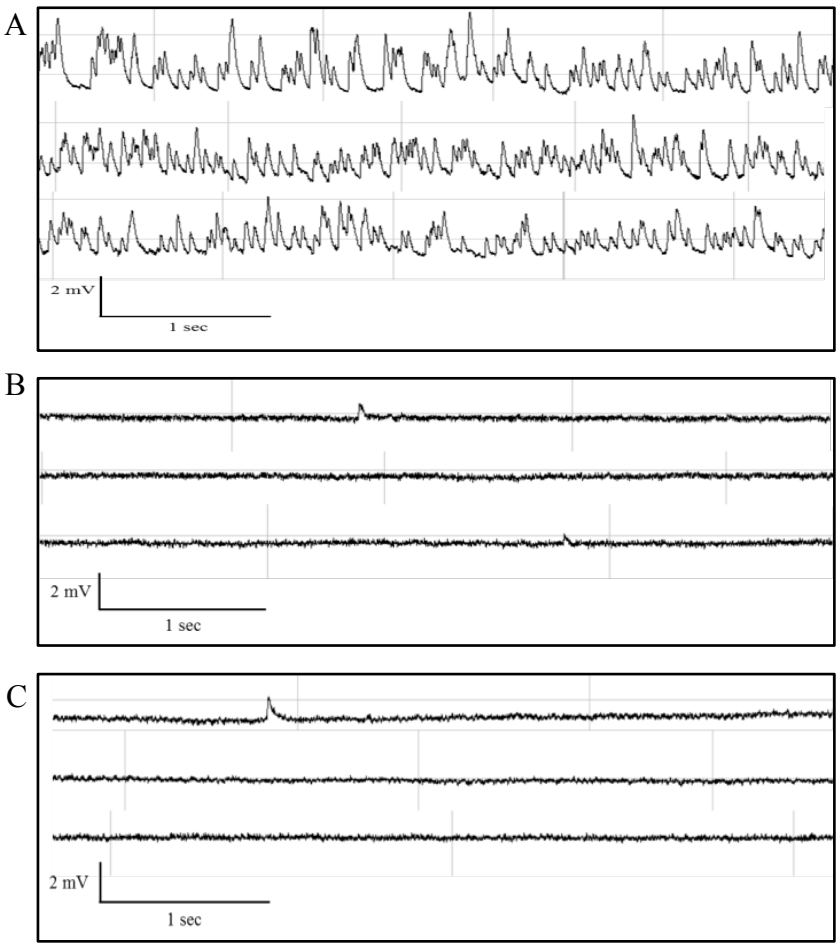

Figure 6.16. Single traces of MEPPs recording in Ca^{2+}-free buffer after the addition of TG (A), and after the addition of LTX^{N4C} (B) and Ca^{2+} (C) once the effects of TG has ceased. The effects of LTX^{N4C} are not able to develop in the presence of TG, with or without the presence of extracellular Ca^{2+}.

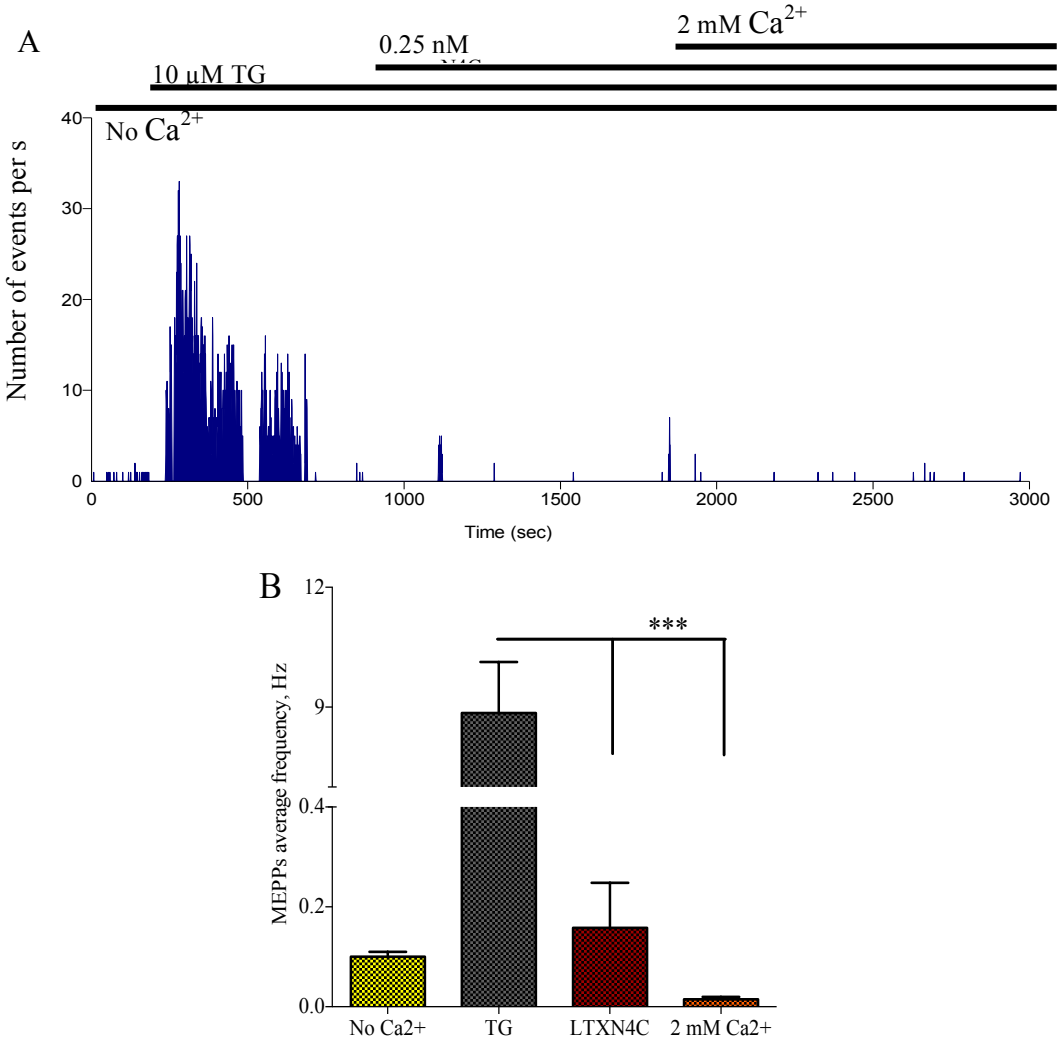

*Figure 6.17. Frequency plot of a MEPPs recording in Ca^{2+}-free buffer, and after the addition of TG, LTX^{N4C}, and 2 mM Ca^{2+}. When added once the peak of exocytosis caused by TG ceased, LTX^{N4C} was not able to increase the frequency of exocytosis even if 2 mM Ca^{2+} was added. B. Average frequency of MEPPs in Ca^{2+}-free buffer, after the addition of TG, LTX^{N4C} and Ca^{2+} (N = 2, n = 5 cells recorded in Ca^{2+}-free buffer, 5 cells after addition of TG, 5 cells after the addition of LTX^{N4C}, and 9 after the addition of 2 mM Ca^{2+}; ***, P < 0.001, Mann – Whitney U test).*

6.2.3 Ba^{2+} and Sr^{2+} support LPHN1-induced exocytosis in the absence of extracellular Ca^{2+}

As I discussed in a previous chapter (see Chapter 4, Section 4.2.8), experiments using LTX^{N4C} to stimulate LPHN1 were conducted replacing the Ca^{2+} in the extracellular buffer either with Ba^{2+} or Sr^{2+}. These experiments, as well as demonstrating that LTX^{N4C} acts via LPHN1 rather than NRX, also help to support the hypothesis that the release of Ca^{2+} from the stores followed by opening of SOCCs and subsequent Ca^{2+} entry in nerve terminals is the mechanism by which LPHN1 works. Here, I specifically investigated the role of divalent cations (other than Ca^{2+}) in mediating the stimulation of Ca^{2+} release from the intracellular stores prestimulated by LPHN1 signalling.

Ba^{2+} and Sr^{2+} are both permeable to TRPC channels and are able to generate I_{CRAC} (Yeromin et al. 2004; Parekh and Putney 2005; Bakowski and Parekh 2007; Ma et al. 2008; Salido, Sage and Rosado 2009; Moreno and Vaca 2011). Furthermore, they can stimulate Ca^{2+} release from intracellular stores, increasing the intracellular [Ca^{2+}] and stimulating neurotransmitter release (Gregoire, Loirand and Pacaud 1993; Przywara et al. 1993; Verhage et al. 1995; Spencer and Berlin 1997).

Neuromuscular preparations incubated in a buffer where Ca^{2+} was substituted with 2 mM Ba^{2+}, were able to respond to the activation of LPHN1 in a manner very similar to that observed in the presence of Ca^{2+}. The overall average frequency of exocytosis reached an average of 9.71 ± 1.35 Hz, and the cells showed the bursting behaviour typical of the activation of LPHN1. The frequency in the bursts reached an average of 41.05 ± 3.02 Hz, and during interburst intervals an average of 0.88 ± 0.19 Hz (Figure 6.19 A and B). However, the time elapsed from the addition of LTX^{N4C} to the appearance of the bursts was slightly increased (it took on average 41 ± 4.04 min) compared to the delay observed in Ca^{2+} buffer (17 ± 2.5 min, Figure 6.22).

The MEPPs average amplitude did not show any significant change between the conditions considered an in respect to the control amplitude in Ca^{2+} buffer (0.82 ±

0.11 mV in Ca^{2+} buffer, 0.92 ± 0.03 mV in Ba^{2+} buffer, and 0.91 ± 0.02 mV in Ba^{2+} buffer after the addition of LTX^{N4C}, Figure 6.19 C).

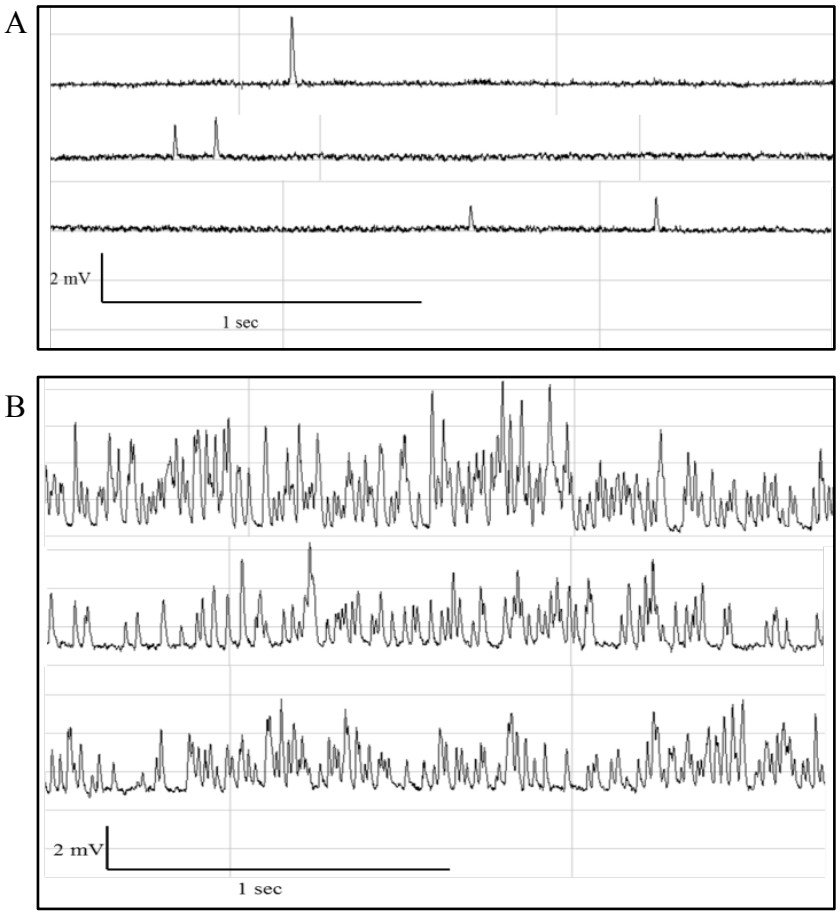

Figure 6.18. Single traces of MEPPs recordings in Ba^{2+} buffer (A) and after the addition of LTX^{N4C} (B). The effects of LPHN1 activation fully develop when Ba^{2+} replaces Ca^{2+} in the extracellular buffer.

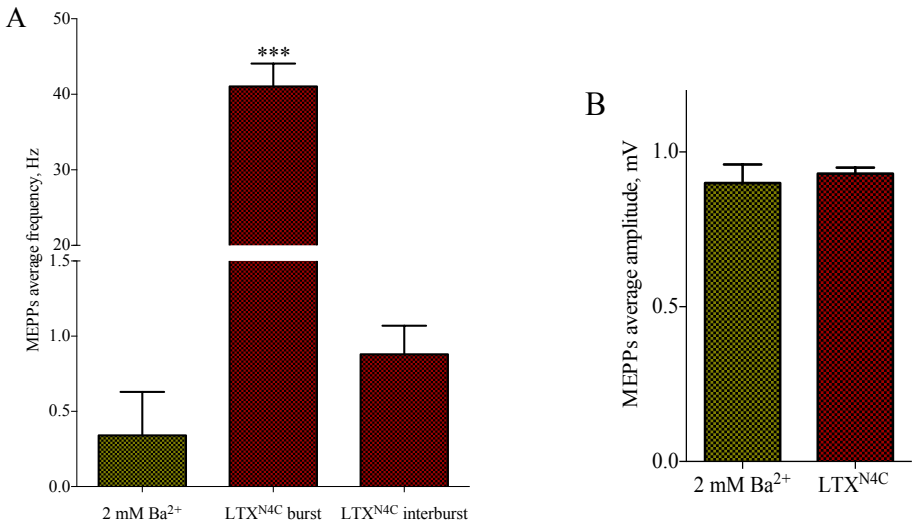

*Figure 6.19. A. Average frequency of MEPPs in Ba^{2+} buffer before and after the addition of LTX^{N4C}. B. Average amplitude of MEPPs in Ba^{2+} buffer before and after the addition of LTX^{N4C}. The difference is not statistically significant (N = 2, n = 16 cells recorded in Ba^{2+} buffer and 70 cells recorded after addition of LTX^{N4C}. ***, P<0.001, Mann – Whitney U test).*

In a similar way, preparations incubated in a buffer where Ca^{2+} was replaced by 2 mM Sr^{2+} responded to the activation of LPHN1 by 0.25 nM LTX^{N4C} with increased exocytosis, that overall reached a frequency of 6.51 ± 2.27 Hz. The cells showed bursting behaviour, with an average frequency of 37.45 ± 17.94 Hz during bursts and 0.84 ± 0.16 Hz during interburst intervals (Figure 6.21 A and B). In this case, it was necessary to wait 92 minutes to see the effects of the activation of LPHN1 on exocytosis (Figure 6.22).

The MEPPs average amplitude was not significantly different between the conditions considered and compared to the control amplitude in Ca^{2+} buffer (0.82 ± 0.11 mV in Ca^{2+} buffer, 0.85 ± 0.08 mV in Sr^{2+} buffer, and 0.78 ± 0.03 mV after the addition of LTX^{N4C}, Figure 6.21 C).

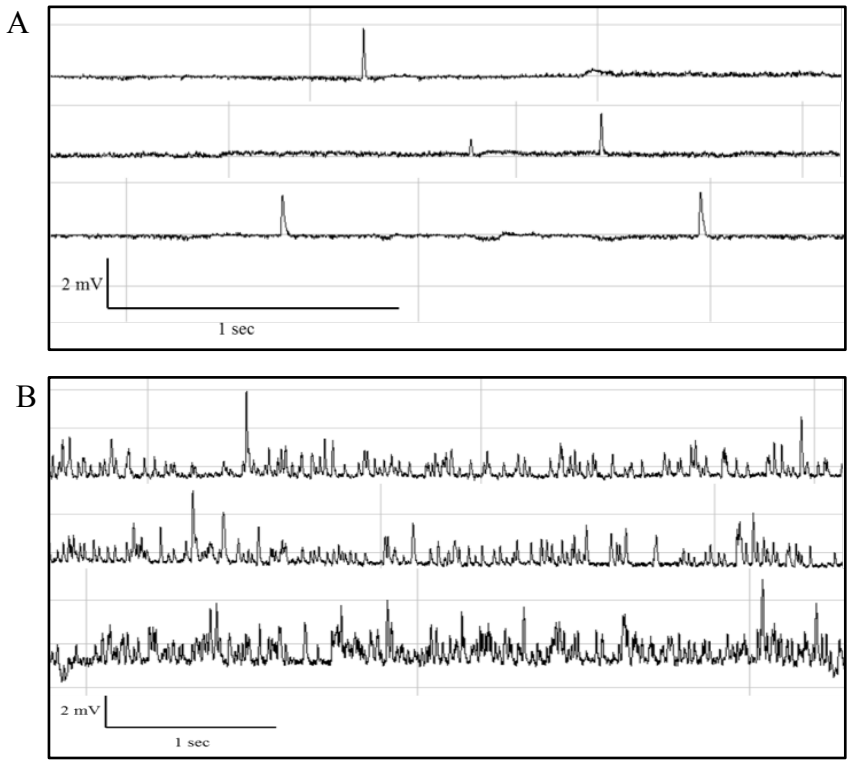

Figure 6.20. Single traces of MEPPs in Sr^{2+} buffer (A) and after the addition of LTX^{N4C} (B). The effects of LPHN1 activation fully develop when Sr^{2+} replaces Ca^{2+} in the extracellular buffer.

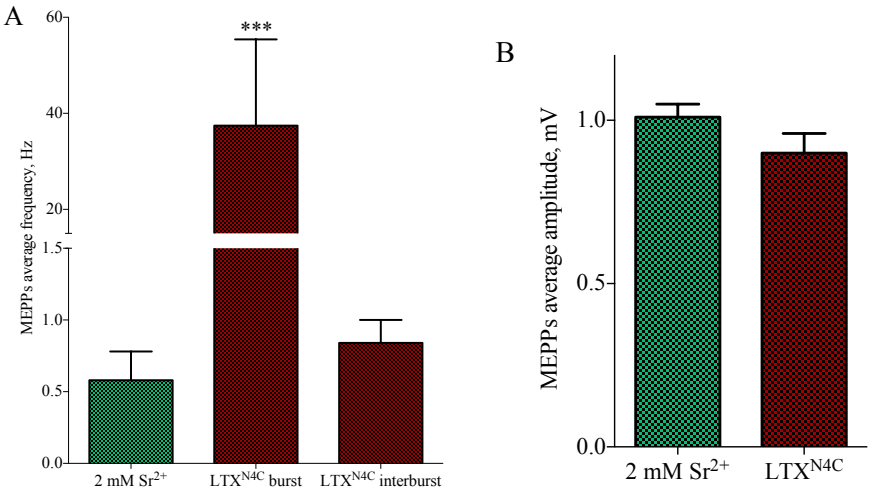

*Figure 6.21. A. Average frequency of MEPPs in Sr^{2+} buffer before and after the addition of LTX^{N4C}. B. Average amplitude of MEPPs before and after the addition of LTX^{N4C} in Sr^{2+}-containing buffer. The difference is not statistically significant (N = 2, n = 5 cells recorded in 2 mM Sr^{2+}, 45 cells recorded after the addition of LTX^{N4C}; ***, P<0.001, Mann – Whitney U test).*

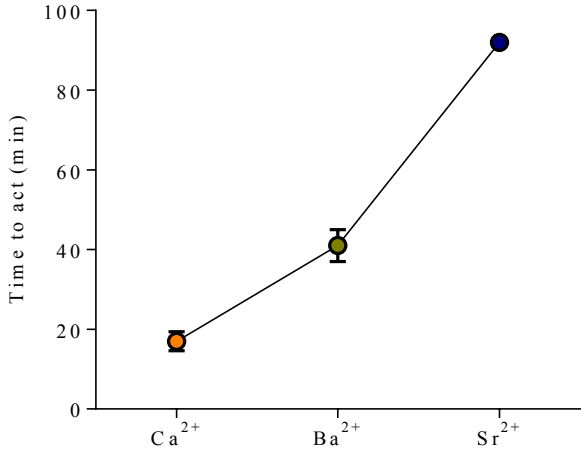

Figure 6.22. Time elapsed between the addition of LTX^{N4C} and the start of its manifested effects on exocytosis in Ca^{2+}, Ba^{2+} and Sr^{2+} buffer. The time LPHN1 needs to react to stimulation consistently increases going from Ca^{2+}, to Ba^{2+} and Sr^{2+}.

6.3 Discussion

The experiments described in this chapter were designed to investigate the involvement of store-operated Ca^{2+} entry (SOCE) downstream of activation of LPHN1. As I previously discussed, the intracellular pathway activated by LPHN1 leads to the increase in cytosolic [Ca^{2+}] by stimulating the release of Ca^{2+} from intracellular Ca^{2+} from IP_3-sensitive Ca^{2+} stores and ultimately the influx of Ca^{2+} through SOCCs.

It has been well described in the literature how the depletion of intracellular Ca^{2+} stores causes the opening of SOCCs located at the plasma membrane (PM): STIM, a transmembrane protein located at the ER, functions as a Ca^{2+} sensor detecting the fall in ER [Ca^{2+}]; it then forms dimers and translocates into puncta in close proximity to the PM, where it contacts Orais and TRPC channels, causing their opening and consequent influx of Ca^{2+} that can then refill the stores. At this point, SARAF detects the elevation of ER [Ca^{2+}] and promotes the disaggregation of STIM dimers, preventing the overfilling of the stores by inhibiting SOCE (for a review see Chapter 1, Section 1.4.2).

Considering this mechanism, the next step of my investigation was directed to test the involvement of these channels in the activity of LPHN1. Several blockers of the SOCE molecular components were used in current clamp experiments where LPHN1 was activated using LTX^{N4C}, and the changes in exocytosis caused by these drugs were analysed.

All drugs used (Gd^{3+}, 2APB, SKF96365, and YM58483) significantly inhibited (or fully blocked) the increase in exocytosis caused by the activation of LPHN1 (see Figure 6.9). Of these drugs, 2APB was the most effective in stopping the effects of LPHN1, likely due to the fact that this drug does not only act on SOCCs, but also on IP_3R; these effects combined resulted in an overall lower cytosolic [Ca^{2+}] and, as a consequence, in a greater inhibition of exocytosis.

The experiments conducted using TG prove the ability of the intracellular Ca^{2+} stores to induce massive spontaneous exocytosis. As I showed (see Figure 6.11), the effects of TG alone (when used in a buffer containing Ca^{2+}) are very similar to the effects observed with the stimulation of LPHN1 by LTX^{N4C}.

However, as we can expect, the bursting behaviour is not present in this case as TG, blocking the SERCA pumps, prevents the refilling of the stores and therefore periodical inactivation of SOCCs. Things take a different direction when TG is used in a Ca^{2+} free buffer: in this case, the increase in exocytosis is only temporary and ceases after a short time; at that point, addition of Ca^{2+} to the extracellular buffer causes the exocytosis to increase again, due to the influx of Ca^{2+} from the SOCCs that have been activated upon store depletion (see Figure 6.13).

The TG experiments also demonstrated the central role of stores in the opening of SOCCs downstream of LTX^{N4C}-induced activation of LPHN1. When TG depletes the stores in a Ca^{2+}-free buffer, then LTX^{N4C} is unable to act, even in the presence of extracellular Ca^{2+} (see Figure 6.17). This was unexpected, taking into consideration that in the absence of LTX^{N4C}, the addition of Ca^{2+} to TG-treated preparation increases the release of neurotransmitter again.

Even more interesting is what happens when TG is added after LTX^{N4C}. In this case, TG causes the sudden and complete cessation of neurotransmitter release (see Figure 6.15) within 3-5 s.

This result is quite difficult to explain unless we hypothesise a non-canonical effect of TG. In the literature, TG is always described as a drug that very specifically targets the SERCA pump in the intracellular Ca^{2+} stores (Thastrup et al. 1990; Lytton, Westlin and Hanley 1991; Treiman, Caspersen and Christensen 1998). However, as the effect of TG (when added after the toxin) develops almost instantaneously, it cannot be due to the inhibition of SERCA. Indeed, (1) the drug cannot penetrate into the cell so quickly (in less than 5 s), and (2) even if it did, the blockade of SERCA would increase cytosolic Ca^{2+} due to its leakage from the stores, leading to an increase rather than a decrease in spontaneous exocytosis. Thus, my findings suggest that TG also has another effect on the cells. One possible way to explain these results is that TG may act as a blocker of a crucial Ca^{2+} channel used by LPHN1 to develop and maintain its effects.

These considerations and also the fact that LTX^{N4C} does not cause an increase in exocytosis in the absence of extracellular Ca^{2+}, but TG does, made us

review the theory according to which Ca^{2+} release from the stores is the only mechanism of LTX^{N4C} action via LPHN1. In fact, it seems clear that LPHN1-mediated stimulation of IP_3R is insufficient to stimulate the release of Ca^{2+} from the stores and the subsequent depletion and opening of SOCCs. It is clear now that at least at the beginning of LPHN1 activation, the influx of Ca^{2+} from extracellular space is necessary to start the mechanism delineated so far. The fast inhibition of the toxin's effect by TG also points at such a possibility.

Moreover, my experiments using Ba^{2+} and Sr^{2+} showed that an influx of not only Ca^{2+}, but also other divalent cations, occurs from the extracellular space, and that these divalent cations can fully replace Ca^{2+} and support the mechanism caused by LPHN1 activation. In the presence of these divalent cations, LTX^{N4C} is able to cause increased neurotransmitter release and bursts of exocytosis in a manner not distinguishable from what happens in Ca^{2+} (see Figures 6.19 and 6.21). The only difference found was in the delay between the addition of the toxin and the rise in exocytosis. In Ca^{2+}, the effect of LPHN1 activation normally takes about 20 minutes to begin; in Ba^{2+} this time goes up to about 40 minutes and in Sr^{2+} it further increases to about 90 minutes. This could be due to the fact that, although these cations can enter the cells during the initial phase and are then capable of stimulating Ca^{2+} release from intracellular Ca^{2+} stores (Gregoire, Loirand and Pacaud 1993; Przywara et al. 1993; Verhage et al. 1995; Spencer and Berlin 1997; Yeromin et al. 2004; Parekh and Putney 2005; Ma et al. 2008; Moreno and Vaca 2011), the extent of this release is not as high as that caused by the initial influx of Ca^{2+} and more time is necessary to reach the level of store depletion needed to start the SOCC-mediated Ca^{2+} influx and bursts of exocytosis (see Figure 6.22).

The bursting exocytosis observed upon activation of LPHN1 can still be explained by the mechanism involving the depletion of intracellular Ca^{2+} stores. Store depletion starts the influx of Ca^{2+} from the extracellular space via SOCCs; however, when the stores are refilled, the influx would stop. Consistent with this, the elevated cytosolic $[Ca^{2+}]$ flowing into the terminals through SOCCs would lead to the elevation of MEPP frequency during the bursts; this frequency would then go down close to control levels once the stores have been refilled, SOCCs are

inactivated and the cytosolic [Ca^{2+}] is decreased by the normal maintenance mechanisms. The stimulation of IP_3R, however, still persists as long as LPHN1 is activated, therefore the stores would start depleting again, and the cycle of activation and inactivation of the SOCCs and exocytosis would start again giving rise to other bursts.

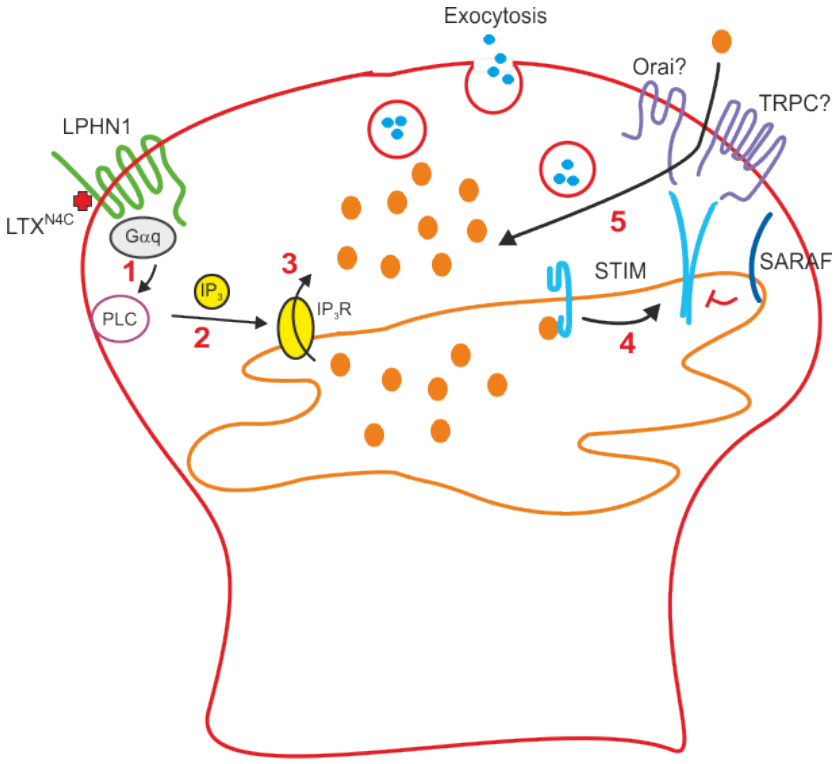

Figure 6.23. Schematic representation of the molecular mechanisms involved in LPHN1 activation. As described previously (Chapter 5, Figure 5.15), activation of LPHN1 activates the $G\alpha_q$ protein pathway, involving activation of PLC (arrow 1), stimulation of IP_3Rs by IP_3 (arrow 2), and release of Ca^{2+} from the ER intracellular stores (arrow 3). Depletion of the stores is sensed by STIM1, a transmembrane protein located at the ER, that under these circumstances dimerises and translocates close to the plasma membrane (arrow 4). Here, STIM1 contacts and opens store-operated Ca^{2+} channels (TRPCs and Orais), that start the influx of Ca^{2+} that allows the refilling of the stores (arrow 5). At this point STIM1 goes back to its monomeric conformation and SOCE stops.

Although these experiments support the hypothesis that the store depletion – opening of SOCCs is the mechanism used by LPHN1 to achieve the burst-like regulation of exocytosis observed upon addition of LTX^{N4C}, they were unable to clearly identify the nature of the channels responsible for this effect. Preliminary data obtained from differentiated neuroblastoma (Nb2a) cells can give us some suggestions about it, however. Nb2a cells stably expressing LPHN1 do not normally respond to LTX^{N4C} unless they are induced to differentiation by serum deprivation or dibutyryl-cAMP. In this condition, the mRNA levels were measured by RT-PCR, and the level of expression of different SOCE proteins in LPHN1 expressing cells were compared to wild type and undifferentiated cells to see if the response to LTX^{N4C} in LPHN1-expressing differentiated cells was due to the upregulation of some SOCE gene/s and consequently to higher expression of particular proteins. Results suggest that the proteins being upregulated in differentiated LPHN1-expressing Nb2a cells are STIM1, SARAF, Orai 3 and TRPC2 (Blackburn, Ushkaryov, data not published). This suggests that all the proteins necessary for a functional SOCE are upregulated in these cells, therefore this could be the reason why they are able to respond to LTX^{N4C} upon differentiation only.

Although this model system can give some suggestions on what channels are used by LPHN1 in a model system, they could be very different in neurons, which can possibly express other Orais and TRPCs, and where LPHN1 could activate more than one type of SOCCs, if not all of them. Experiments on motor neurons cultures where knock down of specific genes is possible would be necessary to clearly identify the specific proteins used by LPHN1 to produce its effects.

Finally, the role of the Ca^{2+} channels crucially involved in the initial activation of the intracellular stores by LTX^{N4C} via LPHN1 remains unexplained by this mechanism of cyclical store depletion/SOCC activation. The next chapter of this dissertation will be dedicated to exploring the involvement of other types of Ca^{2+} channels in the effects on exocytosis caused by the activation of LPHN1.

CHAPTER 7
RESULTS V. LPHN1 and voltage-gated calcium channels (VGCCs)

7.1 Introduction

In the previous chapters I delineated part of the mechanism activated by LPHN1 that causes the increase in exocytosis and the bursting behaviour observed when LTX^{N4C} is used to stimulate the receptor.

As we discussed, the G protein associated to LPHN1 that starts the molecular pathway leading to increased intracellular [Ca^{2+}] is $G\alpha_{q/11}$, that in turn activates PLC promoting the hydrolysis of PIP_2 in IP_3 and DAG. IP_3 then activates IP_3R on the ER, and this leads to the release of Ca^{2+} from intracellular stores into the cytosol. As cytosolic [Ca^{2+}] rises, the frequency of spontaneous exocytosis greatly increases, but then subsides when cytosolic Ca^{2+} is sequestered or chelated. The depletion of the stores in turn causes the activation of SOCE, which allows Ca^{2+} influx, causing a new increase in the intracellular [Ca^{2+}], replenishment of the stores and eventual Ca^{2+} removal from the cytosol. This rise and fall in [Ca^{2+}] produces a new wave of exocytosis. Once the stores have been replenished, the influx of Ca^{2+} from SOCCs stops and the mechanism starts again with the IP_3-induced release of Ca^{2+} from the stores. This causes oscillations in the intracellular [Ca^{2+}], going from relatively low levels when the SOCCs are closed, to higher levels when they are open: these oscillations supposedly give rise to the bursting behaviour that I extensively described in this work.

However, as the experiments using TG and other divalent cations revealed, the initial elevation in cytosolic [Ca^{2+}] caused by LPHN1 through IP_3R activation is not enough to start this whole mechanism: some other source of Ca^{2+} needs to be postulated, which at least at the beginning of LPHN1 activation helps to activate the IP_3R sufficiently to bring the intracellular [Ca^{2+}] to a level high enough to further stimulate the release from the stores and the activation of SOCE.

In this chapter, I investigated the involvement of VGCCs in this mechanism. The potential involvement of VGCCs was hypothesised on the basis of the previous publications which reported the observation of L-type Ca^{2+} current appearing in pancreatic β-cells in response to LTX^{N4C}-induced activation of LPHN1 (Lang et al. 1998; Lajus et al. 2006)

VGCCs, widely expressed in excitable cells, mediate Ca^{2+} influx in response to depolarisation of cells. In neurons, this is achieved after an action potential reaches the terminals and it is the stimulus needed to start synaptic transmission.

Composed of different subunits, VGCCs are classified according to the pore-forming α subunit, which generates diverse Ca^{2+} currents with peculiar physiological and pharmacological characteristics. According to this classification, VGCCs can be divided into Cav1 (1 – 4), Cav2 (1 – 3) and Cav3 (1 – 3), that give rise to L-, P/Q, N-, R- and T-type currents (for a review see Chapter 1, Section 1.5).

7.2 Results

7.2.1 P/Q VGCCs are involved in the activity of LPHN1

To investigate the potential role of VGCCs in the effects observed upon LPHN1 activation, I used drugs and toxins directed to block the major classes of neuronal VGCCs: L-, P/Q and N-types.

Nimodipine

Nimodipine is a dihydropyridine compound used in medicine for the treatment of deficits caused by cerebral vasospasm following subarachnoid haemorrhage. Although it is known that Nimodipine is a selective blocker of L-type VGCCs, its precise mechanism of action is still unknown (http://www.guidetopharmacology.org/GRAC/LigandDisplayForward?tab=summary&ligandId=2523).

In my experiments, I used Nimodipine both after and before the addition of LTX^{N4C} and the consequent activation of LPHN1.

When added after the effects of LPHN1 activation had been already present, Nimodipine was not able to stop or attenuate them (15.58 ± 5.48 Hz vs 15.50 ± 7.07 Hz with LTX^{N4C} only). The cells continued to show bursting behaviour, with the frequency during burst reaching an average of 34.15 ± 5.49 Hz and an interburst frequency of 0.829 ± 0.23 (Figure 7.2 A and B).

The average amplitude of MEPPs was significantly higher when Nimodipine was added to the extracellular buffer (0.82 ± 0.11 mV in Ca^{2+} buffer, 0.92 ± 0.04 after the addition of LTX^{N4C}, and 1.54 ± 0.01 mV in the presence of Nimodipine, Figure 7.2 C).

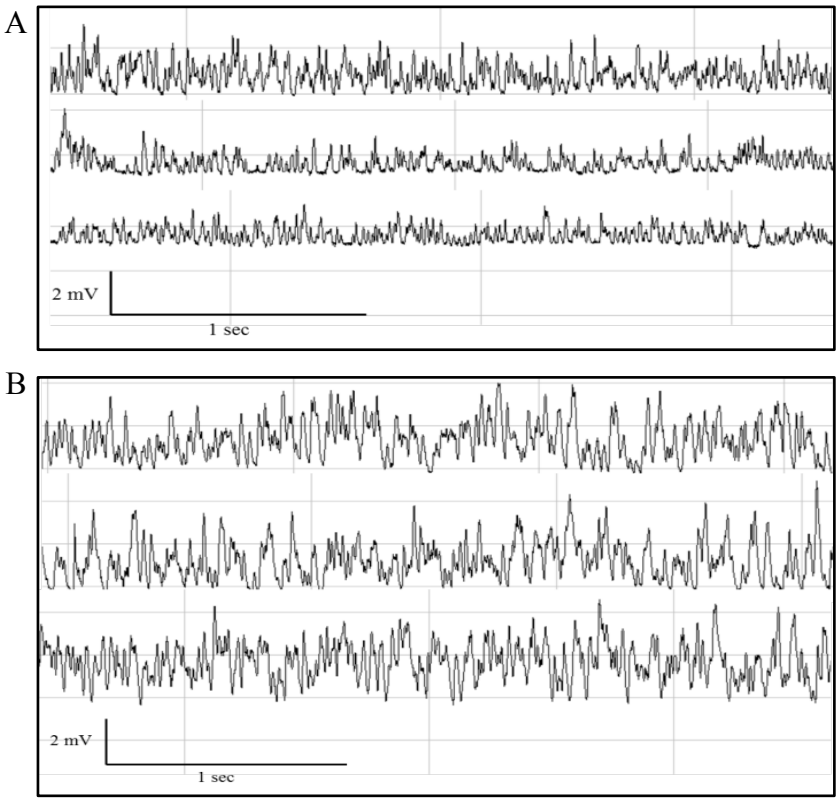

Figure 7.1. Single traces of MEPPs recordings in Ca^{2+} buffer after the addition of LTX^{N4C} (A) and Nimodipine (B). Nimodipine does not stop the effects due to LPHN1 activation; bursts and interburst intervals are still present.

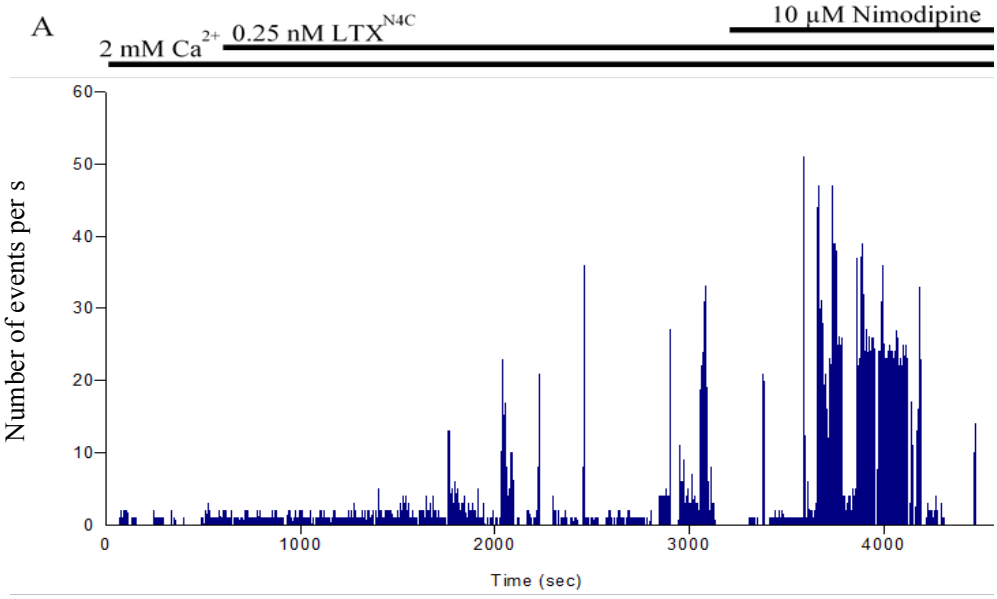

Continued on the next page

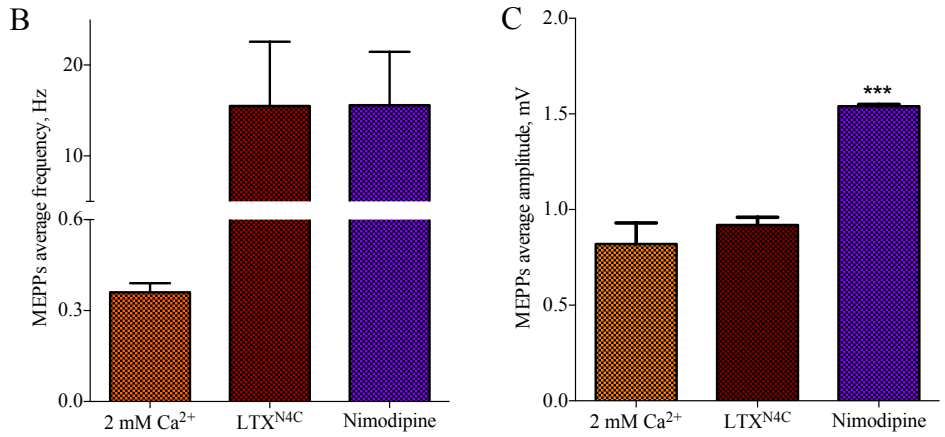

*Figure 7.2. A. Frequency plot of a MEPPs recording in a buffer containing 2 mM Ca^{2+}, and after the consecutive addition of LTX^{N4C} and Nimodipine. The block of L-type VGCCs is not able to suppress LPHN1-mediated exocytosis. B. Average frequency of MEPPs in Ca^{2+} buffer, and after the addition of LTX^{N4C} and Nimodipine. The difference between the conditions is not statistically significant. C. Average amplitude of MEPPs in Ca^{2+} buffer and after the addition of LTX^{N4C} and Nimodipine (N = 2, n = 5 cells recorded in Ca^{2+} buffer, 17 cells after addition of LTX^{N4C}, and 11 cells after the addition of Nimodipine; ***, P < 0.001, Mann – Whitney U test).*

In a reverse order when added before LTX^{N4C}, Nimodipine itself decreased the basal MEPPs frequency, but was not effective in inhibiting the increase in exocytosis typical of the activation of LPHN1 (14.88 ± 2.29 Hz), and the cells showed bursting behaviour with an average of MEPPs of 24.29 ± 0.68 Hz during the bursts, and an interburst frequency of 0.68 ± 0.05 Hz (Figure 7.4 A and B).

Also in this case, addition of Nimodipine itself caused a slight increase in the average MEPPs amplitude that went from the 0.82 ± 0.11 mV of the control in Ca^{2+} buffer, to 1.36 ± 0.55 mV after addition of Nimodipine which did not significantly change after the addition of LTX^{N4C} (1.22 ± 0.02 mV, Figure 7.4 C).

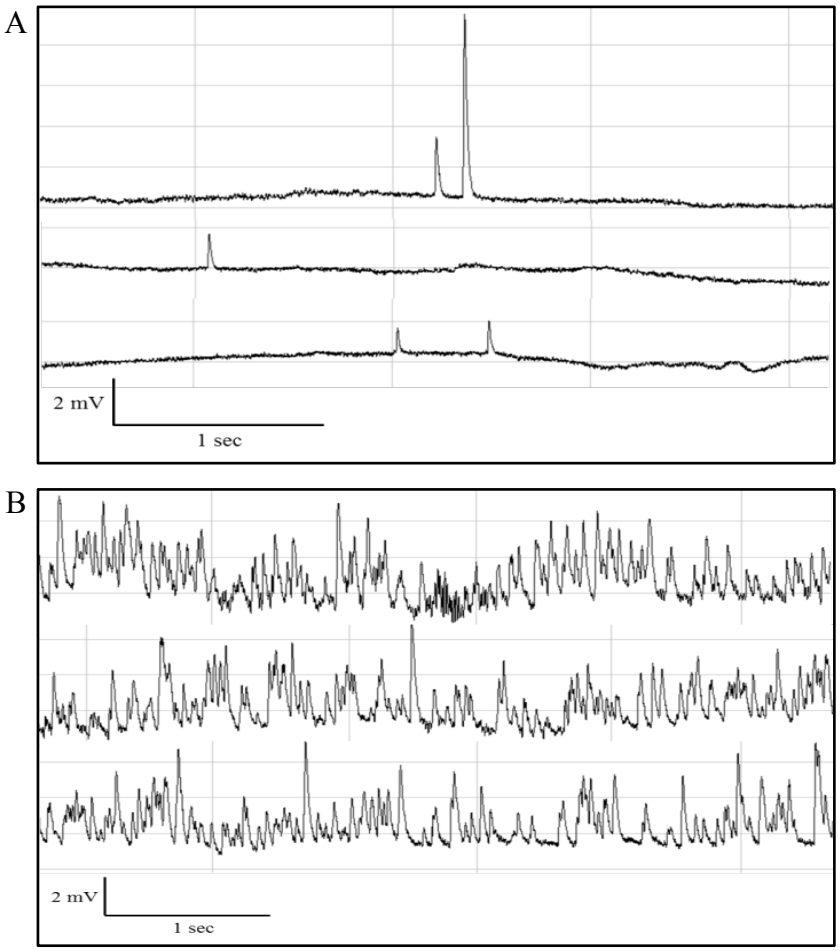

Figure 7.3. Single traces of MEPPs recordings in Ca^{2+} buffer in the presence of Nimodipine (A) and after the addition of LTX^{N4C} (B). The presence of Nimodipine in the buffer does not prevent the development of LPHN1effects on exocytosis.

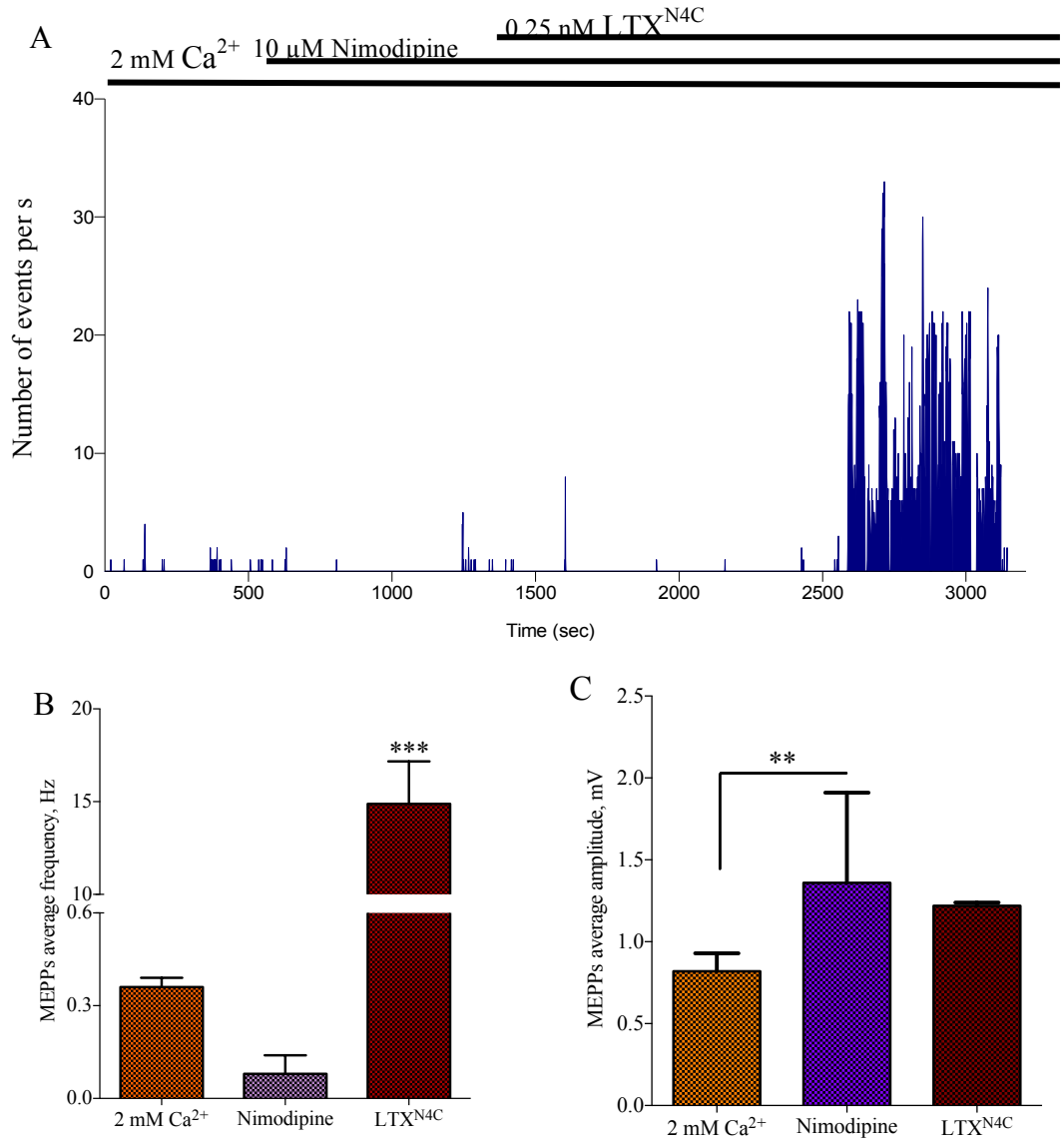

*Figure 7.4. A. Frequency plot of a MEPPs recording in a buffer containing 2 mM Ca^{2+}, and after the addition of Nimodipine and LTX^{N4C}. Nimodipine is not able to prevent the manifestation of the effects due to LPHN1 activation. B. Average frequency of MEPPs in Ca^{2+} buffer, and after the addition of Nimodipine and LTX^{N4C}. C. Average amplitude of MEPPs in Ca^{2+} buffer, and after sequential addition of Nimodipine and LTX^{N4C} (N = 1, n =7 cells recorded in Ca^{2+} buffer, 6 cells recorded with Nimodipine, and 10 cells after the addition of LTX^{N4C}; ***, P < 0.001; **, P < 0.01, Mann – Whitney U test).*

ω-Conotoxin MVIIC

ω-Conotoxin MVIIC (ω-Con MVIIC) is part of a group of neurotoxic peptides isolated from the venom of the marine cone snail. This specific toxin is known to be an inhibitor of P/Q-type VGCCs, and of N-type VGCCs with a lower affinity, although the inhibition of the latter happens much faster compared to the inhibition of the former. In addition, ω-Con MVIIC blocks N-type VGCCs more potently when neurons are at rest compared to the block seen in depolarised neurons (Liu et al. 1996; McDonough et al. 1996; Stocker et al. 1997).

For my experiments, neuromuscular preparations were incubated in Ca^{2+}-containing buffer with ω-Con MVIIC (1 μM) and recording were taken in order to evaluate the basal frequency of exocytosis in the presence of the toxin (0.39 ± 0.09 Hz). 0.25 nM LTX^{N4C} was then added and recordings continued for evaluation of the changes in exocytosis due the activation of LPHN1. The presence of ω-Con MVIIC in the buffer prevented the increase of exocytosis usually observed upon addition of LTX^{N4C} (0.75 ± 0.17 Hz, Figure 7.6 A and B).

The presence of ω-Con MVIIC in the buffer did not significantly change the average amplitude of MEPPs compared to the control in Ca^{2+} buffer (0.82 ± 0.11 mV in Ca^{2+} buffer, 0.94 ± 0.02 mV in the presence of ω-Con MVIIC), neither does the subsequent addition of LTX^{N4C} (0.95 ± 0.03 mV, Figure 7.6 C).

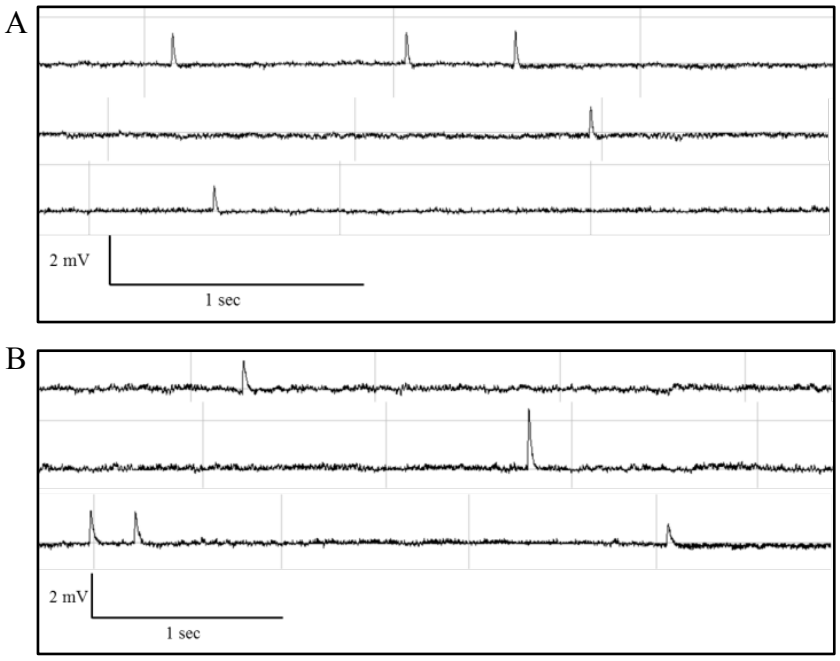

Figure 7.5. A. Single traces of MEPPs in Ca^{2+} buffer after the addition of ω-Con MVIIC (A) and of LTX^{N4C} (B). When LPHN1 is stimulated in the presence of ω-Con MVIIC, no increase in exocytosis develops.

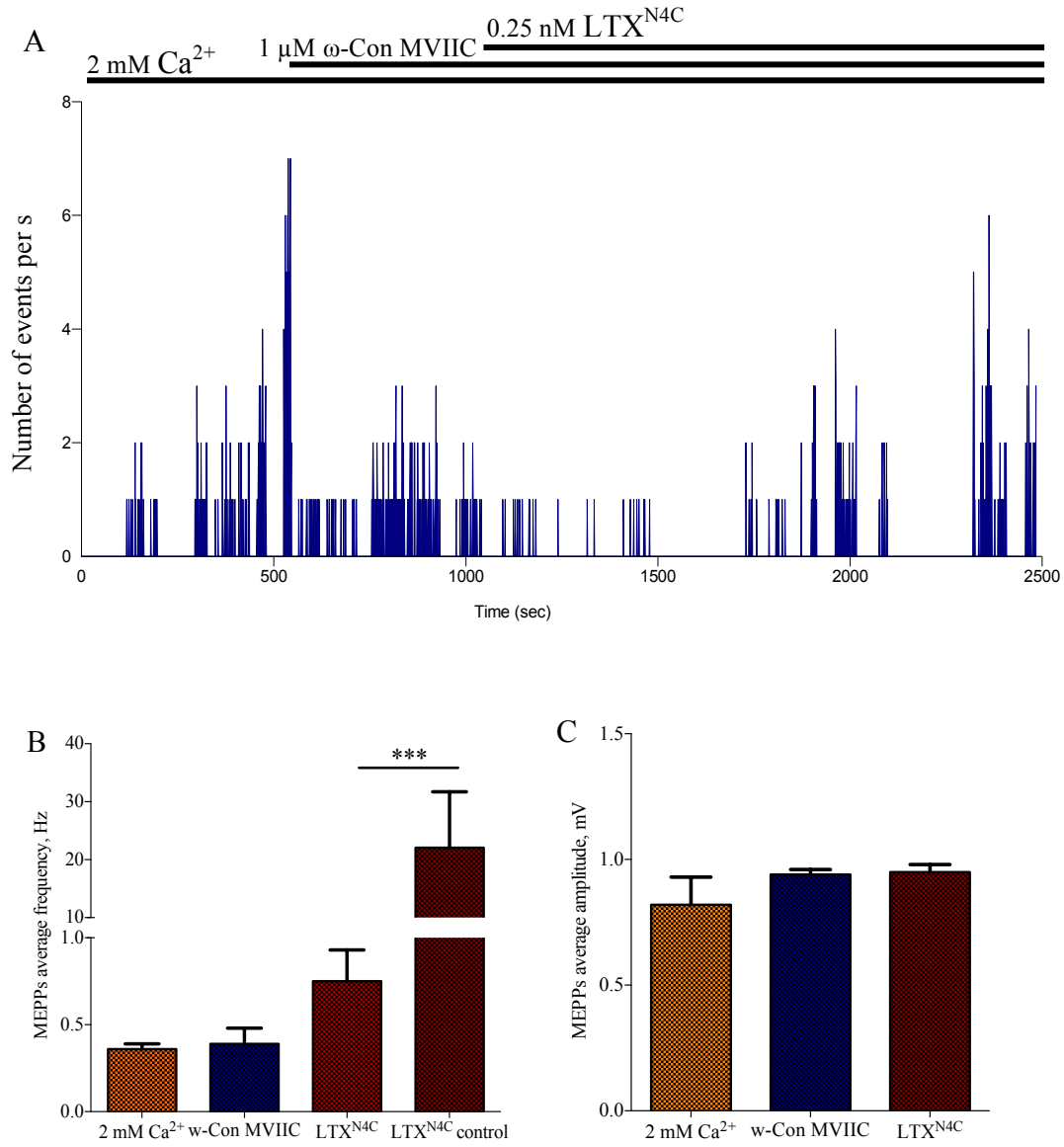

*Figure 7.6. A. Frequency plot of a MEPPs recording in the presence of 2 mM Ca^{2+}, and after the consecutive addition of ω-Con MVIIC and LTX^{N4C}. ω-Con MVIIC successfully inhibits the increase in exocytosis due to the activation of LPHN1. The LTX^{N4C} control was recorded on the same day on a different preparation not treated with ω-Con MVIIC. B. Average frequency of MEPPs in Ca^{2+} buffer and after the addition of ω-Con MVIIC and LTX^{N4C}. The difference between the conditions is not statistically significant. C. Average amplitude of MEPPs in Ca^{2+} buffer, and after sequential addition of ω-Con MVIIC and LTX^{N4C} (N = 3, n = 19 cells recorded in Ca^{2+} buffer, 21 cells with ω-Con MVIIC, and 39 cells after the addition of LTX^{N4C}; ***, P < 0.001, Mann – Whitney U test).*

The situation changed, however, when ω-Con MVIIC (1 μM) was added after LPHN1 had been activated by LTX^{N4C} (0.25 nM), and its effects on exocytosis already started. In this case, ω-Con MVIIC was not able to stop or even attenuate this increase (15.48 ± 0.64 Hz vs. 22.06 ± 9.65 Hz in Ca^{2+} buffer), and the cells continued to burst in the same way they usually did in Ca^{2+} buffer only (32.81 ± 2.65 Hz during bursts and 0.61 ± 0.13 Hz during interburst intervals, Figure 7.8, A and B).

The average amplitude of MEPPs was not significantly different between the conditions considered (0.94 ± 0.01 mV after the addition of LTX^{N4C}, and 0.95 ± 0.01 mV after the addition of ω-Con MVIIC, Figure 7.8 C).

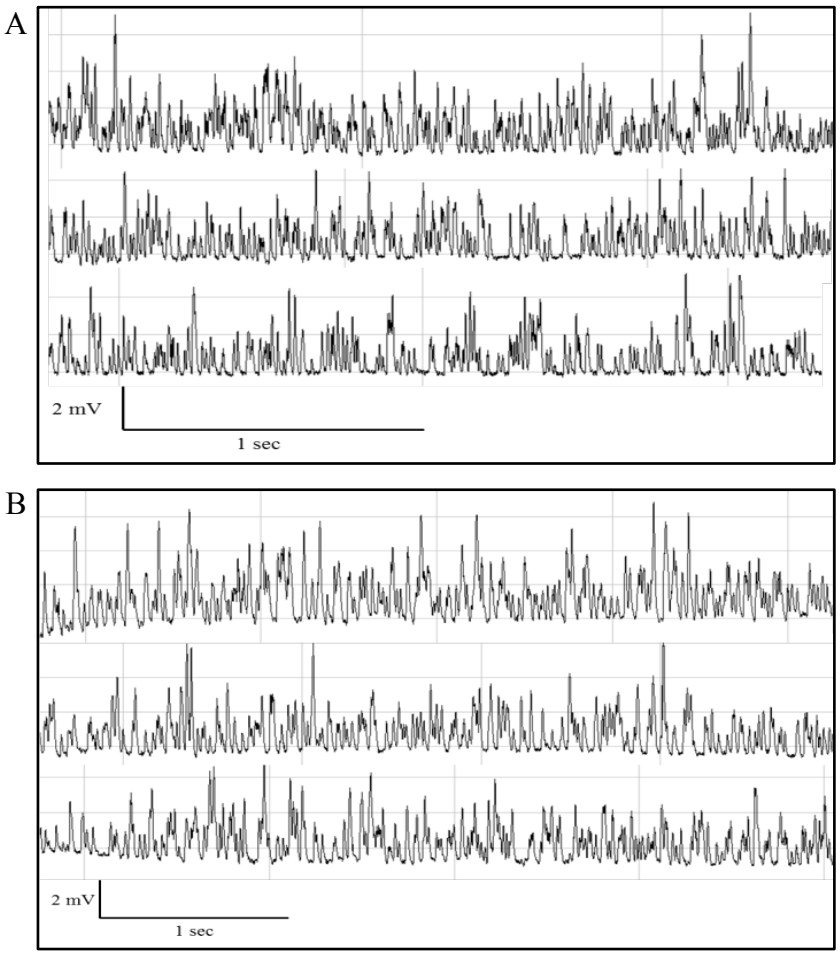

Figure 7.7. Single traces of MEPPs recordings in Ca^{2+} buffer after the addition of LTX^{N4C} (A) and ω-Con MVIIC (B). ω-Con MVIIC is not able to inhibit the effects of LPHN1 activation if added when they have already developed.

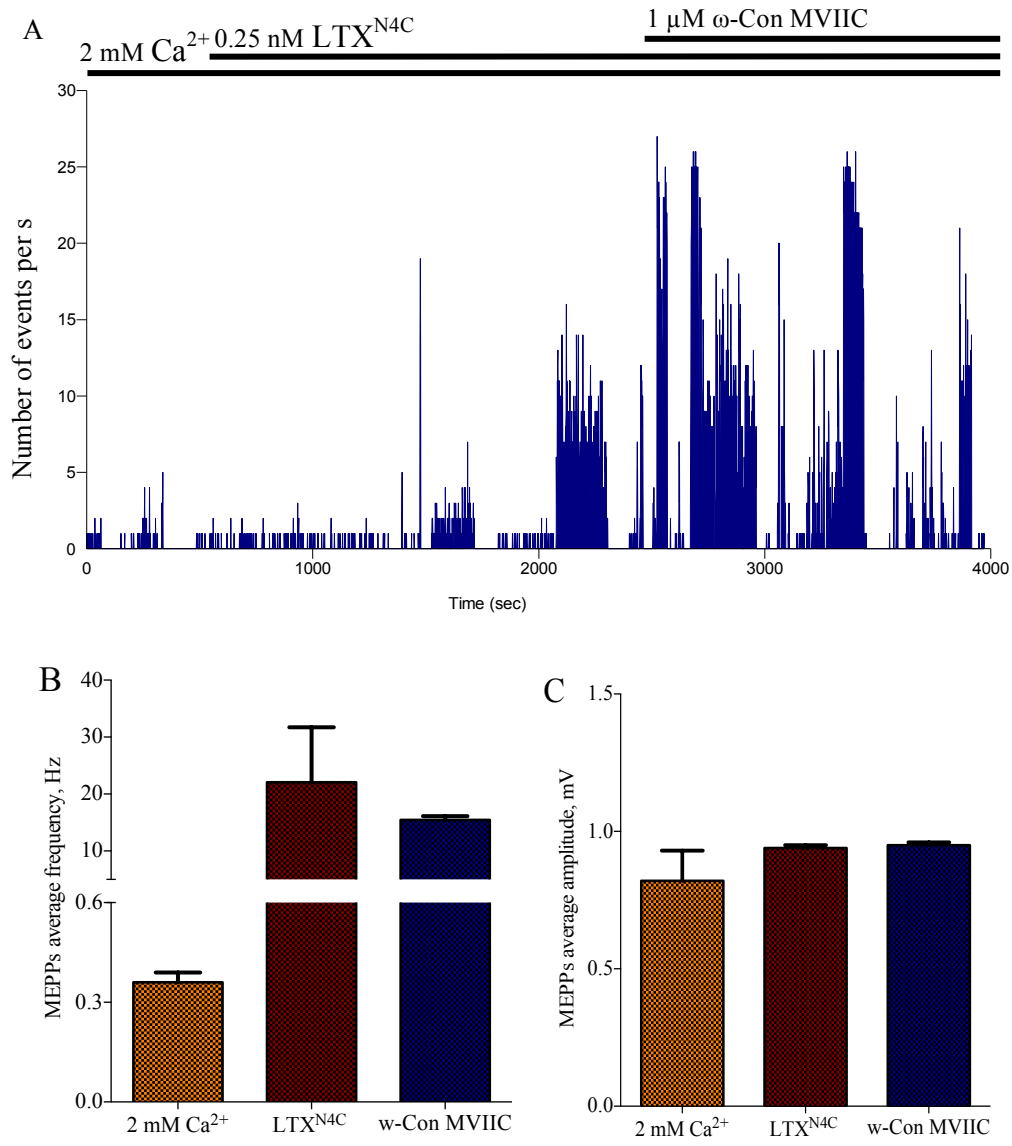

Figure 7.8. A. Frequency plot of a MEPPs recording in a buffer containing 2 mM Ca^{2+}, and after the addition of LTX^{N4C} and ω-Con MVIIC. ω-Con MVIIC added once the increase in exocytosis took place is not able to successfully inhibit it. B. Average frequency of MEPPs in Ca^{2+} buffer, and after the addition of LTX^{N4C} and ω-Con MVIIC. The difference between the conditions is not statistically significant. C. Average amplitude of MEPPs in Ca^{2+} buffer and after sequential addition of LTX^{N4C} and ω-Con MVIIC. The difference is not statistically significant (N = 2, n = 13 cells recorded in Ca^{2+} buffer, 20 cells after the addition of LTX^{N4C}, and 20 after the addition of ω-Con MVIIC, Mann – Whitney U test).

Interestingly, when considering the frequency of MEPPs during interburst intervals after the addition of both LTX^{N4C} and ω-Con MVIIC, this was significantly lower than in the control (LTX^{N4C} in Ca^{2+} buffer only). In fact it went down from a control level of 0.95 ± 0.12 Hz to 0.61 ± 0.13 Hz (Figure 7.9).

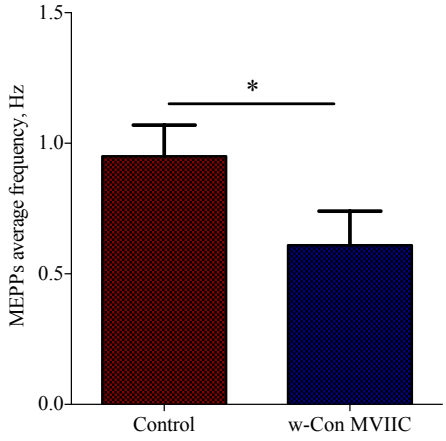

*Figure 7.9. Comparison between the average frequency of MEPPs during interburst intervals in control conditions (LTX^{N4C} in Ca^{2+} buffer) and in the presence of both LTX^{N4C} and ω-Con MVIIC (n = 5 cells for the control condition and 5 with ω-Con MVIIC; *, P < 0.05, Mann – Whitney U test).*

ω-Conotoxin GVIA and ω-Agatoxin IVA

The experiments with ω-Con MVIIC suggested an involvement of N-type and/or P/Q-type VGCCs in LTX^{N4C}-induced activation. However, it was impossible to discriminate the individual contributions of these VGCC types on LPHN1 effects, using this VGCC blocker. To make this distinction possible I used ω-Conotoxin GVIA (ω-Con GVIA), a specific blocker of N-type VGCCs and ω-Agatoxin IVA (ω-Aga IVA), a specific blocker of P/Q-type VGCCs.

Considering that ω-Con MVIIC was able to stop the effects of LPHN1 activation on exocytosis only when added to the preparations before LTX^{N4C}, I used this condition in experiments in order to discriminate the involvement of N-type and P/Q-type VGCCs.

The neuromuscular preparations were incubated in Ca^{2+} buffer with 50 nM ω-Con GIVA and recordings were taken in order to calculate the effects of this toxin on the basal frequency of exocytosis (0.42 ± 0.11 Hz). 0.25 nM LTX^{N4C} was then added and recordings continued for evaluation of the changes in exocytosis due the activation of LPHN1 (12.89 ± 7.12 Hz). The cells showed the typical bursting behaviour observed when LPHN1 was activated by LTX^{N4C} (36.48 ± 8.98 Hz during bursts and 0.92 ± 0.20 Hz during interburst intervals, Figure 7.11 A and B).

The average amplitude of MEPPs was not significantly different between the conditions considered (0.82 ± 0.11 mV in Ca^{2+} buffer, 0.90 ± 0.07 mV in the presence of ω-Con GIVA, and 0.83 ± 0.02 mV after the addition of LTX^{N4C}, Figure 7.11 C).

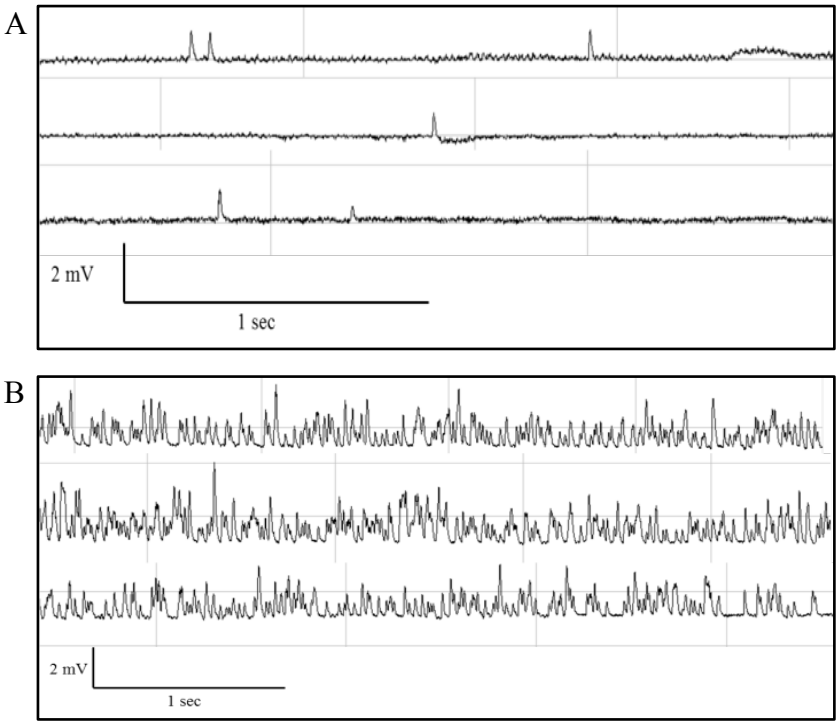

Figure 7.10. Single traces of MEPPs recordings in Ca^{2+} buffer in the presence of ω-Con GVIA (A) and after the addition of LTX^{N4C} (B). The effects of LPHN1 activation are not inhibited by ω-Con GVIA.

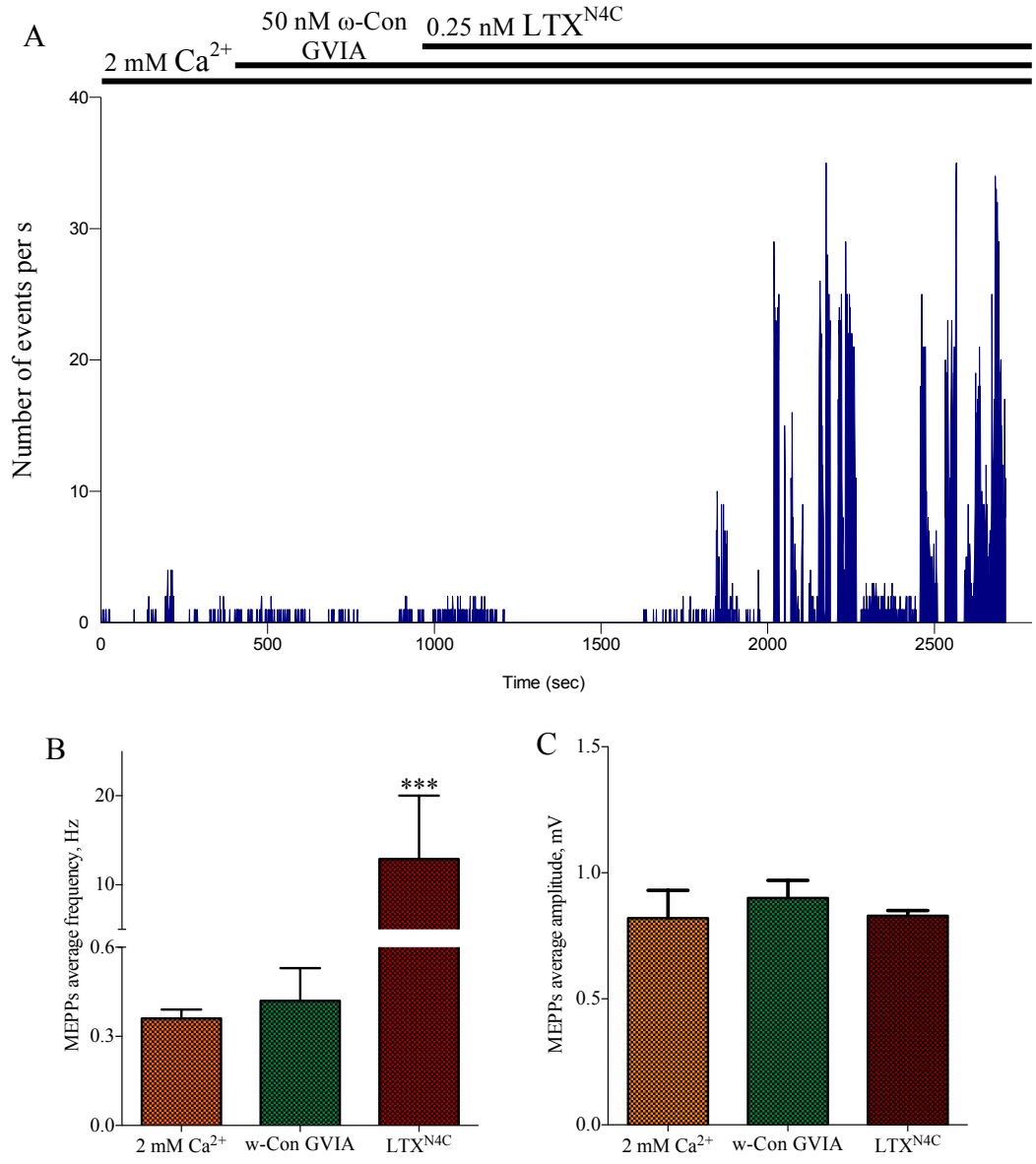

*Figure 7.11. A. Frequency plot of a MEPPs recording in a buffer containing 2 mM Ca^{2+}, and after the addition of ω-Con GVIA and LTX^{N4C}. The presence of ω-Con GVIA in the buffer does not inhibit the effects of LPHN1 activation. B. Average frequency of MEPPs in Ca^{2+} buffer, and after the addition of ω-Con GVIA and LTX^{N4C}. C. Average amplitude of MEPPs in Ca^{2+} buffer, and after the sequential addition of ω-Con GVIA and LTX^{N4C}. The difference is not statistically significant (N = 2, n = 11 cells recorded in Ca^{2+} buffer, 12 cells with ω-Con GVIA, and 30 cells after the addition of LTX^{N4C}; ***, P < 0.001, Mann – Whitney U test).*

The same protocol was used when applying ω-Aga IVA; the preparations were incubated in Ca^{2+} buffer with 200 nM ω-Aga IVA and the basal frequency of exocytosis was calculated (0.477 ± 0.05 Hz). The recordings continued after the addition of 0.25 nM LTX^{N4C}, and no significant changes in the frequency of neurotransmitter release were observed in this instance (0.29 ± 0.19 Hz, Figure 7.13 A and B).

The average amplitude of MEPPs was not significantly different between the conditions considered (0.82 ± 0.11 mV in Ca^{2+} buffer, 0.84 ± 0.07 mV in the presence of ω-Aga IVA, and 0.82 ± 0.04 mV after the addition of LTX^{N4C}, Figure 7.13 C).

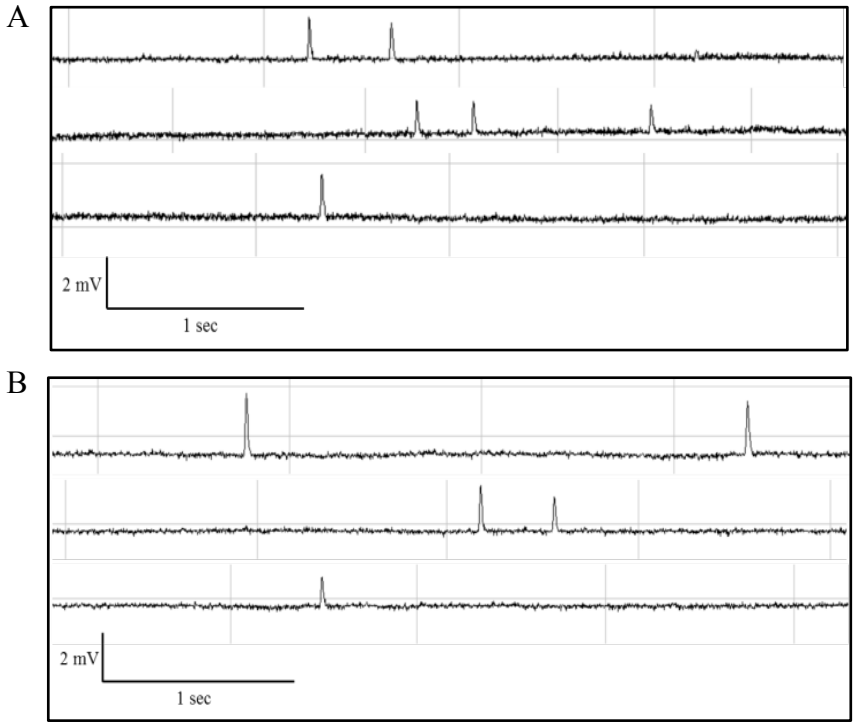

Figure 7.12. Single traces of MEPPs recordings in Ca^{2+} buffer in the presence of ω-Aga IVA (A) and after the addition of LTX^{N4C} (B). The presence of ω-Aga IVA is able to prevent the development of LPHN1 activation.

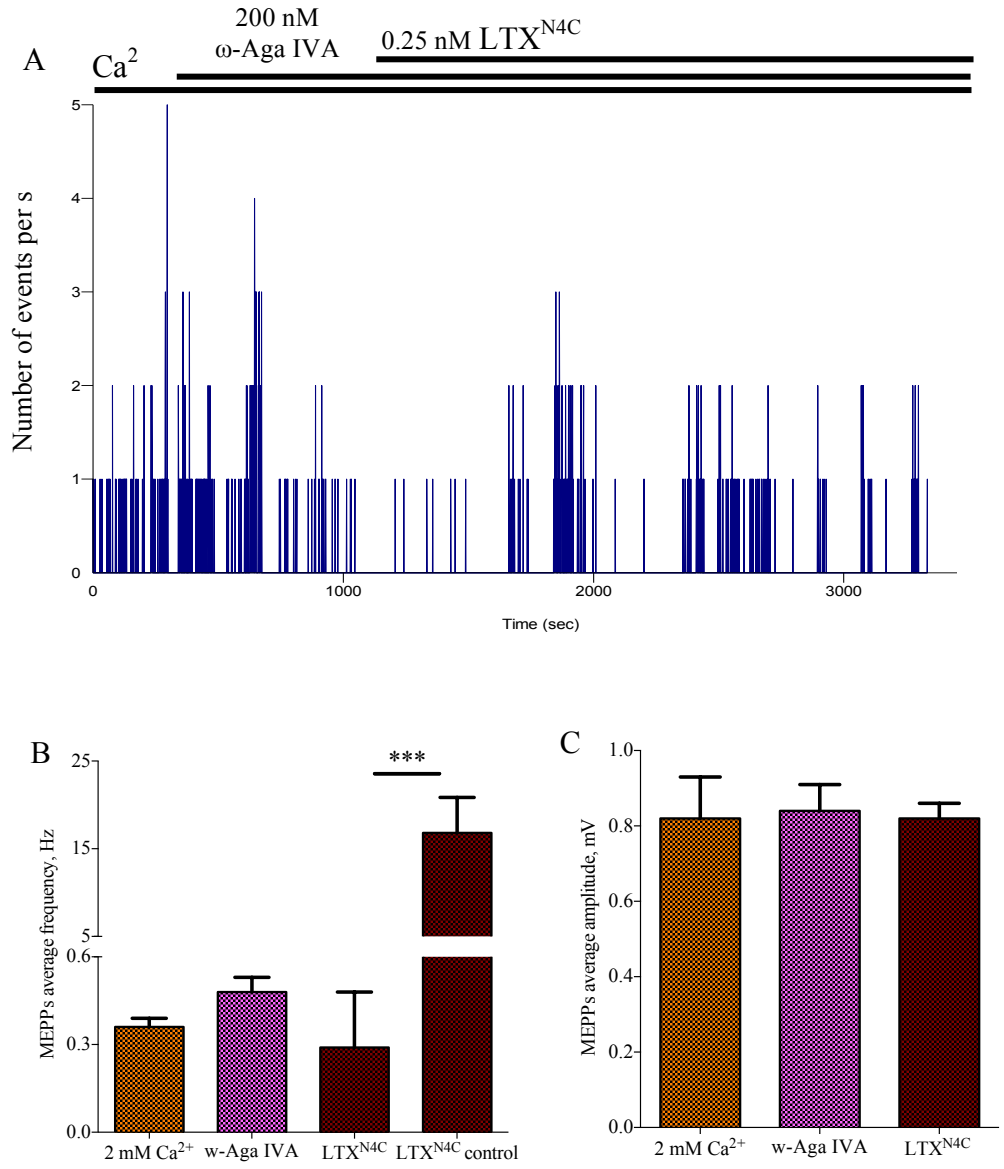

*Figure 7.13. A. Frequency plot of a MEPPs recording in a buffer containing 2 mM Ca^{2+}, and after the addition of ω-Aga IVA and LTX^{N4C}. ω-Aga IVA is able to fully abolish the effects due to the activation of LPHN1. B. Average frequency of MEPPs in buffer A and after the addition of ω-Aga IVA and LTX^{N4C}. The difference between the conditions is not statistically significant. The control of N4C was recorded on the same day on a different preparation not treated with ω-Aga IVA. C. Average amplitude of MEPPs in Ca^{2+} buffer and after the sequential addition of ω-Aga IVA and LTX^{N4C} (N = 3, n = 18 cells recorded in Ca^{2+} buffer, 14 cells with ω-Aga IVA, and 31 cells after the addition of LTX^{N4C}; ***, P< 0.001, Mann – Whitney U test).*

To summarise, of all the VGCCs tested in my experiments, only P/Q-type VGCCs were effective in inhibiting the effects due to the activation of LPHN1. In fact, the frequency of exocytosis was significantly inhibited when using ω-Aga IVA, but not when using Nimodipine or ω-Con GVIA (Figure 7.14 A). Furthermore, my results suggest that the inhibition on exocytosis caused by P/Q VGCCs is effective only if these channels are blocked before LPHN1 gets activated (Figure 7.14 B). This could be therefore the pivotal first Ca^{2+} channel activated by LPHN1, without which the elevation in intracellular [Ca^{2+}] is not sufficient to start the increase in exocytosis.

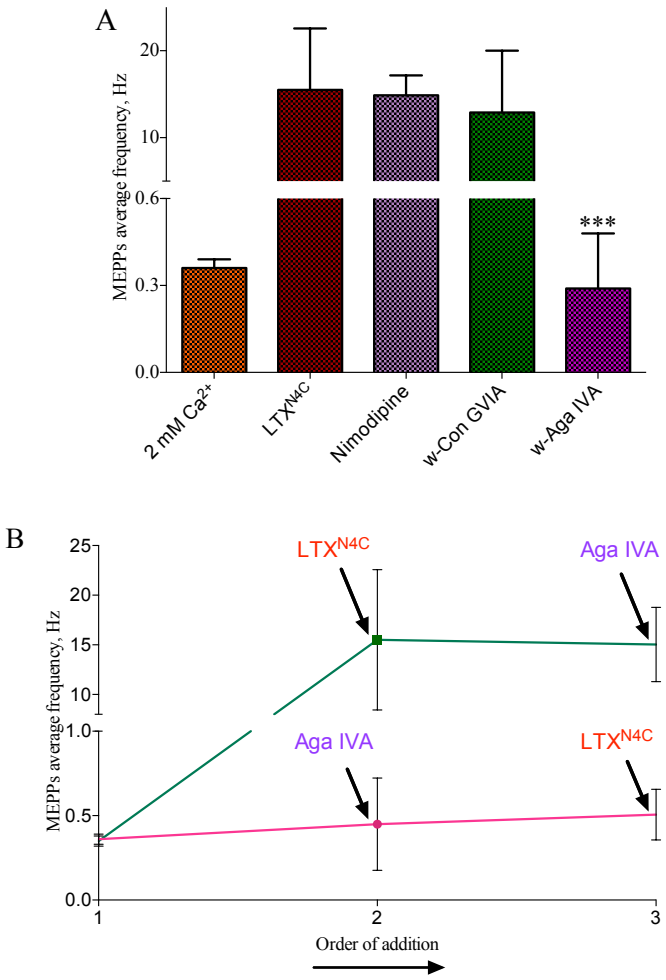

*Figure 7.14. A. Comparison between the averaged frequencies of MEPPs after the addition of LTX^{N4C} in 2 mM Ca^{2+}, and after the addition of VGCCs inhibitors (Nimodipine, ω-Con GVIA, and ω-Aga IVA). Only ω-Aga IVA, a specific blocker of P/Q VGCCs, is able to inhibit the activation of LPHN1 (***P<0.001, Mann – Whitney U test). B. The block of P/Q VGCCs is effective in inhibiting the activation of LPHN1 only when added prior to the addition of LTX^{N4C}. If added once the effects of LPHN1 already developed, blocking these channels does not interfere with the increase in exocytosis normally observed upon activation of LPHN1.*

7.2.2 P/Q-type VGCCs are needed to completely abolish the effects of LPHN1 activation

As shown in Chapter 5 (Section 5.2.1), the inhibition of $G\alpha_{q/11}$ protein drastically and significantly reduces the frequency of neurotransmitter release caused by activation of LPHN1. However, LPHN1 effect is not completely blocked with the inhibition of $G\alpha_{q/11}$, and some cells continue firing MEPPs at a relatively high frequency, with a minority of cells (approximately 30% of the recorded cells) showing a frequency of exocytosis from 6 to 20 Hz. In the light of the results described above (Section 7.2.1), this can be due to the activation of P/Q-type VGCCs, which, by allowing the entry of Ca^{2+} into the cells, cause some cells to respond to it to some extent, although not as strongly as in control, without any inhibition. To test this hypothesis, I performed experiments where the activation of $G\alpha_{q/11}$ and P/Q VGCCs was inhibited at the same time by UBO-QIC and ω-Aga IVA.

The neuromuscular preparations were bathed in a buffer containing 2 mM Ca^{2+} with the addition of 1μM UBO-QIC and 200 nM ω-Aga IVA. Recordings were initially taken in order to evaluate the basal frequency of neurotransmitter release in the presence of both inhibitors (0.34 ± 0.04 Hz). Subsequently, 0.25 nM LTX^{N4C} was added, and no significant changes in the frequency of exocytosis were detectable (0.29 ± 0.06 Hz). No cells showed any signs of effects due to the activation of LPHN1 by LTX^{N4C} (Figure 7.16 A and B).

The average amplitude of MEPPs did not significantly differ between the conditions considered (0.82 ± 0.11 mV in Ca^{2+} buffer, 0.82 ± 0.03 mV after addition of UBO-QIC and ω-Aga IVA, and 0.85 ± 0.04 mV after the addition of LTX^{N4C}, Figure 7.16 C).

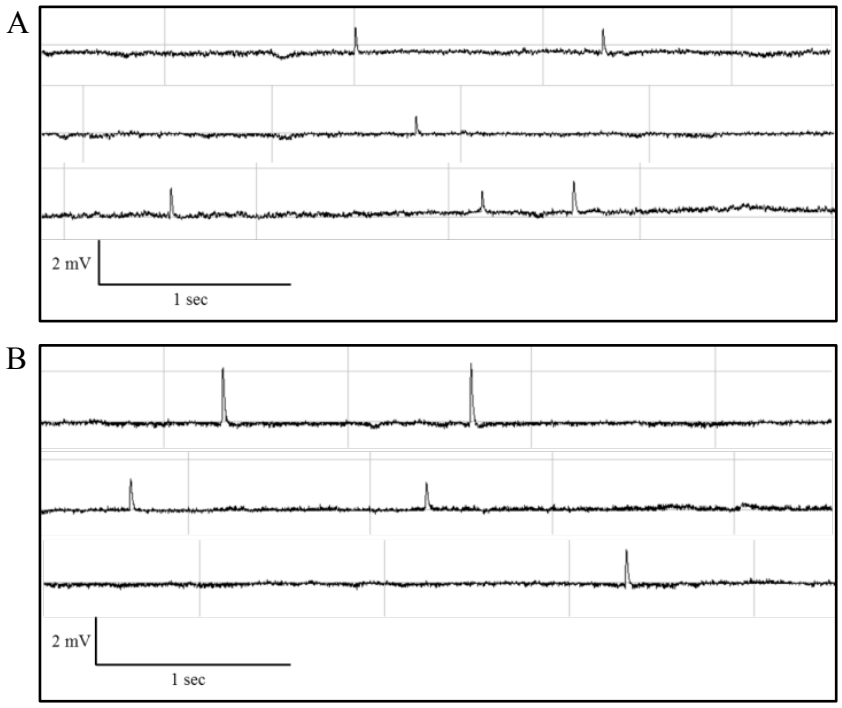

Figure 7.15. Single traces of MEPPs recordings in Ca^{2+} buffer in the presence of UBO-QIC and ω-Aga IVA (A) and after the addition of LTX^{N4C} (B). Whilst when only UBO-QIC is present about 30% of the cells continue responding to LTX^{N4C} with increased exocytosis, the concomitant presence of ω-Aga IVA completely abolishes the effect.

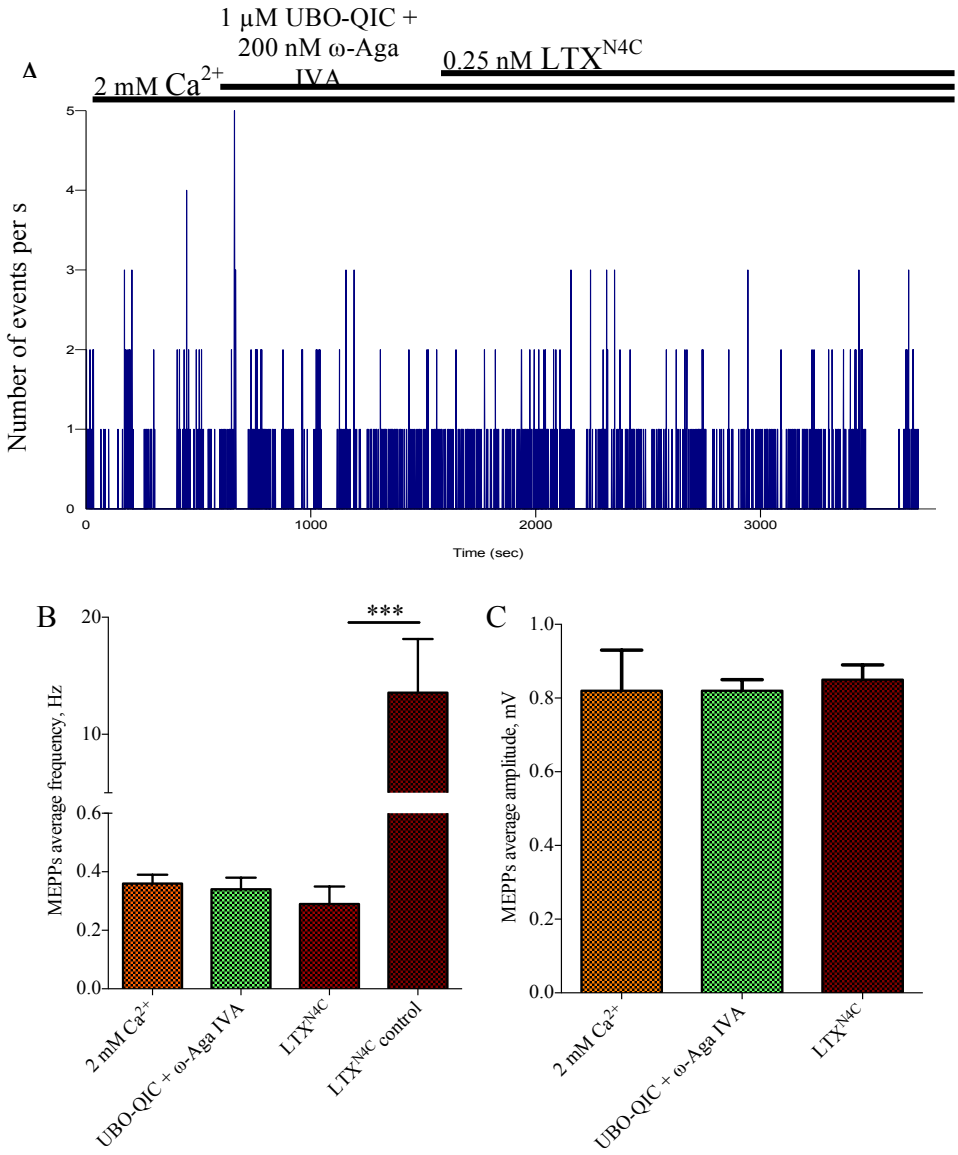

*Figure 7.16. A. Frequency plot of a MEPPs recording in 2 mM Ca^{2+} and after the addition of UBO-QIC and ω-Aga IVA, with subsequent stimulation with 0.25 nM LTX^{N4C}. B. Average frequency of MEPPs in Ca^{2+} buffer and after the addition of UBO-QIC and ω-Aga IVA, and LTX^{N4C}. The difference between the conditions is not statistically significant. The control for LTX^{N4C} was recorded the same day on a different preparation not treated with UBO-QIC and ω-Aga IVA. C. Average amplitude of MEPPs in Ca^{2+} buffer, and after the addition of UBO-QIC and ω-Aga IVA, and after stimulation with LTX^{N4C}. The difference between the conditions is not statistically different (N = 1, n = 5 cells recorded in Ca^{2+} buffer, 12 cells with UBO-QIC and ω-Aga IVA, and 9 cells after the addition of LTX^{N4C}; ***, P < 0.001, Mann – Whitney U test).*

In a similar way, I wanted to explore the possibility of VGCCs being involved in the residual LPHN1 signalling still detectable with $G\alpha_{q/11}$ inhibition. This was accomplished by blocking the P/Q VGCCs with ω-Aga IVA. I incubated the neuromuscular preparations with 1 μM UBO-QIC (0.34 ± 0.9 Hz) and then added 0.25 nM LTX^{N4C}. Although the overall average frequency was low (1.49 ± 0.60 Hz) some cells (approximately 30%) still showed a MEPPs frequency of up to 5 Hz, indicating that they were to some extent responding to the activation of LPHN1, and that this response was not mediated by the $G\alpha_{q/11}$. Addition of 200 nM ω-Aga IVA stopped this residual response and completely inhibited the effects of LPHN1 (0.17 ± 0.01 Hz Figure 7.17).

These results suggested that the signalling induced by LPHN1 activation occurs along two independent pathways: the activation of $G\alpha_{q/11}$ with subsequent sub-threshold activation of IP_3Rs on the calcium stores and the opening of P/Q-type VGCCs. Activation of both signalling pathways is required for the full exocytotic effect of the LPHN1-mediated LTX^{N4C} signalling.

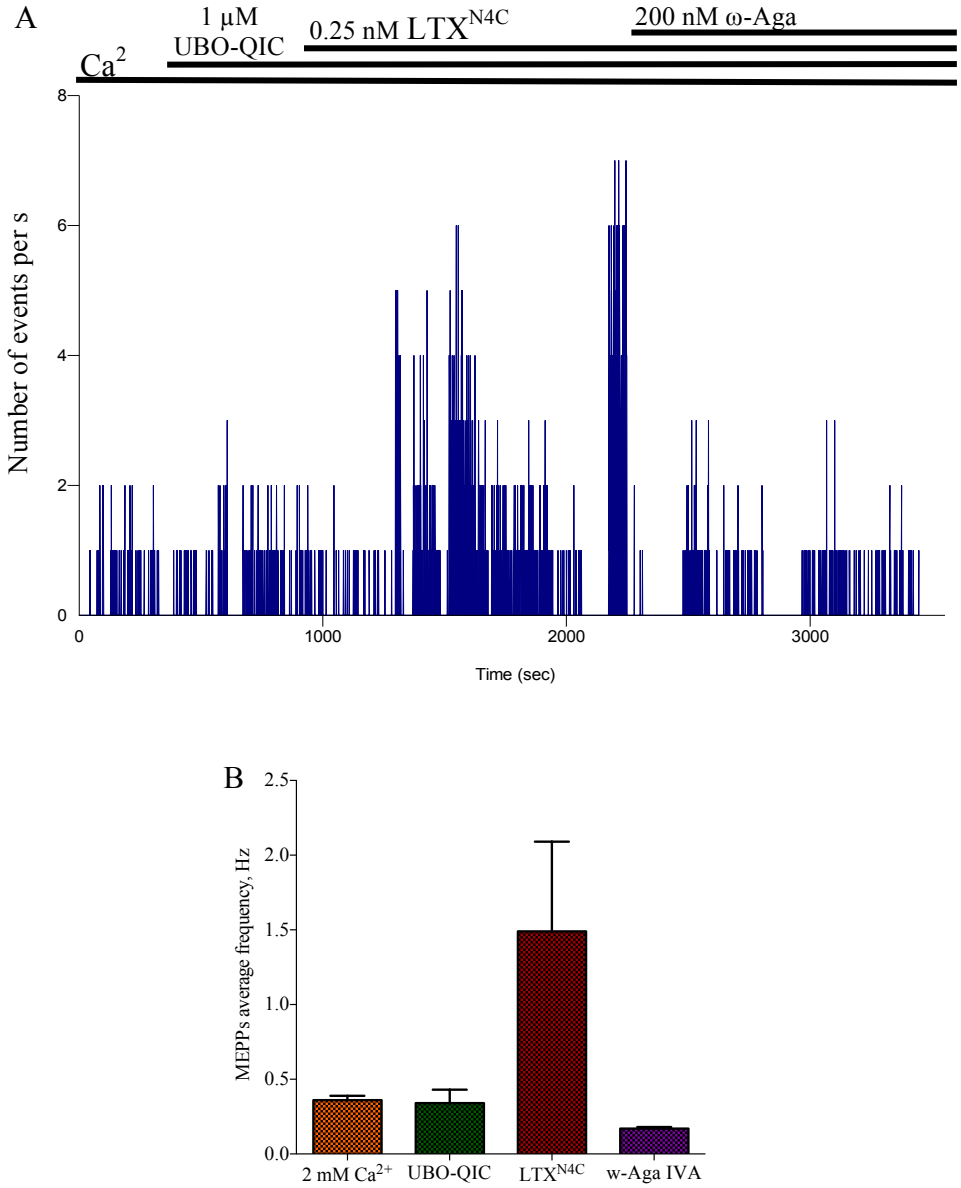

Figure 7.17. A. Frequency plot of a MEPPs recording in 2 mM Ca^{2+} and after the addition of UBO-QIC, LTX^{N4C} and ω-Aga IVA. B. Average frequency of MEPPs in Ca^{2+} buffer, and after the addition of UBO-QIC, LTX^{N4C} and ω-Aga IVA (N = 1, n = 6 cells recorded in Ca^{2+}, 6 with UBO-QIC, 10 after stimulation with LTX^{N4C} and 12 after the addition of ω-Aga IVA).

7.2.3 Cadmium supports the activation of LPHN1

As part of the experiments done to investigate the involvement of the influx of Ca^{2+} in the activation of LPHN1, Cd^{2+} was also used as a blocker of VGCCs. In these experiments I used a buffer where 2 mM Cd^{2+} was used instead of Ca^{2+}, and the effects of the activation of LPHN1 on spontaneous neurotransmitter release were studied using the same protocol as the experiments with Ca^{2+}.

Compared to the basal frequency of exocytosis observed in Ca^{2+} buffer, no significant changes in frequency (0.36 ± 0.03 Hz in Ca^{2+} buffer vs. 0.34 ± 0.06 Hz in Cd^{2+} buffer, Figure 7.18 B) and amplitude (0.82 ± 0.11 mV in Ca^{2+} buffer vs. 0.84 ± 0.16 mV in Cd^{2+} buffer, Figure 7.18 C) were observed when using Cd^{2+} buffer.

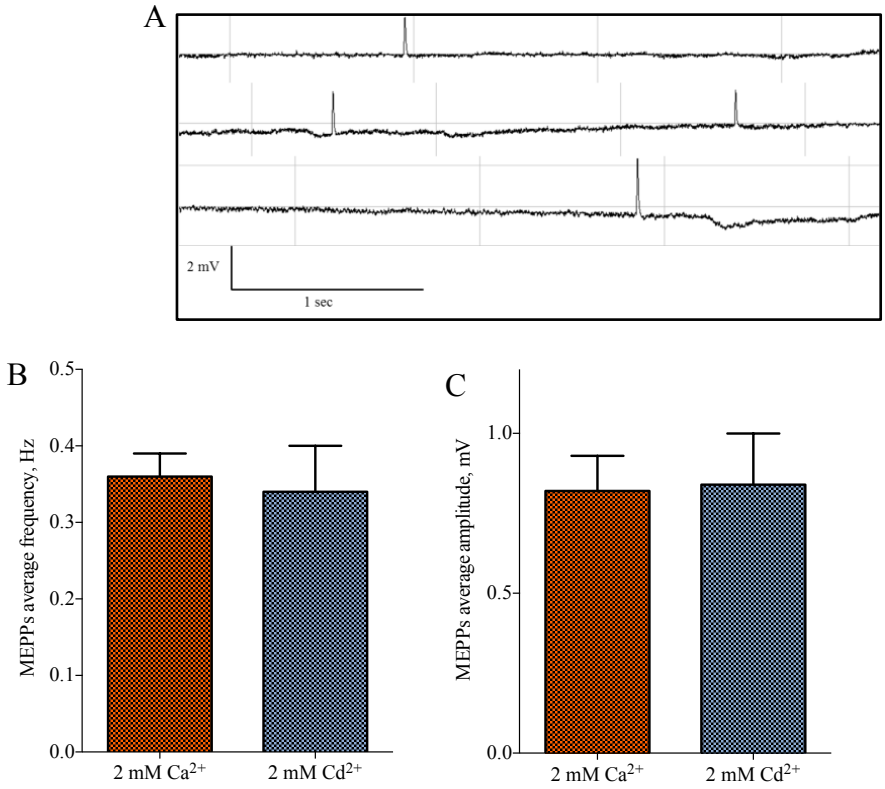

Figure 7.18. A. Single traces of MEPPs recorded at the mouse NMJ in 2 mM Cd^{2+}. B. Average frequency of MEPPs in Ca^{2+} and Cd^{2+} buffer. The difference between the conditions is not statistically significant. C. Average amplitude of MEPPs in Ca^{2+} and Cd^{2+} buffer. The difference is not statistically significant (N = 6, n = 23 cells recorded in Ca^{2+} and 18 in Cd^{2+} buffer).

When stimulated by 0.25 nM LTX^{N4C} in Cd^{2+} buffer, LPHN1 was still able to elicit an increase in exocytosis similar in frequency to the one observed in Ca^{2+} (15.50 ± 7.07 Hz in Ca^{2+} buffer vs. 18.94 ± 1.07 Hz in Cd^{2+} buffer). However, the cells did not show bursting behaviour, rather the frequency of release increased gradually, after about 10 min reaching a peak that lasted for approximately 30 minutes (29.52 ± 6.15 Hz) and then slowly decreased until cessation (Figure 7.20 A and B).

The MEPPs average amplitude was not significantly different between the conditions (0.84 ± 0.16 mV in Cd^{2+}, and 0.85 ± 0.33 mV in after the addition of LTX^{N4C}, Figure 7.20 C).

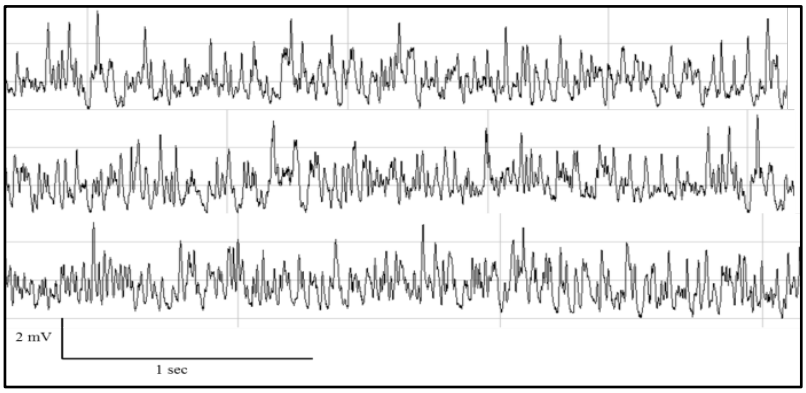

Figure 7.19. Single traces of MEPPs recorded at the mouse NMJ in Cd^{2+} buffer after the addition of LTX^{N4C}. This buffer completely supports the increase in exocytosis caused by the activation of LPHN1.

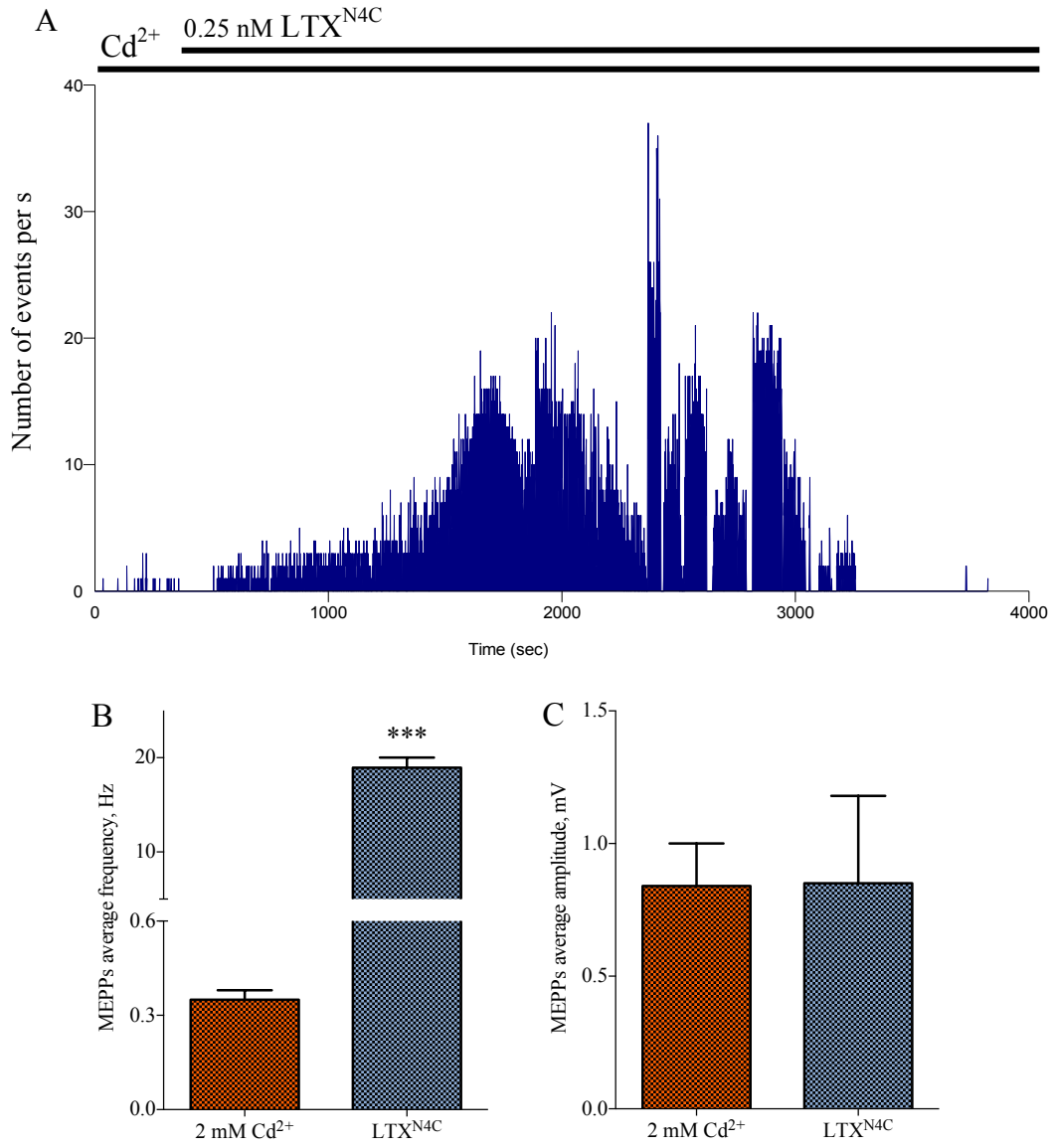

*Figure 7.20. A. Frequency plot of a MEPPs recording in Cd^{2+} buffer and after the addition of LTX^{N4C}. B. Average frequency of MEPPs in Cd^{2+} buffer and after the addition of LTX^{N4C}. C. Average amplitude of MEPPs in Cd^{2+} buffer and after addition of LTX^{N4C} (N = 6, n = 18 cells recorded in Cd^{2+} buffer and 35 after the addition of LTX^{N4C}; ***, P < 0.001, Mann – Whitney U test).*

As described previously, LTX^{N4C} caused no effect in a Ca^{2+}-free buffer, but the subsequent addition of Ca^{2+} triggered massive bursting exocytosis (see Chapter 4, Section 4.2.4, Figure 4.10). Similarly, the frequency of neurotransmitter release rapidly increased upon the addition of 2 mM Cd^{2+} to preparations bathed in a Ca^{2+}-free buffer supplemented with 0.25 nM LTX^{N4C}. The effect was comparable to the one observed when LTX^{N4C} was added in Cd^{2+}-containing buffer, with no bursting behaviour and gradual cessation of release (Figure 4.21).

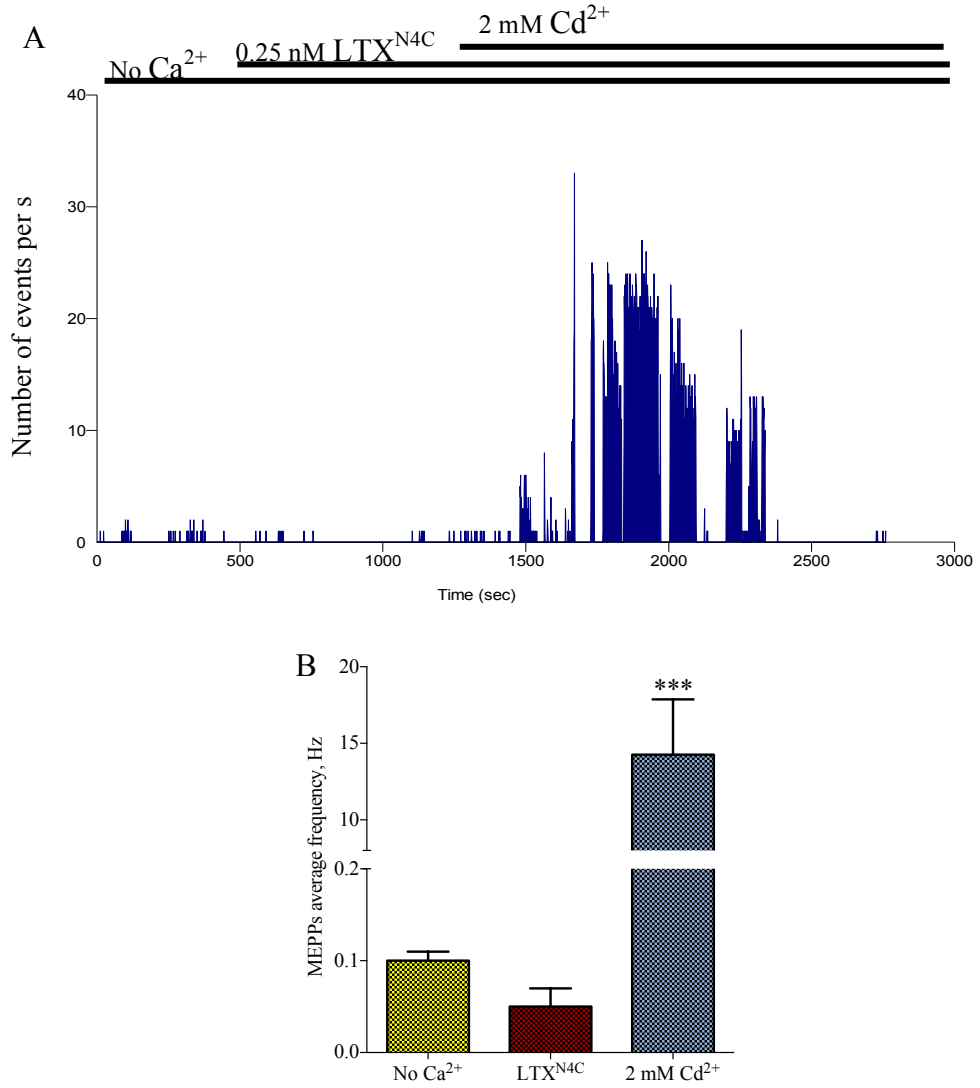

*Figure 7.21. A. Frequency plot of a MEPPs recording inCa^{2+}-free buffer, and after the addition of LTX^{N4C} and Cd^{2+}. B. Average frequency of MEPPs in Ca^{2+}-free buffer, and after the addition of LTX^{N4C} and Cd^{2+} (N = 2, n = 7 cells recorded in Ca^{2+}-free buffer, 9 cells after the addition of LTX^{N4C}, and 26 cells after the addition of Cd^{2+}; ***, P < 0.001, Mann – Whitney U test).*

Experiments with Cd^{2+}, as a universal blocker of VGCCs, were initially meant to test the involvement of VGCCs in LPHN1-mediated exocytosis of neurotransmitter. However, Cd^{2+} seem to support LPHN1-mediated signalling, and the effects of its activation were still present although with different characteristics than that observed in Ca^{2+}. It is therefore likely that Cd^{2+} was able to permeate through some of the channels that caused the increase in exocytosis when LTX^{N4C} was used in Ca^{2+}. To investigate the involvement of the SOCCs and VGCCs in LPHN1 signalling in the presence of Cd^{2+}, I used the pharmacological agents that appeared to be the best blockers of the LPHN1-evoked neurotransmitter release.

Doing this, it was possible to understand that SOCCs are equally involved in the activity of LPHN1 even when Cd^{2+} substituted Ca^{2+} (Figure 7.23). In fact, 2APB (50 μM) was able to significantly reduce the frequency of exocytosis (0.76 ± 0.66 Hz), whilst SKF96365 completely blocked it (0.00 Hz).

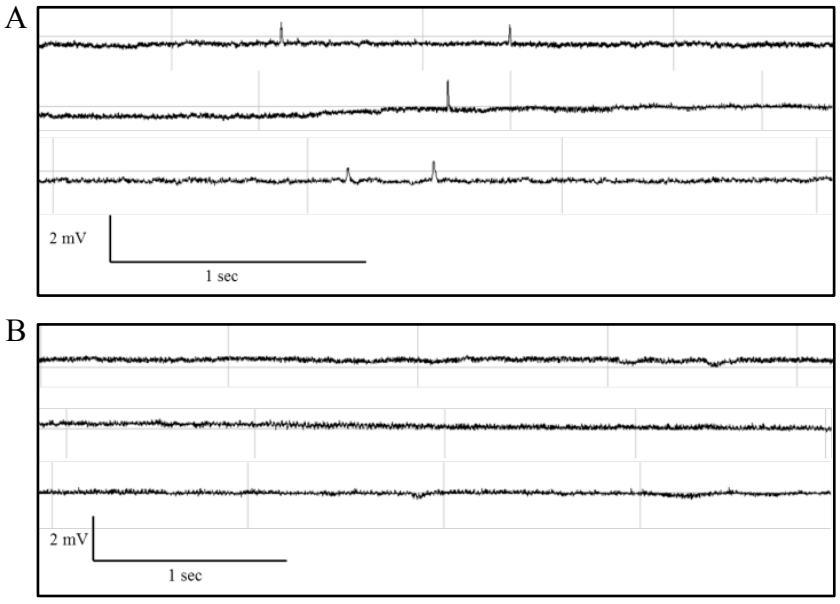

Figure 7.22. Single traces of MEPPs recordings in Cd^{2+} buffer after the addition of LTX^{N4C} and 2APB (A) or SKF96365 (B). These SOCCs blockers are successful in inhibiting LPHN1-mediated increase in exocytosis when Ca^{2+} is replaced by Cd^{2+} in the extracellular buffer.

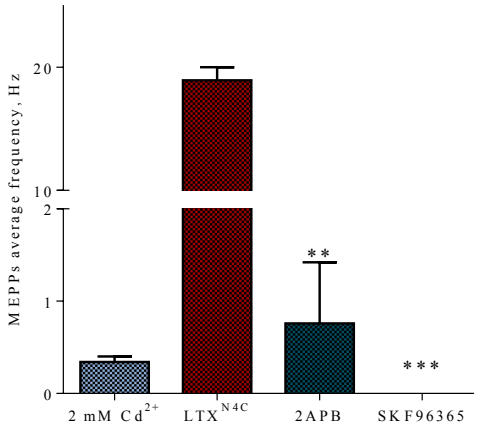

*Figure 7.23. Comparison between the averaged frequency of MEPPs in Cd^{2+} buffer, and after the addition of LTX^{N4C} and of SOCCs blockers 2 APB and SKF96365. Both drugs successfully inhibit LPHN1-mediated exocytosis (n = 15 cells recorded in Cd^{2+}, 29 cells after the addition of LTX^{N4C}, 32 cells after the addition of 2APB, and 15 after the addition of SKF96365; **, P < 0.010; ***, P < 0.001, Mann – Whitney U test).*

To test the involvement of VGCCs, I used ω-Con MVIIC (1 μM) before the activation of LPHN1 by LTX^{N4C} (0.25 nM). Differently to what happened in Ca^{2+} buffer, however, ω-Con MVIIC was less effective in inhibiting the frequency of neurotransmitter release when used in Cd^{2+} buffer (8.37 ± 2.75 Hz, Figure 7.25 A).

The average amplitude of MEPPs was not significantly different between the conditions considered (0.84 ± 0.16 mV in Cd^{2+} buffer, 0.81 ± 0.05 mV in the presence of ω-Con MVIIC, and 0.84 ± 0.02 mV after the addition of LTX^{N4C}, Figure 7.25 B).

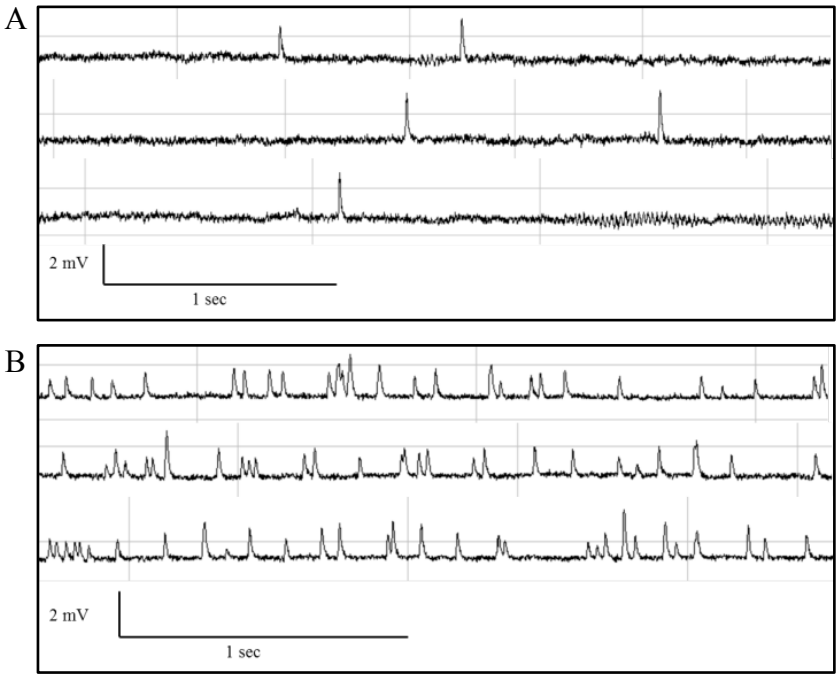

Figure 7.24. Single traces of MEPPs recording in Cd^{2+} buffer in the presence of ω-Con MVIIC before (A) and after (B) the addition of LTX^{N4C}. The inhibition of exocytosis exerted by ω-Con MVIIC is Cd^{2+} buffer is not as strong as in Ca^{2+} buffer.

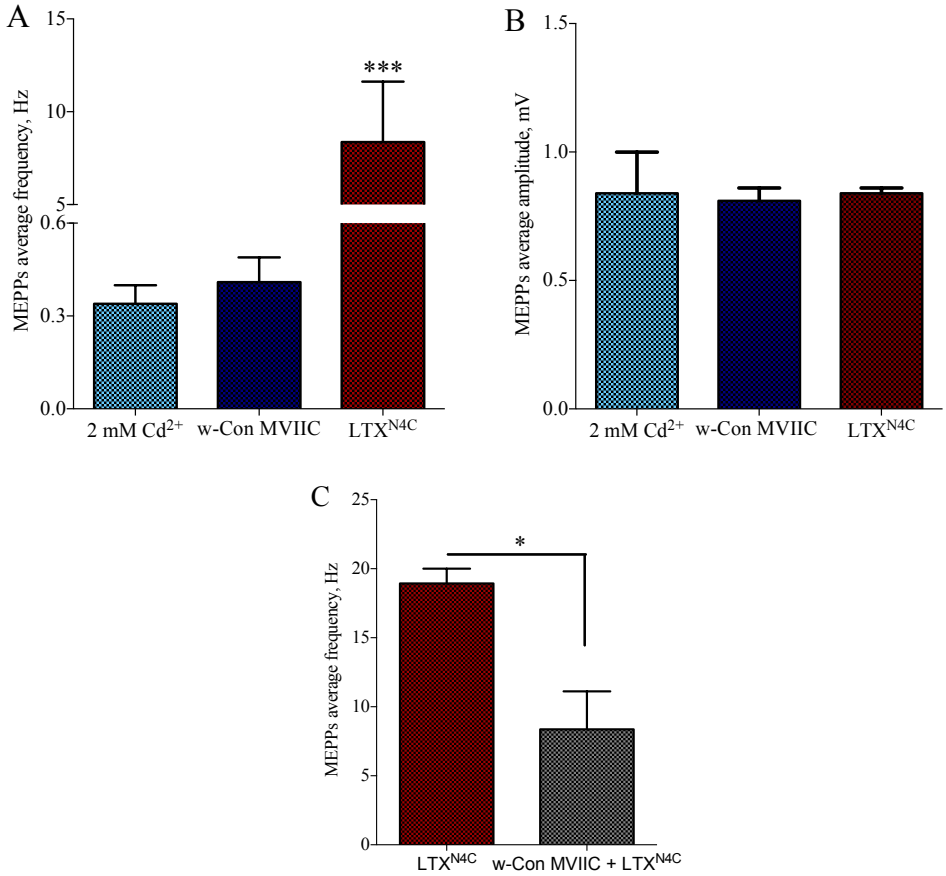

*Figure 7.25. A. Average frequency of MEPPs in 2 mM Cd^{2+}, and after the addition of ω-Con MVIIC and LTX^{N4C}. B. Average amplitude of MEPPs in Cd^{2+} buffer and after the addition of ω-Con MVIIC and LTX^{N4C}. The difference is not statistically significant (N = 1, n = 6 cells recorded in 2 mM Cd^{2+}, 8 cells after the addition of ω-Con MVIIC, and 20 after the addition of LTX^{N4C}; ***, P < 0.001, Mann – Whitney U test). C. Comparison between the effects on frequency of MEPPs after the addition of* LTX^{N4C} *in* Cd^{2+} *buffer in the absence or presence of ω-Con MVIIC (n = 35 cells recorded after the addition of* LTX^{N4C} *in* Cd^{2+} *buffer and 8 cells in the presence of ω-Con MVIIC; *, P < 0.05, Mann – Whitney U test).*

The effects of LPHN1 activation by LTX^{N4C} in Cd^{2+} buffer are similar to the effects that TG has when it is used in this same Cd^{2+}-containing buffer (see below) or indeed in the Ca^{2+}-free buffer (see Chapter 6, Section 6.2.3, Figure 6.17). However, in contrast to what happens in the presence of extracellular Ca^{2+}, addition of 10 µM TG in Cd^{2+} causes a fast increase in exocytosis (within 1 min) that reaches an average frequency not significantly different from that in Ca^{2+} (13.83 ± 3.77 Hz) and then slowly decreases until cessation (Figure 7.27 A and B).

As in Ca^{2+} buffer, the average amplitude of MEPPs after addition of TG was significantly higher (1.81 ± 0.05 mV) than the amplitude in Cd^{2+} buffer only (0.84 ± 0.16 mV, Figure 7.27 C).

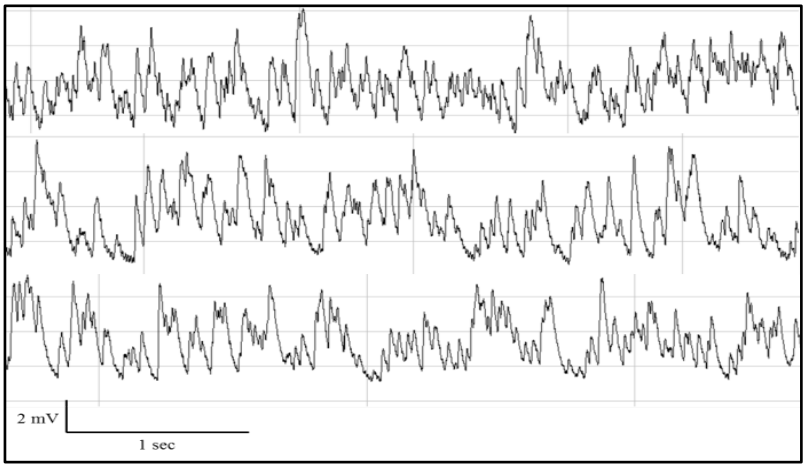

Figure 7.26. Single traces of MEPPs recordings in Cd^{2+} buffer after the addition of TG. Under this condition, exocytosis goes through a gradual increase, then reaches a pick that remain stable for some time before decreasing until cessation.

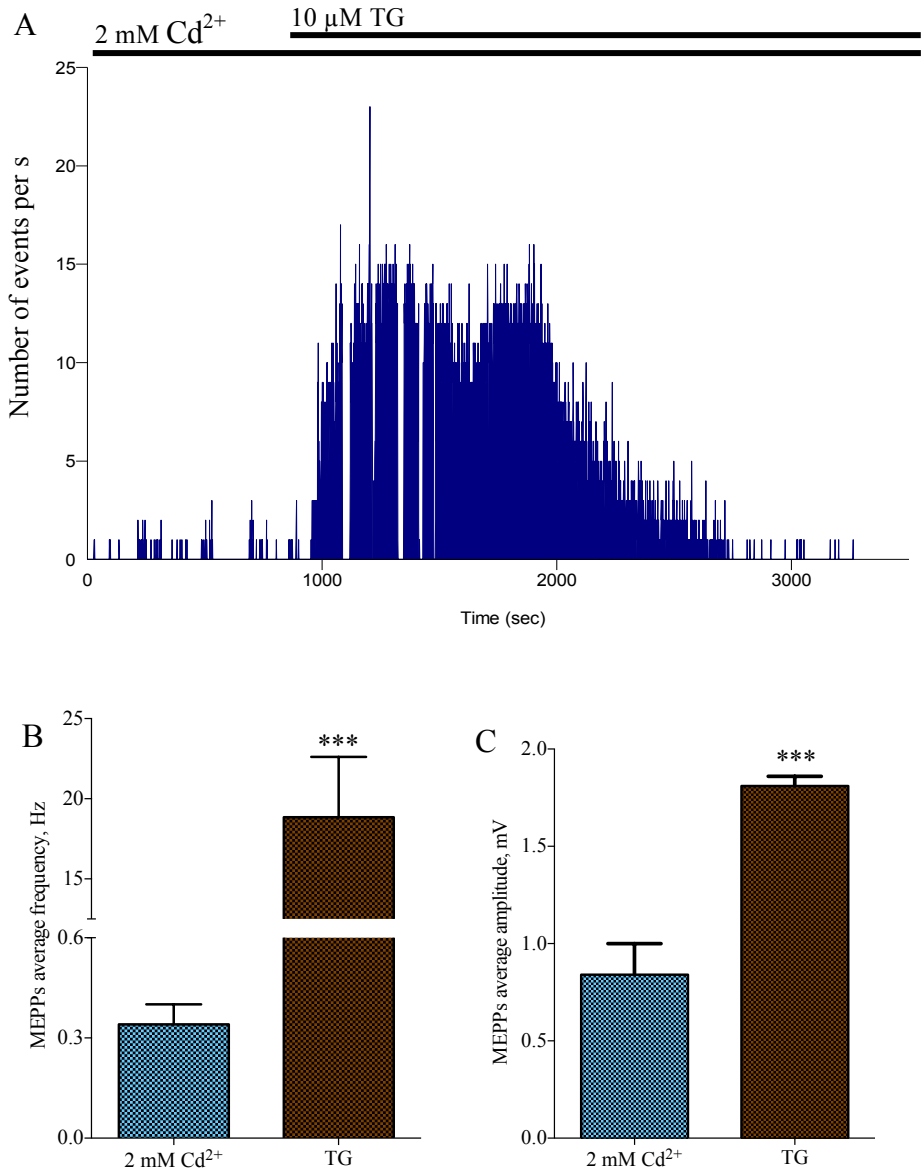

*Figure 7.27. A. Frequency plot of a MEPPs recording in 2 mM Cd^{2+} and after the addition of TG. B. Average frequency of MEPPs in Cd^{2+} buffer and after the addition of TG. C. Average amplitude of MEPPs in Cd^{2+} buffer and after the addition of TG (N = 3, n = 18 cells recorded in Cd^{2+} buffer and 24 cells after the addition of TG; ***, P > 0.001, Mann – Whitney U test).*

Similarly to my experiments in Chapter 6 on the role of Ca^{2+} in LPHN1 signalling, I used TG to test the role of intracellular Ca^{2+} stores and Cd^{2+} in the rise of exocytosis due to the activation of LPHN1. 0.25 nM LTX^{N4C} was added in Cd^{2+}-containing buffer, and 10 μM TG was then added once the increase in exocytosis reached its peak, but before the frequency started to decrease (as demonstrated above, Figure 7.27). In the presence of extracellular Cd^{2+}, I observed the same immediate drop and cessation in neurotransmitter release (0.10 ± 0.07 Hz) as was observed in Ca^{2+} buffer (Figure 7.29).

These experiments suggest that TG very quickly blocks the influx or transport of Cd^{2+} into the nerve terminals, which is crucial for the toxin-triggered exocytosis. Interestingly, because TG causes exactly the same abrupt cessation of LTX^{N4C}-induced exocytosis in the presence of extracellular Ca^{2+}, I can conclude that the channels or transporters that participate in the LPHN1-mediated release are able to conduct both Ca^{2+} and Cd^{2+}.

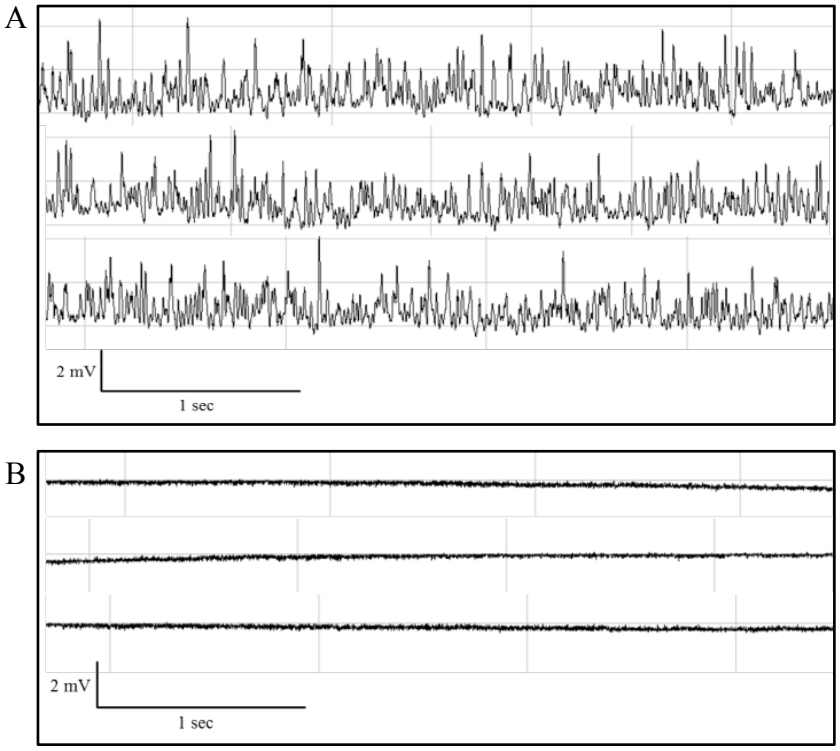

Figure 7.28. Single traces of MEPPs recordings in Cd^{2+} buffer after the addition of LTX^{N4C} (A) and TG (B). TG causes the immediate cessation of release when LTX^{N4C} effects have developed.

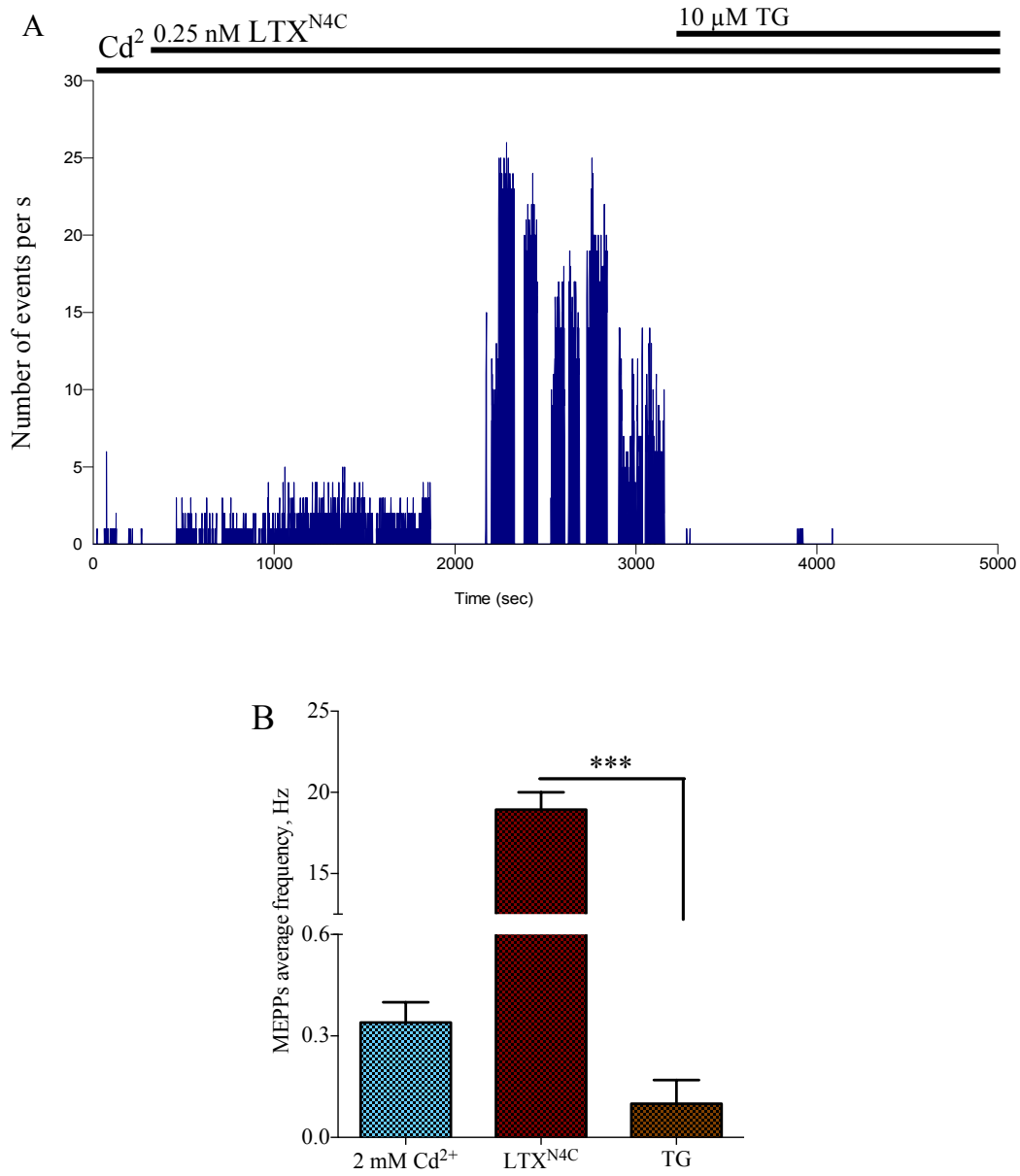

*Figure 7.29. A. Frequency plot of a MEPPs recording in 2 mM Cd^{2+}, and after the addition of LTX^{N4C} and TG. Addition of TG after the rise in exocytosis due to LTX^{N4C} causes a sudden block of release. B. Average frequency of MEPPs in Cd^{2+} buffer, and after the addition of LTX^{N4C} and TG (N = 2, n = 8 cells recorded in Cd^{2+} buffer, 12 cells after the addition of LTX^{N4C}, and 15 cells after the addition of TG; ***, P < 0.001, Mann – Whitney U test).*

7.2.4 Comparison of LPHN1- and depolarisation-mediated neurotransmitter release

As mentioned previously (see Chapter 4, Section 4.2.10, Figure 4.31), to study depolarisation-induced exocytosis I can stimulate nerve terminals using KCl, which is known to cause depolarisation of the neuronal plasma membrane and subsequent influx of Ca^{2+} through VGCCs. To compare the involvement of VGCCs in LPHN1- and depolarisation-induced exocytosis I performed current clamp experiments on neuromuscular preparations stimulated with 20 mM KCl using the pharmacological agents previously used to study LPHN1-mediated neurotransmitter release.

I already described above that normally the addition of 20 mM KCl caused an approximately 50-fold increase in the frequency of exocytosis when used in a buffer containing 2 mM Ca^{2+} (see Chapter 4, Section 4.2.10, Figure 4.31). In this part of the project I conducted similar control experiments, which showed that on the addition of KCl, the frequency of MEPPs gradually increased and reached an average of 16.13 ± 5.34 Hz in about 30 s; nerve terminals maintained this frequency for about 40 min, and then MEPPs frequency started to decrease until all miniature events stop in about 40 min (Figure 7.31).

Upon addition of KCl the resting membrane potential becomes more positive, however the MEPPs average amplitude was not significantly different between the Ca^{2+}-free and the 20 mM KCl conditions (0.90 ± 0.18 mV and 0.88 ± 0.18 mV respectively), whilst is slightly lower when Ca^{2+} is added (0.58 ± 0.01 mV, $P < 0.05$, Mann – Whitney U test).

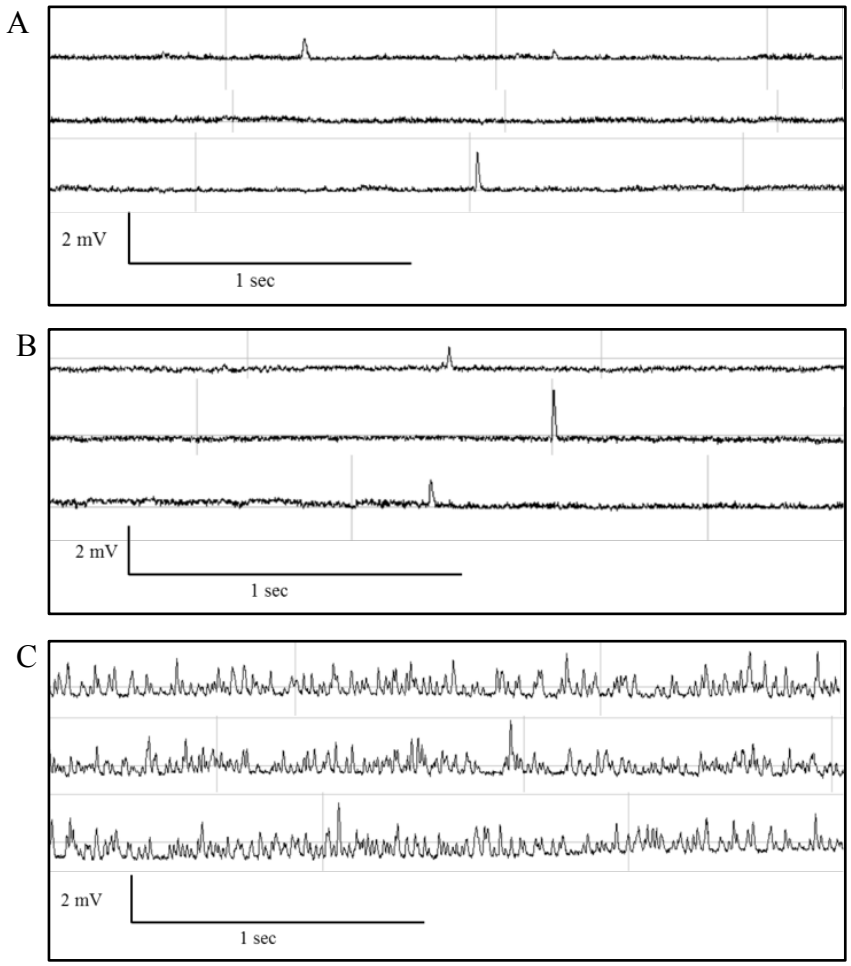

Figure 7.30. Single traces of MEPPs recordings in Ca^{2+}-free buffer (A), and after the sequential addition of KCl (B) and Ca^{2+} (C).

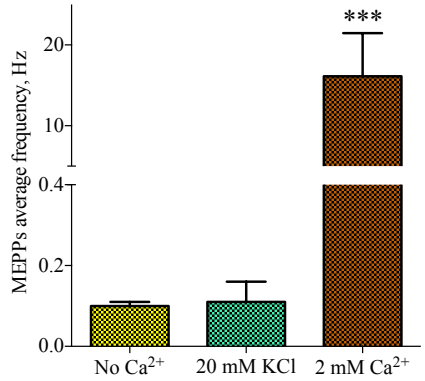

*Figure 7.31. Average frequency of MEPPs in Ca^{2+}-free buffer, and after the addition of 20 mM KCL and 2 mM Ca^{2+}. The increase in exocytosis does not start until Ca^{2+} is added to the extracellular buffer (N = 5, n = 10 cells recorded in Ca^{2+}-free buffer, 21 cells after the addition of KCl, and 38 cells after the addition of Ca^{2+}; ***, P < 0.001, Mann – Whitney U test).*

In experiments with depolarisation-induced exocytosis, I used several VGCCs blockers: Nimodipine (an inhibitor of L-type VGCCs), ω-Aga IVA (an inhibitor of P/Q-type VGCCs), ω-Con MVIIC (an inhibitor of P/Q and N-type VGCCs), and Cd^{2+}. Inhibitors were used one at a time or in conjunction in order to test the contribution of different channel types.

The addition of only Nimodipine (10 μM), ω-Aga IVA (200 nM), or ω-Con MVIIC (1 μM) was not sufficient to significantly decrease the effect of KCl (20 mM) on exocytosis (21.50 ± 1.95 Hz, 14.32 ± 3.32 Hz and 12.18 ± 3.23 Hz respectively, Figure 7.33).

Adding Nimodipine and ω-Con MVIIC at the same time caused an increase in the baseline even in the absence of KCl (5.02 ± 1.05 Hz). Considering this background release, the frequency of KCl-evoked exocytosis significantly dropped (to 3.52 ± 1.78 Hz, Figure 7.33).

Cd^{2+} was either used as a replacement of Ca^{2+} (2 mM), as in previous experiments, or added to Ca^{2+}-containing buffer (500 μM). In both cases, Cd^{2+} completely blocked the effect of KCl on exocytosis (0.12 ± 0.11 Hz and 0.21 ± 0.05 respectively, Figure 7.33).

None of the drugs tested caused a significant change in the amplitude of MEPPs (0.58 ± 0.02 mV in Nimodipine, 0.52 ± 0.01 mV in ω-Con MVIIC, 0.64 ± 0.01 mV when Nimodipine and ω-Con MVIIC were used together, 0.60 ± 0.01 mV in ω-Aga IVA, 0.78 ± 0.16 mV in 2 mM Cd^{2+}, and 0.60 ± 0.06 mV when 500 μM Cd^{2+} was added in Ca^{2+} buffer, Figure 7.33).

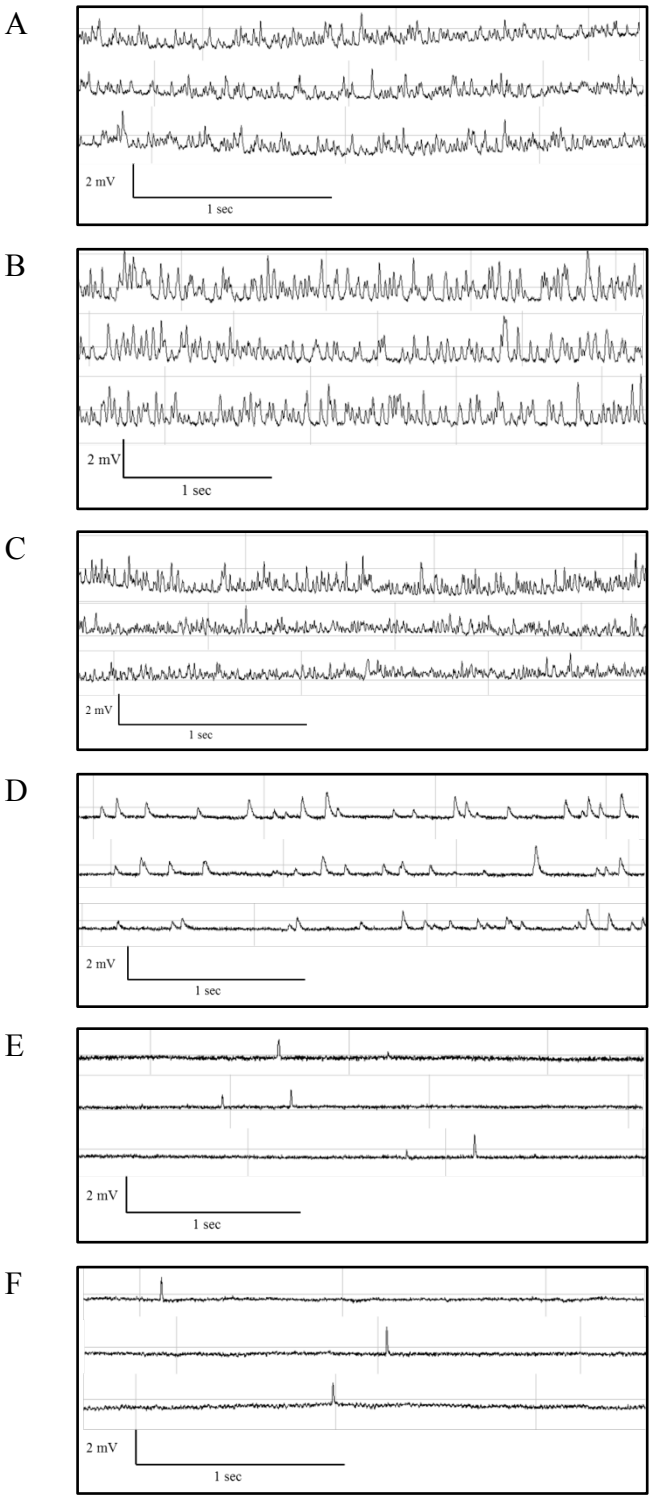

Figure 7.32. Single traces of MEPPs recordings in the presence of 20 mM KCl after the addition of Nimodipine (A), ω-Aga IVA (B), ω-Con MVIIC (C), Nimodipine + ω-Con MVIIC (D), 2 mM Cd^{2+} (E), and 500 µM Cd^{2+} (F).

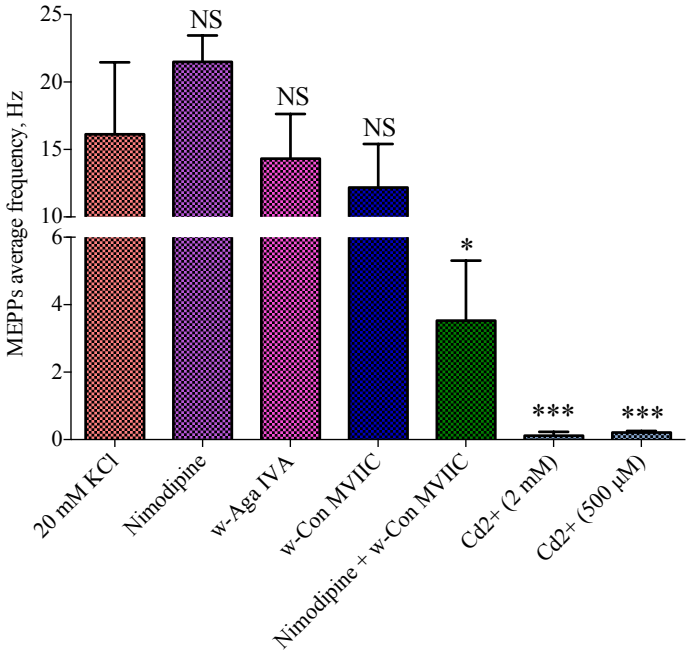

Figure 7.33. Average frequency of MEPPs in 20 mM KCl, and after the addition of VGCCs blockers Nimodipine, ω-Aga IVA, ω-Con MVIIC, Nimodipine and ω-Con MVIIC, and Cd^{2+} (, P < 0.05; ***, P < 0.001, Mann – Whitney U test).*

When comparing the LTX^{N4C} and depolarisation-triggered exocytosis, both stimuli absolutely require the influx of Ca^{2+} into the nerve terminals. However, my findings in this section also show that the two stimuli may either use different types of channels/transporters or they differentially affect the same type of channels/transporters.

7.3 Discussion

The experiments described in this chapter were directed at investigating the role of VGCCs in the effects observed upon the activation of LPHN1. As discussed previously (see Chapter 6, Section 6.3), the release of Ca^{2+} from intracellular stores and subsequent opening of SOCCs only cannot explain all the effects on exocytosis cause by LPHN1 activation. In fact, when compared to the effects of TG in the absence of extracellular Ca^{2+}, it is clear that even if LPHN1 signalling causes any Ca^{2+} release from the stores, this amount of Ca^{2+} release is not high enough to start the increase in exocytosis observed. Another source of Ca^{2+} is needed in order to increase the cytosolic [Ca^{2+}] to a point where the whole mechanism can potentiate and produce the 160-fold increase in exocytosis described.

The involvement of VGCCs was, therefore, investigated as a possible source of Ca^{2+} influx. Blockers of the major neuronal VGCCs were used to test their ability to stop the exocytosis increase upon addition of LTX^{N4C}. Of all the channels tested, only the block of P/Q-type VGCCs was successful in inhibiting the signalling downstream of LPHN1 (see Figure 7.13). In fact, the blockade of the other channels did not significantly decrease the frequency of MEPPs nor did it bring changes to the bursting behaviour observed upon activation of LPHN1 (see Figure 7.14, A).

Interestingly, the block of P/Q-type VGCCs is successful in inhibiting the effects of LPHN1 activation only when the P/Q-types blockers are applied before the addition of LTX^{N4C}, while the block of these channels after the effects of LPHN1 activation already started does not bring about any significant changes in the overall frequency of exocytosis or bursting behaviour (see Figure 7.14, B). The only difference observed in this case is the frequency of MEPPs during the interburst intervals. Application of P/Q blockers to terminals already responding to LTX^{N4C} leads to a significantly lower average frequency of release in between the bursts (see Figure 7.9).

I discussed in the previous chapter how the opening of the SOCCs can explain the increased frequency of exocytosis during the bursts. The opening of

P/Q VGCCs can, instead, explain the frequency during the interburst intervals, which, although not as high as during the bursts, is still much higher than that observed in the absence of LTX^{N4C}. This observation, together with the finding that the blockade of P/Q VGCCs can stop the effects of LPHN1 activation only if applied before the addition of LTX^{N4C}, helps to delineate a more complex, but possibly more complete scheme of the molecular elements activated by LPHN1.

First, the activation of LPHN1 starts the molecular pathway involving $G\alpha_{q/11}$ that leads to the activation of IP_3Rs located at the ER; this in itself, however, is not sufficient to induce Ca^{2+} release, most likely because of the subthreshold activation of the Ca^{2+} release channels (IP_3Rs). At the same time, LPHN1 activation causes the opening of P/Q VGCCs. This triggers an initial increment of cytosolic Ca^{2+} coming from the extracellular space. Although this increase is not enough to cause the dramatic bursts of exocytosis that develops later, it is still sufficient to increase the frequency of MEPPs by about 2 times compared to the basal frequency. More importantly, this P/Q VGCCs-mediated increase in cytosolic Ca^{2+} further stimulates the IP_3Rs, now leading to their massive opening and a further increase in cytosolic $[Ca^{2+}]$. This mechanism leads to the depletion of Ca^{2+} stores, thus, allowing for the opening of SOCCs. At this point, the elevation in cytosolic $[Ca^{2+}]$ reaches a level that translates into the development of a proper burst of exocytosis (when the frequency of spontaneous exocytosis reaches values up to 150 times higher than at rest). The burst continues until the SOCCs are inactivated by the refilling of the stores, and cytosolic Ca^{2+} is largely sequestered or chelated. At that point the burst stops, and the frequency of exocytosis drops to about 2.5 times of that during the rest, being caused by the small but apparently constant and pivotal influx of Ca^{2+} via the P/Q VGCCs.

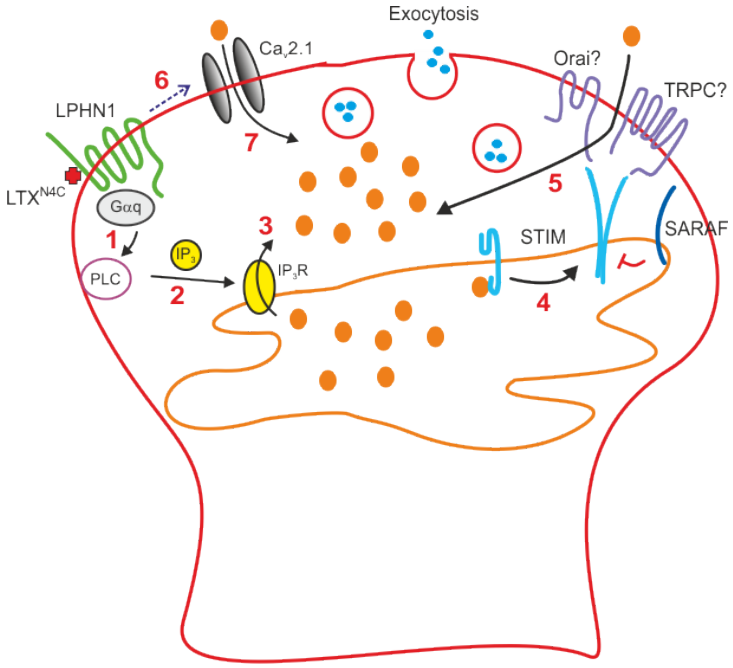

Figure 7.34. Schematic representation of the full mechanism activated by LPHN1. As extensively discussed previously (Chapter 5, Figure 5.15) the stimulation of LPHN1 causes the activation of the Gα_q protein signalling pathway, ultimately leading to the release of Ca^{2+} from IP_3Rs located at the ER (arrows 1 to 5). The decreased concentration of ER intraluminal Ca^{2+} is detected by STIM1, that dimerises in proximity to the plasma membrane and contacts SOCCs (TRPCs and Orais), opening them and allowing influx of Ca^{2+} (arrows 4 – 5, Chapter 6, Figure 6.23). In parallel, activation of LPHN1 causes the opening of P/Q VGCCs (arrow 6), that supply the initial influx of Ca^{2+} necessary to elevate the intracellular Ca^{2+} concentration to a level sufficient to further stimulate IP_3Rs and start the initial increase in exocytosis (arrow 7).

Experiments using Cd^{2+} as a replacement of Ca^{2+}, initially designed to test the involvement of VGCCs in the activation of LPHN1, were instead useful in further confirming the pathway of activation delineated so far. Surprisingly, the replacement of Ca^{2+} with Cd^{2+}, does not inhibit the effects of LPHN1 activation; however, it changes their characteristic. Nerve terminals still respond to the addition of LTX^{N4C} with a high increase in the frequency of exocytosis, that can be compared to the overall increase in the presence of Ca^{2+} (see Figure 7.20, B).

However, the bursts cycles are never produced; instead, the frequency of release gradually increases and then decreases, followed by a complete cessation of exocytosis. This effect can be explained, by postulating that rather than blocking the VGCC conductance, Cd^{2+} acts by interacting with other extracellular proteins. In fact, outside the cells Cd^{2+} is able to upregulate the cytosolic [Ca^{2+}] by activating cell surface G protein-coupled metal binding receptors (Faurskov and Bjerregaard 2002; Martelli et al. 2006). This activates PLC and leads to the production of IP_3, leading to the release of Ca^{2+} from intracellular stores. Moreover, whilst it is certainly true that Cd^{2+} is a blocker of VGCCs at high concentration, this cation is still able to enter the cell through them, especially, but not only, through L-type VGCCs. In other words, Cd^{2+} inhibits the Ca^{2+} current through VGCCs, but it can permeate them itself, and once inside the cells it can fully support exocytosis (Hinkle, Shanshala and Nelson 1992; Usai et al. 1999; Gavazzo, Morelli and Marchetti 2005). To further complete the picture, Cd^{2+} is also able to pass through SOCCs, therefore, allowing the full activation of the LPHN1-mediated exocytosis. In this way, Cd^{2+} may be able to activate all the molecular components that seem to be involved in the exocytosis caused by LPHN1 activation. The only difference in the phenomenology of the effect of Cd^{2+} when compared to Ca^{2+}, is the absence of bursting behaviour, which can be explained by the incapacity of Cd^{2+} to refill the stores, so that the increase in exocytosis will persist as long as there are vesicles and a sufficient [Ca^{2+}]/[Cd^{2+}] is available in the cytosol.

The question that remains to be addressed is the kind of relationship between LPHN1 and P/Q VGCCs. In fact, several kinds of interactions are possible. First of all, one has to consider that usually VGCCs become activated by depolarisation of the cells; however, as I suggest with my experiments using TTX (see Chapter 4, Section 4.2.11), opening of TTX-sensitive voltage-gated Na^{2+} channels and depolarisation of the cells is not needed for the effects of LPHN1 activation (although also other channels might be involved in depolarisation and this conclusion will need more investigation). P/Q channels can also be regulated by G proteins, particularly by the βγ subunits. However, the regulation in this case is inhibitory, switching the state of the channel from the "willing" state (easy to

activate) to the "reluctant" state. This inhibition can be reversed by, among other factors, phosphorylation of the channel by PKC (Herlitze et al. 2001; Colecraft, Brody and Yue 2001). It is therefore possible that LPHN1 facilitates the opening of P/Q VGCCs by activating PKC, which in turn phosphorylates the channel. Another possibility is that the interaction between LPHN1 and P/Q, in addition to being functional, is also physical. If these two proteins physically interact, the conformational changes due to LPHN1 activation might cause the opening of the channel, possibly leading to its continuous activation. If this hypothesis is true, then other question would arise about the nature of this interaction: do LPHN1 and P/Q VGCC normally interact or is the interaction present only upon the activation of LPHN1 with LTX^{N4C}? One way to address this hypothesis would be to perform pull down experiments using a LTX column in order to see if P/Q VGCCs is pulled down together with LPHN1 (although in this case LPHN1 would be at least partially activated by LTX, which might increase the interaction between LPHN1 and VGCC). Other methods to pull down LPHN1, would be needed to ascertain if the interaction between the two proteins is constitutive or it occurs only upon LPHN1 activation. Moreover, patch clamp experiments on cells expressing LPHN1 and P/Q channels are needed in order to evaluate the influx of Ca^{2+} through these channels when LPHN1 is activated.

CHAPTER 8
DISCUSSION

The main purpose of this work was to delineate the molecular mechanisms responsible for the control of spontaneous exocytosis by LPHN1.

First, we studied the physiological effects that LPHN1 exerts on spontaneous exocytosis at the mouse NMJ and in cultured hippocampal neurons in the absence of LPHN1 activation. By comparing LPHN1 WT and KO mice (see Chapter 4, Sections 4.2.2 and 4.2.3), it was possible to observe a consistent increase in the frequency of spontaneous exocytosis in the row from WT, to Het, to KO preparations. This result alone already gives us the idea of LPHN1 as a regulator of neurotransmitter release. When LPHN1 is not activated, it controls the activity of neurons and maintains the basal frequency of spontaneous exocytosis at lower levels. However, as we will see below, the activation of LPHN1 very strongly increases spontaneous neurotransmitter release. This behaviour is fully consistent with a central role of LPHN1 in controlling the resting and induced spontaneous secretion.

Other suggestions about the physiological role of LPHN1 come from the experiments on central synapses. Here, LPHN1 KO neurons showed reduced connectivity and low survival compared to WT neurons. This can suggest a role for LPHN1 in neuronal development, a possibility that has been directly supported by experiments with soluble LPHN1 constructs (Boucard, Maxeiner and Sudhof 2014) and that finds further ground also considering that Lasso, an endogenous ligand of LPHN1, is a member of the teneurin family (Silva et al. 2011), a class of proteins involved in neuronal development, axon guidance and synaptogenesis (Tucker et al. 2007; Young and Leamey 2009).

Second, using the non-pore forming mutant of α-LTX, LTX^{N4C}, as an LPHN1 agonist, we studied the effects of LPHN1 activation on spontaneous exocytosis. Activation of LPHN1 using this toxin causes an increase in exocytosis that goes through bursts of intense release that can reach frequencies of 100 Hz, interspersed with intervals of moderate activity, where the frequency of release

goes back almost to the resting level (see Chapter 4, Section 4.2.5). The bursts and inter-burst intervals are irregular in length, but are always present in each cell recorded when LPHN1 is activated by this agonist. So far this behaviour could not be explained, as the mechanisms underlying these effects were not known. The results we will discuss further in this chapter provide the first most plausible molecular basis for the burst-like spontaneous exocytosis induced by the activation of LPHN1.

However, LTX^{N4C} is known to bind both LPHN1 and NRX-Iα (Ichtchenko et al. 1998; Volynski et al. 2003). Therefore, before investigating the details of the mechanisms underlying LPHN1 activation, it was important to demonstrate that LPHN1 is the α-LTX receptor responsible for the effects described. This was accomplished using several methods: first, the addition of LTX^{N4C} in buffers where Ca^{2+} has been replaced by Ba^{2+} or Sr^{2+} (conditions in which the binding of LTX^{N4C} to all NRXs is not possible; Volynski et al. 2003) causes an increase in exocytosis generally comparable to that described in Ca^{2+} (see Chapter 4, Section 4.2.8).

More importantly, when LTX^{N4C} is used on LPHN1 KO NMJ preparations, none of the effects described in WT preparations are observed (see Chapter 4, Section 4.2.9). The overall frequency of exocytosis does not significantly change with the addition of the toxin, although very few occasional bursts are present. This could be explained, however, if we take into consideration that LPHN2 is also present in these preparation, and that in the absence of LPHN1 the affinity of LPHN2 to LTX^{N4C} is higher than in WT animals, probably due to different post-translational modification of LPHN2 (Yuri Ushkaryov, personal communication). A partial compensation mechanism can, therefore, take place, where LPHN2, taking over some functions of LPHN1, can react to LTX^{N4C}, causing the rare bursts of exocytosis, but not the overall frequency of release.

Furthermore, LTX^{N4C} causes no effect when the interaction between the NTF and the CTF of LPHN1 is prevented by low concentrations of PFOA (see Chapter 4, Section 4.2.10). In this case, in fact, the binding of LTX^{N4C} to the NTF still occurs, however, it cannot cause the conformational changes in the CTF that

are necessary to transduce the signal and to start the molecular pathway responsible for the increased spontaneous exocytosis.

Finally, we delineated the molecular mechanisms responsible for LPHN1-mediated effects using several inhibitors of the G protein pathway and blockers of SOCE and VGCCs.

Figure 8.1 summarises the main findings of this study, delineating the molecular players that are responsible for the elevation in the frequency of spontaneous exocytosis observed upon LPHN1 activation. Our results revealed three main molecular players that work together to generate the effects observed:

- $G\alpha_{q/11}$ protein and its signalling pathway (see Chapter 5);
- Intracellular Ca^{2+} store depletion and activation of SOCE (see Chapter 6);
- P/Q VGCC (see Chapter 7).

The binding of LTX^{N4C} to LPHN1 causes the activation of $G\alpha_{q/11}$ protein; this, in turn, activates PLC, that promotes the hydrolysis of PIP_2 in IP_3 that, binding to IP_3R in the endoplasmic reticulum, ultimately causes the release of Ca^{2+} from intracellular stores and the consequent elevation in cytosolic [Ca^{2+}] (for a review see Kamato et al. 2015). The decrease in the ER [Ca^{2+}] causes the dimerization of STIM, that, aggregating into puncta close to the plasma membrane, contacts and leads to the opening of Orai and TRPC channels, starting SOCE that permits the refilling of the stores and that further increases the cytoplasmic [Ca^{2+}] (Salido, Sage and Rosado 2009).

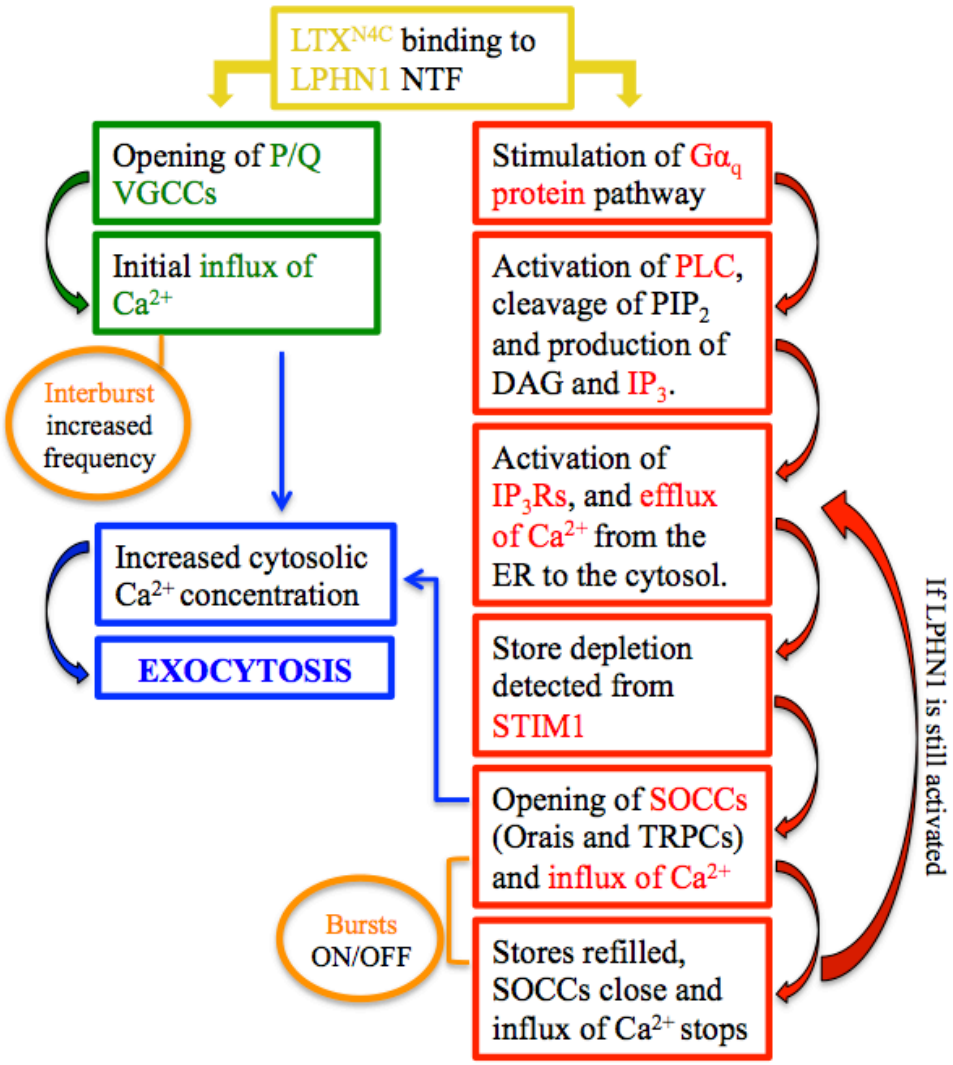

Figure 8.1. Block diagram summarising the molecular mechanisms responsible for the increased exocytosis observed after stimulation of LPHN1 with LTX^{N4C}. Activation of LPHN1 causes the stimulation of the $G\alpha_q$ protein signalling pathway and, in parallel, the opening of P/Q VGCCs. The first leads to the efflux of Ca^{2+} from IP_3-sensitive intracellular Ca^{2+} stores and subsequent opening of SOCCs and initiation of SOCE; the periodic opening/closing of SOCCs is what give rise to the bursts, and it will go on as long as LPHN1 is stimulated. The latter causes the initial influx of Ca^{2+} needed to further stimulate the release of Ca^{2+} from IP_3Rs and start the increase in the frequency of exocytosis; the constant influx of Ca^{2+} from P/Q VGCCs is responsible for the increased frequency of spontaneous release observed during interburst intervals.

None of these mechanisms, however, is able to cause the increase in exocytosis without the initial involvement of the P/Q-type VGCC. In fact, the effects of LPHN1 activation are completely inhibited when this channel is blocked before the increase of release induced by LTX^{N4C} has started. Furthermore, activation of LPHN1 in the absence of extracellular Ca^{2+} also causes no increase in spontaneous exocytosis. These data could mean that the G protein pathway activated by LPHN1 alone is not able to activate IP_3R to an extent where the elevation in Ca^{2+} causes the depletion of the stores and the activation of SOCE; more Ca^{2+} is needed, and this is provided by the activation of the P/Q VGCCs, in order to further stimulate the release of Ca^{2+} from IP_3R and start SOCE. The cyclical process of stores depletion – activation of SOCE and stores refilling – deactivation of SOCE most likely causes the waves in increased – decreased intracellular Ca^{2+} concentration that constitutes the mechanism responsible for the bursting behaviour of spontaneous exocytosis induced via LPHN1. Specifically, the increased cytosolic Ca^{2+} concentration due to its influx through SOCCs is likely to be responsible for the fast increase in exocytosis characterising bursts, that lasts until the refilling of the stores is complete, the SOCCs close again, and the intracellular Ca^{2+} concentration goes back to physiological level. On the other hand, the activation of the P/Q-type VGCC does not seem to follow this burst-like pattern, and therefore, the basal increased cytosolic $[Ca^{2+}]$ caused by the continuous opening of P/Q VGCCs could account for the slightly increased frequency in exocytosis during interburst intervals.

What remains to be understood is the nature of the interaction between LPHN1 and P/Q VGCCs. In fact, regulation of VGCC channels by G proteins has been widely described in the literature (for a review see Dolphin 2003). These channels are operated by direct interaction with the βγ subunit or by phosphorylation through activation of the Gα subunit (Herlitze et al. 2001; Colecraft, Brody and Yue 2001). However, in both cases the interaction with P/Q-type VGCCs is inhibitory in nature. However, the activation of LPHN1, instead, leads to an excitatory effect. This could be due to a novel form of VGCCs modulation. Alternatively, LPHN1 may physically interact with the P/Q VGCC,

leading to channel opening in response to a conformational change in LPHN1 caused by its activation.

8.1 Toxicological aspects of the LPHN1 NTF and CTF dissociation caused by PFOA

Perfluorooctanoic acid (PFOA) is a synthetic, non-biodegradable compound belonging to the perfluorinated compound family (PFCs). Being used as a surfactant in several industrial applications, such as in clothing, carpets, food packaging and cookware, the exposure to these compounds is pervasive and its effects have been studied under different aspects. PFCs have been detected for the first time in human tissues in the 1960s (Taves, 1968) and since then numerous studies have been undertaken to investigate their accumulation in tissues and their potential toxicity. Although less than in other tissues such as blood and liver, PFCs have been found accumulating in the brain, with PFOA reaching levels of 0.5 ng/g (Maestri et al. 2006).

The presence of PFCs in brain tissues has led to concerns about the potential neurotoxicity of these compounds. It has been shown that neonatal exposure to PFCs can lead to altered expression of proteins such as Tau, GAP-43, CaMII and synaptophysin involved in synaptogenesis and neuronal growth; the cholinergic system is also affected, with animals showing a hypoactive response to 80 μg/kg of nicotine 4 month after a single exposure to 1.4 – 21 μM/kg PFOA. Following the same treatment, also spontaneous behaviour (locomotion, rearing and total activity) were deregulated, as well as habituation, a kind of non-associative learning (Johansson, Fredriksson and Eriksson 2008; Johansson, Eriksson and Viberg 2009).

Neonatal exposure to PFOA can also cause alteration of the immune system that, given the predisposition, could lead to the development of symptoms associated to autism and ADHD (Hu et al. 2012).

In vitro, exposure of N2a cells to > 200 μM PFOA and PFOS mediates the disintegration of 3D cultured spheroid into single cell populations, increases the level of necrosis and apoptosis and has inhibitory effect on retinoic acid-induced

differentiation (Choi et al. 2013); the same concentration is able to disrupt calcium homeostasis in cultured hippocampal neurons, stimulating the release of Ca^{2+} from intracellular Ca^{2+} stores (Liu et al. 2011). Exposure to 10 – 30 μM PFCs induces changes in cerebellar Purkinje cells membrane potentials and reduces the rate of fired action potentials (Harada et al. 2006).

In the present work, we showed that PFOA is able to dissociate and differentially solubilise the NTF and CTF of LPHN1, and we described the physiological effects of this dissociation using NMJ preparations.

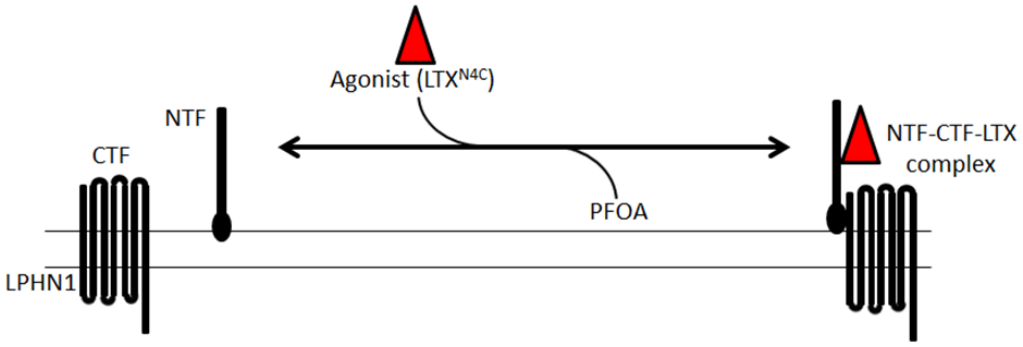

Figure 8.2. Dissociation of LPHN1 NTF and CTF by PFOA. LPHN1 NTF and CTF normally exist as separate fragments independent from each other, and they associate upon binding of an agonist. PFOA supposedly disrupts this association, preventing the effects of LPHN1 activation to develop.

Here, PFOA inhibited, and at 100 μM completely blocked the toxin-evoked exocytosis in a dose-dependent manner. Increasing concentrations of PFOA also delayed depolarisation-induced neurotransmitter release. These results provide new insights into the neurotoxic effect of PFOA on neuronal transmission. The effects described in our experiments can be only compared to an acute intoxication, as the preparations are suddenly exposed to relatively high PFOA concentrations and the effects are observed straight away. Although this type of exposure may not occur in less artificial conditions, the major concern is that PFOA accumulates in tissues; for example, levels of about 2 μg/ml have been

found in the blood of chronically exposed workers (Ehresman et al. 2007). The slow and gradual exposure is likely to lead to the development of compensation mechanisms that, although restoring the impaired function (in our case slow reaction time) to level close to control, may in the long term disrupt some other function changing the balance that characterises the normal physiology.

Caution must be used when using this compound on the large scale, as its effects on human population could cause a general increase in the reaction time of neurons, and consequently a slower response in the action of individuals, that may result in dangerous situations especially when they are involved in activities such as driving or using work-related tools.

8.2 Future work

The work discussed so far allowed us to answer some questions about LPHN1 that were never explored in depth before. However, new questions arise that could not be answered due to limitations in time and in the experimental methods used, and therefore will need to be addressed in the future.

First, it will be interesting to explore in depth the phenomenon of reduced survivability of neurons lacking LPHN1. It could be that the interaction between LPHN1 and Lasso is necessary for the synapse to fully develop and therefore neurons KO for LPHN1, an adhesion molecule, fail to establish functional connections with postsynaptic partners. Interesting suggestions about the role of LPHN1 could also arise studying the survivability of neurons lacking Lasso instead. The same reduced connectivity could be observed, confirming the importance of the LPHN1 – Lasso interaction for synapse formation, or alternatively, if no differences are found compared to WT neurons, it could mean that a molecule different from Lasso (probably FLRT3) also interact with LPHN1 in vivo regulating synaptic formation, and this could reveal new functions of the receptor.

Second, fully formed synapses lacking LPHN1 are more active than the WT ones, showing increased spontaneous neurotransmitter release at rest. This aspect might be crucial for the constitution of functional neuronal networks in the developing nervous system. In fact, there is evidence that we are born with more synaptic connections than we retain, and that the interaction with the environment helps the system to select the synapses that, being more active, have to be maintained (Edelman 1987; Edelman 1992). It is therefore possible that mice lacking LPHN1 (and probably humans with expressing a defective form of it) develop abnormal neuronal networks, that in the long run could lead to pathological outcomes such as autism, where subjects affected have been shown to have more synapses than the control (Tang et al. 2014), or Alzheimer's disease, in which hyperactivity of the medial temporal regions and a general increased magnitude of brain activation (especially hippocampal, parietal and prefrontal regions) during memory tasks have been shown to be common in subjects at risk

of the disease, and could be able to predict the subsequent future decline in memory (Bookheimer et al. 2000; Putcha et al. 2011).

Third, more precision is needed in defining the molecular partners involved in LPHN1 activation, particularly in respect of SOCCs. First of all, having the limitation of not allowing genetic manipulations of the specimen, the experiments on NMJ did not allow us to test if the defective expression of particular SOCCs would alter the response of LPHN1 to LTX^{N4C}. As mentioned in Chapter 4, differentiated Nb2a cells acquire the ability to respond to LTX^{N4C} when expressing LPHN1 (response that is not present in non-differentiated Nb2a cells, even when expressing LPHN1). Preliminary data suggest that the proteins necessary for a functional SOCE are upregulated in these cells, particularly STIM1, SARAF, Orai 3 and TRPC2 (Blackburn and Ushkaryov, data not published). Whether or not these are the major SOCE proteins involved in LPHN1 activation at the NMJ or in other tissues is not clear at the moment, and experiments where it will be possible to knock down single genes to analyse the possible changes in the response of LPHN1 to its agonist are needed, using for example motor or pyramidal neurons primary cultures.

Finally, the regulation operated by LPHN1 on P/Q VGCCs needs to be investigated with more attention. In this regard, two possibilities are plausible: on the one hand LPHN1 could facilitate the opening of P/Q VGCCs by activating PKC, which in turn phosphorylates the channel allowing its transition from a "reluctant" to a "willing" state (Herlitze et al. 2001; Colecraft, Brody and Yue 2001). Alternatively, the interaction between LPHN1 and P/Q could be physical. In this case, conformational changes of LPHN1 would physically open the channel, leading to a much faster Ca^{2+} influx than in the case of phosphorylation by PKC. If this is true, other questions present themselves for future investigation, such as whether the interaction is constitutive or only occurs upon activation of LPHN1.

BIBLIOGRAPHY

Ahlijanian, M. K., Westenbroek, R. E. and Catterall, W. A. (1990). Subunit structure and localization of dihydropyridine-sensitive calcium channels in mammalian brain, spinal cord, and retina. *Neuron* [Online], 4(6), 819-832.

Almo, S. C., et al. (2007). Structural genomics of protein phosphatases. *Journal of Structural and Functional Genomics* [Online], 8(2-3), 121-140.

Ashton, A. C., et al. (2000). Tetramerisation of alpha-latrotoxin by divalent cations is responsible for toxin-induced non-vesicular release and contributes to the Ca(2+)-dependent vesicular exocytosis from synaptosomes. *Biochimie* [Online], 82(5), 453-468.

Ashton, A. C., et al. (2001). α-Latrotoxin, Acting via Two Ca2+-dependent Pathways, Triggers Exocytosis of Two Pools of Synaptic Vesicles. [Online]. Vol. 276., pp. 44695-44703.

Awatramani, G. B., Price, G. D. and Trussell, L. O. (2005). Modulation of transmitter release by presynaptic resting potential and background calcium levels. *Neuron* [Online], 48(1), 109-121.

Bai, J., et al. (2004). Fusion pore dynamics are regulated by synaptotagmin*t-SNARE interactions. *Neuron* [Online], 41(6), 929-942.

Bakowski, D. and Parekh, A. B. (2007). Voltage-dependent Ba2+ permeation through store-operated CRAC channels: implications for channel selectivity. *Cell Calcium* [Online], 42(3), 333-339.

Berna-Erro, A., Redondo, P. C. and Rosado, J. A. (2012). Store-operated Ca(2+) entry. *Advances in Experimental Medicine and Biology* [Online], 740, 349-382.

Birks, R., Huxley, H. E. and Katz, B. (1960). The fine structure of the neuromuscular junction of the frog. *The Journal of Physiology* [Online], 150, 134-144.

Bernard, R., et al. (2014). Assessing the role of Gαq/11 in cellular responses: an analysis of investigative tools. *Clinical and Experimental Pharmacology* [online], 4:164.

Bleasdale, J. E., et al. (1990). Selective inhibition of receptor-coupled phospholipase C-dependent processes in human platelets and polymorphonuclear neutrophils. *The Journal of Pharmacology and Experimental Therapeutics* [Online], 255(2), 756-768.

Bleasdale, J. E. and Fisher, S. K. (1993). Use of U-73122 as an Inhibitor of Phospholipase C-Dependent Processes. *Neuroprotocols* [Online], 3(2), 125-133.

Bookheimer, S. Y., et al. (2000). Patterns of brain activation in people at risk for Alzheimer's disease. *The New England Journal of Medicine* [Online], 343(7), 450-456.

Bootman, M. D., et al. (2002). 2-Aminoethoxydiphenyl borate (2-APB) is a reliable blocker of store-operated Ca2+ entry but an inconsistent inhibitor of InsP3-induced Ca2+ release. *The FASEB Journal* [Online], 16(10), 1145-1150.

Boucard, A. A., Maxeiner, S. and Sudhof, T. C. (2014). Latrophilins function as heterophilic cell-adhesion molecules by binding to teneurins: regulation by alternative splicing. *The Journal of Biological Chemistry* [Online], 289(1), 387-402.

Bouron, A. (2001). Modulation of spontaneous quantal release of neurotransmitters in the hippocampus. *Progress in Neurobiology* [Online], 63(6), 613-635.

Brose, N., et al. (1992). Synaptotagmin: A calcium sensor on the synaptic vesicle surface. *Science* [Online], 256(5059), 1021-1025 [Accessed 22 July 2014].

Burgess, T. L. and Kelly, R. B. (1987). Constitutive and regulated secretion of proteins. *Annual Review of Cell Biology* [Online], 3, 243-293.

Capogna, M., Gahwiler, B. H. and Thompson, S. M. (1996). Calcium-independent actions of alpha-latrotoxin on spontaneous and evoked synaptic transmission in the hippocampus. *Journal of Neurophysiology* [Online], 76(5), 3149-3158.

Capogna, M., et al. (2003). The alpha-latrotoxin mutant LTXN4C enhances spontaneous and evoked transmitter release in CA3 pyramidal neurons. *The Journal of Neuroscience : The Official Journal of the Society for Neuroscience* [Online], 23(10), 4044-4053.

Catterall, W. A. (2011). Voltage-gated calcium channels. *Cold Spring Harbor Perspectives in Biology* [Online], 3(8), a003947.

Catterall, W. A. (2000). Structure and regulation of voltage-gated Ca2+ channels. *Annual Review of Cell and Developmental Biology* [Online], 16, 521-555.

Ceccarelli, B., Grohovaz, F. and Hurlbut, W. P. (1979). Freeze-fracture studies of frog neuromuscular junctions during intense release of neurotransmitter. I. Effects of black widow spider venom and Ca2+-free solutions on the structure of the active zone. *The Journal of Cell Biology* [Online], 81(1), 163-177.

Ceccarelli, B. and Hurlbut, W. P. (1980a). Ca2+-dependent recycling of synaptic vesicles at the frog neuromuscular junction. *The Journal of Cell Biology* [Online], 87(1), 297-303.

Ceccarelli, B. and Hurlbut, W. P. (1980b). Vesicle hypothesis of the release of quanta of acetylcholine. *Physiological Reviews* [Online], 60(2), 396-441.

Ceccarelli, B., Hurlbut, W. P. and Mauro, A. (1973). Turnover of transmitter and synaptic vesicles at the frog neuromuscular junction. *The Journal of Cell Biology* [Online], 57(2), 499-524.

Ceccarelli, B., Hurlbut, W. P. and Mauro, A. (1972). Depletion of vesicles from frog neuromuscular junctions by prolonged tetanic stimulation. *The Journal of Cell Biology* [Online], 54(1), 30-38.

Chapman, E. R., et al. (1995). Ca2+ Regulates the Interaction between Synaptotagmin and Syntaxin 1. *Journal of Biological Chemistry* [Online], 270(40), 23667-23671.

Chieregatti, E., Witkin, J. W. and Baldini, G. (2002). SNAP-25 and synaptotagmin 1 function in Ca2+-dependent reversible docking of granules to the plasma membrane. *Traffic (Copenhagen, Denmark)* [Online], 3(7), 496-511.

Choi, S., Klingauf, J. and Tsien, R. W. (2003). Fusion pore modulation as a presynaptic mechanism contributing to expression of long-term potentiation. *Philosophical Transactions of the Royal Society of London.Series B, Biological Sciences* [Online], 358(1432), 695-705.

Choi, S., Klingauf, J. and Tsien, R. W. (2000). Postfusional regulation of cleft glutamate concentration during LTP at 'silent synapses'. *Nature Neuroscience* [Online], 3(4), 330-336.

Choi, S. K., et al. (2013). Cytotoxicity and inhibition of intercellular interaction in N2a neurospheroids by perfluorooctanoic acid and perfluorooctanesulfonic acid. *Food and Chemical Toxicology : An International Journal Published for the British Industrial Biological Research Association* [Online], 60, 520-529.

Cole, K. S. (1949). Some physical aspects of bioelectric phenomena. *Proceedings of the National Academy of Sciences of the United States of America* [Online], 35(10), 558-566.

Colecraft, H. M., Brody, D. L. and Yue, D. T. (2001). G-protein inhibition of N- and P/Q-type calcium channels: distinctive elementary mechanisms and their functional impact. *The Journal of Neuroscience : The Official Journal of the Society for Neuroscience* [Online], 21(4), 1137-1147.

D'Amour F., Becker F. E., van Riper W. (1936). The black widow spider. *The Quarterly Review of Biology*. 11, 123-160.

Davletov, B. A., et al. (1998a). Vesicle exocytosis stimulated by alpha-latrotoxin is mediated by latrophilin and requires both external and stored Ca2+. *The EMBO Journal* [Online], 17(14), 3909-3920.

Davletov, B. A., et al. (1998b). Vesicle exocytosis stimulated by alpha-latrotoxin is mediated by latrophilin and requires both external and stored Ca2+. *The EMBO Journal* [Online], 17(14), 3909-3920.

Davletov, B. A., et al. (1996a). Isolation and biochemical characterization of a Ca2+-independent alpha-latrotoxin-binding protein. *The Journal of Biological Chemistry* [Online], 271(38), 23239-23245.

Davletov, B. A., et al. (1995). High Affinity Binding of a-Latrotoxin to Recombinant Neurexin Ia. *Journal of Biological Chemistry* [Online], 270(41), 23903-23905.

Davletov, B. A., et al. (1996b). Isolation and Biochemical Characterization of a Ca2+-independent a-Latrotoxin-binding Protein. *Journal of Biological Chemistry* [Online], 271(38), 23239-23245.

De Robertis, E. (1958). Submicroscopic morphology and function of the synapse. *Experimental Cell Research* [Online], 14(Suppl 5), 347-369.

Deak, F., et al. (2009). Alpha-latrotoxin stimulates a novel pathway of Ca2+-dependent synaptic exocytosis independent of the classical synaptic fusion machinery. *The Journal of Neuroscience : The Official Journal of the Society for Neuroscience* [Online], 29(27), 8639-8648.

del Castillo, J. and Katz, B. (1956). Biophysical aspects of neuro-muscular transmission. *Progress in Biophysics and Biophysical Chemistry* [Online], 6, 121-170.

del Castillo, J. and Katz, B. (1954). Quantal components of the end-plate potential. *The Journal of Physiology* [Online], 124(3), 560-573.

Dixon, R. A., et al. (1987). Structural features required for ligand binding to the beta-adrenergic receptor. *The EMBO Journal* [Online], 6(11), 3269-3275.

Dolphin A. C., (2003). G protein modulation of voltage-gated calcium channels. *Pharmacological reviews*, 55, 607-627.

Duchen, L. W., Gomez, S. and Queiroz, L. S. (1981). The neuromuscular junction of the mouse after black widow spider venom. *The Journal of Physiology* [Online], 316, 279-291.

Dulubova, I. E., et al. (1996). Cloning and Structure of -Latroinsectotoxin, a Novel Insect-specific Member of the Latrotoxin Family: FUNCTIONAL EXPRESSION REQUIRES C-TERMINAL TRUNCATION. *Journal of Biological Chemistry* [Online], 271(13), 7535-7543.

Dunlap, K., Luebke, J. I. and Turner, T. J. (1995). Exocytotic Ca2+ channels in mammalian central neurons. *Trends in Neurosciences* [Online], 18(2), 89-98.

Edelman G. (1987). Neural Darwinism. The theory of neuronal group selection. *Basic Books*, New York.

Edelman G. (1993). Bright air, brilliant fire: on the matter of the mind. *Basic Books*, New York. ;

Ehresman, D. J., et al. (2007). Comparison of human whole blood, plasma, and serum matrices for the determination of perfluorooctanesulfonate (PFOS), perfluorooctanoate (PFOA), and other fluorochemicals. *Environmental Research* [Online], 103(2), 176-184.

Elrick, D. B. and Charlton, M. P. (1999). Alpha-Latrocrustatoxin Increases Neurotransmitter Release by Activating a Calcium Influx Pathway at Crayfish Neuromuscular Junction. *Journal of Neurophysiology* [Online], 82(6), 3550-3562.

Emptage, N. J., Reid, C. A. and Fine, A. (2001). Calcium Stores in Hippocampal Synaptic Boutons Mediate Short-Term Plasticity, Store-Operated Ca2+ Entry, and Spontaneous Transmitter Release. *Neuron* [Online], 29(1), 197-208.

Ermolyuk, Y. S., et al. (2013). Differential triggering of spontaneous glutamate release by P/Q-, N- and R-type Ca2+ channels. *Nature Neuroscience* [Online], 16(12), 1754-1763.

Fatt, P. and Katz, B. (1952). Spontaneous subthreshold activity at motor nerve endings. *The Journal of Physiology* [Online], 117(1), 109-128.

Faurskov, B. and Bjerregaard, H. F. (2002). Evidence for cadmium mobilization of intracellular calcium through a divalent cation receptor in renal distal epithelial A6 cells. *Pflugers Archiv : European Journal of Physiology* [Online], 445(1), 40-50.

Fernandez, I., et al. (2001). Three-dimensional structure of the synaptotagmin 1 C2B-domain: synaptotagmin 1 as a phospholipid binding machine. *Neuron* [Online], 32(6), 1057-1069.

Fesce, R., et al. (1986). Effects of black widow spider venom and Ca2+ on quantal secretion at the frog neuromuscular junction. *The Journal of General Physiology* [Online], 88(1), 59-81.

Finkelstein, A., Rubin, L. L. and Tzeng, M. C. (1976). Black widow spider venom: effect of purified toxin on lipid bilayer membranes. *Science (New York, N.Y.)* [Online], 193(4257), 1009-1011.

Fredriksson, R., et al. (2003). The G-Protein-Coupled Receptors in the Human Genome Form Five Main Families. Phylogenetic Analysis, Paralogon Groups, and Fingerprints. *Molecular Pharmacology* [Online], 63(6), 1256-1272.

Fredriksson, R. and Schiöth, H. B. (2005). The Repertoire of G-Protein–Coupled Receptors in Fully Sequenced Genomes. *Molecular Pharmacology* [Online], 67(5), 1414-1425.

Frontali, N., et al. (1976). Purification from black widow spider venom of a protein factor causing the depletion of synaptic vesicles at neuromuscular junctions. *The Journal of Cell Biology* [Online], 68(3), 462-479.

Gavazzo, P., Morelli, E. and Marchetti, C. (2005). Susceptibility of insulinoma cells to cadmium and modulation by L-type calcium channels. *Biometals : An International Journal on the Role of Metal Ions in Biology, Biochemistry, and Medicine* [Online], 18(2), 131-142.

Geppert, M., et al. (1998). Neurexin Ia Is a Major a-Latrotoxin Receptor That Cooperates in a-Latrotoxin Action. *Journal of Biological Chemistry* [Online], 273(3), 1705-1710.

Giovannini, F., et al. (2002). Calcium channel subtypes contributing to acetylcholine release from normal, 4-aminopyridine-treated and myasthenic syndrome auto-antibodies-affected neuromuscular junctions. *British Journal of Pharmacology* [Online], 136(8), 1135-1145.

Glitsch, M. D. (2008). Spontaneous neurotransmitter release and Ca2+--how spontaneous is spontaneous neurotransmitter release?. *Cell Calcium* [Online], 43(1), 9-15.

Grassi, F., et al. (1994). TNF-α increases the frequency of spontaneous miniature synaptic currents in cultured rat hippocampal neurons. *Brain Research* [Online], 659(1), 226-230.

Grasso, A. and Mercanti-Ciotti, M. T. (1993). The secretion of amino acid transmitters from cerebellar primary cultures probed by α-latrotoxin. *Neuroscience* [Online], 54(3), 595-604.

Grasso, A., Rufini, S. and Senni, I. (1978). Concanavalin a blocks black widow spider toxin stimulation of transmitter release from synaptosomes. *FEBS Letters* [Online], 85(2), 241-244.

Gregoire, G., Loirand, G. and Pacaud, P. (1993). Ca2+ and Sr2+ entry induced Ca2+ release from the intracellular Ca2+ store in smooth muscle cells of rat portal vein. *The Journal of Physiology* [Online], 472, 483-500.

Grigoriev, I., et al. (2008). STIM1 is a MT-plus-end-tracking protein involved in remodeling of the ER. *Current Biology : CB* [Online], 18(3), 177-182.

Grishin, E. V. (1998). Black widow spider toxins: the present and the future. *Toxicon* [Online], 36(11), 1693-1701.

Hamann, J., et al. (2015). International Union of Basic and Clinical Pharmacology. XCIV. Adhesion G Protein–Coupled Receptors. *Pharmacological Reviews* [Online], 67(2), 338-367.

Hannon, H. E. and Atchison, W. D. (2013). Omega-conotoxins as experimental tools and therapeutics in pain management. *Marine Drugs* [Online], 11(3), 680-699.

Harada, K. H., et al. (2006). Effects of perfluorooctane sulfonate on action potentials and currents in cultured rat cerebellar Purkinje cells. *Biochemical and Biophysical Research Communications* [Online], 351(1), 240-245.

Harris, J. B. and Ribchester, R. R. (1979). The relationship between end-plate size and transmitter release in normal and dystrophic muscles of the mouse. *The Journal of Physiology* [Online], 296, 245-265.

He, L. and Wu, L. G. (2007). The debate on the kiss-and-run fusion at synapses. *Trends in Neurosciences* [Online], 30(9), 447-455.

Herlitze, S., et al. (2001). Allosteric modulation of Ca2+ channels by G proteins, voltage-dependent facilitation, protein kinase C, and Ca(v)beta subunits. *Proceedings of the National Academy of Sciences of the United States of America* [Online], 98(8), 4699-4704.

Hestrin, S., et al. (1990). Analysis of excitatory synaptic action in pyramidal cells using whole-cell recording from rat hippocampal slices. *The Journal of Physiology* [Online], 422, 203-225.

Heuser, J. E. (1989). Review of electron microscopic evidence favouring vesicle exocytosis as the structural basis for quantal release during synaptic transmission. *Quarterly Journal of Experimental Physiology (Cambridge, England)* [Online], 74(7), 1051-1069.

Heuser, J. E. and Reese, T. S. (1973). Evidence for recycling of synaptic vesicle membrane during transmitter release at the frog neuromuscular junction. *The Journal of Cell Biology* [Online], 57(2), 315-344.

Hinkle, P. M., Shanshala, E. D.,2nd and Nelson, E. J. (1992). Measurement of intracellular cadmium with fluorescent dyes. Further evidence for the role of calcium channels in cadmium uptake. *The Journal of Biological Chemistry* [Online], 267(35), 25553-25559.

Hlubek, M. D., et al. (2000). Calcium-Independent Receptor for a-Latrotoxin and Neurexin 1a Facilitate Toxin-Induced Channel Formation: Evidence That Channel Formation Results from Tethering of Toxin to Membrane. *Molecular Pharmacology* [Online], 57(3), 519-528.

Hlubek, M., Tian, D. and Stuenkel, E. L. (2003). Mechanism of α-latrotoxin action at nerve endings of neurohypophysis. *Brain Research* [Online], 992(1), 30-42.

Hu, K., et al. (2002). Vesicular restriction of synaptobrevin suggests a role for calcium in membrane fusion. *Nature* [Online], 415(6872), 646-650.

Hu, Q., et al. (2012). Does developmental exposure to perflurooctanoic acid (PFOA) induce immunopathologies commonly observed in neurodevelopmental disorders?. *Neurotoxicology* [Online], 33(6), 1491-1498.

Hubbard J. I. and Kwanbunbumpen S. (1968). Evidence for the vesicle hypothesis. *Journal of Physiology* [Online], 194, 407-420.

Ichtchenko, K., et al. (1998). Alpha-Latrotoxin Action Probed with Recombinant Toxin: Receptors Recruit Alpha-Latrotoxin but do Not Transduce an Exocytotic Signal. *The EMBO Journal* [Online], 17(21), 6188-6199.

Ichtchenko, K., et al. (1999). A Novel Ubiquitously Expressed a-Latrotoxin Receptor Is a Member of the CIRL Family of G-protein-coupled Receptors. *Journal of Biological Chemistry* [Online], 274(9), 5491-5498.

Isaacson, J. S., Solis, J. M. and Nicoll, R. A. (1993). Local and diffuse synaptic actions of GABA in the hippocampus. *Neuron* [Online], 10(2), 165-175.

Ishikawa, J., et al. (2003). A pyrazole derivative, YM-58483, potently inhibits store-operated sustained Ca2+ influx and IL-2 production in T lymphocytes. *Journal of Immunology (Baltimore, Md.: 1950)* [Online], 170(9), 4441-4449.

IUPHAR/BPS Guide to Pharmacology. G protein-coupled receptors. Available at <http://www.guidetopharmacology.org/GRAC/ReceptorFamiliesForward?type=GPCR>, November 2015.

IUPHAR/BPS Guide to Pharmacology. Nimodipine. Available at <http://www.guidetopharmacology.org/GRAC/LigandDisplayForward?ligandId=2523>, November 2015.

Jahn, R. and Fasshauer, D. (2012). Molecular machines governing exocytosis of synaptic vesicles. *Nature* [Online], 490(7419), 201-207.

Ji, T. H., Grossmann, M. and Ji, I. (1998). G Protein-coupled Receptors: I. DIVERSITY OF RECEPTOR-LIGAND INTERACTIONS. *Journal of Biological Chemistry* [Online], 273(28), 17299-17302.

Johansson, N., Eriksson, P. and Viberg, H. (2009). Neonatal exposure to PFOS and PFOA in mice results in changes in proteins which are important for neuronal growth and synaptogenesis in the developing brain. *Toxicological Sciences : An Official Journal of the Society of Toxicology* [Online], 108(2), 412-418.

Johansson, N., Fredriksson, A. and Eriksson, P. (2008). Neonatal exposure to perfluorooctane sulfonate (PFOS) and perfluorooctanoic acid (PFOA) causes neurobehavioural defects in adult mice. *Neurotoxicology* [Online], 29(1), 160-169.

Kamato D., et al. (2015). Structure, function, pharmachology, and therapeutic potential of the G protein Gαq/11. *Frontiers in Cardiovascular Medicine*, 2:14.

Karnik, S. S., et al. (2003). Activation of G-protein-coupled receptors: a common molecular mechanism. *Trends in Endocrinology & Metabolism* [Online], 14(9), 431-437.

Kasahara K., Ui M. (2011). G protein alpha o. *UCSD Nature Molecule Pages*, UCSD Nature Signaling Gateway (www.signaling-gateway.org).

Katz, B. and Thesleff, S. (1957). A study of the desensitization produced by acetylcholine at the motor end-plate. *The Journal of Physiology* [Online], 138(1), 63-80.

Khow, O. and Suntrarachun, S. (2012). Strategies for production of active eukaryotic proteins in bacterial expression system. *Asian Pacific Journal of Tropical Biomedicine* [Online], 2(2), 159-162.

Khvotchev, M., et al. (2007). Dual modes of Munc18-1/SNARE interactions are coupled by functionally critical binding to syntaxin-1 N terminus. *The Journal of Neuroscience : The Official Journal of the Society for Neuroscience* [Online], 27(45), 12147-12155.

Kiyatkin, N. I., et al. (1995). Functional Characterization of Black Widow Spider Neurotoxins Synthesised in Insect Cells. *European Journal of Biochemistry* [Online], 230(3), 854-859.

Koh, T. W. and Bellen, H. J. (2003). Synaptotagmin I, a Ca2+ sensor for neurotransmitter release. *Trends in Neurosciences* [Online], 26(8), 413-422.

Krasnoperov, V. G., et al. (1996). The Calcium-Independent Receptor of α-Latrotoxin Is Not a Neurexin. *Biochemical and Biophysical Research Communications* [Online], 227(3), 868-875.

Krasnoperov, V. G., et al. (1997). α-Latrotoxin Stimulates Exocytosis by the Interaction with a Neuronal G-Protein-Coupled Receptor. *Neuron* [Online], 18(6), 925-937.

Krasnoperov, V., et al. (2002). *Protein-tyrosine Phosphatase-ς Is a Novel Member of the Functional Family of α-Latrotoxin Receptors*. [Online]. Vol. 277., pp. 35887-35895.

Kristiansen, K. (2004). Molecular mechanisms of ligand binding, signaling, and regulation within the superfamily of G-protein-coupled receptors: molecular modeling and mutagenesis approaches to receptor structure and function. *Pharmacology & Therapeutics* [Online], 103(1), 21-80.

Lajus, S., et al. (2006). Alpha-latrotoxin induces exocytosis by inhibition of voltage-dependent K+ channels and by stimulation of L-type Ca2+ channels via latrophilin in beta-cells. *The Journal of Biological Chemistry* [Online], 281(9), 5522-5531.

Lalonde, J., Saia, G. and Gill, G. (2014). Store-operated calcium entry promotes the degradation of the transcription factor Sp4 in resting neurons. *Science Signaling* [Online], 7(328), ra51.

Lang, J., et al. (1998a). Ca2+-independent insulin exocytosis induced by alpha-latrotoxin requires latrophilin, a G protein-coupled receptor. *The EMBO Journal* [Online], 17(3), 648-657.

Lang, J., et al. (1998b). Ca2+-independent insulin exocytosis induced by alpha-latrotoxin requires latrophilin, a G protein-coupled receptor. *The EMBO Journal* [Online], 17(3), 648-657.

Lelianova, V. G., et al. (1997). Alpha-latrotoxin receptor, latrophilin, is a novel member of the secretin family of G protein-coupled receptors. *The Journal of Biological Chemistry* [Online], 272(34), 21504-21508.

Lelyanova, V. G., et al. (2009). Activation of alpha-latrotoxin receptors in neuromuscular synapses leads to a prolonged splash acetylcholine release. *Bulletin of Experimental Biology and Medicine* [Online], 147(6), 701-703.

Li, Y., et al. (2005). Essential role of TRPC channels in the guidance of nerve growth cones by brain-derived neurotrophic factor. *Nature* [Online], 434(7035), 894-898.

Li, Y. X., et al. (1998). Enhancement of neurotransmitter release induced by brain-derived neurotrophic factor in cultured hippocampal neurons. *The Journal of Neuroscience : The Official Journal of the Society for Neuroscience* [Online], 18(24), 10231-10240.

Lievremont, J., Bird, G. S. and Putney, J. W. (2005). Mechanism of Inhibition of TRPC Cation Channels by 2-Aminoethoxydiphenylborane. *Molecular Pharmacology* [Online], 68(3), 758-762.

Liu, H., et al. (1996). Identification of Three Subunits of the High Affinity ω-Conotoxin MVIIC-sensitive Ca2+ Channel. *Journal of Biological Chemistry* [Online], 271(23), 13804-13810.

Liu, X., et al. (2011). Possible mechanism of perfluorooctane sulfonate and perfluorooctanoate on the release of calcium ion from calcium stores in primary cultures of rat hippocampal neurons. *Toxicology in Vitro : An International Journal Published in Association with BIBRA* [Online], 25(7), 1294-1301.

Llano, I., et al. (2000). Presynaptic calcium stores underlie large-amplitude miniature IPSCs and spontaneous calcium transients. *Nature Neuroscience* [Online], 3(12), 1256-1265.

Lu, Y., et al. (2015). Structural Basis of Latrophilin-FLRT-UNC5 Interaction in Cell Adhesion. *Structure* [Online], 23(9), 1678-1691.

Lytton, J., Westlin, M. and Hanley, M. R. (1991). Thapsigargin inhibits the sarcoplasmic or endoplasmic reticulum Ca-ATPase family of calcium pumps. *The Journal of Biological Chemistry* [Online], 266(26), 17067-17071.

Ma, H. T., et al. (2008). Canonical transient receptor potential 5 channel in conjunction with Orai1 and STIM1 allows Sr2+ entry, optimal influx of Ca2+, and degranulation in a rat mast cell line. *Journal of Immunology (Baltimore, Md.: 1950)* [Online], 180(4), 2233-2239.

Maestri, L., et al. (2006). Determination of perfluorooctanoic acid and perfluorooctanesulfonate in human tissues by liquid chromatography/single quadrupole mass spectrometry. *Rapid Communications in Mass Spectrometry : RCM* [Online], 20(18), 2728-2734.

Majewski, L. and Kuznicki, J. (2015). SOCE in neurons: Signaling or just refilling?. *Biochimica Et Biophysica Acta* [Online].

Martelli, A., et al. (2006). Cadmium toxicity in animal cells by interference with essential metals. *Biochimie* [Online], 88(11), 1807-1814.

Maruyama, T., et al. (1997). 2APB, 2-Aminoethoxydiphenyl Borate, a Membrane-Penetrable Modulator of Ins(1,4,5)P3-Induced Ca2+ Release. *Journal of Biochemistry* [Online], 122(3), 498-505.

Matsushita, H., Lelianova, V. G. and Ushkaryov, Y. A. (1999). The latrophilin family: multiply spliced G protein-coupled receptors with differential tissue distribution. *FEBS Letters* [Online], 443(3), 348-352.

McDonough, S. I., et al. (1996). Inhibition of calcium channels in rat central and peripheral neurons by omega-conotoxin MVIIC. *The Journal of Neuroscience : The Official Journal of the Society for Neuroscience* [Online], 16(8), 2612-2623.

McEnery, M. W., et al. (1991). Purified omega-conotoxin GVIA receptor of rat brain resembles a dihydropyridine-sensitive L-type calcium channel. *Proceedings of the National Academy of Sciences of the United States of America* [Online], 88(24), 11095-11099.

McKinney, R. A., et al. (1999). Miniature synaptic events maintain dendritic spines via AMPA receptor activation. *Nature Neuroscience* [Online], 2(1), 44-49.

McLachlan, E. M. and Martin, A. R. (1981). Non-linear summation of end-plate potentials in the frog and mouse. *The Journal of Physiology* [Online], 311, 307-324.

Miledi, R. (1956). Strontium as a substrate for calcium in the process of transmitter release at the neuromuscular junction. *Nature* [Online], 212, 1233-1234.

Mintz, I. M., Adams, M. E. and Bean, B. P. (1992). P-type calcium channels in rat central and peripheral neurons. *Neuron* [Online], 9(1), 85-95.

Misler, S. and Hurlbut, W. P. (1979). Action of black widow spider venom on quantized release of acetylcholine at the frog neuromuscular junction: dependence upon external Mg2+. *Proceedings of the National Academy of Sciences of the United States of America* [Online], 76(2), 991-995.

Moreno, C. and Vaca, L. (2011a). SOC and now also SIC: store-operated and store-inhibited channels. *IUBMB Life* [Online], 63(10), 856-863.

Moreno, C. and Vaca, L. (2011b). SOC and now also SIC: Store-operated and store-inhibited channels. *IUBMB Life* [Online], 63(10), 856-863.

Mozrzymas, J. W., Barberis, A. and Cherubini, E. (1999). Facilitation of miniature GABAergic currents by chlorpromazine in cultured rat hippocampal cells. *Neuroreport* [Online], 10(11), 2251-2254.

Nimmrich, V. and Gross, G. (2012). P/Q-type calcium channel modulators. *British Journal of Pharmacology* [Online], 167(4), 741-759.

Occhi, G., et al. (2002). Identification and characterization of heart-specific splicing of human neurexin 3 mRNA (NRXN3). *Biochemical and Biophysical Research Communications* [Online], 298(1), 151-155.

O'Dowd, B. F., et al. (1989). Palmitoylation of the human beta 2-adrenergic receptor. Mutation of Cys341 in the carboxyl tail leads to an uncoupled nonpalmitoylated form of the receptor. *Journal of Biological Chemistry* [Online], 264(13), 7564-7569.

Orlova, E. V., et al. (2000). Structure of alpha-latrotoxin oligomers reveals that divalent cation-dependent tetramers form membrane pores. *Nature Structural Biology* [Online], 7(1), 48-53.

O'Sullivan, M. L., et al. (2012). FLRT proteins are endogenous latrophilin ligands and regulate excitatory synapse development. *Neuron* [Online], 73(5), 903-910.

Palty, R., et al. (2012). SARAF Inactivates the Store Operated Calcium Entry Machinery to Prevent Excess Calcium Refilling. *Cell* [Online], 149(2), 425-438.

Pani, B. and Singh, B. B. (2009). Lipid rafts/caveolae as microdomains of calcium signaling. *Cell Calcium* [Online], 45(6), 625-633.

Parekh, A. B. and Putney, J. W.,Jr (2005a). Store-operated calcium channels. *Physiological Reviews* [Online], 85(2), 757-810.

Parekh, A. B. and Putney, J. W.,Jr (2005b). Store-operated calcium channels. *Physiological Reviews* [Online], 85(2), 757-810.

Park, C. Y., Shcheglovitov, A. and Dolmetsch, R. (2010). The CRAC channel activator STIM1 binds and inhibits L-type voltage-gated calcium channels. *Science (New York, N.Y.)* [Online], 330(6000), 101-105.

Park, Y. and Kim, K. (2009). Short-term plasticity of small synaptic vesicle (SSV) and large dense-core vesicle (LDCV) exocytosis. *Cellular Signalling* [Online], 21(10), 1465-1470.

Peterson, M. E. (2006). Black widow spider envenomation. *Clinical Techniques in Small Animal Practice* [Online], 21(4), 187-190.

Petrenko, A. G., et al. (1990). Isolation and properties of the alpha-latrotoxin receptor. *The EMBO Journal* [Online], 9(6), 2023-2027.

Picotti, G. B., Bondiolotti, G. P. and Meldolesi, J. (1982). Peripheral catecholamine release by alpha-latrotoxin in the rat. *Naunyn-Schmiedeberg's Archives of Pharmacology* [Online], 320(3), 224-229.

Poskanzer, K. E., et al. (2003). Synaptotagmin I is necessary for compensatory synaptic vesicle endocytosis in vivo. *Nature* [Online], 426(6966), 559-563.

Prakriya, M. (2013). Store-operated Orai channels: structure and function. *Current Topics in Membranes* [Online], 71, 1-32.

Przywara, D. A., et al. (1993). Barium-induced exocytosis is due to internal calcium release and block of calcium efflux. *Proceedings of the National Academy of Sciences of the United States of America* [Online], 90(2), 557-561.

Pulido, R., et al. (1995). The LAR/PTP delta/PTP sigma subfamily of transmembrane protein-tyrosine-phosphatases: multiple human LAR, PTP delta, and PTP sigma isoforms are expressed in a tissue-specific manner and associate with the LAR-interacting protein LIP.1. *Proceedings of the National Academy of Sciences of the United States of America* [Online], 92(25), 11686-11690.

Purves, D. (2012). Neuroscience. [Online]. Sunderland, Mass.: Sinauer Associates.

Putcha, D., et al. (2011). Hippocampal hyperactivation associated with cortical thinning in Alzheimer's disease signature regions in non-demented elderly adults. *The Journal of Neuroscience : The Official Journal of the Society for Neuroscience* [Online], 31(48), 17680-17688.

Putney, J. W.,Jr (2007). Recent breakthroughs in the molecular mechanism of capacitative calcium entry (with thoughts on how we got here). *Cell Calcium* [Online], 42(2), 103-110.

Qanbar, R. and Bouvier, M. (2003). Role of palmitoylation/depalmitoylation reactions in G-protein-coupled receptor function. *Pharmacology & Therapeutics* [Online], 97(1), 1-33.

Rahman, M. A., et al. (1999). Norepinephrine exocytosis stimulated by alpha-latrotoxin requires both external and stored Ca2+ and is mediated by latrophilin, G proteins and phospholipase C. *Philosophical Transactions of the Royal Society of London.Series B, Biological Sciences* [Online], 354(1381), 379-386.

Ramirez, D. M. and Kavalali, E. T. (2011). Differential regulation of spontaneous and evoked neurotransmitter release at central synapses. *Current Opinion in Neurobiology* [Online], 21(2), 275-282.

Ranaivoson, F., et al. (2015). Structural and Mechanistic Insights into the Latrophilin3-FLRT3 Complex that Mediates Glutamatergic Synapse Development. *Structure* [Online], 23(9), 1665-1677.

Rauber, A. (1983). Black widow spider bites. *Journal of Toxicology.Clinical Toxicology* [Online], 21(4-5), 473-485.

Rens-Domiano, S. and Hamm, H. E. (1995). Structural and functional relationships of heterotrimeric G-proteins. *The FASEB Journal* [Online], 9(11), 1059-1066.

Ribchester, R. R. (2009). Mammalian neuromuscular junctions: modern tools to monitor synaptic form and function. *Current Opinion in Pharmacology* [Online], 9(3), 297-305.

Robertson J. D. (1956). The ultrastructure of a reptilian myoneural junction. *Journal of Biophysics and Biochemical Cytology* [online], 2(4):381-94.

Robinson, M., et al. (2004). FLRT3 is expressed in sensory neurons after peripheral nerve injury and regulates neurite outgrowth. *Molecular and Cellular Neurosciences* [Online], 27(2), 202-214.

Rohou, A., Nield, J. and Ushkaryov, Y. A. (2007). Insecticidal toxins from black widow spider venom. *Toxicon : Official Journal of the International Society on Toxinology* [Online], 49(4), 531-549.

Salido, G. M., Sage, S. O. and Rosado, J. A. (2009a). Biochemical and functional properties of the store-operated Ca2+ channels. *Cellular Signalling* [Online], 21(4), 457-461.

Salido, G. M., Sage, S. O. and Rosado, J. A. (2009b). TRPC channels and store-operated Ca(2+) entry. *Biochimica Et Biophysica Acta* [Online], 1793(2), 223-230.

Sampayo, R. R. L. (1944). Pharmacological action of the venom of Latrodectus Mactans and other Latrodectus spiders. *Journal of Pharmacology and Experimental Therapeutics* [Online], 80(4), 309-322.

Sampieri, A., et al. (2009). Visualizing the store-operated channel complex assembly in real time: Identification of SERCA2 as a new member. *Cell Calcium* [Online], 45(5), 439-446.

Schaefer, M., et al. (2000). Receptor-mediated Regulation of the Nonselective Cation Channels TRPC4 and TRPC5. *Journal of Biological Chemistry* [Online], 275(23), 17517-17526.

Schiavo, G., et al. (1996). Calcium-dependent switching of the specificity of phosphoinositide binding to synaptotagmin. [Online]. Vol. 93., pp. 13327-13332.

Schiavo, G., et al. (1997). Binding of the synaptic vesicle v-SNARE, synaptotagmin, to the plasma membrane t-SNARE, SNAP-25, can explain docked vesicles at neurotoxin-treated synapses. [Online]. Vol. 94., pp. 997-1001.

Schwarz, G., Droogmans, G. and Nilius, B. (1994). Multiple effects of SK&F 96365 on ionic currents and intracellular calcium in human endothelial cells. *Cell Calcium* [Online], 15(1), 45-54.

Sedgwick, S. G. and Smerdon, S. J. (1999). The ankyrin repeat: a diversity of interactions on a common structural framework. *Trends in Biochemical Sciences* [Online], 24(8), 311-316.

Shackleford, R., et al. (2015). The black widow spider bite: differential diagnosis, clinical manifestations, and treatment options. *The Journal of the Louisiana State Medical Society : Official Organ of the Louisiana State Medical Society* [Online], 167(2), 74-78.

Shim, S., Zheng, J. Q. and Ming, G. L. (2013). A critical role for STIM1 in filopodial calcium entry and axon guidance. *Molecular Brain* [Online], 6, 51-6606-6-51.

Silva, J. P., et al. (2011). Latrophilin 1 and its endogenous ligand Lasso/teneurin-2 form a high-affinity transsynaptic receptor pair with signaling capabilities. *Proceedings of the National Academy of Sciences of the United States of America* [Online], 108(29), 12113-12118.

Silva, J. P., Suckling, J. and Ushkaryov, Y. (2009). Penelope's web: using alpha-latrotoxin to untangle the mysteries of exocytosis. *Journal of Neurochemistry* [Online], 111(2), 275-290.

Silva, J. P. and Ushkaryov, Y. A. (2010). The latrophilins, "split-personality" receptors. *Advances in Experimental Medicine and Biology* [Online], 706, 59-75.

Silva, J., et al. (2009). Functional Cross-interaction of the Fragments Produced by the Cleavage of Distinct Adhesion G-protein-coupled Receptors. *Journal of Biological Chemistry* [Online], 284(10), 6495-6506.

Singh, A., et al. (2010). The transient receptor potential channel antagonist SKF96365 is a potent blocker of low-voltage-activated T-type calcium channels. *British Journal of Pharmacology* [Online], 160(6), 1464-1475.

Smith, R. J., et al. (1990). Receptor-coupled signal transduction in human polymorphonuclear neutrophils: effects of a novel inhibitor of phospholipase C-dependent processes on cell responsiveness. *The Journal of Pharmacology and Experimental Therapeutics* [Online], 253(2), 688-697.

Smith, S. M., et al. (2012). Calcium regulation of spontaneous and asynchronous neurotransmitter release. *Cell Calcium* [Online], 52(3-4), 226-233.

Smyth, J. T., et al. (2010). Activation and regulation of store-operated calcium entry. *Journal of Cellular and Molecular Medicine* [Online], 14(10), 2337-2349.

Sollner, T., et al. (1993a). A protein assembly-disassembly pathway in vitro that may correspond to sequential steps of synaptic vesicle docking, activation, and fusion. *Cell* [Online], 75(3), 409-418.

Sollner, T., et al. (1993b). SNAP receptors implicated in vesicle targeting and fusion. *Nature* [Online], 362(6418), 318-324.

Spencer, C. I. and Berlin, J. R. (1997). Calcium-induced release of strontium ions from the sarcoplasmic reticulum of rat cardiac ventricular myocytes. *The Journal of Physiology* [Online], 504 (Pt 3)(Pt 3), 565-578.

Stathopulos, P. B. and Ikura, M. (2013). Structural aspects of calcium-release activated calcium channel function. *Channels (Austin, Tex.)* [Online], 7(5), 344-353.

Stevens, C. F. and Williams, J. H. (2000). “Kiss and run” exocytosis at hippocampal synapses. *Proceedings of the National Academy of Sciences* [Online], 97(23), 12828-12833.

Stocker, J. W., et al. (1997). Preferential interaction of omega-conotoxins with inactivated N-type Ca2+ channels. *The Journal of Neuroscience : The Official Journal of the Society for Neuroscience* [Online], 17(9), 3002-3013.

Sudhof, T. C. (2004). The synaptic vesicle cycle. *Annual Review of Neuroscience* [Online], 27, 509-547.

Sudhof, T. C. and Rizo, J. (2011). Synaptic vesicle exocytosis. *Cold Spring Harbor Perspectives in Biology* [Online], 3(12), 10.1101/cshperspect.a005637.

Südhof, T. (2013). Neurotransmitter Release: The Last Millisecond in the Life of a Synaptic Vesicle. *Neuron* [Online], 80(3), 675-690.

Sutton, M. A., et al. (2004). Regulation of dendritic protein synthesis by miniature synaptic events. *Science (New York, N.Y.)* [Online], 304(5679), 1979-1983.

Sutton, R. B., et al. (1998). Crystal structure of a SNARE complex involved in synaptic exocytosis at 2.4 A resolution. *Nature* [Online], 395(6700), 347-353.

Tang, G., et al. (2014). Loss of mTOR-dependent macroautophagy causes autistic-like synaptic pruning deficits. *Neuron* [Online], 83(5), 1131-1143.

Taves, Donald R. (1968). Evidence that there are two forms of fluoride in human serum. *Nature*, 217, 1050-1051.

Thastrup, O., et al. (1990). Thapsigargin, a tumor promoter, discharges intracellular Ca2+ stores by specific inhibition of the endoplasmic reticulum Ca2(+)-ATPase. *Proceedings of the National Academy of Sciences of the United States of America* [Online], 87(7), 2466-2470.

Treiman, M., Caspersen, C. and Christensen, S. B. (1998). A tool coming of age: thapsigargin as an inhibitor of sarco-endoplasmic reticulum Ca(2+)-ATPases. *Trends in Pharmacological Sciences* [Online], 19(4), 131-135.

Tse, F. W. and Tse, A. (1999). α-Latrotoxin Stimulates Inward Current, Rise in Cytosolic Calcium Concentration, and Exocytosis in at Pituitary Gonadotropes. *Endocrinology* [Online], 140(7), 3025-3033. Available from: http://dx.doi.org/10.1210/endo.140.7.6849.

Tucker, R. P., et al. (2007). Teneurins: Transmembrane proteins with fundamental roles in development. *The International Journal of Biochemistry & Cell Biology* [Online], 39(2), 292-297.

Tzeng, M. C., Cohen, R. S. and Siekevitz, P. (1978). Release of neurotransmitters and depletion of synaptic vesicles in cerebral cortex slices by alpha-latrotoxin from black widow spider venom. *Proceedings of the National Academy of Sciences of the United States of America* [Online], 75(8), 4016-4020.

Tzeng, M. and Siekevitz, P. (1978). The effect of the purified major protein factor (α-latrotoxin) of black widow spider venom on the release of acetylcholine and norepinephrine from mouse cerebral cortex slices. *Brain Research* [Online], 139(1), 190-196.

Ubach, J., et al. (1998). Ca2+ binding to synaptotagmin: how many Ca2+ ions bind to the tip of a C2-domain?. *The EMBO Journal* [Online], 17(14), 3921-3930.

Ulloa-Aguirre, A., et al. (1999). Structure-Activity Relationships of G Protein-Coupled Receptors. *Archives of Medical Research* [Online], 30(6), 420-435.

Ullrich, B., Ushkaryov, Y. A. and Südhof, T. C. (1995). Cartography of neurexins: More than 1000 isoforms generated by alternative splicing and expressed in distinct subsets of neurons. *Neuron* [Online], 14(3), 497-507.

Usai, C., et al. (1999). Pathways of cadmium influx in mammalian neurons. *Journal of Neurochemistry* [Online], 72(5), 2154-2161.

Ushkaryov, Y. A., et al. (1994). Conserved domain structure of beta-neurexins. Unusual cleaved signal sequences in receptor-like neuronal cell-surface proteins. *Journal of Biological Chemistry* [Online], 269(16), 11987-11992.

Ushkaryov, Y. (2002). α-Latrotoxin: from structure to some functions. *Toxicon* [Online], 40(1), 1-5.

Ushkaryov, Y. A., et al. (1992). Neurexins: synaptic cell surface proteins related to the alpha-latrotoxin receptor and laminin. *Science (New York, N.Y.)* [Online], 257(5066), 50-56.

Ushkaryov, Y. A., Rohou, A. and Sugita, S. (2008). alpha-Latrotoxin and its receptors. *Handbook of Experimental Pharmacology* [Online], (184)(184), 171-206.

Ushkaryov, Y. A., Volynski, K. E. and Ashton, A. C. (2004). The multiple actions of black widow spider toxins and their selective use in neurosecretion studies. *Toxicon : Official Journal of the International Society on Toxinology* [Online], 43(5), 527-542.

Vaca, L. (2010). SOCIC: the store-operated calcium influx complex. *Cell Calcium* [Online], 47(3), 199-209.

Varnai, P., Hunyady, L. and Balla, T. (2009). STIM and Orai: the long-awaited constituents of store-operated calcium entry. *Trends in Pharmacological Sciences* [Online], 30(3), 118-128.

Verhage, M., et al. (1995). Ba2+ replaces Ca2+/calmodulin in the activation of protein phosphatases and in exocytosis of all major transmitters. *European Journal of Pharmacology: Molecular Pharmacology* [Online], 291(3), 387-398.

Verhage, M., et al. (2000). Synaptic Assembly of the Brain in the Absence of Neurotransmitter Secretion. *Science* [Online], 287(5454), 864-869.

Vicentini L. M., Meldolesi J. (1984). Alpha Latrotoxin of black widow spider venom binds to a specific receptor coupled to phosphoinositide breakdown in PC12 cells. *Biochemical and Biophysical Research Communications*, 121(2), 538-544.waz`

Volynski, K. E., et al. (2003). Mutant alpha-latrotoxin (LTXN4C) does not form pores and causes secretion by receptor stimulation: this action does not require neurexins. *The Journal of Biological Chemistry* [Online], 278(33), 31058-31066.

Volynski, K. E., et al. (1999). Functional expression of alpha-latrotoxin in baculovirus system. *FEBS Letters* [Online], 442(1), 25-28.

Volynski, K. E., et al. (2004). Latrophilin fragments behave as independent proteins that associate and signal on binding of LTX(N4C). *The EMBO Journal* [Online], 23(22), 4423-4433.

Volynski, K. E., et al. (2000). Latrophilin, Neurexin, and Their Signaling-deficient Mutants Facilitate a-Latrotoxin Insertion into Membranes but Are Not Involved in Pore Formation. *Journal of Biological Chemistry* [Online], 275(52), 41175-41183.

Wang, L., et al. (2005). Teneurin proteins possess a carboxy terminal sequence with neuromodulatory activity. *Molecular Brain Research* [Online], 133(2), 253-265.

Wang, Y., et al. (2010). The calcium store sensor, STIM1, reciprocally controls Orai and CaV1.2 channels. *Science (New York, N.Y.)* [Online], 330(6000), 105-109.

Wightman, R. M. and Haynes, C. L. (2004). Synaptic vesicles really do kiss and run. *Nature Neuroscience* [Online], 7(4), 321-322.

Wu, M. N., et al. (2001). The ROP-Syntaxin interaction inhibits neurotransmitter release. *European Journal of Cell Biology* [Online], 80(2), 196-199.

Xu, T. and Xu, P. (2008). Differential Regulation of Small Clear Vesicles and Large Dense-Core Vesicles - Wang, Z-T. In: *Molecular Mechanisms of Neurotransmitter Release*. Humana Press, pp. 327-339.

Yamagishi, S., et al. (2011). FLRT2 and FLRT3 act as repulsive guidance cues for Unc5-positive neurons. *The EMBO Journal* [Online], 30(14), 2920-2933.

Yang, B., et al. (2000). nSec1 binds a closed conformation of syntaxin1A. *The Journal of Cell Biology* [Online], 148(2), 247-252.

Yeromin, A. V., et al. (2004). A store-operated calcium channel in Drosophila S2 cells. *The Journal of General Physiology* [Online], 123(2), 167-182.

Young, T. R. and Leamey, C. A. (2009). Teneurins: Important regulators of neural circuitry. *The International Journal of Biochemistry & Cell Biology* [Online], 41(5), 990-993.

Zhao, C., et al. (2010). Dissecting the N-ethylmaleimide-sensitive factor: required elements of the N and D1 domains. *The Journal of Biological Chemistry* [Online], 285(1), 761-772.

Zitt, C., et al. (2004). Potent Inhibition of Ca2+ Release-activated Ca2+ Channels and T-lymphocyte Activation by the Pyrazole Derivative BTP2. *Journal of Biological Chemistry* [Online], 279(13), 12427-12437.